ESD-TR-67-425
ESTI FILE COPY

ESD-TR-67-425
ESD RECORD COPY
RETURN TO
SCIENTIFIC & TECHNICAL INFORMATION DIVISION
(ESTI), BUILDING 1211

ESD ACCESSION LIST
ESTI Call No. AL 58882
Copy No. 1 of 2 cys.

MTP-52

POLARIZATION PROPERTIES OF THE PARABOLOIDAL ANTENNA: AN ANALYTICAL STUDY

ESLE

DECEMBER 1967

Jerome L. Altman

Prepared for

DEVELOPMENT ENGINEERING DIVISION
DIRECTORATE OF PLANNING AND TECHNOLOGY

ELECTRONIC SYSTEMS DIVISION
AIR FORCE SYSTEMS COMMAND
UNITED STATES AIR FORCE
L. G. Hanscom Field, Bedford, Massachusetts

This document has been approved for public release and sale; its distribution is unlimited.

Project 8052
Prepared by
THE MITRE CORPORATION
Bedford, Massachusetts
Contract AF19(628)-5165

AD0664564

When U.S. Government drawings, specifications, or other data are used for any purpose other than a definitely related government procurement operation, the government thereby incurs no responsibility nor any obligation whatsoever; and the fact that the government may have formulated, furnished, or in any way supplied the said drawings, specifications, or other data is not to be regarded by implication or otherwise, as in any manner licensing the holder or any other person or corporation, or conveying any rights or permission to manufacture, use, or sell any patented invention that may in any way be related thereto.

Do not return this copy. Retain or destroy.

POLARIZATION PROPERTIES OF THE PARABOLOIDAL ANTENNA: AN ANALYTICAL STUDY

DECEMBER 1967

Jerome L. Altman

Prepared for

DEVELOPMENT ENGINEERING DIVISION
DIRECTORATE OF PLANNING AND TECHNOLOGY

ELECTRONIC SYSTEMS DIVISION
AIR FORCE SYSTEMS COMMAND
UNITED STATES AIR FORCE
L. G. Hanscom Field, Bedford, Massachusetts

This document has been approved for public release and sale; its distribution is unlimited.

Project 8052
Prepared by
THE MITRE CORPORATION
Bedford, Massachusetts
Contract AF19(628)-5165

FOREWORD

The work reported in this document was performed by The MITRE Corporation, Bedford, Massachusetts, for the Development Engineering Division, Directorate of Planning and Technology, Electronic Systems Division, of the Air Force Systems Command, under Contract AF 19(628)-5165.

The research was supported by the Advanced Research Projects Agency, Project Defender, and was monitored by Col. B. I. Hill under Contract No. AF 19(628)-5165.

REVIEW AND APPROVAL

Publication of this technical report does not constitute Air Force approval of the report's findings or conclusions. It is published only for the exchange and stimulation of ideas.

ANTHONY P. TRUNFIO, Technical Advisor
Development Engineering Division
Directorate of Planning and Technology

ABSTRACT

This study is a theoretical investigation of the polarization properties of the paraboloidal antenna for both the focal feed system and the Cassegrain feed system when the feed horn is either circularly or linearly polarized. The properties are analyzed in terms of general analytic equations and also in terms of quantitative graphs pertaining to the specific case of the 30-foot diameter paraboloidal antenna which is part of The MITRE Corporation's Bedford Radar Installation.

ACKNOWLEDGMENT

It is gratefully acknowledged that Mr. J. L. Pearlman was responsible for all the programmings and computations involved in this study.

TABLE OF CONTENTS

TABLE OF CONTENTS (Continued)

TABLE OF CONTENTS (Concluded)

LIST OF ILLUSTRATIONS

LIST OF ILLUSTRATIONS (Continued)

LIST OF ILLUSTRATIONS (Continued)

LIST OF ILLUSTRATIONS (Continued)

LIST OF ILLUSTRATIONS (Concluded)

SECTION I

INTRODUCTION AND SUMMARY

SCOPE OF THE STUDY

The scope of this study is primarily confined to the theoretical investigation of the polarization properties of the paraboloidal antenna. Thus, answers are sought to the questions: What is the ellipticity (ratio of major to minor axes) in the near- and far-fields when the feed is circularly polarized? What sort of polarization prevails in the near- and far-fields when the feed is linearly polarized?

The answers are given in terms of general analytic equations (Section II, for the focal feed system; Section III, for the Cassegrain system), and also in terms of quantitative graphs pertaining to the MITRE Antenna (Section IV, for the focal feed system; Section V, for the Cassegrain system).

Field amplitude distributions (as functions of various parameters) are given considerable attention since this information must be obtained for polarization purposes, and since amplitude comparisons with known or experimental values serve as checks on the equations and computations. Effects of paraboloid imperfections and of defocusing both in the focal plane and along the boresight axis are also considered.

SUMMARY OF RESULTS

Some of the more important findings of the study are as follows:

(1) For any circularly polarized primary illumination, ellipticity on boresight is 0 db (perfect circularity).

(2) Off boresight, ellipticity is strongly dependent on the primary illumination distribution whose practical extremes are the ideal equibeam and the dipole-like distributions. Within the 3-db beamwidth, the ellipticity may be practically 0 db (as with the equibeam distribution in the focal feed system), or as high as 0.8 db (as with the dipole-like distribution in the focal feed system). The Cassegrain feed system is relatively less exacting regarding the type of primary illumination, and, within the 3-db beamwidth, ellipticity is about 0.15 db for either distribution.

Ellipticity increases in the region of the null and decreases again in the region of the sidelobe peaks.

The magnitude of the ellipticity is constant with azimuth (at a given elevation angle), provided that the source can be considered as infinitely small in extent (as with the equibeam and dipole-like distributions, but not with the pseudo-equibeam distribution, which represents another extreme case of illumination imperfection).

(3) When linear polarization is applied at the feed, the polarization of the near- and far-fields suffer a deviation angle from the direction of primary illumination which depends on azimuth and increases (or decreases) as would ellipticity, were circular polarization applied.

(4) For the focal feed system, ellipticity (at a given elevation angle) is lower as the main dish is flatter (longer focal length), or as the flat portion of the dish is favored at the expense of the periphery region (as achieved by a large tapering of the primary illumination).

(5) For an imperfect primary distribution, such as the dipole-like, the Cassegrain system is superior insofar as the subreflector subtends a smaller angle from the source than that subtended by the main dish from its virtual source. The overall improvement over the focal feed system is comparable to that afforded by the effective "magnification" of focal length of ray optics. Another viewpoint (Section V) is that illumination defects at the edge of the subreflector are not magnified at the edge of the main dish, although their angular locations are magnified.

(6) Near-field and far-field ellipticities are almost equal in magnitude within the half-power beamwidth, but show large differences near the nulls. The far-field can be even more closely simulated at close range, even with regard to gain, by judicious de-focusing along the boresight axis.

(7) Ellipticity is hardly affected by random but sizeable (one tenth of a wavelength) imperfections on the surface of the paraboloidal main dish – although gain (but not directivity) is lowered. Semi-correlated imperfections of comparable magnitude are far more detrimental.

(8) Ray optics methods of treating the Cassegrain system are somewhat inexact; yet they afford worthwhile qualitative information.

MECHANISMS OF POLARIZATION

The polarization mechanisms involve, for the focal feed system, the interplay of the reflector paraboloidal surface with the primary illumination, and, for the Cassegrain system, interplay of reflecting surfaces with primary and secondary illuminations.

Dipole-Like Distribution

Consider first the dipole-like distribution.* This type of illumination originates from a single point source (phase center) to which is associated a spherical wavefront. On this spherical wavefront, the H-field is oriented along parallel "latitude" lines and its strength varies with azimuth (for a given elevation angle) so that its magnitude in the H-plane is different from its magnitude in the E-plane (Figure 1a).

On the paraboloidal dish, the tangential components of the parallel "latitude" H-lines give rise to current lines, which are no longer parallel, but contain "cross-polarized" components. Thus, an x-oriented dipole gives rise not only to x-oriented currents but also to y-currents which are functions of azimuth and peak up in the planes 45 degrees away from the x-z plane. It is those currents which are mostly responsible for the cross-polarized components in the near- and far-fields and for shifting the linear polarization direction. The concavity of the paraboloidal dish induces z-currents which also produce cross-polarized components, but their effect is small compared to that of the y-directed currents. All the extraneous currents (y- and z-directed) produce a cross-polarized pattern which does not correspond to that produced by the x-directed currents. As a result, cross-polarized terms are most effective in the "null" region where the in-polarized components are weakest.

---

*This distribution is considered in: E. U. Condon, "Theory of Radiation from Paraboloid Reflectors," Research Report SR-105, 24 Sep 1941; S. Silver, "Microwave Antenna Theory and Design," p. 419, Rad. Lab. Series, Vol. 12, 1947; L. Thourel, "The Antenna," pp. 269-270, John Wiley and Sons, Inc., New York, 1960.

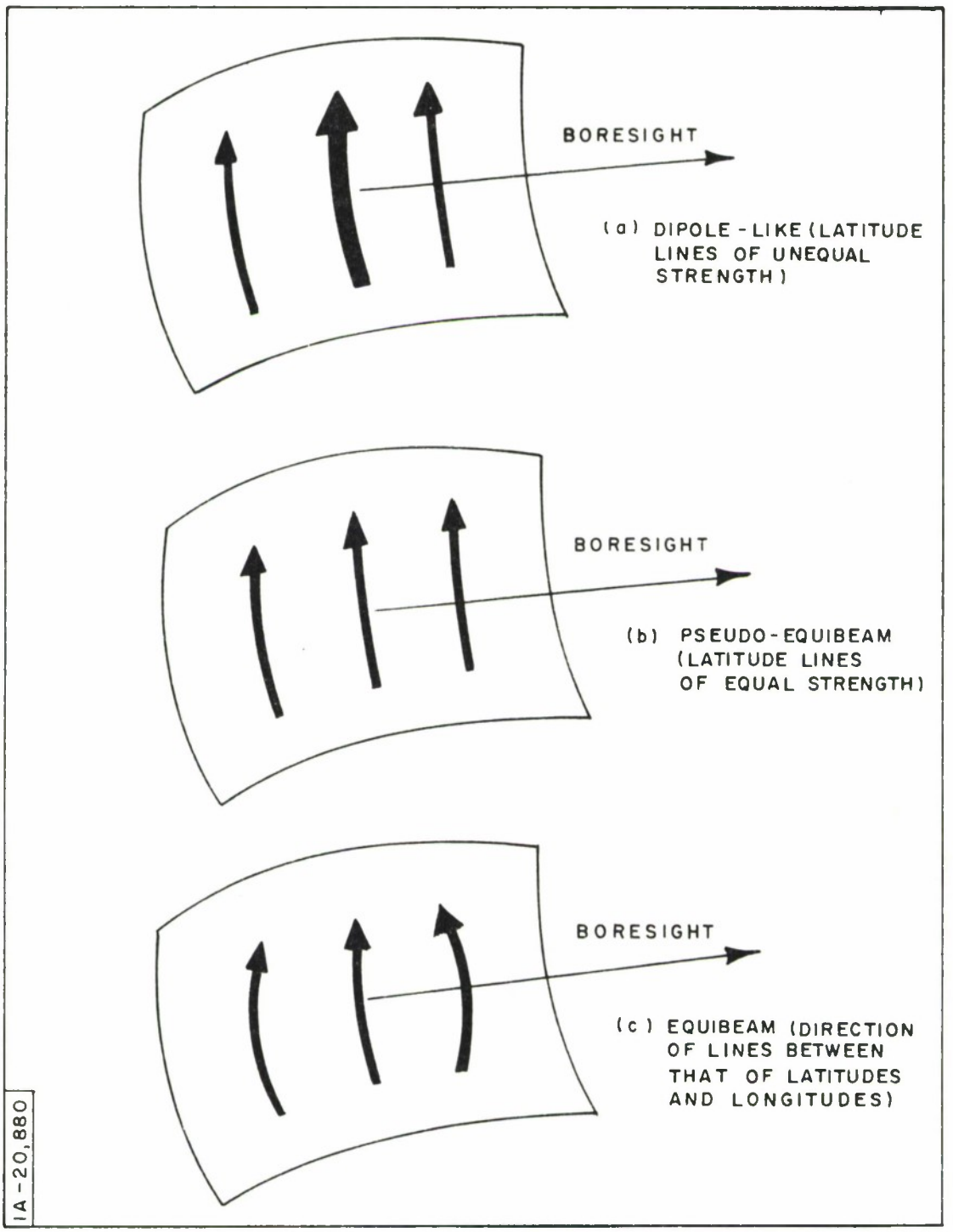

Figure 1. Distributions on Spherical Wavefront

When the feed is circularly polarized (with dipole-like distribution), the field on the spherical wavefront is elliptically polarized, except on the boresight axis. Although the ellipticity arises both from the fact that the magnitude of each quadrature component varies with azimuth, and from the fact that the direction of each quadrature component is along "latitude" lines, the ellipticity on the spherical wavefront is constant in amplitude with azimuth and, furthermore, the directions of the major axes of the ellipses present cylindrical symmetry with the boresight axis. These elliptically polarized fields induce elliptically polarized currents on the paraboloidal dish. These currents can be considered as the sums of two counter-rotating circularly polarized currents which give rise to counter-rotating circularly polarized fields. Again, because of different distributions over the dish for the counter-rotating current components, the ratio of the two counter-rotating circularly polarized fields at the observation point is not constant with elevation, but is constant with azimuth.

Pseudo-Equibeam Distribution

For the pseudo-equibeam distribution, the situation is somewhat different. This distribution is like the dipole-like insofar as the direction of the H-field is still along parallel "latitude" lines. However, the H-field strength, on the spherical wavefront, is made independent of azimuth (Figure 1b).

Under linear polarization, the H-field still induces y-directed current components which peak up in the 45-degree planes and give rise to cross-polarized components in the near- and far-fields. The situation is similar to that of the previous case.

When the source is circularly polarized, the field on the wavefront no longer exhibits constant ellipticity with azimuth. There are now "preferred" planes (corresponding to the source quadrature component planes) where the field is circularly polarized, whereas it is strongly elliptically polarized in

in planes 45 degrees away. As a result, the near- and far-fields exhibit an ellipticity which depends on azimuth.

Equibeam Distribution

With the equibeam distribution, the field strength on the spherical wavefront is constant with azimuth, as for pseudo-equibeam distribution. However, the field direction is no longer along parallel "latitude" lines but is so directed that two space orthogonal sources produce fields which are orthogonal, not only on the boresight axis, but everywhere on the spherical wavefront (Figure 1c). It turns out that the projection of this non-parallel field on the paraboloidal surface induces parallel currents. Thus, an x-directed source produces no y-directed current. Moreover, the x-directed current magnitude is independent of azimuth. The only mechanism by which ellipticity comes into play is through the z-directed currents which give rise, in the near- and far-fields, to x- and y-components, as the elevation angle is increased from zero. Again, this effect, which is now small compared to the other two cases, becomes maximum in the "null" region where the normal components are small.

Cassegrain System

In the Cassegrain system, the three distributions are almost the same on the subreflector because it subtends a much smaller angle from the source. However, even with the equibeam distribution (whose field on the spherical wavefront is circularly polarized everwhere), the currents induced on the hyperboloidal subreflector have rather small, but finite, cross-polarized components. Through a process related to the effective magnification of the main dish focal length (ray optics viewpoint), the relative magnitudes of the various components are essentially preserved; whereas, the angular locations are "magnified" from the subreflector to the main dish.

Distribution Models

From a practical standpoint, the equibeam distribution can be considered as the ideal distribution (ideal feed-horn compensation). It can be experimentally verified by applying circular polarization to the horn and measuring the circularity of the primary illumination on the spherical wavefront. The dipole-like distribution is a fair approximation to the uncompensated square or circular horn; whereas, the pseudo-equibeam distribution represents an attempt to compensate the horn for equal amplitude in two orthogonal planes without regard to cylindrical symmetry. Those are the three arbitrary mathematical models of primary distributions which are considered in this study.

ANALYTICAL APPROACH

In Section II, the paraboloidal dish is considered as a scatterer to the primary illumination. The starting point of the study is the exact integral equation for perfect conductors (form of Kirchhoff's Equation) relating the scattered H-field to the field on the scatterer. Simplifying physical optics assumptions involving size, curvature, etc., and certain range assumptions are introduced. The various geometrical vectors related to the paraboloid are expressed in Cartesian components, and each component is expressed in terms of elevation angle, azimuth angle, and constants of the system. The geometry of the observation point is also reduced to elevation, azimuth, and range.

As the "geometry" is expressed analytically, so is the illumination function. Cartesian components in terms of elevation and azimuth are obtained for the three distributions discussed in the preceding subsection. Those distributions, in turn, can be "tapered" by appropriate amplitude functions independent of azimuth. Those functions are set forth arbitrarily

or are taken from measurements. Circular polarization is introduced immediately, since it is a simple matter, when considering linear polarization, to suppress one of the quadrature components.

After all the elements have been expressed analytically, the various field components can be separated in terms of space directions and time phases. Concurrently, some "tools" are developed to compute ellipticity magnitude and orientation in terms of the various field components and, when necessary, to change the coordinate system for a more meaningful "view" of the field.

In Section III, the Cassegrain system is analyzed by considering the field at the paraboloidal dish as that being scattered by the subreflector. The "geometry" of the hyperboloidal subreflector must then be treated analytically, although the primary illumination functions are the same as those considered in Section II. After it has been solved, the field on the paraboloid is treated as the primary illumination of Section II.

The geometrical problems, primary distributions, and other "tools" transcending the limited scope of this study are relegated to the Appendices.

COMPUTER PROGRAMS*

A number of computer programs are developed to perform the calculations described in this study. Listings of some typical programs are reproduced in Appendix K.

The programs, written in FORTRAN IV, are run on the IBM 7030 (STRETCH) Computer of MITRE's SDL facility.

---

*Written by J. L. Pearlman

Since several of the programs are time consuming, a deliberate effort is made to eliminate, wherever possible, the recalculation of often used intermediate results. This is accomplished by devoting large amounts of memory to the storage of these results. In certain cases, the programs are written in two parts, with the output of the first part being stored on tape to be used as input to the second part, as in the case of the Cassegrain system. In this case, the field scattered onto the parabolic reflector from the hyperbolic subreflector is computed and stored on tape for further processing by programs which compute the field components at various points.

SECTION II

ANALYSIS OF FOCAL FEED SYSTEM

SYMBOLIC FIELD EQUATIONS AND APPROXIMATIONS

A paraboloidal dish illuminated from a source located at its focus acts as a scatterer to the primary illumination (Figure 2), and the exact equation for the scattered H-field at the observation point P, $\vec{H}_{S|P}$, is:

$$\vec{H}_{S|P} = \frac{1}{4\pi} \iint_S (\hat{n} \times \vec{H}) \times \nabla_Q \left(\frac{e^{-jkr}}{r} \right) dA \qquad (1)$$

where

$\vec{H}$ = total H-field at point Q on the surface of the paraboloid,

$\hat{n}$ = outward normal unit vector at point Q,

k = propagation constant, equal to $2\pi/\lambda$,

r = distance from the observation point P to point Q,

dA = differential area element at point Q, and

S = surface of the paraboloid.

An exact expression for $\nabla_Q (e^{-jkr}/r)$ is:

$$\nabla_Q \left(\frac{e^{-jkr}}{r} \right) = \left(j \frac{2\pi}{\lambda} + \frac{1}{r} \right) \left(\frac{e^{-jkr}}{r} \right) \hat{a}_1 \qquad (2)$$

It is seen that when r is greater than 15 wavelengths, the magnitude of the 1/r term is but one percent the magnitude of k. Furthermore, if the

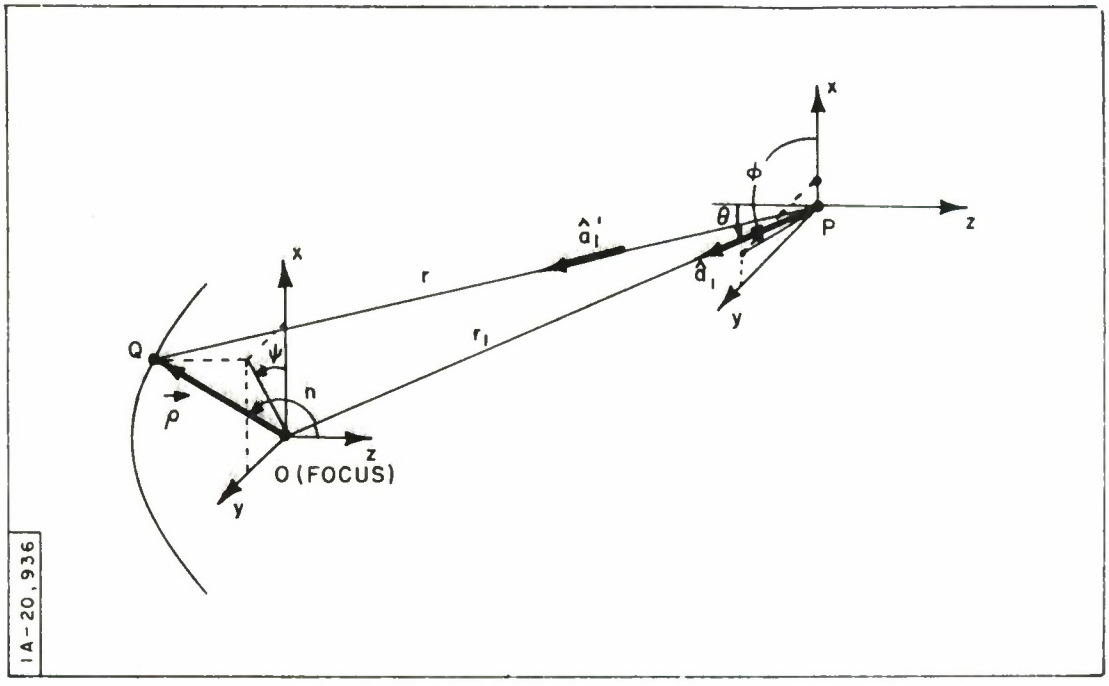

Figure 2. Geometry of the Problem

observation point P is at least 15 focal lengths from the apex of the paraboloid, then, as far as amplitude is concerned, r can safely be replaced by the constant factor r_1, the distance from the observation point P to the focus (coordinate center) of the paraboloid. An approximate expression for Equation (2), valid everywhere but in the very near field, becomes

$$\nabla_Q \left(\frac{e^{-jkr}}{r}\right) = \frac{jk}{r_1} e^{-jkr} \hat{a}_1', \tag{3}$$

where $\hat{a}_1'$ is the unit vector directed from point P to the running point Q.

Since it can be assumed that the paraboloid is large compared to wavelength, and smooth, the approximation

$$\hat{n} \times \vec{H} = 2 (\hat{n} \times \vec{H}_i) \tag{4}$$

essentially prevails, where $\vec{H}_i$ is the magnetic field incident on the paraboloid at point Q. The phase of $\vec{H}_i$ can be explicitly brought out according to

$$\vec{H}_i = \vec{H}_{io}\, e^{-jk\rho} \tag{5}$$

where ρ is the distance from the origin-phase center to the running point Q. The magnitude and orientation of $\vec{H}_{io}$ will be subsequently restricted. Finally, an implication of Equation (4) is that S is to be taken as only that portion which is directly illuminated.

With all those approximations, Equation (1) becomes

$$\vec{H}_{S|P} = \frac{jk}{2\pi r_1} \iint (\hat{n} \times \vec{H}_{io}) \times \hat{a}_1' \, e^{-jk(r+\rho)}\, dA \tag{6}$$

where the quantities $\hat{n}$, $\vec{H}_{io}$, ρ, and dA are functions of the running point Q only, where r_1 is a function of the observation point P only, and where $\hat{a}_1'$ and r are functions of both P and Q.

The assumptions on which the approximations of Equation (6) are based can be summarized as follows:

(1) Dish dimensions are large compared to wavelength,
(2) Observation point is at least 15 focal lengths away,
(3) System is fed from a phase center located at the focus.

The next task is obtaining analytical expressions for the various quantities in Equation (6) in terms of the coordinates of point Q, defined by the elevation angle η and the azimuthal angle ψ, and of point P, defined by r_1 and by the elevation angle θ and the azimuthal angle ϕ.

GEOMETRY OF THE PROBLEM

The "geometry" of the paraboloid is illustrated in Figure 3 (cross-section through the x-z plane) and Figure 4 (coordinates of running point Q on the paraboloid). Briefly, Q is a general point of coordinates x, y, z.

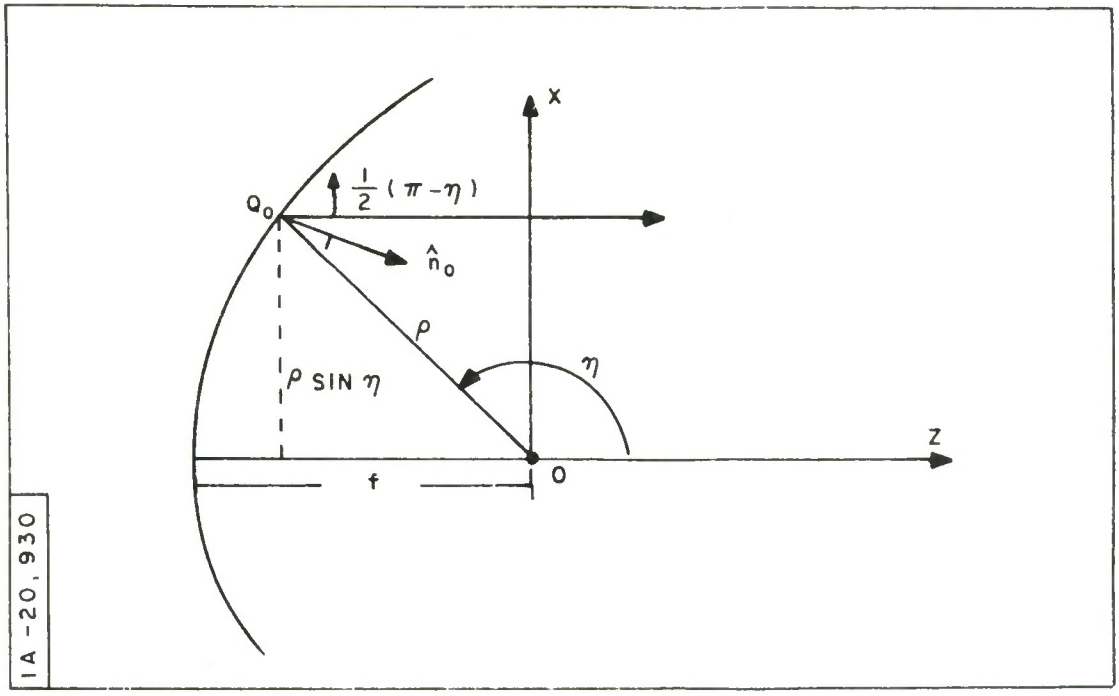

Figure 3. Geometry of the Paraboloid: Cross-Section through x-z Plane

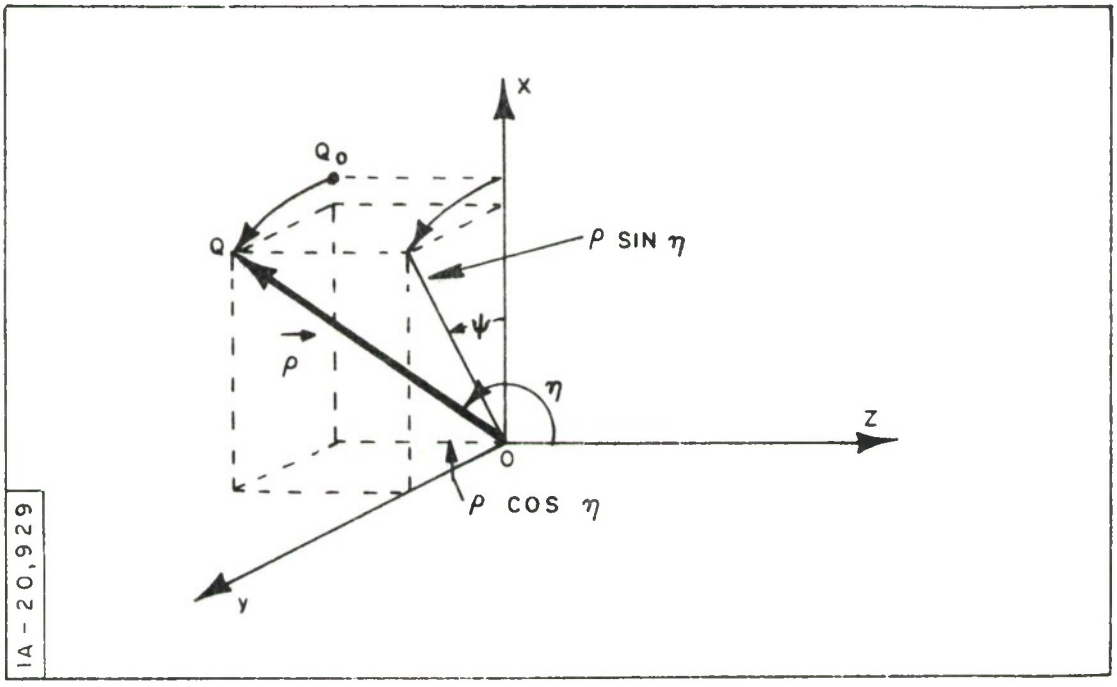

Figure 4. Geometry of the Paraboloid: Point Q_O Rotated through ψ to Q

It can be considered as the rotation of point Q_O, in the x-z plane, through an angle ψ. The distance between the origin (focus) and Q_O is ρ. The focal length is f. In the final analysis, Q (and all the quantities dependent on it) will be determined by η, the angle between the z-axis and $\vec{\rho}$ (the vector from O and Q), and by ψ, the angle between the x-axis and the projection of $\vec{\rho}$ on the x-y plane.

It is shown, in Appendix A, that because of the geometric properties of the the paraboloid, the Cartesian coordinates of $\hat{n}$ are

$$\hat{n} = \begin{vmatrix} n_x \\ n_y \\ n_z \end{vmatrix} = \begin{vmatrix} -\cos\psi\cos\eta/2 \\ -\sin\psi\cos\eta/2 \\ \sin\eta/2 \end{vmatrix} \qquad (7)$$

In Appendix B, it is shown that the expression for $\vec{\rho}$, the vector from the origin to point Q, is

$$\vec{\rho} = \frac{f}{\sin^2\eta/2}(\hat{x}\sin\eta\cos\psi + \hat{y}\sin\eta\sin\psi + \hat{z}\cos\eta) \qquad (8)$$

According to Appendix C, the expression for the differential area dA assumes the form

$$dA = \frac{f^2\sin\eta}{\sin^5\eta/2}\, d\eta\, d\psi \qquad (9)$$

In order to evaluate the unit vector $\hat{a}_1'$ (Figure 1) directed from the observation point, P, to the running point, Q, and the quantity r (the distance from P to Q), introduce first the unit vector $\hat{a}_1$, directed from the observation point P to the origin (focus). The unit vector can be

expressed in terms of θ (its angle with the negative z-axis) and of ϕ (the angle of its projection in the x-y plane with the x-axis) as:

$$\hat{a}_1 = - \begin{vmatrix} \sin\theta\cos\phi \\ \sin\theta\sin\phi \\ \cos\theta \end{vmatrix} \tag{10}$$

The reason for taking the origin of θ as the negative z-axis is only for convenience when referring to measurements.

Now r, being the magnitude of $(\hat{a}_1 r + \vec{\rho})$, is, by Equations (8) and (10):

$$r = \text{magnitude of} \begin{vmatrix} \frac{f}{\sin^2\eta/2}\sin\eta\cos\psi - r_1\sin\theta\cos\phi \\ \frac{f}{\sin^2\eta/2}\sin\eta\sin\psi - r_1\sin\theta\sin\phi \\ \frac{f}{\sin^2\eta/2}\cos\eta - r_1\cos\theta \end{vmatrix}$$

which is evaluated as

$$r = \left\{ r_1^2 + \frac{f^2}{\sin^4\eta/2} - \frac{2fr_1}{\sin^2\eta/2}\left[\sin\eta\sin\theta\cos(\psi-\phi) + \cos\theta\cos\eta\right] \right\}^{1/2} \tag{11}$$

The exact expression for the vector $\hat{a}_1'$ is $(\hat{a}_1 r_1 + \vec{\rho}) / r$. However, in this expression which enters Equation (6) as a magnitude (and not as a phase), the denominator, r, can be approximated as r_1, provided that the observation point is at least 10 focal lengths away from the antenna. The approximate expression for $\hat{a}_1'$ becomes $\left(\hat{a}_1 + \vec{\rho}/r_1\right)$, that is

$$\hat{a}_1' \approx \begin{vmatrix} \frac{f}{r_1\sin^2\eta/2}\sin\eta\cos\psi - \sin\theta\cos\phi \\ \frac{f}{r_1\sin^2\eta/2}\sin\eta\sin\psi - \sin\theta\sin\phi \\ \frac{f}{r_2\sin^2\eta/2}\cos\eta - \cos\theta \end{vmatrix}$$

Except if θ is unduly large (larger than 5 degrees), the z-component of $\hat{a}_1'$ can be approximated as -1. Thus, the final expression for $\hat{a}_1'$ becomes

$$\hat{a}_1' \approx \begin{vmatrix} \frac{2f}{r_1} \cot \eta/2 \cos \psi - \sin \theta \cos \phi \\ \frac{2f}{r_1} \cot \eta/2 \sin \psi - \sin \theta \sin \phi \\ -1 \end{vmatrix} \tag{12}$$

This expression is essentially valid everywhere for amplitude purposes, except in the very near field (r_1 less than 10 focal lengths).

PRIMARY PATTERNS

The primary patterns are discussed in Appendix D. Any particular primary pattern is strictly a function of the feed system, and it can assume an infinity of different forms. One can consider the equibeam distribution distinguished by the fact that, when the field is linearly polarized, the strength of the field on the spherical wavefront has cylindrical symmetry. The orientation of the field on the spherical wavefront must obey clearly defined relationships. Under conditions of feed circular polarization, the expression for $\vec{H}_{io}$ (which is circularly polarized at each point of the spherical wavefront) is

$$\vec{H}_{io} = h(\eta) \sin^2 \eta/2 \begin{vmatrix} (-\cos^2 \psi \cos \eta + \sin^2 \psi) \cos \omega t \\ \quad + (-\cos \psi \sin \psi [1 + \cos \eta]) \sin \omega t \\ (-\cos \psi \sin \psi [1 + \cos \eta]) \cos \omega t \\ \quad + (-\sin^2 \psi \cos \eta + \cos^2 \psi) \sin \omega t \\ \sin \eta \cos \psi \cos \omega t + \sin \eta \sin \psi \sin \omega t \end{vmatrix} \tag{13}$$

where $\sin^2 \eta/2$ reflects the dependence of the field strength on the distance ρ, $h(\eta)$ is an amplitude function independent of azimuth, and $\cos \omega t$ and

sin ωt are temporary labels designed to tag the "vertical" and "horizontal" components, respectively.

It has been found experimentally that

$$h(\eta) = \cos^{1.5}(\pi - \eta) \tag{14}$$

fits the polar amplitude pattern very closely for an equibeam feed, with a 10 db taper at the edge of the dish (η_o = 118 degrees).

The dipole-like distribution is characterized by the fact that when the feed is linearly polarized, the orientation of the H-field is along "latitude" lines on the spherical wavefront. The field strength depends on the azimuth angle. Under conditions of feed circular polarization, the expression for $\vec{H}_{io}$ (circularly polarized on-axis only, but of ellipticity constant with azimuth angle) is

$$\vec{H}_{io} = h(\eta) \sin^2 \eta/2 \begin{vmatrix} -\cos\eta\cos\omega t \\ -\cos\eta\sin\omega t \\ \sin\eta\cos\psi\cos\omega t + \sin\eta\sin\psi\sin\omega t \end{vmatrix} \tag{15}$$

The pseudo-equibeam distribution is derived from the dipole-like distribution. The field strength has been made independent of azimuth angle. However, the H-field still lies along "latitude" lines on the spherical wavefront. Under conditions of feed circular polarization, the expression for $\vec{H}_{io}$ (whose ellipticity depends on the azimuth angle and which is circularly polarized on the "vertical" and "horizontal" planes only) is

$$\vec{H}_{io} = h(\eta) \sin^2 \eta/2 \begin{vmatrix} -\cos\eta\gamma_c\cos\omega t \\ -\cos\eta\gamma_s\sin\omega t \\ (\sin\eta\cos\psi\gamma_c)\cos\omega t + (\sin\eta\sin\psi\gamma_s)\sin\omega t \end{vmatrix} \tag{16}$$

where

$$\gamma_c = (\cos^2\eta + \sin^2\eta\cos^2\psi)^{-1/2}$$
$$\gamma_s = (\cos^2\eta + \sin^2\eta\sin^2\psi)^{-1/2} \qquad (17)$$

Linear polarization can be studied by suppressing either the $\cos\omega t$ terms or the $\sin\omega t$ terms. Other non-equibeam distributions can be approximated by appropriate modifications of γ_c and γ_s .

FIELD FORMULATION FOR THE EQUIBEAM DISTRIBUTION

Analytic expressions for each quantity in the fundamental equation (Equation 6) are now available. Before evaluating the integral, it remains to calculate the exponential factor, $e^{-jk(r+\rho)}$, and the cross-product

$$[(\hat{n}\times\vec{H}_{io})\times\hat{a}_{1'}].$$

By Equations (11) and (173) of Appendix B,

$$e^{-jk(r+\rho)} = \exp.-jk\left\{\left[r_1^2 + \frac{f^2}{\sin^4\eta/2} - \frac{2fr_1}{\sin^2\eta/2}[\sin\eta\sin\theta\cos(\psi-\phi)+\cos\theta\cos\eta]\right]^{1/2} + \frac{f}{\sin^2\eta/2}\right\} \qquad (18)$$

By Equations (7) and (13), $(\hat{n}\times\vec{H}_{io})$ is the vector whose components are the cofactors of the determinant of

$$\begin{vmatrix} \hat{x} & \hat{y} & \hat{z} \\ -\cos\psi\cos\eta/2 & -\sin\psi\cos\eta/2 & \sin\eta/2 \\ (-\cos^2\psi\cos\eta+\sin^2\psi)\cos\omega t & (-\cos\psi\sin\psi[\cos\eta+1])\cos\omega t & (\sin\eta\cos\psi\cos\omega t) \\ +(-\cos\psi\sin\psi[1+\cos\eta])\sin\omega t & +(-\sin^2\psi\cos\eta+\cos^2\psi)\sin\omega t & +(\sin\eta\sin\psi\sin\omega t) \end{vmatrix}$$

times $h(\eta)\sin^2\eta/2$.

This expression simplifies considerably to become

$$(\hat{n}\times\vec{H}_{io}) = h(\eta)\sin^2\eta/2 \begin{vmatrix} -\sin\eta/2\sin\omega t \\ \sin\eta/2\cos\omega t \\ \sin\psi\cos\eta/2\cos\omega t - \cos\psi\cos\eta/2\sin\omega t \end{vmatrix} \qquad (19)$$

or, symbolically,

$$(\hat{n} \times \vec{H}_{io}) = \begin{vmatrix} A \sin \omega t \\ -A \cos \omega t \\ E \sin \omega t - F \cos \omega t \end{vmatrix} \qquad (20)$$

where

$$A = (-)\, h\,(\eta) \sin^2 \eta/2 \sin \eta/2 \quad = A'$$

$$E = (-)\, h\,(\eta) \sin^2 \eta/2 \cos \eta/2 \cos \psi \quad = E' \cos \psi$$

$$F = (-)\, h\,(\eta) \sin^2 \eta/2 \cos \eta/2 \sin \psi \quad = E' \sin \psi$$

It is remarkable that no cross-polarized term is present, that is, vertical polarization in the feed ($\cos \omega t$ terms) gives rise to x- and z-directed currents only (no y-component of current), whereas horizontal linear polarization gives rise to the no x-component of current.

The cross-product of $(\hat{n} \times \vec{H}_{io})$ and $\hat{a}_1'$ (Equation 12) is the vector whose components are the co-factors of

$$\begin{vmatrix} \hat{x} & \hat{y} & \hat{z} \\ A \sin \omega t & -A \cos \omega t & [E \sin \omega t - F \cos \omega t] \\ \left[\frac{2f}{r_1} \cot \eta/2 \cos \psi - \sin \theta \cos \phi\right] & \left[\frac{2f}{r_1} \cot \eta/2 \sin \psi - \sin \theta \sin \phi\right] & -1 \end{vmatrix}$$

that is, $[(\hat{n} \times \vec{H}_{io}) \times \hat{a}_1']$ =

$$\begin{vmatrix} A \cos \omega t - \left(\frac{2f}{r_1} \cot \eta/2 \sin \psi - \sin \theta \sin \phi\right) (E \sin \omega t - F \cos \omega t) \\ A \sin \omega t + \left(\frac{2f}{r_1} \cot \eta/2 \cos \psi - \sin \theta \cos \phi\right) (E \sin \omega t - F \cos \omega t) \\ A \sin \omega t \left(\frac{2f}{r_1} \cot \eta/2 \sin \psi - \sin \theta \sin \phi\right) + A \cos \omega t \left(\frac{2f}{r_1} \cot \eta/2 \cos \psi - \sin \theta \cos \phi\right) \end{vmatrix}$$

(21)

Consider now the x-component of $\vec{H}_{S|P}$. The "in-phase" terms are

$$X1 = + \int_0^{2\pi} \int_{\eta_o}^{\pi} A' \exp\{\{ g(\eta)\, d\eta\, d\psi \tag{22}$$

$$X3 = + \int_0^{2\pi} \int_{\eta_o}^{\pi} E' \exp\{\{ g(\eta) \sin\psi \left(\frac{2f}{r_1} \cot \eta/2 \sin\psi - \sin\theta \sin\phi\right) d\eta\, d\psi \tag{23}$$

The phase-quadrature term arising from the "horizontal" components (through the z-directed current) in the primary pattern is

$$X5 = - \iint E' \exp\{\{ g(\eta) \cos\psi \left(\frac{2f}{r_1} \cot \eta/2 \sin\psi - \sin\theta \sin\phi\right) d\eta\, d\psi \tag{24}$$

For the y-components, the "in-phase" terms are

$$Y1 = X1 \tag{25}$$

$$Y3 = + \iint E' \exp\{\{ g(\eta) \cos\psi \left(\frac{2f}{r_1} \cot \eta/2 \cos\psi - \sin\theta \cos\phi\right) d\eta\, d\psi \tag{26}$$

The phase-quadrature term arising from the "vertical" components in the primary pattern is

$$Y5 = - \iint E' \exp\{\{ g(\eta) \sin\psi \left(\frac{2f}{r_1} \cot \eta/2 \cos\psi - \sin\theta \cos\phi\right) d\eta\, d\psi$$

where

$\exp\{\{$ is given by Equation (18),

$g(h) = \dfrac{f^2 \sin\eta}{\sin^5 \eta/2}$ or $\dfrac{\sin\eta}{\sin^5 \eta/2}$ (Equation (9)),

$A' = - [h(\eta) \sin^2 \eta/2] \sin \eta/2$

$E' = - [h(\eta) \sin^2 \eta/2] \cos \eta/2$

In the case of small values of $|\theta|$, the z-component is neglected, although it could be obtained from Equation (21).

FIELD FORMULATION FOR DIPOLE-LIKE DISTRIBUTIONS

The dipole-like distribution (Equation 15) and the pseudo-equibeam distribution (Equation 16) will be carried together for the sake of convenience. It will be understood that

$$\gamma_c = \gamma_s = 1$$

for the dipole distribution, and that

$$\gamma_c = (\cos^2\eta + \sin^2\eta \cos^2\psi)^{-1/2}$$

$$\gamma_s = (\cos^2\eta + \sin^2\eta \sin^2\psi)^{-1/2}$$

for the pseudo-equibeam distribution, as given by Equation (17).

The same exponential factor (Equation 18) still applies as in the preceding section. By Equations (7) and (16), $(\hat{n} \times \vec{H}_{io})$ is the vector whose components are the cofactors of the determinant of

$$h(\eta)\sin^2\eta/2 \begin{vmatrix} \hat{x} & \hat{y} & \hat{z} \\ (-\cos\psi\cos\eta/2) & (-\sin\psi\cos\eta/2) & (\sin\eta/2) \\ (-\cos\eta\,\gamma_c\cos\omega t) & (-\cos\eta\,\gamma_s\sin\omega t) & (\sin\eta\cos\psi\,\gamma_c\cos\omega t + \sin\eta\sin\psi\,\gamma_s\sin\omega t) \end{vmatrix}$$

that is, $(\hat{n} \times \vec{H}_{io}) =$

$$h(\eta)\sin^2\eta/2 \begin{vmatrix} -\sin\eta\cos\eta/2\sin\psi(\cos\psi\gamma_c\cos\omega t + \sin\psi\gamma_s\sin\omega t) + \sin\eta/2\cos\eta\gamma_s\sin\omega t \\ \sin\eta\cos\eta/2\cos\psi(\cos\psi\gamma_c\cos\omega t + \sin\psi\gamma_s\sin\omega t) - \sin\eta/2\cos\eta\gamma_s\cos\omega t \\ \cos\eta\cos\eta/2(\cos\psi\gamma_s\sin\omega t - \sin\psi\gamma_c\cos\omega t) \end{vmatrix}$$

or symbolically,

$$(\hat{n} \times \vec{H}_{io}) = \begin{vmatrix} (A + B)\gamma_s\sin\omega t + C\gamma_c\cos\omega t \\ (-A + D)\gamma_c\cos\omega t - C\gamma_s\sin\omega t \\ E\gamma_s\sin\omega t - F\gamma_c\cos\omega t \end{vmatrix} \qquad (27)$$

where

$$A = h(\eta)\sin^2\eta/2\sin\eta/2\cos\eta = A'$$

$$B = -h(\eta)\sin^2\eta/2\sin\eta\cos\eta/2\sin^2\psi = B'\sin^2\psi$$

$$C = -h(\eta)\sin^2\eta/2\sin\eta\cos\eta/2\sin\psi\cos\psi = B'\sin\psi\cos\psi$$

$$D = h(\eta)\sin^2\eta/2\sin\eta\cos\eta/2\cos^2\psi = -B'\cos^2\psi$$

$$E = h(\eta)\sin^2\eta/2\cos\eta\cos\eta/2\cos\psi = E'\cos\psi$$

$$F = h(\eta)\sin^2\eta/2\cos\eta\cos\eta/2\sin\psi = E'\sin\psi$$

Note that the "vertical" polarization components (cos ωt terms) give rise not only to x- and z-directed currents, but also to y-directed currents (cross-polarized terms). In the same manner, the "horizontal" polarized components ($\sin\omega t$ terms) give rise not only to y- and z-currents, but also to x-currents. This effect does not arise in the true equibeam distribution (see preceding sub-section). It will be appreciated later on how those cross-polarized terms give rise to sizeable ellipticities in the near- and far-fields.

The cross-product of $(\hat{n} \times \vec{H}_{io})$ and $\hat{a}_1'$ Equation (12) is the vector whose components are the co-factors of

$$\begin{vmatrix} \hat{x} & \hat{y} & \hat{z} \\ [(A+B)\gamma_s\sin\omega t + C\gamma_c\cos\omega t] & [(-A+D)\gamma_c\cos\omega t - C\gamma_s\sin\omega t] & [E\gamma_s\sin\omega t - F\gamma_c\cos\omega t] \\ \left[\frac{2f}{r_1}\cot\eta/2\cos\psi - \sin\theta\cos\phi\right] & \left[\frac{2f}{r_1}\cot\eta/2\sin\psi - \sin\theta\sin\phi\right] & -1 \end{vmatrix}$$

that is, $[(\hat{n}\times\vec{H}_{io}) \times \hat{a}_1']$ =

$$\begin{vmatrix} (A-D)\gamma_c\cos\omega t + C\gamma_s\sin\omega t - \left(\frac{2f}{r_1}\cot\eta/2\sin\psi - \sin\theta\sin\phi\right) & (E\gamma_s\sin\omega t - F\gamma_c\cos\omega t) \\ (A+B)\gamma_s\sin\omega t + C\gamma_c\cos\omega t + \left(\frac{2f}{r_1}\cot\eta/2\cos\psi - \sin\theta\cos\phi\right) & (E\gamma_s\sin\omega t - F\gamma_c\cos\omega t) \\ [(A+B)\gamma_s\sin\omega t + C\gamma_c\cos\omega t]\left(\frac{2f}{r_1}\cot\eta/2\sin\psi - \sin\theta\sin\phi\right) + [(A-D)\gamma_c\cos\omega t + C\gamma_s\sin\omega t]\cdot & \\ \left(\frac{2f}{r_1}\cot\eta/2\cos\psi - \sin\theta\cos\phi\right) & \end{vmatrix}$$

Consider now the x-component of $\vec{H}_{S|P}$. The "in-phase" terms are

$$X1 = + \int_{0}^{2\pi} \int_{\eta_o}^{\pi} A' \gamma_c \exp\{\} g(\eta)\, d\eta\, d\psi \tag{29}$$

$$X2 = + \iint B' \gamma_c \exp\{\} g(\eta) \cos^2 \psi\, d\eta\, d\psi \tag{30}$$

$$X3 = + \iint E' \gamma_c \exp\{\} g(\eta) \sin \psi \left(\frac{2f}{r_1} \cot \eta/2 \sin \psi - \sin \theta \sin \phi \right) d\eta\, d\psi \tag{31}$$

The phase-quadrature terms arising from the "horizontal" components in the primary pattern are

$$X4 = + \iint B' \gamma_s \exp\{\} g(\eta) \sin \psi \cos \psi\, d\eta\, d\psi \tag{32}$$

$$X5 = - \iint E' \gamma_s \exp\{\} g(\eta) \cos \psi \left(\frac{2f}{r_1} \cot \eta/2 \sin \psi - \sin \theta \sin \phi \right) d\eta\, d\psi \tag{33}$$

For the y-components, the "in-phase" terms are

$$Y1 = + \iint A' \gamma_s \exp\{\} g(\eta)\, d\eta\, d\psi \tag{34}$$

$$Y2 = + \iint B' \gamma_s \exp\{\} g(\eta) \sin^2 \psi\, d\eta\, d\psi \tag{35}$$

$$Y3 = + \iint E' \gamma_s \exp\{\} g(\eta) \cos \psi \left(\frac{2f}{r_1} \cot \eta/2 \cos \psi - \sin \theta \cos \phi \right) d\eta\, d\psi \tag{36}$$

The phase-quadrature terms arising from the "vertical" components in the primary pattern are

$$Y4 = + \iint B' \gamma_c \exp\{\} \, g(\eta) \sin\psi \cos\psi \, d\eta \, d\psi \tag{37}$$

$$Y5 = - \iint E' \gamma_c \exp\{\} \, g(\eta) \sin\psi \left(\frac{2f}{r_1} \cot \eta/2 \cos\psi - \sin\theta \cos\phi \right) d\eta \, d\psi \tag{38}$$

where

$\exp\{\}$ is given by Equation (18),

$$g(h) = \frac{f^2 \sin\eta}{\sin^5 \eta/2} \quad \text{or} \quad \frac{\sin\eta}{\sin^5 \eta/2} \quad \text{(see Equation (9))},$$

$$A' = + [h(\eta) \sin^2 \eta/2] \sin \eta/2 \cos\eta$$

$$B' = - [h(\eta) \sin^2 \eta/2] \sin\eta \cos \eta/2$$

$$E' = + [h(\eta) \sin^2 \eta/2] \cos\eta \cos \eta/2$$

In the case of small values of θ, the z-component is neglected, although it could also be obtained from Equation (28).

FAR-FIELD APPROXIMATIONS

When $r_1 >> f$, then, from Figure 1,

$$r \approx r_1$$

$$\hat{a} \approx \hat{a}_1'$$

Those approximations are valid when r and $\hat{a}_1'$ enter amplitude factors, but are still not valid when they enter the exponential term which, because of its modulo 2π characteristic, is very sensitive to minor differences, even if those differences are minute compared to the total argument.

First, consider the expression for r (Equation 11), and re-write it as

$$r = r_1 \left\{ 1 + \frac{f^2}{r_1^2 \sin^4 \eta/2} - \frac{2f}{r_1 \sin^2 \eta/2} [\sin \eta \sin \theta \cos (\psi - \phi) + \cos \theta \cos \eta] \right\}^{1/2}$$

We can expand it as a power series of the form

$$(1 + X)^{1/2} = 1 + \frac{X}{2} - \frac{X^2}{4} + \frac{3X^3}{8} - \ldots$$

and retain but the first two terms, that is

$$r = r_1 \left\{ 1 + \frac{f^2}{2r_1^2 \sin^4 \eta/2} - \frac{f}{r_1 \sin^2 \eta/2} [\sin \eta \sin \theta \cos (\psi - \phi) + \cos \theta \cos \eta] \right\}$$

Furthermore, we are assured that, for r_1 large enough,

$$r_1 \left(\frac{f^2}{2r_1^2 \sin^4 \eta/2} \right) \to 0$$

Consequently, the expression for r in the far-field becomes

$$r = r_1 - \frac{f}{\sin^2 \eta/2} [\sin \eta \sin \theta \cos (\psi - \phi) + \cos \theta \cos \eta] \tag{39}$$

The expression for the exponential term (Equation 18) in the far-field becomes

$$e^{-jk(r+\rho)} = \exp. - jk \left(r_1 - \frac{f}{\sin^2 \eta/2} [\sin \eta \sin \theta \cos (\psi - \phi) + \cos \theta \cos \eta - 1] \right) \tag{40}$$

$$= \exp. - jk r_1 \cdot \exp. j 2k f \left[\sin \theta \cot \eta/2 \cos (\psi - \phi) + \frac{\cos \theta \cos \eta - 1}{2 \sin^2 \eta/2} \right]$$

The term e^{-jkr_1} is independent of the paraboloid coordinates and can be placed outside the integral (or neglected).

A further simplification results if θ is small (point P near boresight). When this is the case, then Equation (40) becomes

$$\text{exp. } j2kf\,[\sin\theta\cot\eta/2\cos(\psi-\phi) - 1]$$

or

$$\text{exp. } -jk(r+\rho) = \text{exp. } j2kf\sin\theta\cot\eta/2\cos(\psi-\phi) \qquad (41)$$

where again the term e^{-j2kf} has been placed outside the integral (or neglected). From Equation (176) of Appendix B, the exponent can be expressed in terms of the aperture D(Q) of the dish at point Q according to

$$\text{exp. } -jk(r+\rho) = \text{exp. } j\frac{D(Q)}{2}\sin\theta\cos(\psi-\phi) \qquad (42)$$

Thus, for small values of θ, the exponent is independent of f, the focal length, and depends only on D(Q) and on θ.

Aside from the simplification of exp. { }, one can discard the r_1-dependent components of X3, X5, and Y3, Y5 in the equibeam or dipole-like distributions.

If, furthermore, the study is confined to small values of θ ($\theta < 5$ degrees), the new terms X3, X5, and Y3, Y5, which are all products of $\sin\theta$, will be negligible with respect to the dominant terms X1 and Y1 in the equibeam distribution. For the dipole-like distribution, those terms will be smaller than the "correction" terms X2, X4, Y2, Y4 which arise from the quadrature currents by one (or more) orders of magnitude.

Thus, under conditions of far-field and small elevation angles, the components of $\vec{H}_{S|P}$ are as follows:

For equibeam distribution:

In-phase x-component:

$$X1 = -\iint 2h(\eta) \exp\{\} \cot \eta/2 \, d\eta \, d\psi \tag{43}$$

In-phase y-component:

$$Y1 = -\iint 2h(\eta) \exp\{\} \cot \eta/2 \, d\eta \, d\psi \tag{44}$$

For dipole-like distributions:

In-phase x-components:

$$X1 = +\int_0^{2\pi} \int_{\eta_0}^{\pi} h(\eta) \gamma_c \exp\{\} \sin \eta/2 \cos \eta \, \frac{\sin \eta}{\sin^3 \eta/2} \, d\eta \, d\psi \tag{45}$$

$$X2 = -\iint h(\eta) \gamma_c \exp\{\} \sin \eta \cos \eta/2 \cos^2 \psi \, \frac{\sin \eta}{\sin^3 \eta/2} \, d\eta \, d\psi \tag{46}$$

Quadrature-phase x-component:

$$X4 = -\iint h(\eta) \gamma_s \exp\{\} \sin \eta \cos \eta/2 \sin \psi \cos \psi \, \frac{\sin \eta}{\sin^3 \eta/2} \, d\eta \, d\psi \tag{47}$$

In-phase y-components:

$$Y1 = +\iint h(\eta) \gamma_s \exp\{\} \sin \eta/2 \cos \eta \, \frac{\sin \eta}{\sin^3 \eta/2} \, d\eta \, d\psi \tag{48}$$

$$Y2 = -\iint h(\eta)\, y_s \exp\{\{\sin\eta \cos\eta/2 \sin^2\psi \, d\eta \, d\psi \qquad (49)$$

Quadrature-phase y-component:

$$Y4 = -\iint h(\eta)\, y_c \exp\{\{\sin\eta \cos\eta/2 \sin\psi \cos\psi \, \frac{\sin\eta}{\sin^3\eta/2} \, d\eta \, d\psi \qquad (50)$$

where exp {{ stands for Equation (41).

FIELD AMPLITUDE AND POLARIZATION

Consider the case of small values of θ, so that the x and y coordinates, at the observation point P, are essentially perpendicular to the line of sight. (A coordinate transformation, suitable for any value of θ, is suggested in Appendix E).

It is now time to substitute, for the real time functions $\cos\omega t$ and $\sin\omega t$, appropriate phasors:

$$\cos\omega t \rightarrow 1$$

$$\sin\omega t \rightarrow j$$

For a circularly polarized feed system, the total component of $\vec{H}_{S|P}$ is then

$$X = (X1 + X2 + X3) + j(X4 + X5) \qquad (51)$$

and the total y-component

$$Y = j(Y1 + Y2 + Y3) + (Y4 + Y5) \qquad (52)$$

where some of the terms may be zero, depending on the distribution and the conditions.

By the considerations of Appendix F, the ellipticity is obtained as follows: the magnitude of thr right-hand wave is

$$|S^+| = \frac{1}{2}\left[(\mathrm{Re}\,X - \mathrm{Im}\,Y)^2 + (\mathrm{Im}\,X + \mathrm{Re}\,Y)^2\right]^{1/2} \tag{53}$$

and of the left-hand wave

$$|S^-| = \frac{1}{2}\left[(\mathrm{Re}\,X + \mathrm{Im}\,Y)^2 + (\mathrm{Im}\,X - \mathrm{Re}\,Y)^2\right]^{1/2} \tag{54}$$

The "voltage" ellipticity at point P is then

$$\text{Ellipticity} = \left|\frac{|S^+| + |S^-|}{|S^+| - |S^-|}\right| \tag{55}$$

or, in db,

$$\text{Ellipticity (db)} = 20\log_{10}\left|\frac{|S^+| + |S^-|}{|S^+| - |S^-|}\right| \tag{56}$$

If one linear component in the primary pattern is suppressed, so that the x-component only ($\cos \omega t$) is applied, then the x- and y-components of $\vec{H}_{S|P}$ become respectively

$$X' = X_1 + X_2 + X_3 \tag{57}$$

$$Y' = Y_4 + Y_5 \tag{58}$$

The overall amplitude is then

$$\text{Amplitude} = \sqrt{|X'|^2 + |Y'|^2} \tag{59}$$

and the deviation angle from the primary polarization to the polarization at point P is

$$\alpha = \tan^{-1}\frac{Y'}{X'} \tag{60}$$

Equations (59), (56), and (60) have been computed and plotted under various conditions, and the results are found in Section IV. But before considering the actual quantitative results, it is proper to examine the equations for general qualitative characteristics. This is accomplished in the next subsection.

DISCUSSION OF FIELD EQUATIONS

For the equibeam distribution, it is clear, from Equations (43) and (44), that in the far-field and within small elevation angles, the field at the observation point, P , will be circularly polarized, not only on boresight but for any value of θ and ϕ . Thus, the behavior is similar to that of a flat circular plate illuminated by a plane wave, a case that is discussed in Appendix H.

As the range is decreased and/or as θ becomes larger, there will be a certain amount of ellipticity caused by the z-directed current originating from both orthogonal polarizations.

In contradistinction with the equibeam case, the dipole-like distributions will produce different results with respect to ellipticity. Components X4 and Y4 arise from cross-polarized currents which, in turn, are caused by the distortion of the "latitude" lines when projected onto the paraboloid. Components X2 and Y2 are extraneous, in-phase components which arise from the same source. Those two sets of components will tend to become smaller as the dish is "flatter," that is, as the focal length increases. As in the case of the equibeam distribution, the X3 and X5 components on the one hand, the Y3 and Y5 on the other, arise because of near-field and off-boresight effects combined with the z-directed current. Except in the very near-field

or within large elevation angles, those terms are small and provide but small corrections to the sidelobe formation which is determined primarily by the exponential factor.

For dipole-like distributions, on boresight ($\theta = 0$), both the general expressions and the far-field approximations for the exponential term (Equations (18) and (41)) simplify considerably insofar as they become independent of ψ. It follows that

$$X1 = Y1 \tag{61}$$

$$X2 = Y2 \tag{62}$$

$$X3 = Y3 \tag{63}$$

$$X4 = Y4 = 0 \tag{64}$$

$$X5 = Y5 = 0 \tag{65}$$

regardless of whether $\gamma_c = \gamma_s = 1$, or whether Equation 17 applies since

$$\int_0^{2\pi} \gamma_c \, d\psi = \int_0^{2\pi} \gamma_s \, d\psi \tag{66}$$

$$\int_0^{2\pi} \gamma_{c,s} \cos^2 \psi \, d\psi = \int_0^{2\pi} \gamma_{s,c} \sin^2 \psi \, d\psi \tag{67}$$

$$\int_0^{2\pi} \gamma_s \sin \psi \cos \psi \, d\psi = \int_0^{2\pi} \gamma_c \sin \psi \cos \psi \, d\psi = 0 \tag{68}$$

It follows that, on boresight, the field is circularly polarized if the feed is circularly polarized.

Now consider the far-field equations, which are somewhat simpler when the observation point is off-boresight ($\theta \neq 0$). The exponential term (Equation (41)) is

$$\exp\{\} = e^{j2kf \sin\theta \cot\eta/2 \cos(\psi - \phi)} = e^{j a \cos(\psi - \phi)}$$

$$= \cos[a \cos(\psi - \phi)] + j \sin[a \cos(\psi - \phi)] \tag{69}$$

where a stands for $2kf \sin\theta \cot\eta/2 \cos(\psi - \phi)$.

For $\psi' = \psi \pm \pi$

$$\exp\{\} = \cos[a \cos(\psi - \phi)] - j \sin[a \cos(\psi - \phi)] \tag{70}$$

Consequently, when the integrands are even functions of ψ (as in the case of X1, Y1, X2, Y2), that is, when

$$f(\psi) = f(\psi'),$$

then the limits of integration ψ (0 to 2π) can be replaced by 0 to π, and $\exp\{\}$ by $2\cos[a(\psi - \phi)]$. Note that $e^{-j a \cos(\psi - \phi)}$ would give the same result.

It is clear that, for any value of ϕ,

$$X1 = Y1 \tag{71}$$

provided that $\gamma_c = \gamma_s$. But if Equation (17) applies, then Equation (71) does not hold, except when $\phi = \pm \pi/4$, since $\cos\psi$ and $\sin\psi$ now

have the same weights. Furthermore

$$X2 = Y2 \tag{72}$$

when $\phi = \pm \pi/4$ and Equation (17) prevails.

Finally, even for the pseudo-equibeam distribution,

$$X1|_{\phi} = Y1|_{\phi \pm \pi/2} \tag{73}$$

$$X2|_{\phi} = X2|_{\phi \pm \pi/2} \tag{74}$$

since

$$\int_0^{2\pi} f(\cos^2 \psi)\, e^{j a \cos(\psi - \phi)}\, d\psi = \int_0^{2\pi} f(\sin^2 \psi)\, e^{-j a \cos(\psi - \phi + \pi/2)} d\psi$$

$$= \int_0^{2\pi} f(\sin^2 \psi)\, e^{j a \sin(\psi - \phi)}\, d\psi \tag{75}$$

Regarding the quadrature terms X4 and Y4 , it is shown, in Appendix G, that they are zero for $\phi = 0, \pi/2, \pi$ and $3\pi/2$.

It will be shown that, when $\gamma_c = \gamma_s = 1$, ellipticity is constant with the azimuthal angle ϕ, for a given elevation θ.

By Equations (215) and (216), of Appendix F, the circularly polarized waves, S^+ and S^- are, respectively,

$$S^{+} = \frac{1}{2}(X + jY) = \frac{1}{2}[(X1 + X2 - Y1 - Y2) + j(X4 + Y4)]$$

$$= \frac{1}{2}[(X2 - Y2) + j(X4 + Y4)]$$

$$S^{-} = \frac{1}{2}(X - jY) = \frac{1}{2}[(X1 + X2 + Y1 + Y2) + j(X4 - Y4)]$$

$$= \frac{1}{2}[2X1 + (X2 + Y2)]$$

S^{+} involves integration of

$$-(\cos^2\psi - \sin^2\psi) - j\,2\sin\psi\cos\psi$$

$$= -\cos 2\psi - j\sin 2\psi = -e^{j2\psi}$$

so that

$$S^{+} \propto \int_0^{2\pi} e^{j[a\cos(\psi - \phi) + 2\psi]}\,d\psi = e^{-j2\phi}\int_0^{2\pi} e^{j[a\cos\xi + 2\xi]}\,d\xi$$

$$= -2\pi\, e^{-j2\phi} J_2(a) \qquad (76)$$

which is independent of ϕ, except for phase.

S^- involves integration of constants, so that

$$S^- \propto \int_0^{2\pi} e^{j[a \cos(\psi - \phi)]}\, d\psi = 2\pi J_0(a) \qquad (77)$$

which is independent of ϕ. Because the phase of the circularly polarized wave S^+ depends on 2ϕ and the phase of S^- is independent of ϕ, the orientation of the ellipse will vary directly as ϕ, although the ratio of major axis to minor axis is independent of ϕ.

In general, ellipticity can be inferred from a linear polarization pattern (linearly polarized feed) by superimposing the same pattern rotated by $\pi/2$. Thus, ellipticity in the $\phi = 0$ and $\phi = \pi/2$ planes is attributable directly to the difference in "beamwidth" in the $\phi = 0$ and $\phi = \pi/2$ planes (since the quadrature terms are zero). Where such beamwidths are equal, the ellipticity will be 1. Ellipticity in the $\phi = \pm \pi/4$ planes is attributable to the phase-quadrature components (since X1 = Y1, X2 = Y2 at those planes). It is remarkable that, for $\gamma_c = \gamma_s = 1$, all those terms balance one another, as shown above. Physically, this must be so, since there is no "preferred" plane regarding amplitude. This property does not hold for the pseudo-equibeam distribution because, as discussed in Appendix D, there are preferred planes.

Appendix H considers the case of a flat circular plate, illuminated by a plane, circularly polarized wave. It is shown that in that case, the far-field is everywhere circularly polarized, if the feed is circularly polarized.

DEFOCUSING IN FOCAL PLANE

Before concluding the analytical study of the focal feed system, the effects of defocusing the source (phase center) in the focal plane are considered in this subsection. Defocusing along the axis of symmetry will be considered in the next subsection.

Let the phase center be located at point O', in the focal plane, such that O' is determined by the vector $\vec{d}$ in the x-direction:

$$\vec{d} = \begin{vmatrix} d \\ 0 \\ 0 \end{vmatrix} \tag{78}$$

where d is small compared to the focal length f (Figure 5). It will be assumed that, because $d << f$, the amplitude of $\vec{H}_i$ is essentially the same as if the phase center were located at the origin. Hence, $\vec{H}_{io}$ will be given by Equations (13), (15), (16). However, because d is not necessarily small compared to a wavelength, the phase of $\vec{H}_i$ at the running point Q can be substantially different.

For the far-field, the exponential term is given by

$$\exp. - jk(r + \Re) = \exp j2kf\left[\sin\theta \cot\eta/2 \cos(\psi - \phi) + \frac{\cos\theta\cos\eta}{2\sin^2\eta/2} - \frac{\Re}{2f}\right] \tag{79}$$

according to Equation (39), where the term e^{-jkr_1} has been neglected (it is a constant), and where $\Re$ is the distance from O' to Q.

From Figure 5, it is seen that

$$\vec{\mathcal{R}} = \vec{\rho} - \vec{d} = \frac{f}{\sin^2 \eta/2} \begin{vmatrix} \sin\eta\cos\psi - \frac{d}{f}\sin^2\eta/2 \\ \sin\eta\sin\psi \\ \cos\eta \end{vmatrix} \tag{80}$$

by Equations (8) and (78). The magnitude of $\vec{\mathcal{R}}$ is

$$\mathcal{R} = \frac{f}{\sin^2\eta/2}\left[\left(\sin\eta\cos\psi - \frac{d}{f}\sin^2\eta/2\right)^2 + (\sin\eta\sin\psi)^2 + \cos^2\eta\right]^{1/2}$$

$$= \frac{f}{\sin^2\eta/2}\left[1 + \frac{d^2\sin^4\eta/2}{f^2} - \frac{2d\sin^2\eta/2\sin\eta\cos\psi}{f}\right]^{1/2} \tag{81}$$

Consequently, the exponential term becomes

$$\exp. - jk(r+\mathcal{R}) =$$

$$\exp. j2kf\left\{\sin\theta\cot\eta/2\cos(\psi-\phi) + \frac{1}{2\sin^2\eta/2}\left[\cos\theta\cos\eta - \left(1 + \frac{d^2\sin^4\eta/2}{f^2} - 2\frac{d}{f}\sin^2\eta/2\sin\eta\cos\psi\right)^{1/2}\right]\right\} \tag{82}$$

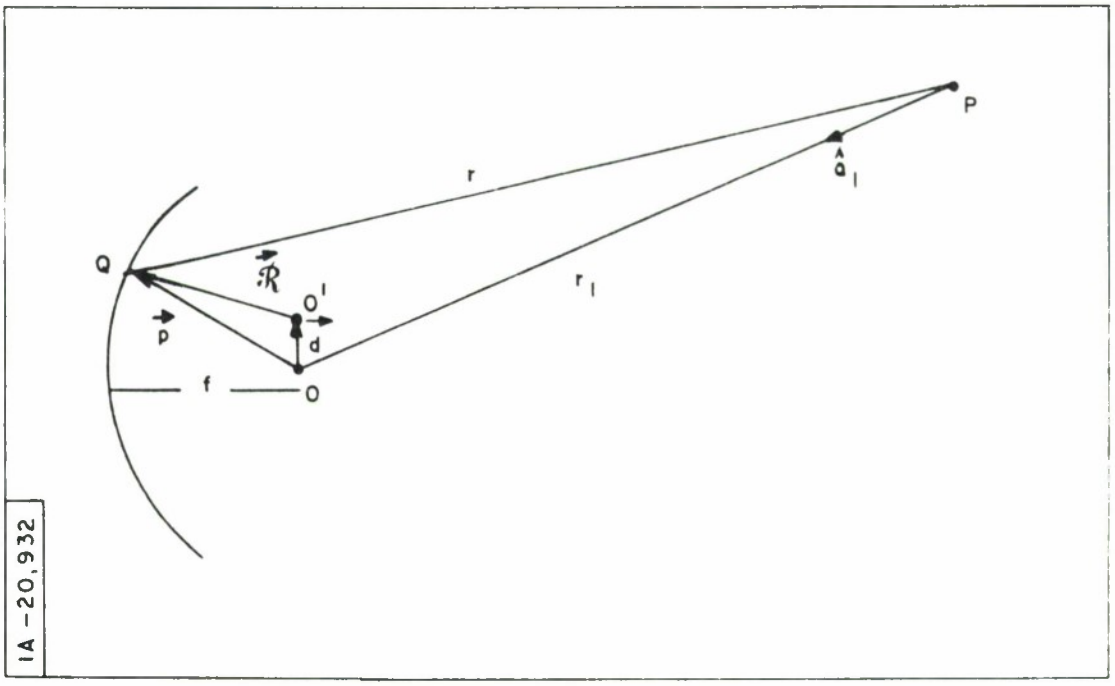

Figure 5. Defocusing in Focal Plane

When d/f is very small (a criterion for "smallness" might be that $2kf\,(d/f)^2 < 0.1$), Equation (81) can be expanded as a power series with the second and higher degree terms neglected. Equation (81) becomes

$$\mathcal{R} = \frac{f}{\sin^2 \eta/2} - d \sin \eta \cos \psi \tag{83}$$

and Equation (82) becomes

$$\exp. - jk\,(r + \mathcal{R}) \approx \exp. j2kf \left[\sin \theta \cot \eta/2 \cos (\psi - \phi) + \frac{d}{2f} \sin \eta \cos \psi\right] \tag{84}$$

if θ is small.

In order to get an estimate of θ_o, the angle at which the beam now peaks up, consider that it arises from the situation when all the contributions

from the differential areas dA are most nearly in phase. This situation will prevail when

$$\sin \theta_o = \frac{d}{f} \sin^2 \eta_m/2 \cos \eta_m \tag{85}$$

and

$$\phi = \pi \tag{86}$$

where η_m is some "mean" value of η between π and η_o .

For η_m = 160 degrees, an estimate of θ_o would be

$$\theta_o \approx 0.91 \left(\frac{d}{f}\right)$$

Equation (86) states that as the phase center is shifted "up," the beam shifts "down."

The sum of two beams arising from a phase center located at x = d and a second phase center located at x = - d would have components of the form given by Equations (45) through (50), but with the exponential term replaced by

$$e^{j2kf \sin \theta \cot \eta/2 \cos (\psi - \phi)} \left(e^{jkd \sin \eta \cos \psi} + e^{-jkd \sin \eta \cos \psi}\right)$$

$$= 2 \cos (k d \sin \eta \cos \psi)\, e^{j2kf \sin \theta \cot \eta/2 \cos (\psi - \phi)} \tag{87}$$

Amplitude and ellipticity plots are presented in Section IV.

DEFOCUSING ALONG AXIS

Let the phase center be located at point O' , on the axis, such that O' is determined by the vector $\vec{d}$ in the z-direction:

$$\vec{d} = \begin{vmatrix} 0 \\ 0 \\ d \end{vmatrix} \tag{88}$$

where d is small compared to the focal length (Figure 6). It will be assumed that, because $d << f$, the amplitude of $\vec{H}_i$ is essentially the same as if the phase center were located at the origin. Hence, $\vec{H}_{io}$ will be given by Equation (13), (15) or (16). However, because d is not necessarily small compared to a wavelength. the phase of $\vec{H}_i$ at the running point Q can be substantially different.

Let $\vec{\mathcal{R}}$ be the vector from O' to the running point Q. From Figure 6 it is seen that

$$\vec{\mathcal{R}} = \vec{\rho} - \vec{a} = \frac{f}{\sin^2 \eta/2} \begin{vmatrix} \sin\eta\cos\psi \\ \sin\eta\sin\psi \\ \cos\eta - \dfrac{\sin^2\eta/2\, d}{f} \end{vmatrix} \tag{89}$$

by Equations (8) and (88). The magnitude of $\vec{\mathcal{R}}$ is

$$\mathcal{R} = \frac{f}{\sin^2\eta/2}\left[(\sin\eta\cos\psi)^2 + (\sin\eta\sin\psi)^2 + \left(\cos\eta - \frac{\sin^2\eta/2\, d}{f}\right)^2\right]^{1/2}$$

$$= \frac{f}{\sin^2\eta/2}\left[1 + \frac{\sin^4\eta/2\, d^2}{f^2} - \frac{2\cos\eta\sin^2\eta/2\, d}{f}\right]^{1/2} \tag{90}$$

The expression for the near-field exponential term (Equation (18)) becomes

$$e^{-jk(r+\mathcal{R})} =$$

$$\exp. - jk\left\{\left[r_1^2 + \frac{f^2}{\sin^4\eta/2} - \frac{2fr_1}{\sin^2\eta/2}\left[\sin\eta\sin\theta\cos(\psi-\phi) + \cos\theta\cos\eta\right]\right]^{1/2} + \left[d^2 + \frac{f^2}{\sin^4\eta/2} - \frac{2fd}{\sin^2\eta/2}\cos\eta\right]^{1/2}\right\} \tag{91}$$

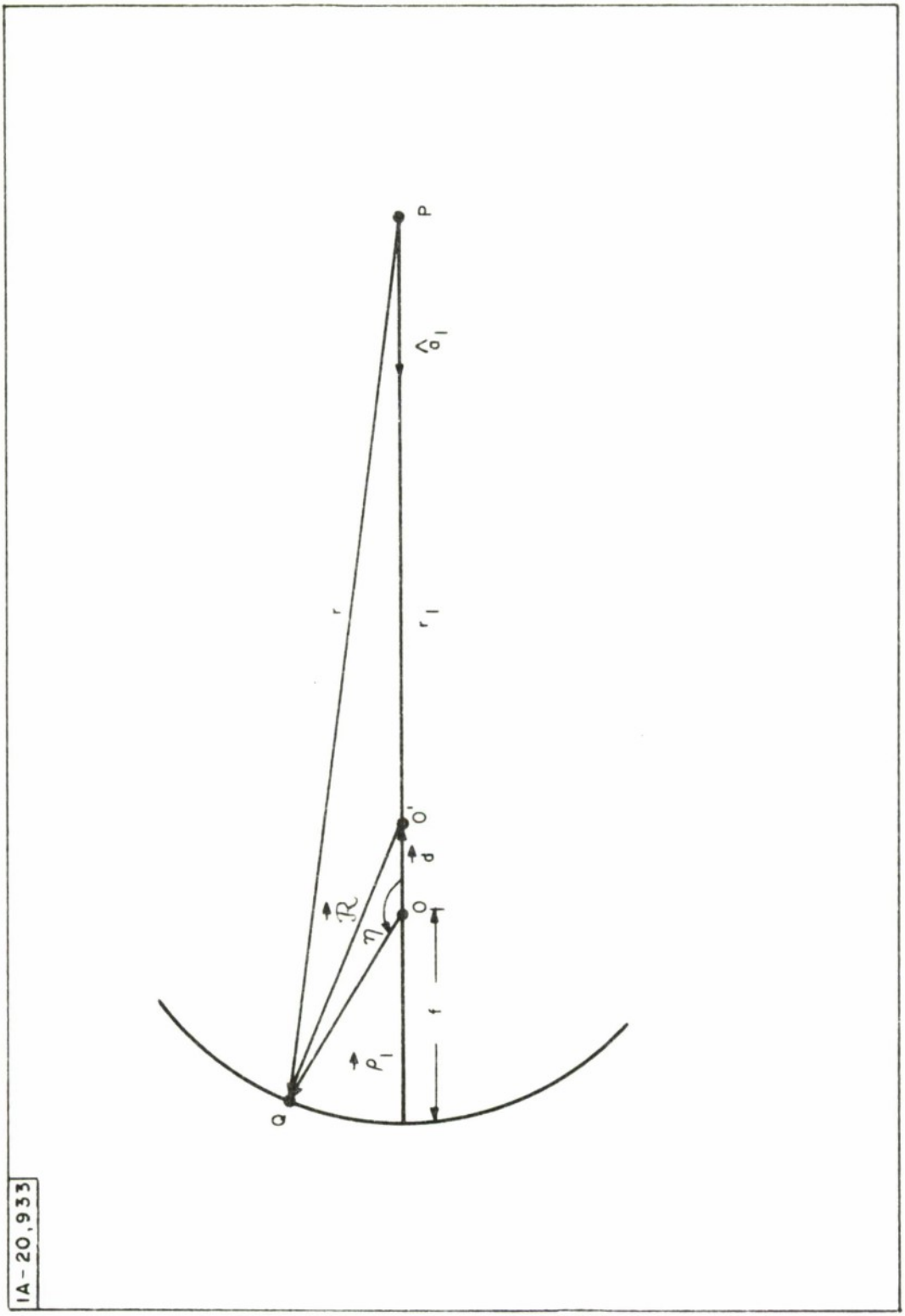

Figure 6. Defocusing Along Axis

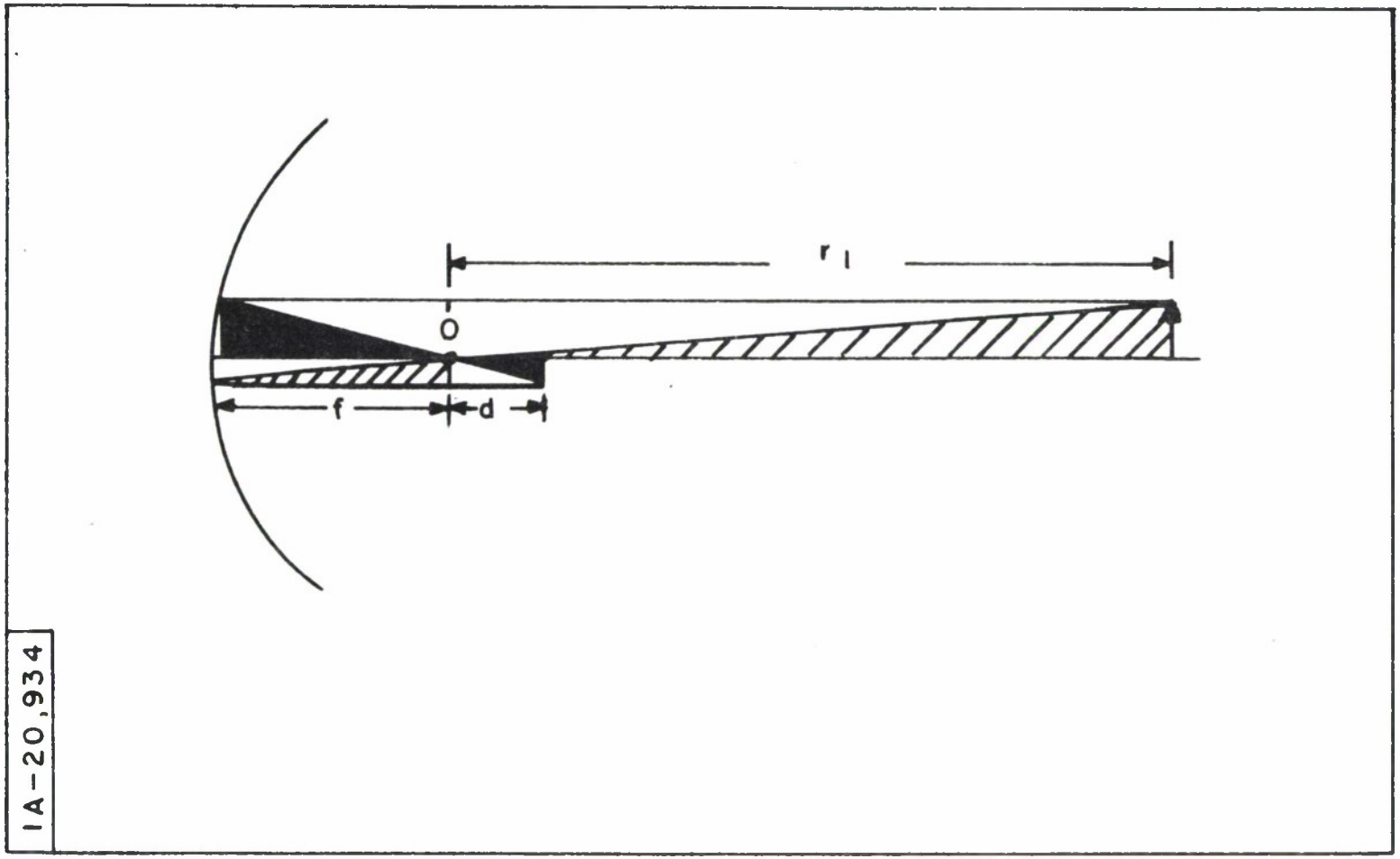

Figure 7. Near-Field Focusing: Geometric Construction

From ray optics constructions (Figure 7), it is found that the value of d that will result in a focused condition at r_1 is

$$d = \frac{f^2}{r_1} \tag{92}$$

This equation is an approximation which becomes more exact as the aperture becomes smaller. From a physical optics standpoint, near-field focusing can be construed as the condition when the contributions from the various differential areas, dA , add up almost in phase. Of course, this condition is impossible to achieve, but an attempt can be made by imposing certain restrictions. Let $A(\eta)$ be the complete phase term (Equation (91)) when $\theta = 0$ (focusing on-axis, at range r_1) :

$$A(\eta) = \left[r_1^2 + \frac{f^2}{\sin^4 \eta/2} - \frac{2 f r_1}{\sin^2 \eta/2} \cos\eta \right]^{1/2} + \left[d^2 + \frac{f^2}{\sin^4 \eta/2} - \frac{2 f r_1}{\sin^2 \eta/2} \cos\eta \right]^{1/2} \tag{93}$$

When $dA/d\eta|_{\eta(Q)} = 0$, that is, when the phase associated with a region around point Q does not vary, then the contributions from the points in that region will reinforce at the observation point, P .

Thus,

$$\frac{dA}{d\eta} = \frac{1}{2} \sin\eta \left\{ \left[r_1^2 + \frac{f^2}{\sin^4 \eta/2} - \frac{2 f r_1}{\sin^2 \eta/2} \cos\eta \right]^{-1/2} \left(\frac{-f^2}{\sin^6 \eta/2} + \frac{f r_1 \cos\eta}{\sin^4 \eta/2} + \frac{2 f r_1}{\sin^2 \eta/2} \right) \right.$$

$$\left. + \left[d^2 + \frac{f^2}{\sin^4 \eta/2} - \frac{2 f d}{\sin^2 \eta/2} \cos\eta \right]^{-1/2} \left(\frac{-f^2}{\sin^6 \eta/2} + \frac{f d \cos\eta}{\sin^4 \eta/2} + \frac{2 f d}{\sin^2 \eta/2} \right) \right. \tag{94}$$

In order for this equation to be zero,

$$\left[d^2 + \frac{f^2}{\sin^4 \eta_m/2} - \frac{2fd}{\sin^2 \eta_m/2} \cos \eta_m \right]^{1/2} \left(\frac{-f^2}{\sin^6 \eta_m/2} + \frac{f r_1 \cos \eta_m}{\sin^4 \eta_m/2} + \frac{2 f r_1}{\sin^2 \eta_m/2} \right)$$

$$= - [r_1, f]^{1/2} \left(\frac{-f^2}{\sin^6 \eta_m/2} + \frac{f d \cos \eta_m}{\sin^4 \eta_m/2} + \frac{2fd}{\sin^2 \eta_m/2} \right) \qquad (95)$$

where η_m is some weighted "mean" value of η. If, arbitrarily, $\eta_m = 160°$

$$d = 1.065 \frac{f^2}{r_1} \qquad 96)$$

Amplitude and ellipticity plots are presented in Section IV.

SECTION III

ANALYSIS OF CASSEGRAIN SYSTEM

GENERAL FORMULATION OF THE FIELD INCIDENT UPON THE PARABOLOID

The general procedure that was applied to obtain analytic expressions for the field of a focal feed paraboloidal antenna is now applied to the Cassegrain feed system. Actually, this procedure must be applied twice: first, the field on the paraboloid is considered as the field scattered by the hyperboloidal subreflector; then, this first scattered field is substituted for the "primary distribution" of the focal feed system in order to obtain the near-field and far-field of the complete antenna.

Consider the hyperboloidal subreflector illuminated by a source located at one of its foci (point 0, Figure 8). The second focus of the hyperboloid coincides with the focus of the paraboloidal dish at point C. An arbitrary point on the paraboloid is still referred as Q, of coordinates η and ψ, but the running point on the subreflector has been designated as P, of coordinates ρ, θ, and ϕ. Distances from the subreflector to the paraboloid are designated as r and r_1. It is hoped that those quantities will not be mistaken for the coordinates of the entire antenna field observation point, since the derivations of the field on the dish and of the space field are conceptually separate problems.*

First, one wants to know what is the field $\vec{H}_S\big|_Q$ at any arbitrary point, Q, on the paraboloid. Subsequently, it will become possible to compute the far-field (and also the near-field) of the paraboloidal dish.

---

*The reason for not introducing new symbols is the traditional association of θ with elevation, ϕ with azimuth, r with distance, etc.

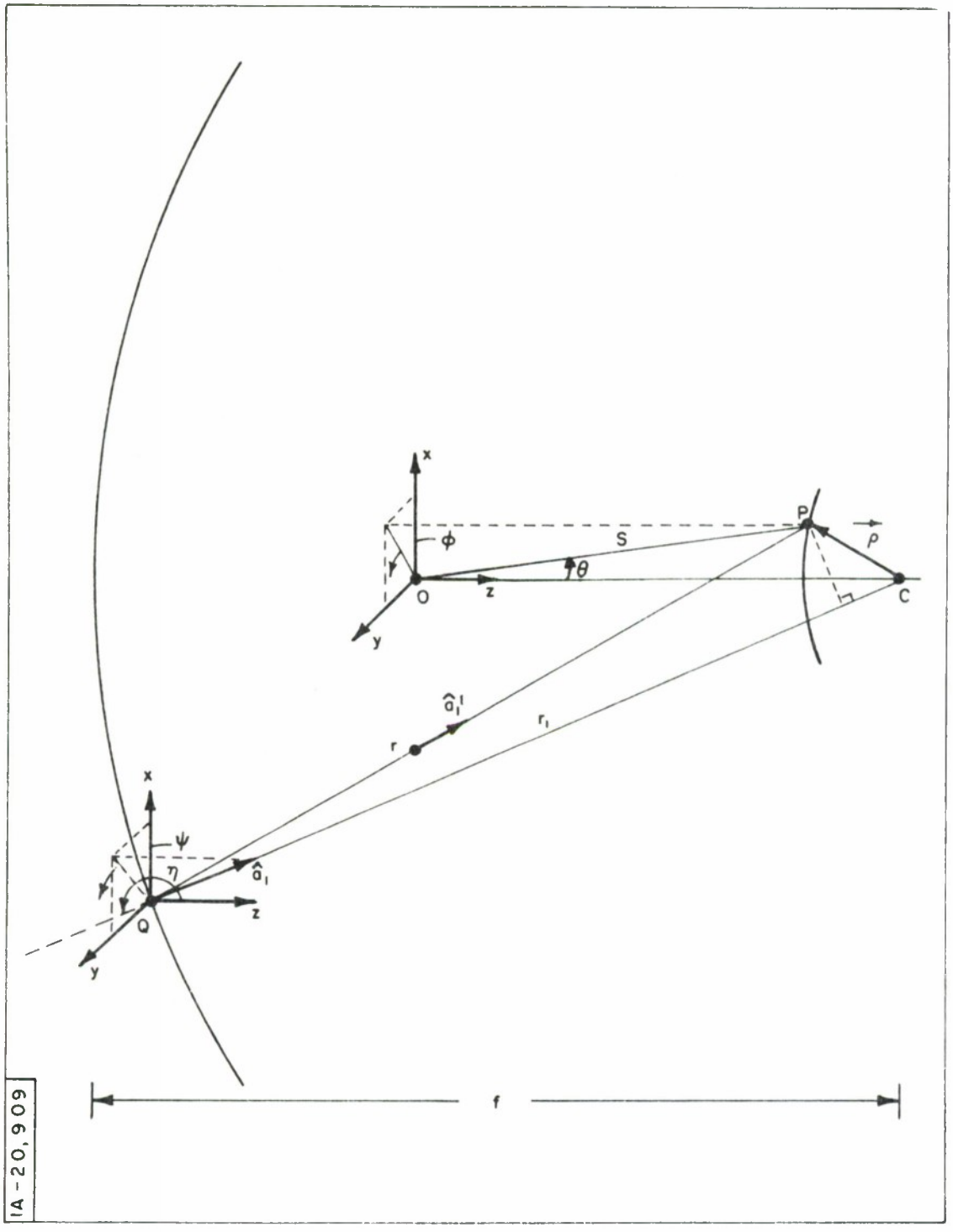

Figure 8. Cassegrain Feed System

An exact expression for $\vec{H}_{S|Q}$ is*

$$\vec{H}_{S|Q} = \frac{1}{4\pi} \iint_S (\hat{n} \times \vec{H}) \times \nabla_p \left(\frac{e^{-jkr}}{r}\right) dA \qquad (97)$$

where

$\hat{n}$ = the outward normal unit vector at a point Q on the surface of the hyperboloid,

$\vec{H}$ = the total H-field at point P

dA = the differential element of area at point P

r = the distance from the observation point Q to P

k = the propagation constant, equal to $2\pi/\lambda$

∇_p = the gradient, taken at point P

S = the total surface of the hyperboloid

Equation (97), as it stands, is truly formidable, and some judicious approximations are in order. The total field $\vec{H}$, or rather the expression $(\hat{n} \times \vec{H})$, will be approximated by $2(\hat{n} \times \vec{H}_i)$, that is

$$(\hat{n} \times \vec{H}) = 2(\hat{n} \times \vec{H}_i) \qquad (98)$$

where $\vec{H}_i$ is the incident H-field at point P. Furthermore, S is taken as only that portion of the hyperboloid which is directly illuminated. Those approximations appear to be valid if the diameter is at least a few wavelengths.

The expression for $\nabla_p (e^{-jkr}/r)$ is exactly

$$\nabla_p \left(\frac{e^{-jkr}}{r}\right) = \left(j\frac{2\pi}{\lambda} + \frac{1}{r}\right) \left(\frac{e^{-jkr}}{r}\right) \hat{a}_1' \qquad (99)$$

---

*See Equation (1).

where $\hat{a}_1'$ is the unit vector pointing from Q to P. But, if $r \gg \lambda$, then

$$\nabla_P \left(\frac{e^{-jkr}}{r} \right) \approx \frac{jk\, e^{-jkr}}{r} \hat{a}_1' \tag{100}$$

Again, this appears to be a safe approximation in the practical cases one is liable to encounter.

An approximation which is not safe, and which must be re-examined for a specific geometry, is one consisting in letting

$$\hat{a}_1' \approx \hat{a}_1$$

where $\hat{a}_1$ is the unit vector directed from Q to C, the focus of the hyperboloid (and of the paraboloid). The excursion angle from $\hat{a}_1'$ to $\hat{a}_1$, when viewed from point Q for any point P on the hyperboloid, may not be negligible.

The distance from point Q to point P, r, is exactly

$$r = |\vec{r}_1 + \vec{\rho}| = |\hat{a}_1 r_1 + \vec{\rho}| \tag{101}$$

Vector $\hat{a}_1'$ is exactly

$$\hat{a}_1' = \frac{\hat{a}_1 r_1 + \vec{\rho}}{|\hat{a}_1 r_1 + \vec{\rho}|} \tag{102}$$

The quantities $\hat{a}_1$, r_1, and $\vec{\rho}$ will be obtained in the following subsection.

The approximation involving $\vec{H}_i$ is that it originates from a point source (phase center) and that it is a spherical wave, with no longitudinal component. It will be written

$$\vec{H}_i = \vec{H}_{io}\, e^{-jks} \tag{103}$$

where the phase, ks , is brought out explicitly (s being the distance from the origin, or second focus, to the running point P). The 1/s amplitude dependency will be taken into account in the overall amplitude function of $\vec{H}_{io}$ which is discussed in Appendix D. In practice, the only requirement imposed by the approximation is that the subreflector be outside the very near-zone of the feed.

By means of Equations (98), (100), (101), (102), and (103), Equation (97) becomes

$$\vec{H}_{S|Q} = \frac{jk}{2\pi} \iint \frac{1}{r} (\hat{n} \times \vec{H}_{io}) \times \hat{a}_1' \, e^{-jk(s+r)} \, dA \qquad (104)$$

where r and $\hat{a}_1'$ are functions of both P and Q , and $\hat{n}$, $\vec{H}_{io}$, s , and dA are functions of P only.

The vectors will be broken up into Cartesian components, and those components – in turn – will be expressed in terms of elevation and azimuth angles, θ and ϕ respectively for the hyperboloid, η and ψ respectively for the paraboloid.

GEOMETRY OF THE PROBLEM

Point Q on the paraboloid (Figure 8) can be described by the elevation angles η and the azimuth angle ψ of the ray CQ , where C is at the focus of both paraboloid and hyperboloid. The quantity r_1 , a function of η and of f , the focal length, is

$$r_1 = \frac{f}{\sin^2(\eta/2)} \qquad (105)$$

The unit vector $\hat{a}_1$ is expressed in Cartesian coordinates as *

$$\hat{a}_1 = - \begin{vmatrix} \sin\eta \cos\psi \\ \sin\eta \sin\psi \\ \cos\eta \end{vmatrix} \tag{106}$$

The polar equation of the hyperbola is

$$s = \frac{a(1-e^2)}{1-e\cos\theta} \tag{107}$$

which is derived in Appendix J, where the constants a and e are also defined.

The magnitude of vector $\vec{\rho}$ from C to P is derived, in Appendix J, as

$$\rho = s - 2a = \frac{a[2e\cos\theta - (1+e^2)]}{1-e\cos\theta} \tag{108}$$

whereas the vector $\vec{\rho}$ itself, in Cartesian coordinates, is

$$\vec{\rho} = \frac{a}{1-e\cos\theta} \begin{vmatrix} (1-e^2)\sin\theta\cos\phi \\ (1-e^2)\sin\theta\sin\phi \\ [(1+e^2)\cos\theta - 2e] \end{vmatrix} \tag{109}$$

Still in Appendix J, the unit vector normal to the surface at point Q, $\hat{n}$, is derived as

$$\hat{n} = \frac{1}{(1+e^2-2e\cos\theta)^{1/2}} \begin{vmatrix} \sin\theta\cos\phi \\ \sin\theta\sin\phi \\ (\cos\theta - e) \end{vmatrix} \tag{110}$$

---

* See Equation (10).

and the expression for the differential area, dA , is derived as

$$dA = \frac{a^2(1-e^2)^2}{(1-e\cos\theta)^3}(1+e^2-2e\cos\theta)\sin\theta\, d\theta\, d\phi \qquad (111)$$

It follows, by Equation (101), that

$$r = \text{magnitude of} \begin{vmatrix} \frac{-f}{\sin^2\eta/2}(\sin\eta\cos\psi) + \frac{a}{1-e\cos\theta}(1-e^2)\sin\theta\cos\phi \\ \frac{-f}{\sin^2\eta/2}(\sin\eta\sin\psi) + \frac{a}{1-e\cos\theta}(1-e^2)\sin\theta\sin\phi \\ \frac{-f}{\sin^2\eta/2}\cos\eta + \frac{a}{1-e\cos\theta}[(1+e^2)\cos\theta - 2e] \end{vmatrix}$$

or

$$r = \left[\frac{f^2}{\sin^4\eta/2} + \frac{a^2[2e\cos\theta-(1+e^2)]^2}{(1-e\cos\theta)^2} - \frac{2fa}{\sin^2\eta/2(1-e\cos\theta)}[(\sin\eta\sin\theta(1-e^2)\cos(\psi-\phi) + (1+e^2)\cos\theta\cos\eta - 2e\cos\eta)]\right]^{1/2} \qquad (112)$$

and that

$$\hat{a}_1' = \frac{\begin{vmatrix} \frac{-f}{\sin^2\eta/2}(\sin\eta\cos\psi) + \frac{a}{1-e\cos\theta}(1-e^2)\sin\theta\cos\phi \\ \frac{-f}{\sin^2\eta/2}(\sin\eta\sin\psi) + \frac{a}{1-e\cos\theta}(1-e^2)\sin\theta\sin\phi \\ \frac{-f}{\sin^2\eta/2}\cos\eta + \frac{a}{1-e\cos\theta}[(1+e^2)\cos\theta - 2e] \end{vmatrix}}{\left[\frac{f^2}{\sin^4\eta/2} + \frac{a^2[2e\cos\theta-(1+e^2)]^2}{(1-e\cos\theta)^2} - \frac{2fa}{\sin^2\eta/2(1-e\cos\theta)}[\sin\eta\sin\theta(1-e^2)\cos(\psi-\phi) + (1+e^2)\cos\theta\cos\eta - 2e\cos\eta]\right]^{1/2}} \qquad (113)$$

PRIMARY PATTERNS

The primary patterns are discussed in Section II and in Appendix D. When η (of Figure 2) is replaced by θ (of Figure 8), the signs must be changed. Another modification in the analytic expressions occur insofar as the field strength dependence on the range is now $(e \cos\theta - 1)$, by Equation (107).

Thus, the equibeam distribution is given by

$$\vec{H}_{io} = h(\theta)(e\cos\theta - 1) \left| \begin{array}{l} (\cos^2\phi\cos\theta + \sin^2\phi)\cos\omega t \\ \quad + (\cos\phi\sin\phi[\cos\theta - 1])\sin\omega t \\ \\ (\cos\phi\sin\phi[\cos\theta - 1])\cos\omega t \\ \quad + (\sin^2\phi\cos\theta + \cos^2\phi)\sin\omega t \\ \\ -\sin\theta\cos\phi\cos\omega t - \sin\theta\sin\phi\sin\omega t \end{array} \right| \tag{114}$$

whereas the dipole-like and pseudo-equibeam distributions are given by

$$\vec{H}_{io} = h(\theta)(e\cos\theta - 1) \left| \begin{array}{c} \gamma_c\cos\theta\cos\omega t \\ \gamma_s\cos\theta\sin\omega t \\ -[(\sin\theta\cos\phi)\gamma_c\cos\omega t + (\sin\theta\sin\phi)\gamma_s\sin\omega t \end{array} \right| \tag{115}$$

with

$$\gamma_c = \gamma_s = 1 \tag{116}$$

for the dipole-like distribution, and

$$\gamma_c = (\cos^2\theta + \sin^2\theta\cos^2\phi)^{-\frac{1}{2}}$$

$$\gamma_s = (\cos^2\theta + \sin^2\theta\sin^2\phi)^{-\frac{1}{2}} \qquad (117)$$

for the pseudo-equibeam distribution.

In Appendix J, it is shown that

$$h(\theta) = \cos^2(2\theta) \qquad (118)$$

fits, very closely, an experimental pattern with a 12-db taper at the edge of the sub-dish (θ_o = 30 degrees).

FORMULATION OF THE FIELD ON THE PARABOLOID: EQUIBEAM DISTRIBUTION

Equations (107) through (114) or (115) can now be substituted into Equation (104). The exponential term becomes, by Equations (107) and (112)

$$\exp. - jk(s + r) = \exp. - jk \left\{ \frac{a(1-e^2)}{1 - e\cos\theta} \right.$$

$$+ \left[\frac{f^2}{\sin^4 \eta/2} + \frac{a^2[2e\cos\theta - (1+e^2)]^2}{(1 - e\cos\theta)^2} \right.$$

$$- \frac{2fa}{\sin^2 \eta/2(1 - e\cos\theta)}[\sin\eta\sin\theta(1-e^2)\cos(\psi - \phi)$$

$$\left. \left. + (1+e^2)\cos\theta\cos\eta - 2e\cos\eta] \right]^{\frac{1}{2}} \right\} \qquad (119)$$

The cross-product of $\hat{n}$ and $\vec{H}_{io}$ is the vector whose components are the co-factors of

$$\begin{vmatrix} \hat{x} & \hat{y} & \hat{z} \\ \sin\theta\cos\phi & \sin\theta\cos\phi & (\cos\theta - e) \\ (\cos^2\phi\cos\theta + \sin^2\phi)\cos\omega t + (\cos\phi\sin\phi[\cos\theta - 1])\sin\omega t & (\cos\phi\sin\phi[\cos\theta - 1]) + (\sin^2\phi\cos\theta + \cos^2\phi) & -\sin\theta(\cos\phi\cos\omega t + \sin\phi\sin\omega t) \end{vmatrix}$$

times $$\frac{h(\theta)\,(e\cos\theta - 1)}{(1 + e^2 - 2e\cos\theta)^{1/2}}$$

This expression simplifies considerably to become

$$\begin{vmatrix} [-\sin\phi\cos\phi(1+e)(1-\cos\theta)]\cos\omega t + [(e-\cos\theta) - \sin^2\phi(1-\cos\theta)(1+e)]\sin\omega t \\ [\sin\phi\cos\phi(1+e)(1-\cos\theta)]\sin\omega t - [(e-\cos\theta) - \cos^2\phi(1-\cos\theta)(1+e)]\cos\omega t \\ \sin\theta\cos\phi\sin\omega t - \sin\theta\sin\phi\cos\omega t \end{vmatrix}$$

times $$\frac{h(\theta)\,(e\cos\theta - 1)}{(1 + e^2 - 2e\cos\theta)^{1/2}} \qquad (120)$$

or, symbolically

$$(\hat{n} \times \vec{Hi}_o) = \begin{vmatrix} (A + B) \sin \omega t + C \cos \omega t \\ (-A + D) \cos \omega t - C \sin \omega t \\ E \sin \omega t - F \cos \omega t \end{vmatrix} \tag{121}$$

where

$$A = + h'(\theta) (e - \cos \theta) \tag{122}$$

$$B = - h'(\theta) (1 + e) (1 - \cos \theta) \sin^2 \phi \tag{123}$$

$$C = - h'(\theta) (1 + e) (1 - \cos \theta) \sin \phi \cos \phi \tag{124}$$

$$D = + h'(\theta) (1 + e) (1 - \cos \theta) \cos^2 \phi \tag{125}$$

$$E = + h'(\theta) \sin \theta \cos \phi \tag{126}$$

$$F = + h'(\theta) \sin \theta \sin \phi \tag{127}$$

and

$$h'(\theta) = \frac{+ h (\theta) (e \cos \theta - 1)}{(1 + e^2 - 2e \cos \theta)^{1/2}} \tag{128}$$

Since further derivations of the expressions for the field on the paraboloid are common to the cases of dipole-like distributions (after the symbols A through F have been established), they will be postponed to the next subsection.

FORMULATION OF THE FIELD ON THE PARABOLOID: DIPOLE-LIKE DISTRIBUTIONS

The dipole-like distributions Equations (115) and (116) and the pseudo-equibeam distribution Equations (115) and (117) will be carried together, for the sake of convenience.

The cross-product $(\hat{n} \times \vec{H}_{io})$ is the vector whose components are the co-factors of

$$\frac{h(\theta)(e\cos\theta - 1)}{(1 + e^2 - 2e\cos\theta)^{1/2}} \begin{vmatrix} \hat{x} & \hat{y} & \hat{z} \\ \sin\theta\cos\phi & \sin\theta\sin\phi & (\cos\theta - e) \\ (\gamma_c \cos\theta\cos\omega t) & (\gamma_s \cos\theta \sin\omega t) & -[(\gamma_c \sin\theta\cos\phi)\cos\omega t + (\gamma_s \sin\theta\sin\phi)\sin\omega t] \end{vmatrix}$$

that is

$$\frac{h(\theta)(e\cos\theta - 1)}{(1 + e^2 - 2e\cos\theta)^{1/2}} \begin{vmatrix} -\sin^2\theta\sin\phi(\gamma_c\cos\phi\cos\omega t + \gamma_s\sin\phi\sin\omega t) & -\gamma_s\cos\theta(\cos\theta - e)\sin\omega t \\ +\sin^2\theta\cos\phi(\gamma_c\cos\phi\cos\omega t + \gamma_s\sin\phi\sin\omega t) & +\gamma_c\cos\theta(\cos\theta - e)\cos\omega t \\ \sin\theta\cos\theta(\gamma_s\cos\phi\sin\omega t - \gamma_c\sin\phi\cos\omega t) & \end{vmatrix} \tag{129}$$

or, symbolically

$$(\hat{n} \times \vec{H}_{io}) = \begin{vmatrix} (A - B)\gamma_s \sin\omega t + C\gamma_c \cos\omega t \\ (-A + D)\gamma_c \cos\omega t - C\gamma_s \sin\omega t \\ E\gamma_s \sin\omega t - F\gamma_c \cos\omega t \end{vmatrix} \tag{130}$$

where

$$A = +h'(\theta)\cos\theta(e - \cos\theta) \tag{131}$$

$$B = -h'(\theta)\sin^2\theta\sin^2\phi \tag{132}$$

$$C = -h'(\theta)\sin^2\theta\sin\phi\cos\phi \tag{133}$$

$$D = +h'(\theta)\sin^2\theta\cos^2\phi \tag{134}$$

$$E = + h'(\theta) \sin\theta \cos\theta \cos\phi \tag{135}$$

$$F = + h'(\theta) \sin\theta \cos\theta \sin\phi \tag{136}$$

and

$$h'(\theta) = \frac{+ h(\theta)(e\cos\theta - 1)}{(1 + e^2 - 2e\cos\theta)^{1/2}}$$

as in Equation (128).

The cross-product of $(\hat{n} \times \vec{H}_{io})$ and $\hat{a}_1'$ (Equation (113)) is the vector whose components are the co-factors of

$$\begin{vmatrix} \hat{x} & \hat{y} & \hat{z} \\ [(A+B)\gamma_s \sin\omega t + C\gamma_c \cos\omega t] & [(-A+D)\gamma_c \cos\omega t - C\gamma_s \sin\omega t] & [E\gamma_s \sin\omega t - F\gamma_c \cos\omega t] \\ a_{1x}' & a_{1y}' & a_{1z}' \end{vmatrix}$$

that is

$$(\hat{n} \times \vec{H}_{io}) \times \hat{a}_1' = \begin{vmatrix} a_{1z}'[(-A+D)\gamma_c \cos\omega t - C\gamma_s \sin\omega t] - a_{1y}'(E\gamma_s \sin\omega t - F\gamma_c \cos\omega t) \\ -a_{1z}'[(A+B)\gamma_s \sin\omega t + C\gamma_c \cos\omega t] + a_{1x}'(E\gamma_s \sin\omega t - F\gamma_c \cos\omega t) \\ a_{1y}'[(A+B)\gamma_s \sin\omega t + C\gamma_c \cos\omega t] - a_{1x}'[(-A+D)\gamma_c \cos\omega t - C\gamma_s \sin\omega t] \end{vmatrix} \tag{137}$$

or, by rearranging the terms

$$(\hat{n} \times \vec{H}_{io}) \times \hat{a}_1' = \begin{vmatrix} [a_{1z}'(-A+D) + a_{1y}'F]\gamma_c \cos\omega t - [a_{1z}'C + a_{1y}'E]\gamma_s \sin\omega t \\ [-a_{1z}'(A+B) + a_{1x}'E]\gamma_s \sin\omega t - [a_{1z}'C + a_{1x}'F]\gamma_c \cos\omega t \\ [a_{1y}'C - a_{1x}'(-A+D)]\gamma_c \cos\omega t + [a_{1y}'(A+B) + a_{1x}'C]\gamma_s \sin\omega t \end{vmatrix} \tag{138}$$

where

$$a_{1x}' = \frac{1}{r}\left[\frac{-f}{\sin^2 \eta/2}(\sin\eta\cos\psi) + \frac{a}{1-e\cos\theta}(1-e^2)\sin\theta\cos\phi\right] \quad (139)$$

$$a_{1y}' = \frac{1}{r}\left[\frac{-f}{\sin^2 \eta/2}(\sin\eta\sin\psi) + \frac{a}{1-e\cos\theta}(1-e^2)\sin\theta\sin\phi\right] \quad (140)$$

$$a_{1z}' = \frac{1}{r}\left\{\frac{-f}{\sin^2 \eta/2}\cos\eta + \frac{a}{1-e\cos\theta}[(1+e^2)\cos\theta - 2e]\right\} \quad (141)$$

and r is given by Equation (112).

The incident magnetic field vector at any point Q on the paraboloid becomes

$$\vec{H}_s|_Q \propto \begin{vmatrix} X1\cos\omega t + X2\sin\omega t \\ Y1\sin\omega t + Y2\cos\omega t \\ Z1\cos\omega t + Z2\sin\omega t \end{vmatrix} \quad (142)$$

where

$$X_1 = (+)\int_{\phi=0}^{\phi=2\pi}\int_{\theta=0}^{\theta=\theta_0}\gamma_c \exp\{\{\frac{1}{r}[a_{1z}'(-A+D) - a_{1y}'F]\,dA \quad (143)$$

$$X2 = (-)\iint\gamma_s \exp\{\{\frac{1}{r}[a_{1z}'C + a_{1y}'E]\,dA \quad (144)$$

$$Y1 = (+)\iint\gamma_s \exp\{\{\frac{1}{r}[-a_{1z}'(A+B) + a_{1x}'E]\,dA \quad (145)$$

$$Y2 = (-)\iint\gamma_c \exp\{\{\frac{1}{r}[a_{1z}'C + a_{1x}'F]\,dA \quad (146)$$

$$Z1 = (+) \iint \gamma_c \exp\{\} \frac{1}{r} [a_{ly}' C - a_{lx}' (-A + D)] \, dA \tag{147}$$

$$Z2 = (+) \iint \gamma_s \exp\{\} \frac{1}{r} [a_{ly}' (A + B) + a_{lx}' C] \, dA \tag{148}$$

Instead of the form given by Equation (104), it may be advantageous to bring out and suppress the phase factor e^{-jkr_1} in order to provide a direct comparision with direct focal point feed. Equation (104) must be modified to the form

$$\vec{H}_s|_{Q'} = \frac{jk}{2\pi} \iint \frac{1}{r} (\hat{n} \times \vec{H}_{io}) \times \hat{a}_1' e^{-jk(s+r-r_1)} \, dA \tag{149}$$

where the phase of $\vec{H}_S|_{Q'}$ is now referred back to the paraboloid focus. Equation (142) must be modified according to

$$\vec{H}_s|_p = \begin{vmatrix} X1' \cos \omega t + X2' \sin \omega t \\ Y1' \sin \omega t + Y2' \cos \omega t \\ Z1' \cos \omega t + Z2' \sin \omega t \end{vmatrix} \tag{150}$$

where the primes denote that the exponential terms have been modified, in Equations (143) through (148), to the form

$$e^{-jk(s+r-r_1)}$$

It is understood that, for the equibeam distribution, the symbols A through F are given by Equations (122) through (127), and that

$$\gamma_c = \gamma_s = 1$$

For the dipole-like distribution, the symbols A through F are given by Equations (131) through (136), and

$$\gamma_c = \gamma_s = 1$$

For the pseudo-equibeam distribution, the symbols A through F are also given by Equations (131) through (136), but γ_c and γ_s are given by Equation (117).

Symbols pertaining to the "modified" Equations (143) through (148), where the phase is referred back to the paraboloid focus, are summarized in Table I.

PARABOLOID ILLUMINATION FROM SUB-REFLECTOR

Before considering the space field (as will be done in the next subsection), it is worthwhile to transform the field on the paraboloid in a form that will enable comparisons with measurements.

Let the feed be linearly polarized by suppressing the $\sin \omega t$ component. By Equation (150), the field on the paraboloid, in Cartesian coordinates, is

$$\vec{H} = \begin{vmatrix} X1' \\ Y2' \\ Z1' \end{vmatrix}$$

But Cartesian coordinates are not appropriate to measurements since the measuring probe will generally be aligned with the vector $-\hat{a}_1$ (Figure 8). Coordinate transformations can be effected by means of Equations (208) and (209).

Table I

Symbols for Modified Equations (143) Through (148)

$$\vec{H}_s|'_Q = \frac{jk}{2\pi} \int_{\phi=0}^{\phi=2\pi} \int_{\theta=0}^{\theta=\theta_o} \frac{1}{r} (\hat{n} \times \vec{H}_{io}) \times \hat{a}_1' e^{-jk(s+r-r_1)} \, dA$$

$$r = \left\{ \frac{f^2}{\sin^4 \eta/2} + \frac{a^2 [2e\cos\theta - (1+e^2)]^2}{(1-e\cos\theta)^2} - \frac{2fa}{\sin^2\eta/2(1-e\cos\theta)} [\sin\eta\sin\theta(1-e^2)\cos(\psi-\phi) + (1+e^2)\cos\theta\cos\eta - 2e\cos\eta] \right\}^{1/2}$$

$$dA = \frac{a^2(1-e^2)^2}{(1-e\cos\theta)^3} (1+e^2-2e\cos\theta)\sin\theta \, d\theta \, d\phi$$

$$\exp\{\} = \exp.-jk\left[\frac{a(1-e^2)}{1-e\cos\theta} - \frac{f}{\sin^2\eta/2} + r\right]$$

$$a_{1x}' = \frac{1}{r}\left[-\frac{f}{\sin^2\eta/2}(\sin\eta\cos\psi) + \frac{a}{1-e\cos\theta}(1-e^2)\sin\theta\cos\phi\right]$$

$$a_{1y}' = \frac{1}{r}\left[\frac{-f}{\sin^2\eta/2}(\sin\eta\sin\psi) + \frac{a}{1-e\cos\theta}(1-e^2)\sin\theta\sin\phi\right]$$

$$a_{1z}' = \frac{1}{r}\left\{-\frac{f}{\sin^2\eta/2}\cos\eta + \frac{a}{1-e\cos\theta}[(1+e^2)\cos\theta - 2e]\right\}$$

$$h'(\theta) = \frac{+h(\theta)}{(1+e^2-2e\cos\theta)^{1/2}}$$

	EQUIBEAM	DIPOLE-LIKE	PSEUDO-EQUIBEAM
A =	$+h'(\theta)(e-\cos\theta)$	$+h'(\theta)\cos\theta(e-\cos\theta)$	
B =	$-h'(\theta)(1+e)(1-\cos\theta)\sin^2\phi$	$-h'(\theta)\sin^2\theta\sin^2\phi$	
C =	$-h'(\theta)(1+e)(1-\cos\theta)\sin\phi\cos\phi$	$-h'(\theta)\sin^2\theta\sin\phi\cos\phi$	
D =	$+h'(\theta)(1+e)(1-\cos\theta)\cos^2\phi$	$+h'(\theta)\sin^2\theta\cos^2\phi$	
E =	$+h'(\theta)\sin\theta\cos\phi$	$+h'(\theta)\sin\theta\cos\theta\cos\phi$	
F =	$+h'(\theta)\sin\theta\sin\phi$	$+h'(\theta)\sin\theta\cos\theta\sin\phi$	
γ_c =	1	1	$(\cos^2\theta+\sin^2\theta\cos^2\phi)^{-1/2}$
γ_s =	1	1	$(\cos^2\theta+\sin^2\theta\sin^2\phi)^{-1/2}$

In particular, for an H-plane cut ($\psi = 0$ or π), a rotation through the angle ($\eta - \pi$) about the y-axis is in order. It is described by the rotation matrix

$$[T]_{(\eta-\pi),y} = \begin{vmatrix} -\cos\eta & 0 & \sin\eta \\ 0 & 1 & 0 \\ -\sin\eta & 0 & -\cos\eta \end{vmatrix} \tag{151}$$

where η must be considered negative when $\psi = \pi$, whereas for an E-plane cut ($\psi = \pm\pi/2$), a rotation through the angle ($\eta - \pi$) about the x-axis is required. It is described by the rotation matrix

$$[T]_{(\eta-\pi),x} = \begin{vmatrix} 1 & 0 & 0 \\ 0 & -\cos\eta & \sin\eta \\ 0 & -\sin\eta & -\cos\eta \end{vmatrix} \tag{152}$$

Consequently, the field on the paraboloid in the H-plane is

$$\vec{H}_H = \begin{vmatrix} -X1'\cos\eta \pm Z1'\sin\eta \\ Y2' \\ \mp X1'\sin\eta - Z1'\cos\eta \end{vmatrix} \tag{153}$$

where the lower signs apply when $\psi = \pi$.

In the E-plane, the field on the paraboloid becomes

$$\vec{H}_E = \begin{vmatrix} X1' \\ -Y2'\cos\eta + Z1'\sin\eta \\ -Y2'\sin\eta - Z1'\cos\eta \end{vmatrix} \tag{154}$$

Other cuts can be obtained by the appropriate applications of $[T]_{\phi}$ and $[T]_{\eta}$.

Plots relative to H_H and H_V are given in Section V.

ANALYTIC FORMULATION OF THE SPACE FIELD*

The procedure for finding the space field when the paraboloid is excited by a Cassegrain feed system is now the same as for the case of a focal feed system. But the distribution of the incident field on the paraboloid is now different, and adequate modifications must be provided. Essentially, $\vec{H}_S\big|_Q$ (Equation 142) is the field incident on the paraboloid and now takes the place of $\vec{H}_i$ in Equation (5).

Thus, the starting point is Equation (6) modified with regard to both modulus and argument of $\vec{H}_i$. If one uses the "modified" form of $\vec{H}_i$ (Equation 149) where the phase of H is referred back to the focus of the paraboloid, then Equation (18) is the right expression for the exponential factor

$$\exp. - jk \left\{ \left[r_1^2 + \frac{f^2}{\sin^4 \eta/2} - \frac{2 f r_1}{\sin^2 \eta/2} \left[\sin\eta \sin\theta \cos(\psi - \phi) + \cos\theta \cos\eta \right] \right]^{1/2} + \frac{f}{\sin^2 \eta/2} \right\}$$

The field on the paraboloid is given by Equation (150). The expression for $\hat{n}$ is given in Equation (7). Consequently, $(\hat{n} \times \vec{H}_{io})$ is the vector formed by the cofactors of

---

* In this and the following sections, the symbols refer back to Figures 2 and 3 since point P is no longer on the hyperboloid, but is now an arbitrary observation point in space.

$$\begin{vmatrix} \hat{x} & \hat{y} & \hat{z} \\ -(\cos\psi\cos\eta/2) & -(\sin\psi\cos\eta/2) & \sin\eta/2 \\ [X1'\cos\omega t + X2'\sin\omega t] & [Y1'\sin\omega t + Y2'\cos\omega t] & [Z1'\cos\omega t + Z2'\sin\omega t] \end{vmatrix}$$

or

$$(\hat{n}\times\vec{H}_{io}) = \begin{vmatrix} (-\sin\psi\cos\eta/2)(Z1'\cos\omega t + Z2'\sin\omega t) & -\sin\eta/2\,(Y1'\sin\omega t + Y2'\cos\omega t) \\ (\cos\psi\cos\eta/2)(Z1'\cos\omega t + Z2'\sin\omega t) & +\sin\eta/2\,(X1'\cos\omega t + X2'\sin\omega t) \\ (-\cos\psi\cos\eta/2)(Y1'\sin\omega t + Y2'\cos\omega t) & +(\sin\psi\cos\eta/2)(X1'\cos\omega t + X2'\sin\omega t) \end{vmatrix} \tag{155}$$

or, in symbolic form

$$(\hat{n}\times\vec{H}_{io}) = \begin{vmatrix} A_1\sin\omega t + A_2\cos\omega t \\ B_1\cos\omega t + B_2\sin\omega t \\ C_1\cos\omega t + C_2\sin\omega t \end{vmatrix} \tag{156}$$

where

$$\begin{aligned} A_1 &= -(Y_1'\sin\eta/2 + Z_2'\sin\psi\cos\eta/2) \\ A_2 &= -(Y_2'\sin\eta/2 + Z_1'\sin\psi\cos\eta/2) \\ B_1 &= +(X_1'\sin\eta/2 + Z_1'\cos\psi\cos\eta/2) \\ B_2 &= +(X_2'\sin\eta/2 + Z_2'\cos\psi\cos\eta/2) \\ C_1 &= +(X_1'\sin\psi\cos\eta/2 - Y_2'\cos\psi\cos\eta/2) \\ C_2 &= +(X_2'\sin\psi\cos\eta/2 - Y_1'\cos\psi\cos\eta/2) \end{aligned}$$

An expression for $\hat{a}_1'$ is provided by Equation (12). Consequently, the cross-product $(\hat{n} \times \vec{H}_{io}) \times \hat{a}_1'$ is the vector whose components are the co-factors of

$$\begin{vmatrix} \hat{x} & \hat{y} & \hat{z} \\ (A_1 \sin\omega t + A_2 \cos\omega t) & (B_1 \cos\omega t + B_2 \sin\omega t) & (C_1 \cos\omega t + C_2 \sin\omega t) \\ \left(\frac{2f}{r_1} \cot\eta/2 \cos\psi - \sin\theta\cos\phi\right) & \left(\frac{2f}{r_1} \cot\eta/2 \sin\psi - \sin\theta\sin\phi\right) & -1 \end{vmatrix}$$

that is, $(\hat{n} \times \vec{H}_{io}) \times \hat{a}_1' =$

$$\begin{vmatrix} -\left[(B_1 \cos\omega t + B_2 \sin\omega t) + (C_1 \cos\omega t + C_2 \sin\omega t)\left(\frac{2f}{r_1} \cot\eta/2 \sin\psi - \sin\theta\sin\phi\right)\right] \\ +\left[(A_1 \sin\omega t + A_2 \cos\omega t) + (C_1 \cos\omega t + C_2 \sin\omega t)\left(\frac{2f}{r_1} \cot\eta/2 \cos\psi - \sin\theta\cos\phi\right)\right] \\ +\left[(A_1 \sin\omega t + A_2 \cos\omega t)\left(\frac{2f}{r_1} \cot\eta/2 \sin\psi - \sin\theta\sin\phi\right)\right. \\ \left. -(B_1 \cos\omega t + B_2 \sin\omega t)\left(\frac{2f}{r_1} \cot\eta/2 \cos\psi - \sin\theta\cos\phi\right)\right] \end{vmatrix} \tag{157}$$

Finally, after substitution of the expression for dA as given by Equation (9), the components of the field at point P assume the following forms:

$$XP = \cos\omega t \int_0^{2\pi} \int_{\eta_o}^{\pi} (-)\left[B_1 + C_1\left(\frac{2f}{r_1} \cot\eta/2 \sin\psi - \sin\theta\sin\phi\right)\right] \exp\{\{\frac{\sin\eta}{\sin^5\eta/2}\, d\eta\, d\psi \tag{158}$$

$$XQ = \sin\omega t \iint (-)\left[B_2 + C_2\left(\frac{2f}{r_1} \cot\eta/2 \sin\psi - \sin\theta\sin\phi\right)\right] \exp\{\{\frac{\sin\eta}{\sin^5\eta/2}\, d\eta\, d\psi \tag{159}$$

$$YP = \sin\omega t \iint \left[A_1 + C_2\left(\frac{2f}{r_1} \cot\eta/2 \cos\psi - \sin\theta\cos\phi\right)\right] \exp\{\{\frac{\sin\eta}{\sin^5\eta/2}\, d\eta\, d\psi \tag{160}$$

$$YQ = \cos\omega t \iint \left[A_2 + C_1\left(\frac{2f}{r_1} \cot\eta/2 \cos\psi - \sin\theta\cos\phi\right)\right] \exp\{\{\frac{\sin\eta}{\sin^5\eta/2}\, d\eta\, d\psi \tag{161}$$

and z-components which are neglected for $\theta < 5$ degrees.

Table II summarizes the symbols used in Equations (158) through (161).

Table II

Symbols for Equations (158) Through (161)

$$A_1 = -(Y_1' \sin \eta/2 + Z_2' \sin \psi \cos \eta/2)$$

$$A_2 = -(Y_2' \sin \eta/2 + Z_1' \sin \psi \cos \eta/2)$$

$$B_1 = +(X_1' \sin \eta/2 + Z_1' \cos \psi \cos \eta/2)$$

$$B_2 = +(X_2' \sin \eta/2 + Z_2' \cos \psi \cos \eta/2)$$

$$C_1 = +(X_1' \sin \psi \cos \eta/2 - Y_2' \cos \psi \cos \eta/2)$$

$$C_2 = +(X_2' \sin \psi \cos \eta/2 - Y_1' \cos \psi \cos \eta/2)$$

$$\exp\{\} = \exp.- jk \left(\left[r_1^2 + \frac{f^2}{\sin^4 \eta/2} - \frac{2 f r_1}{\sin^2 \eta/2} [\sin \eta \sin \theta \cos(\psi - \phi) + \cos \theta \cos \eta] \right]^{1/2} + \frac{f}{\sin^2 \eta/2} \right)$$

Polarization effects at point P can be computed by means of Equations (53) through (60), where now the total x-component of $\vec{H}_S\big|_P$ (circularly polarized feed system) is

$$X = (XP + jXQ) \tag{162}$$

and the total y-component is

$$Y = (jYP + YQ) \tag{163}$$

whereas, if the primary pattern is linearly polarized (for instance, only x-component applied),

$$X' = XP \tag{164}$$

$$Y' = YQ \tag{165}$$

Amplitudes and ellipticities for the Cassegrain system have been computed under various conditions and plotted. The results are found in Section V.

SECTION IV

COMPUTED RESULTS – FOCAL FEED SYSTEM

AMPLITUDES

Figures 9 through 25 are plots of the overall field amplitude at the observation point P as a function of elevation angle, θ, when the feed system is linearly polarized. Those plots are computed values of Equation (59). Those are plots of directivity rather than of gain, since no attempt was made to integrate and normalize the primary illumination. The peaks of the beams are always taken as the 0 db level, although – in certain cases – gain differences are indicated (Figure 16, 18 and 20 through 25). The actual orientation of the total field at point P is considered in detail in Figures 42 through 49. Quantities constant from graph to graph are the frequency (ω = 1288 Mc), and the paraboloid aperture (diameter = 30 ft).

Figures 9 through 14 show amplitude variations in the far-field, from graph to graph, as the primary illumination is varied in its basic distribution (equibeam, dipole-like, pseudo-equibeam) and the tapering function $h(\eta)$. Figure 15 pertains to changes in focal length. Figures 16 through 19 reflect amplitude variations, from graph to graph, caused by changes in the range of the observation point P. Finally, Figures 20 through 25 reflect amplitude variation changes as the surface of the paraboloid is perturbed.

Figure 9 whose tapering function is given by $\sin^2\eta/2\ h(\eta) = \sin^2\eta/2 \cos^{1.5}(\pi - \eta)$ (10 db taper, exclusive of the paraboloid range factor $\sin^2\eta/2$), can be considered as the case resulting from some "standard" primary illumination: equibeam, with taper at the edge of the dish optimum for gain, sidelobe level, and directivity considerations. The far-field beam

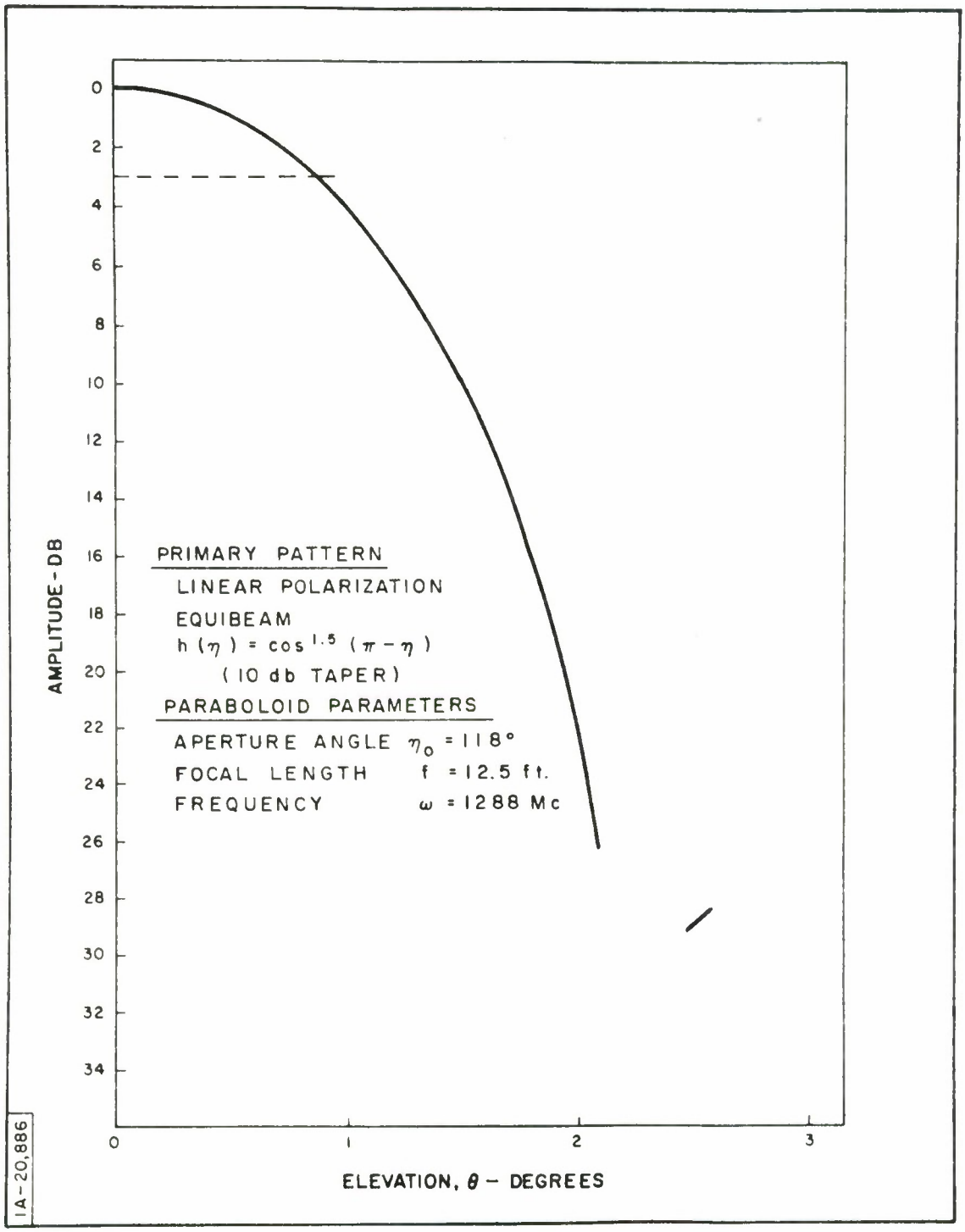

Figure 9. Focal Feed System: Amplitude Related to Primary Distribution (Far-Field)

is perfeetly symmetrieal (no azimuth variations) over the range of elevations considered. The 3-db half-beamwidth is 0.86 degrees. This graph ean be referred to Figures 13 and 14 which pertain to the same tapering function, but to dipole-like and pseudo-equibeam basie distributions, respectively.

In Figure 10, the basic distribution is dipole-like (H-field direetion along parallel "latitude" lines: H-field amplitude varying with azimuth). There is no taper, and the factor reflecting range variations from the phase center to the various points on the paraboloid (factor $\sin^2 \eta/2$) is not taken in consideration. The plots of this graph show that, in the far-field, the beam is not cylindrical. Since the paraboloid is illuminated more effectively in the H-plane than in the E-plane, the beam is narrower in the H-plane than in the E-plane. The H-plane 3-db half-beamwidth is 0.74 degrees, and the E-plane 3-db half-beamwidth is 0.825 degrees. Both values are smaller than the value of Figure 9, because of the absence of tapering.

In Figure 11, the distribution is dipole-like and the tapering function is implied in $\sin^2 \eta/2 \; h(\eta) = \cos \eta'$

where $\eta' = \dfrac{\pi}{2(\eta - \eta_o)} (\eta + \pi - 2\eta_o)$

The illumination function is essentially the same as in Figure 10, except that it is multiplied by an overall eosine funetion which tapers the amplitude to zero at the edge of the dish. This tapering results in an increase in beamwidth. The H-plane 3-db half-beamwidth is now 0.96 degrees, whereas the E-plane 3-db half-beamwidth is 1.05 degrees. Not shown in the graph is the fact that the sidelobe level is down, as eompared to Figure 10 (about 40 db down, for $\theta = 4.5$ degrees).

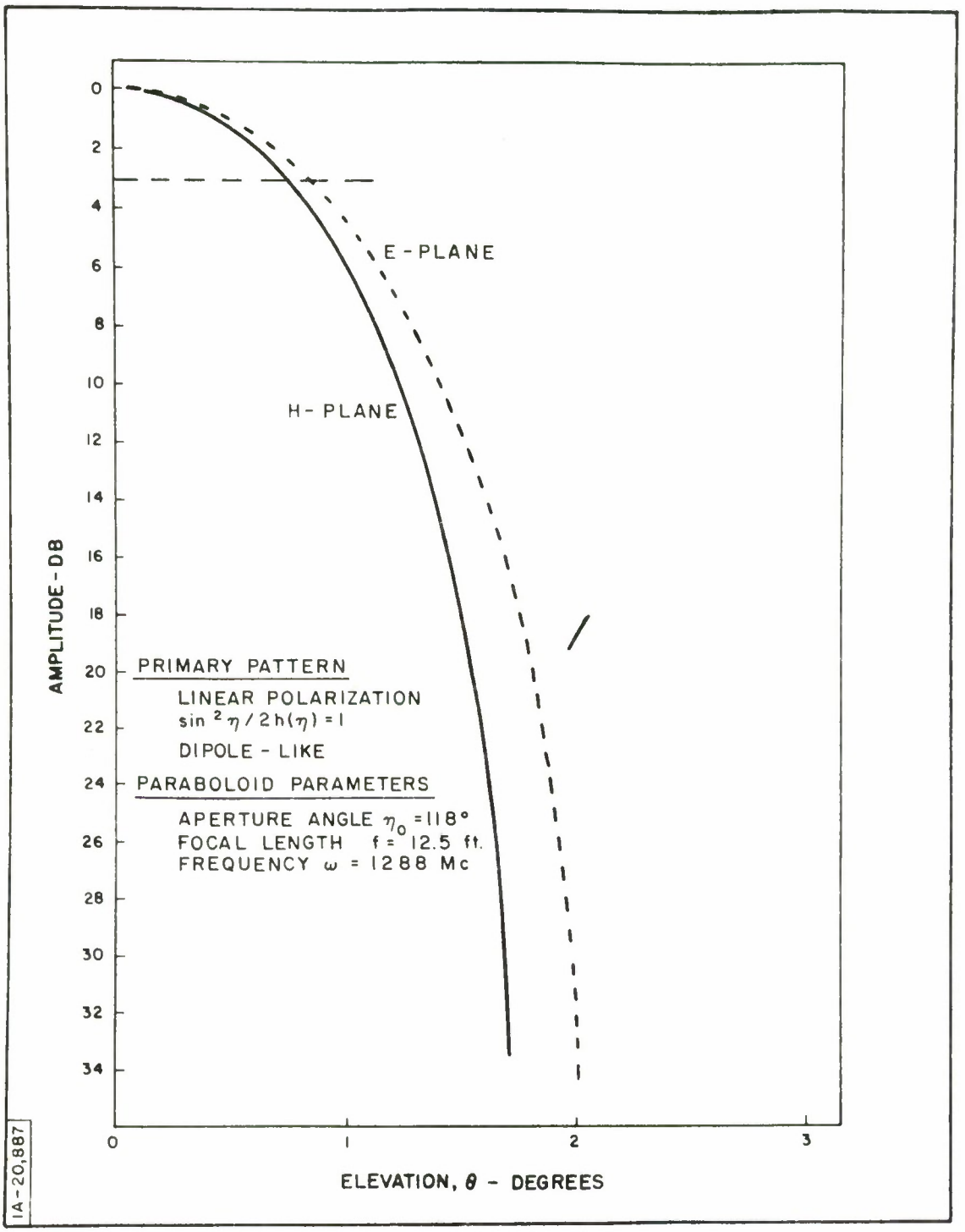

Figure 10. Focal Feed System: Amplitude Related to Primary Illumination (Far-Field)

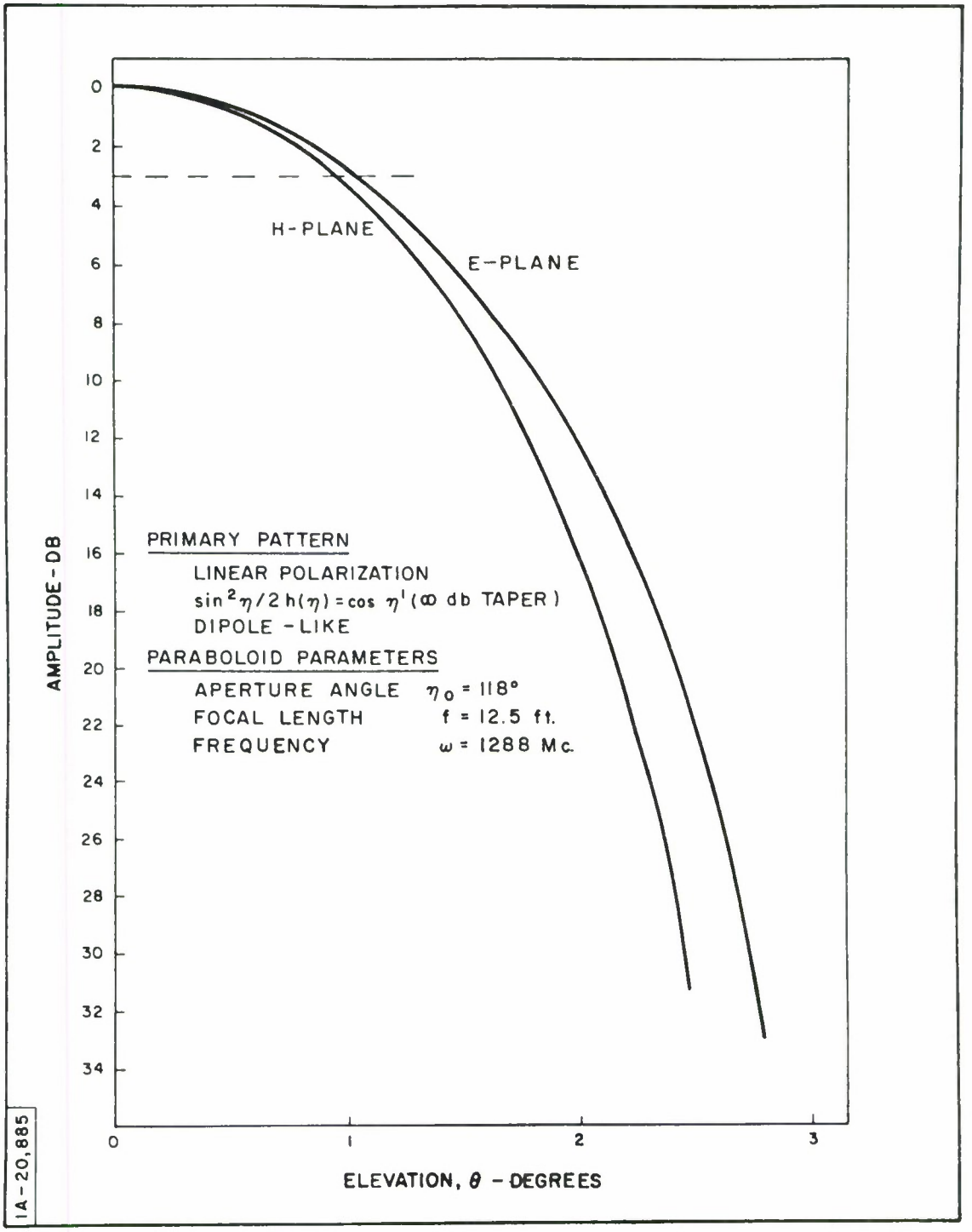

Figure 11. Focal Feed System: Amplitude Related to Primary Illumination (Far-Field)

In Figure 12, the distribution is dipole-like and $\sin^2 \eta/2\ h(\eta) = \cos^2 \eta'$. The primary illumination has the same character as in the preceding case, except that it is even more concentrated around the center of the paraboloid at the expense of the periphery region. The half-beamwidths are even wider: for the H-plane, it is 1.15 degrees, and for the E-plane, 1.24 degrees. Not shown in the graph is the fact that the sidelobe level becomes very low (about 60 db down, for $\theta = 5$ degrees).

In Figure 13, the illumination is dipole-like and

$$\sin^2 \eta/2\ h(\eta) = \sin^2/2 \cos^{1.5} (\pi - \eta)$$

This illumination corresponds to a 10 db taper (exclusive of range effect) as in Figure 9, but, because of the cos η variation in the E-plane, the actual taper in the E-plane is 16.5 db. The 3-db half-beamwidth for the H-plane, which is 0.84 degrees, is comparable to that of Figure 9. In the E-plane, the 3-db half-beamwidth is 0.95 degrees.

In the preceding graphs dealing with the dipole-like distribution (Figures 10 through 13), the beamwidth increases continuously from the H-plane to the E-plane where it becomes maximum. The beamwidth at the 45 degree plane is about half-way between the two extremes. In the case that follows, the situation is different and somewhat like that of Figure 9.

In Figure 14, the dipole-like distribution has been made "pseudo-equibeam" by making the amplitude of H independent of azimuth. However, the direction of the H-field is still held along parallel "latitude" lines, just as in the dipole-like distribution. As explained in Appendix D, the 45-degree planes on the paraboloid still contain "cross-polarized" current components. The tapering function is again $\sin^2 \eta/2\ h(\eta) = \sin^2 \eta/2 \cos^{1.5} (\pi - \eta)$, and now corresponds to a 10 db taper (exclusive of range effect) at the edge

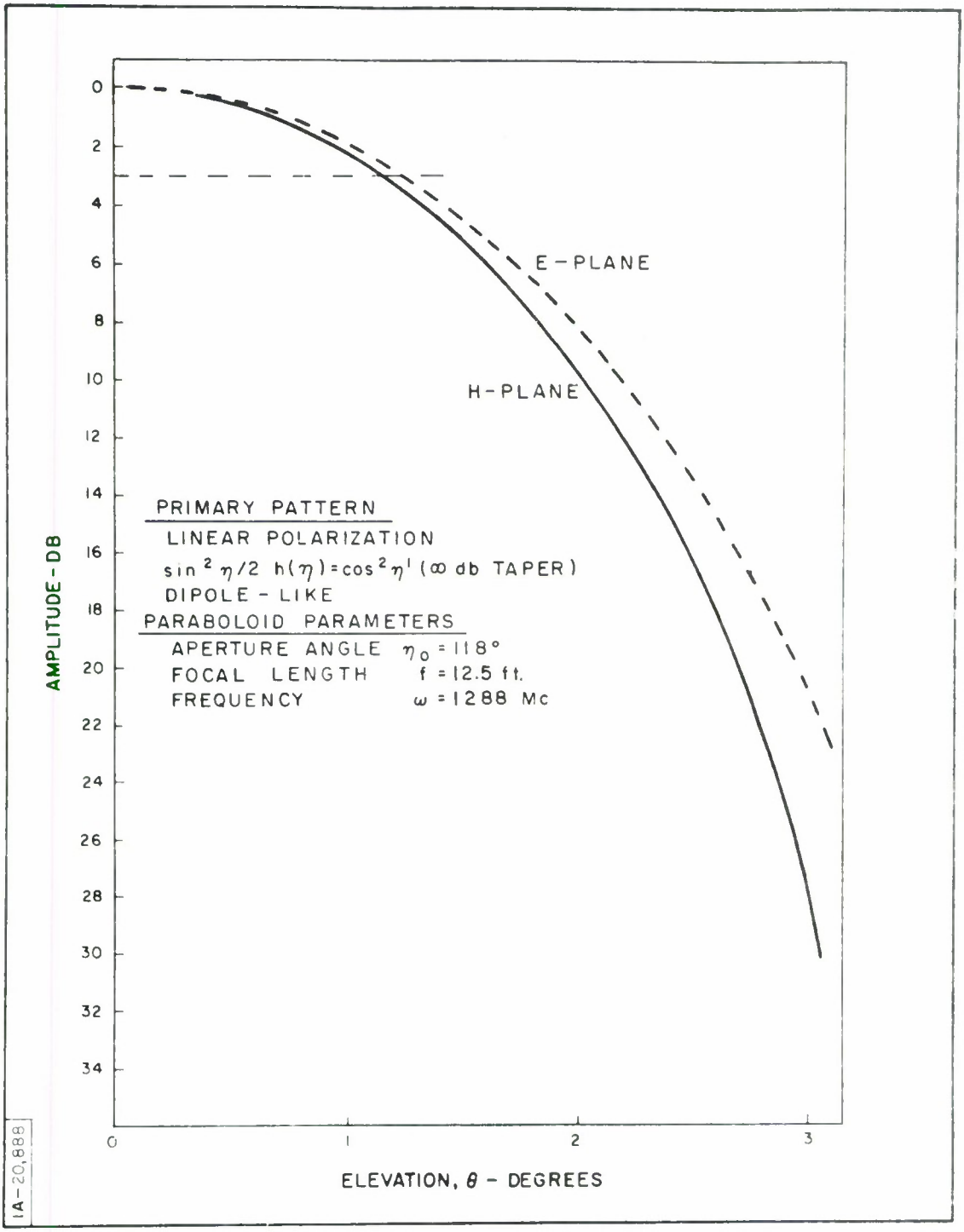

Figure 12. Focal Feed System: Amplitude Related to Primary Illumination (Far-Field)

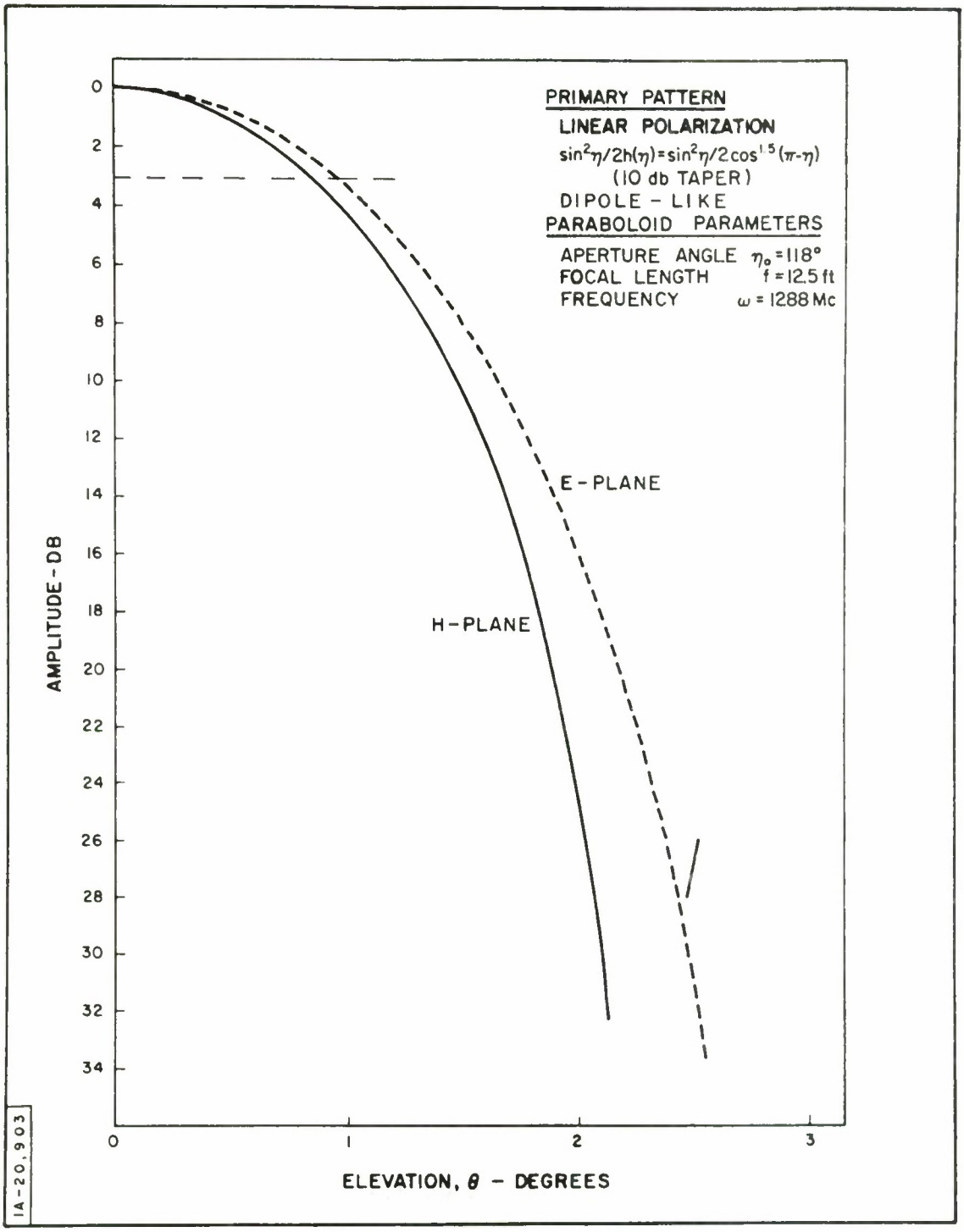

Figure 13. Focal Feed System: Amplitude Related to Primary Illumination (Far-Field)

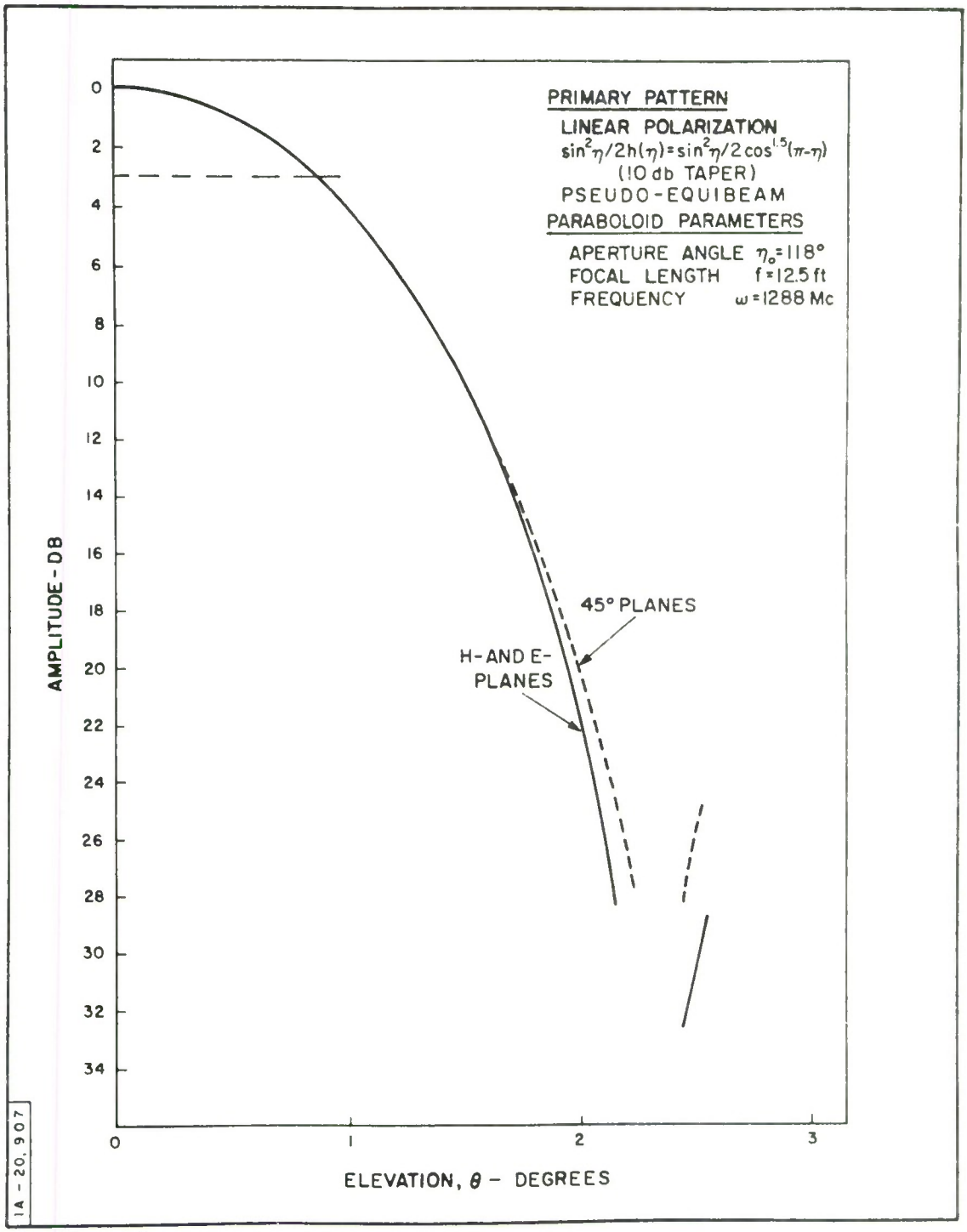

Figure 14. Focal Feed System: Amplitude Related to Primary Illumination (Far-Field)

of the dish, independent of azimuth. It is noted that the H- and E-plane 3-db half-beamwidths are equal to each other and to the value obtained in Figure 9. However, about 12 db below the peak of the beam on boresight, the beam no longer exhibits cylindrical symmetry. It broadens more in the 45-degree planes than in either the H- or E-planes.

In Figure 15, interest shifts to the effects of focal length on amplitude for the dipole-like distribution. The plots pertain to paraboloids having the same apertures as in the preceding cases (30 ft), but with focal lengths increased from 12.5 ft to 29.7 ft and to 68 ft. By Equation (176), it is found that the aperture angles, η_o, are respectively 151.6 and 167.4 degrees. The tapering used in the plots is of the form

$$\sin^2 \eta/2\, h(\eta) = \sin^2 \eta/2 \cos^{1.5}(\pi - \eta)$$

to correspond to Figure 13. However, the η-variation is so small (from 151.6 degrees and 167.4 degrees to 180 degrees) that Figure 15 is better referred to Figure 10. Because the illumination is now almost constant and equal in both H- and E-planes and thus approaches the equibeam condition, the far-field H- and E-plane patterns are essentially equal and, for the 68-ft focal length case, the beam exhibits cylindrical symmetry down to 30 db. The 3-db half-beamwidths, which are 0.80 degrees, fall between the H-plane and E-plane half-beamwidths of Figure 10.

Figures 16 through 19 exhibit the effect of range at the observation point, P, on the amplitude pattern.

Figure 16 (equibeam, 10 db taper; see Figure 9) compares the amplitude in the far-field to the amplitude at a 400-ft range. At 400 ft, the 3-db

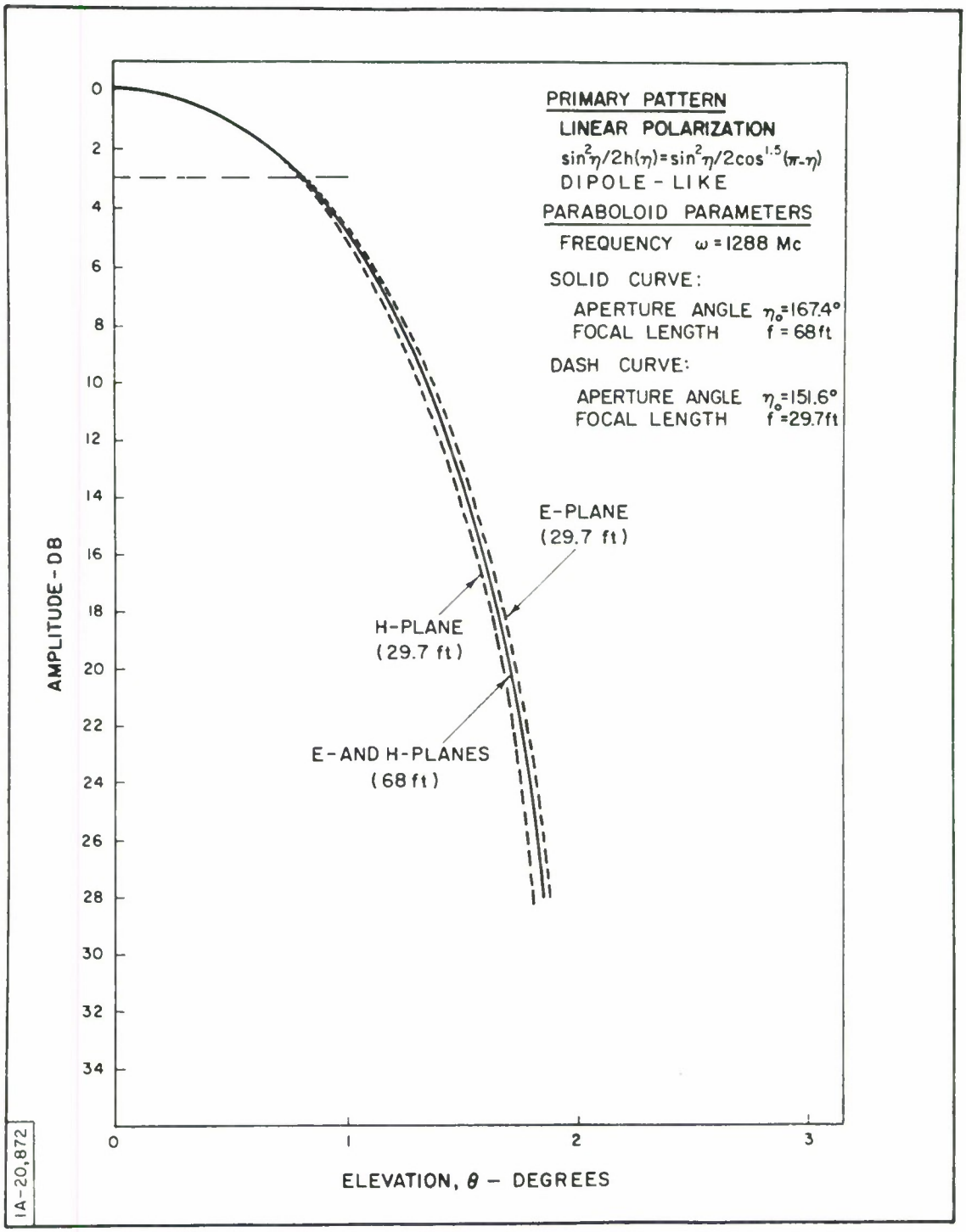

Figure 15. Focal Feed System: Amplitude Related to Focal Length (Far-Field)

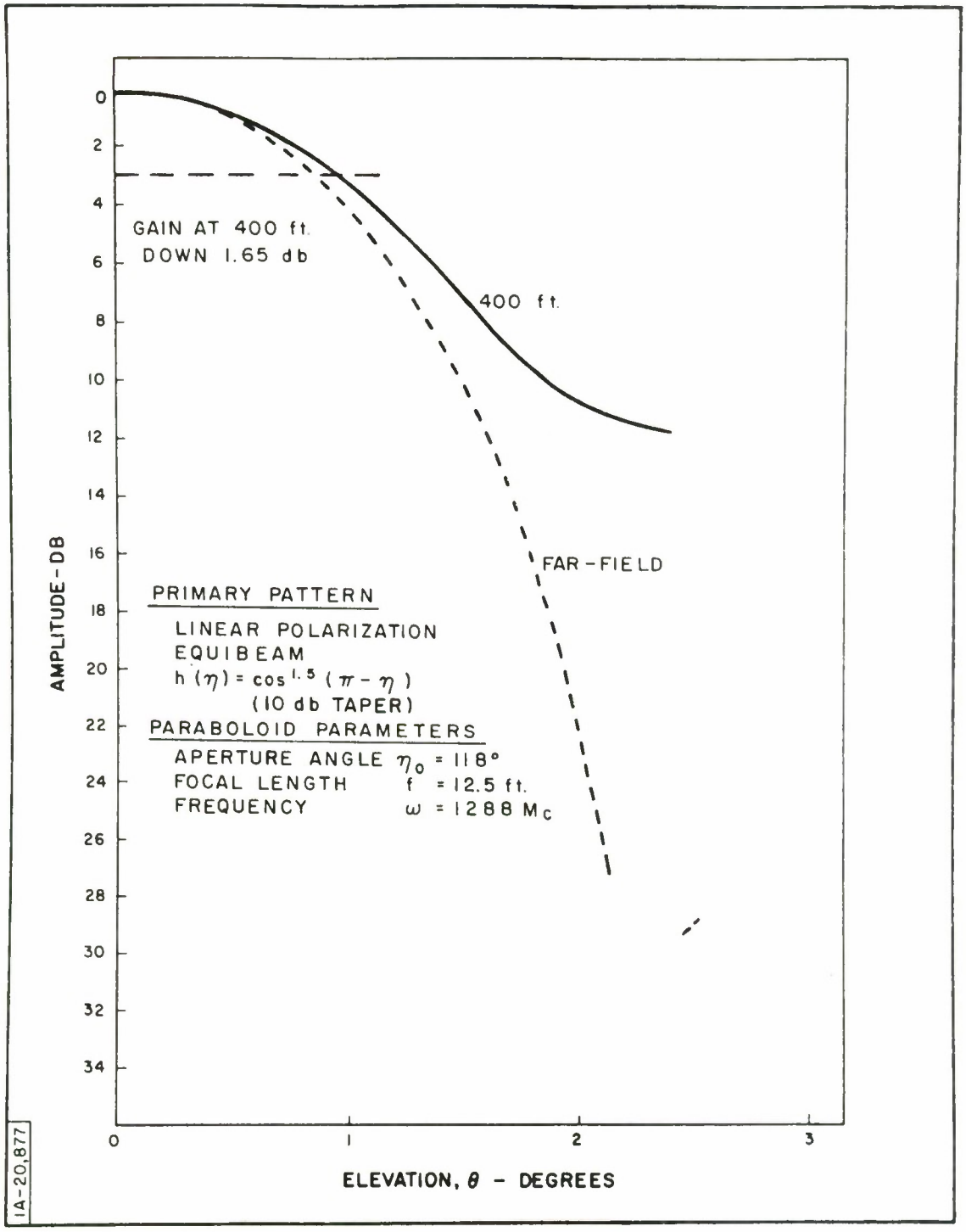

Figure 16. Focal Feed System: Amplitude Related to Range

half-beamwidth is increased from 0.86 degrees to 9.95 degrees. The null is filled in and shifted toward a larger elevation angle. Gain on boresight is down 1.65 db.

Figure 17 corresponds to the same illumination as Figure 10, but the range of point P is taken at 400 ft, 300 ft, and 200 ft. Near boresight, and roughly within the 3-db points, the character of the curves is about the same for ranges of 400 ft and 300 ft as for the far-field. However, the far-field "nulls" fill in rapidly as the range decreases. For the 200-ft range, the character of the curve is lost, and the former "nulls" are almost as high as the beam on boresight, in anticipation of "beam splitting" at a probably slightly closer range.

Figure 18 compares the amplitude pattern at a range of 400 ft to the amplitude pattern in the far-field, for the dipole-like, 10-db taper illumination. The near-field pattern is characterized by a broadening of the 3-db beamwidth and a "filling-in" of the null region.

Figure 19 compares the amplitude pattern at a range of 400 ft to the amplitude pattern in the far-field for the pseudo-equibeam, 10 db taper illumination. Qualitatively, the same characteristics of Figures 16 and 18 apply to this graph: slight broadening of the beamwidth, "filling-in" of the null region.

Figures 20 through 25 reflect amplitude variations (or lack thereof) when the paraboloidal surface is perturbed.

In Figures 20, 21, and 22, randomly distributed imperfections on the paraboloidal surface are simulated by letting the focal length, f, become a function of η and ψ. Thus, in the integration process, to each point (η_i , ψ_j) corresponds

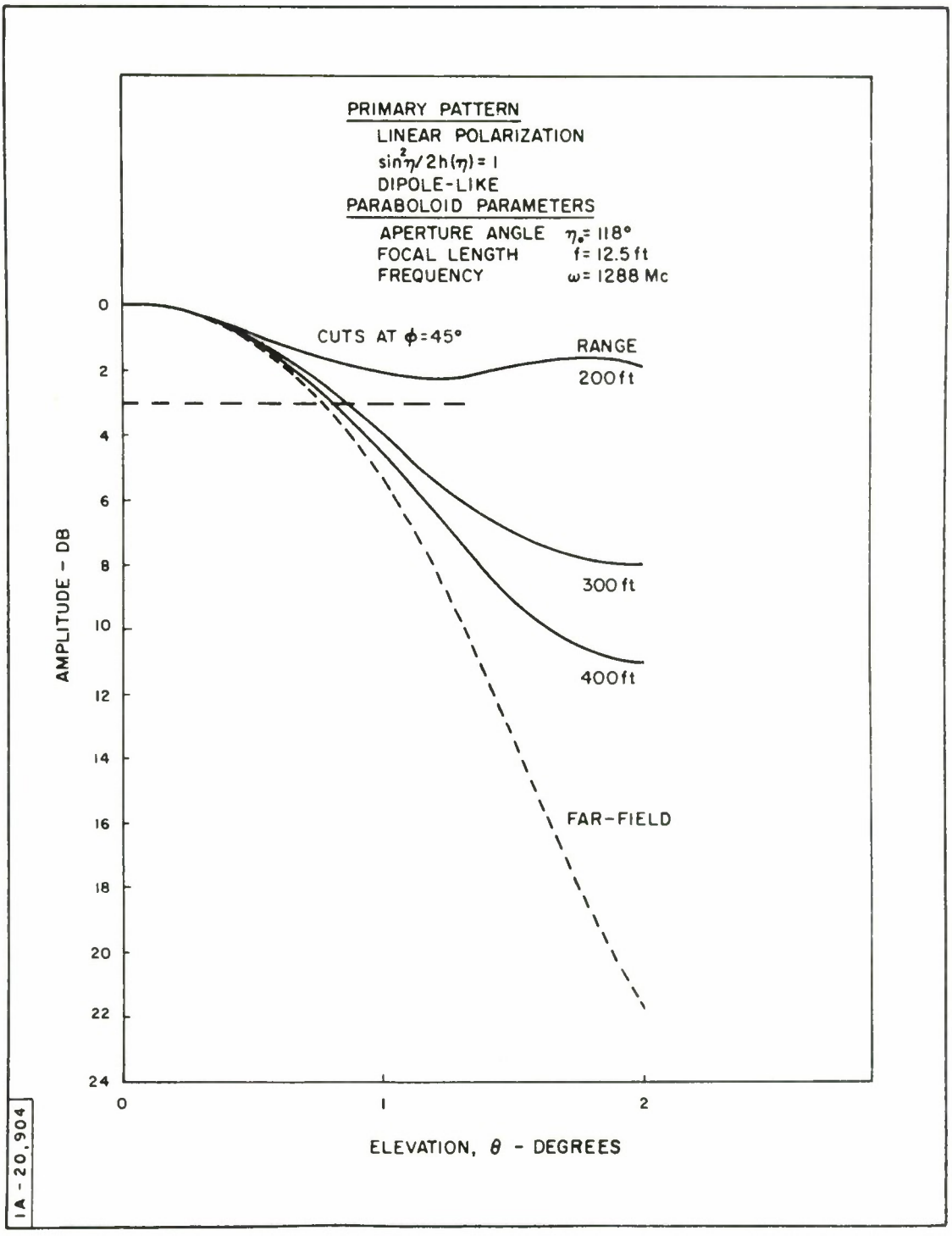

Figure 17. Focal Feed System: Amplitude Related to Range

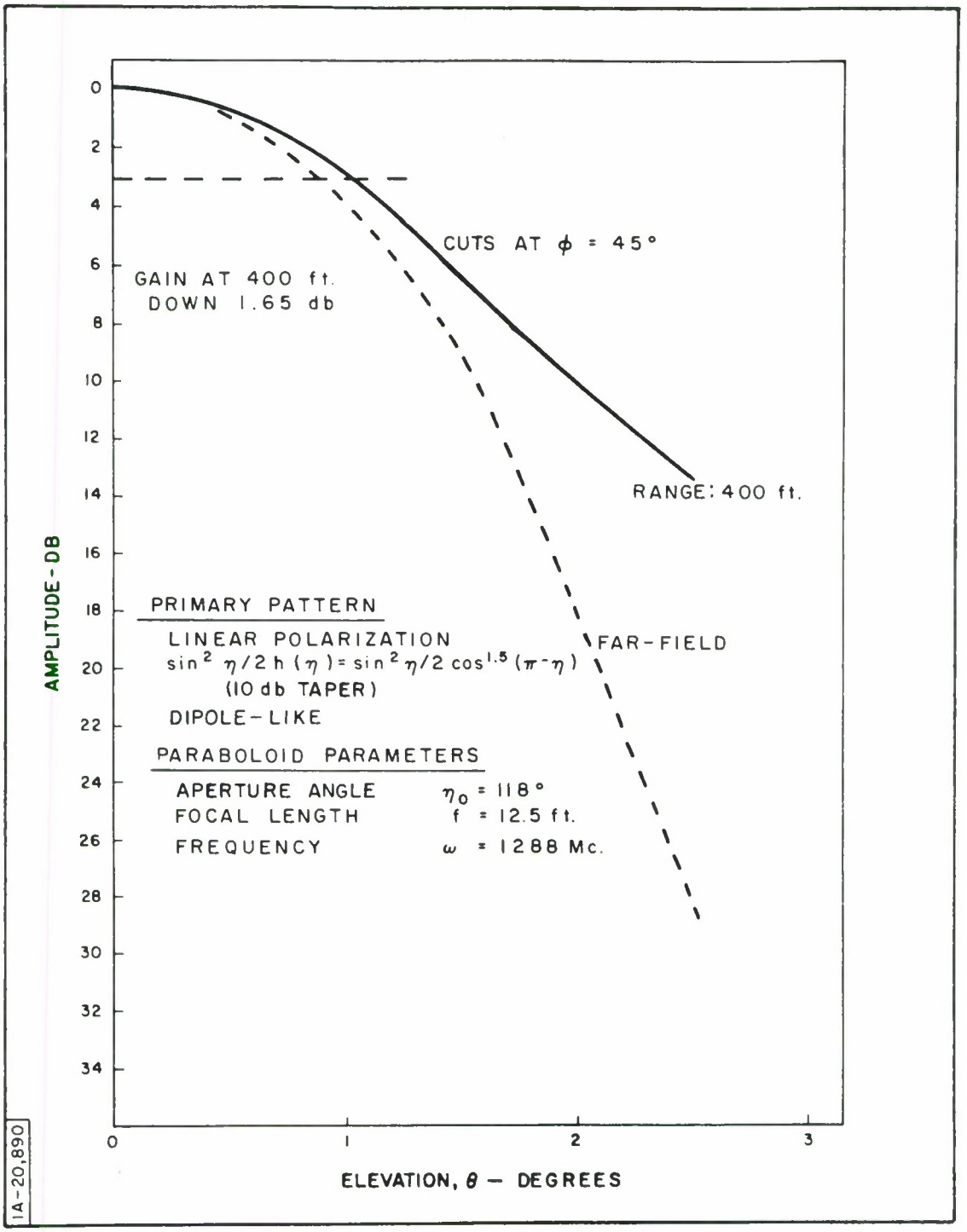

Figure 18. Focal Feed System: Amplitude Related to Range

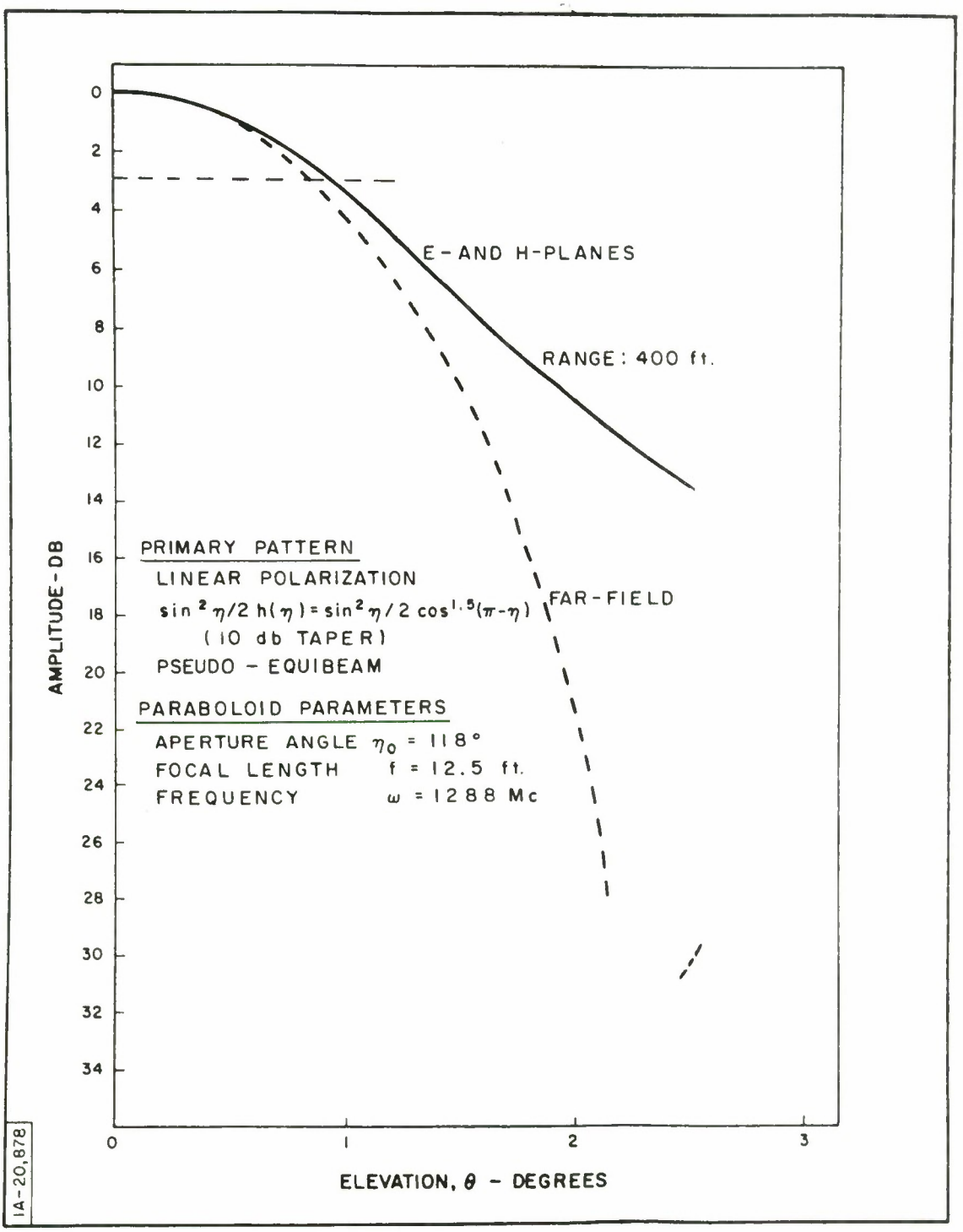

Figure 19. Focal Feed System: Amplitude Related to Range

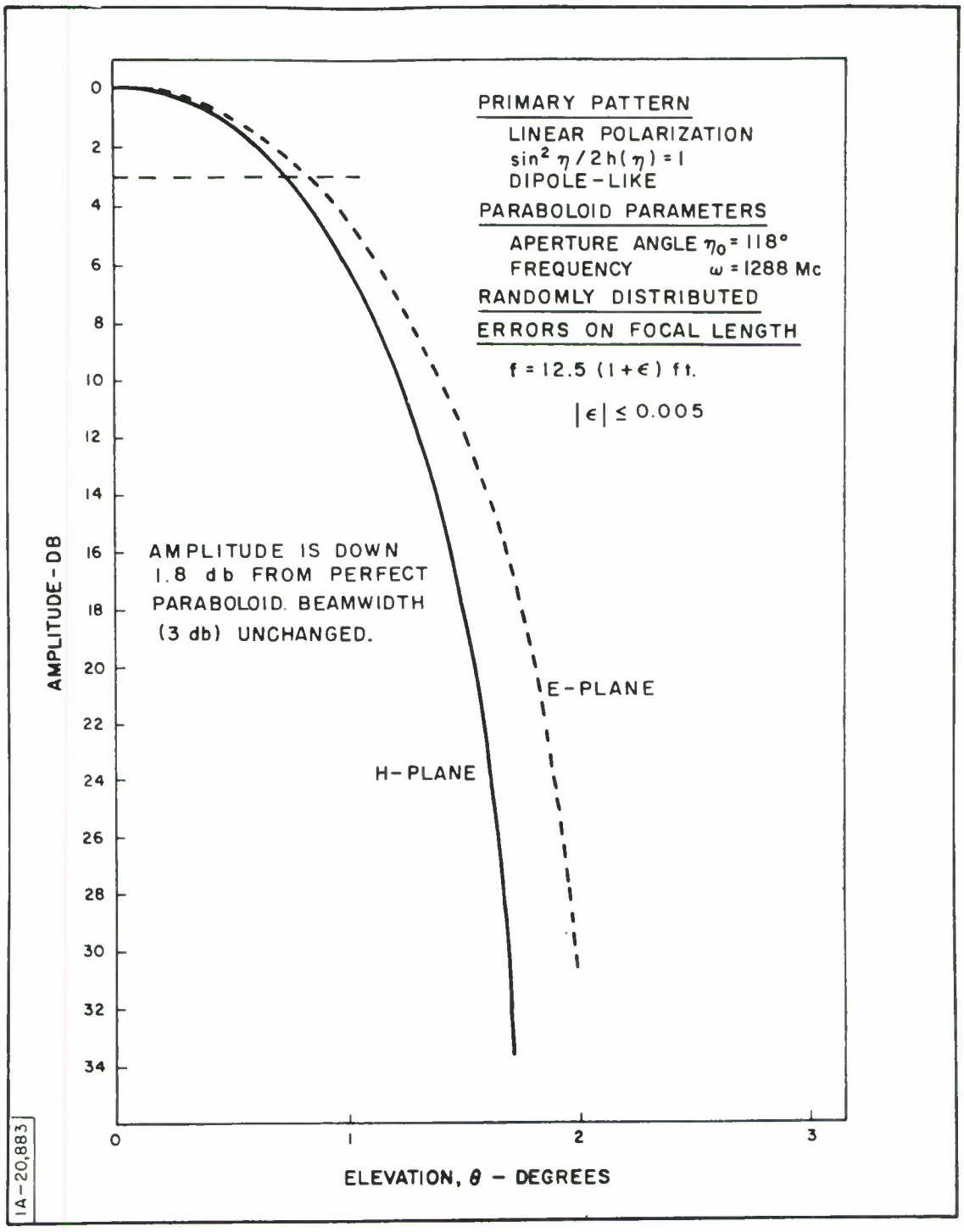

Figure 20. Focal Feed System: Amplitude Related to Paraboloid Imperfections (Far-Field)

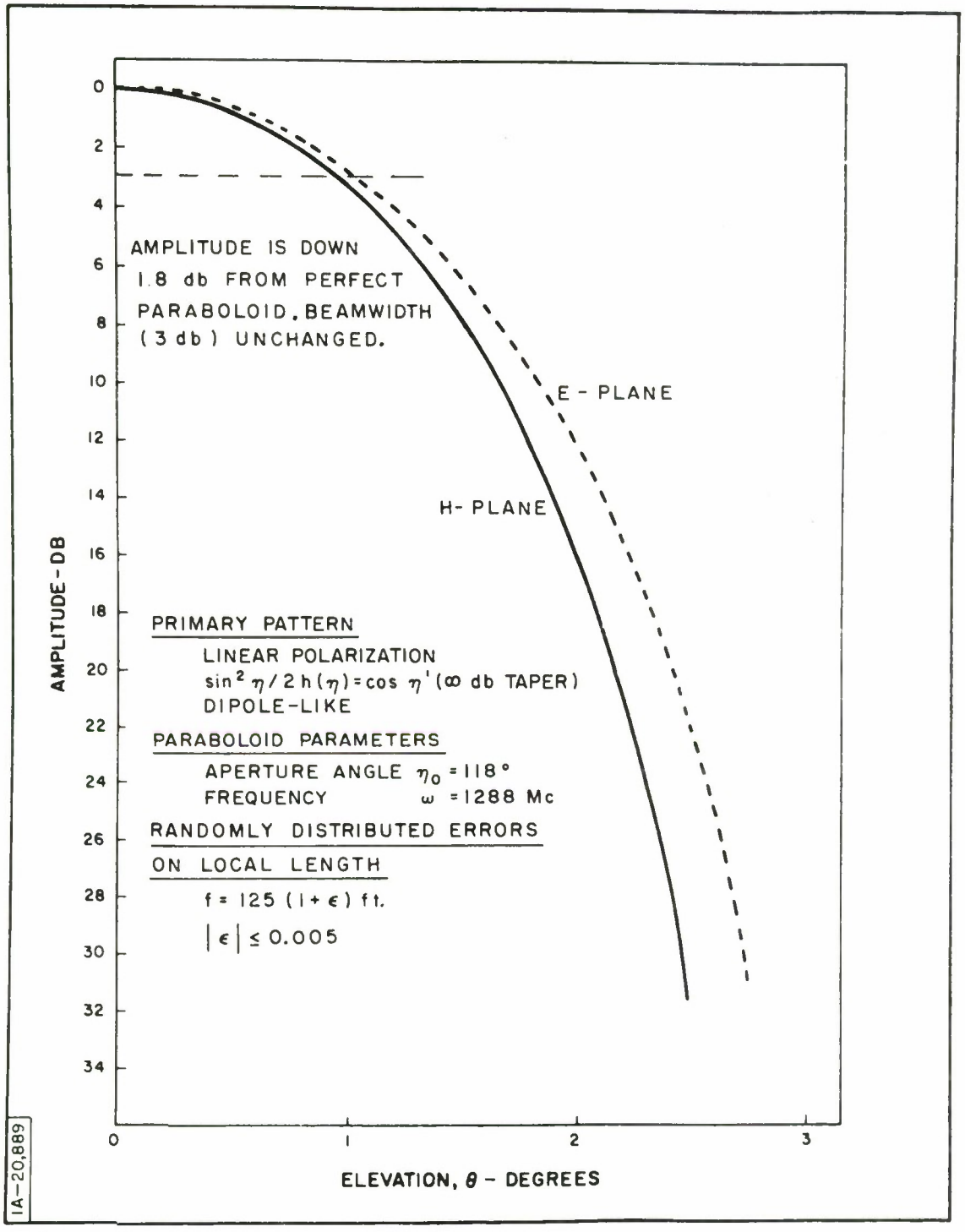

Figure 21. Focal Feed System: Amplitude Related to Paraboloid Imperfections (Far-Field)

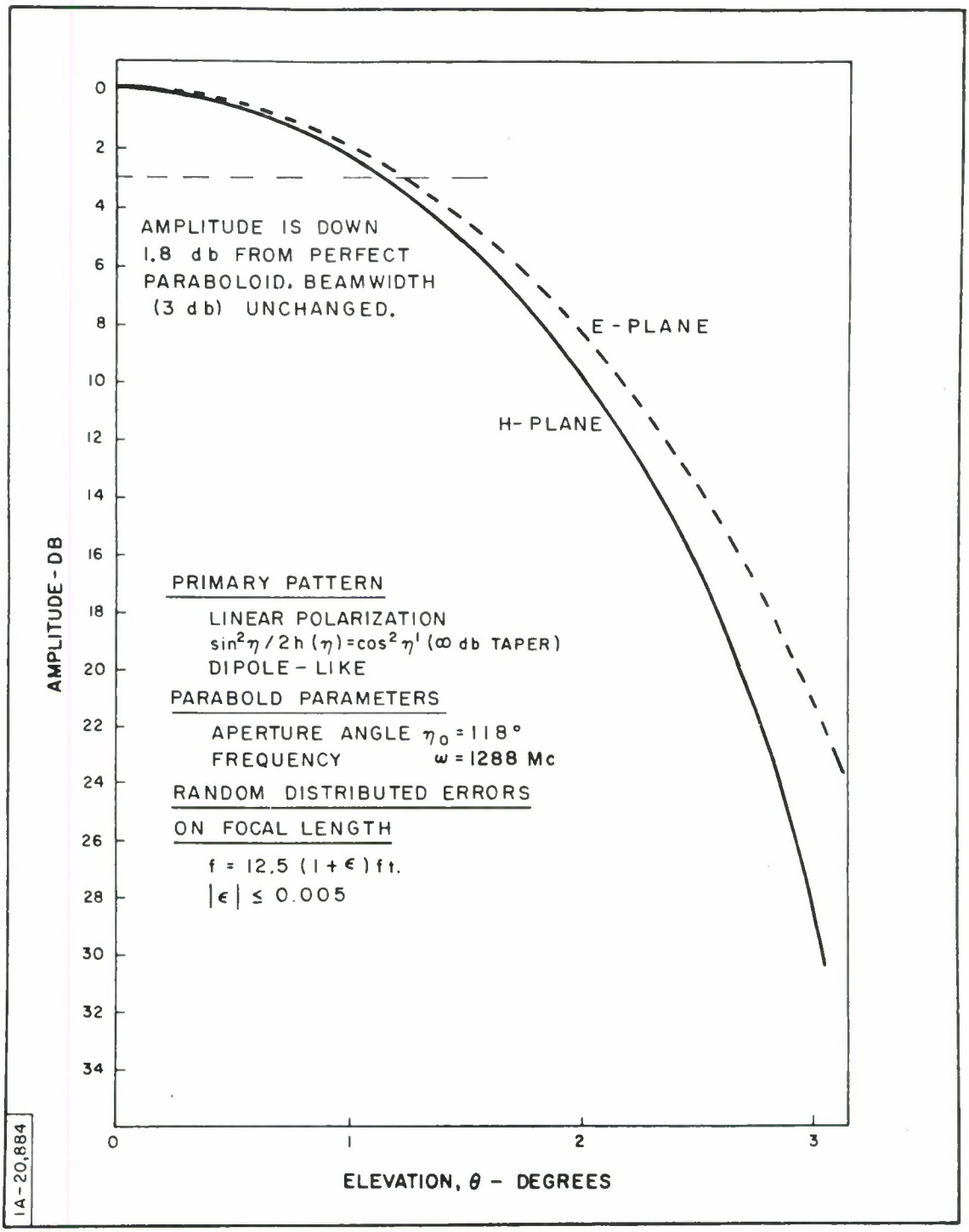

Figure 22. Focal Feed System: Amplitude Related to Paraboloid Imperfections (Far-Field)

$$f_{i,j} = f(\eta_i, \psi_j)$$

The function

$$f_{i,j} = (1 + \epsilon_{ij})\, f$$

$$= (1 + \epsilon_{ij})\ 12.5 \text{ ft}$$

has been generated and stored, and it is the same one that is used in Figures 20 through 22. The error (or imperfection) function ϵ_{ij} is randomly distributed, but limited such that

$$|\epsilon_{ij}| \leq 0.005$$

Consequently, the maximum deviation on f is

$$0.005 \times 12.5 \text{ ft} = \pm 0.75''$$

$$\text{or} \qquad \pm 0.082\ \lambda$$

$$\text{or} \qquad \pm 30 \text{ degrees}$$

The far-field approximation equations must be used cautiously. Thus, the term e^{-j2kf} (neglected from Equation (41)) must be brought back under the integral sign, since it is no longer a constant.

The illumination functions used in Figures 20, 21 and 22 are, respectively, those of Figures 10, 11, and 12. The amplitude patterns are strikingly similar to those of the unperturbed surfaces (same beamwidth, same null regions). However, the level of the curves (the gain) is down 1.8 db from the levels of the unperturbed cases. *

*See Dr. Ruze's findings, NEREM Record, 1964, pp. 166-167.

For Figures 23, 24, and 25, the focal length was made to vary discontinuously as a function of ψ only, in a random manner. Thus, each equal pie-shaped slice, covering 15 degrees, has a random (but bounded) focal length, given by

$$f_i = f(\psi_i) \quad , i = 1, 2, \ldots, 24$$

$$= [1 + \epsilon(\psi_i)]\ 12.5 \text{ ft}$$

Since there are only 24 values of $[1 + \epsilon(\psi_i)]$, they are listed in the following table:

Table III

Values of $[1 + \epsilon(\psi_i)]$ *

0.998878	0.995612	1.003482	0.995667	0.995607	0.995452
0.999624	0.999905	0.995332	0.999547	1.000148	0.998926
0.998794	1.002547	1.000484	0.998315	1.003611	0.998473
0.997937	0.998034	1.004276	1.000725	1.001686	1.002419

The illumination functions used in Figures 23, 24 and 25 are, respectively, those used in Figures 10, 11, and 12. The amplitude patterns show gross distortions as the amplitude varies considerably as a function of φ, although it is noteworthy that the "average" 3-db half-beamwidths remain about the same as in the corresponding cases of the perfect paraboloid. On boresight, the amplitudes are down 1.35 db from those corresponding to the perfect paraboloid. Another salient feature of all three plots is that the maximum amplitude is reached for $\theta = 0.25$ degrees rather than on boresight. Hence, a "pointing error" is introduced by the pie-shaped segments of unequal focal length. **

* Read across.

**The reason is that the 24 values of Table I are "randomly "but not "evenly" distributed.

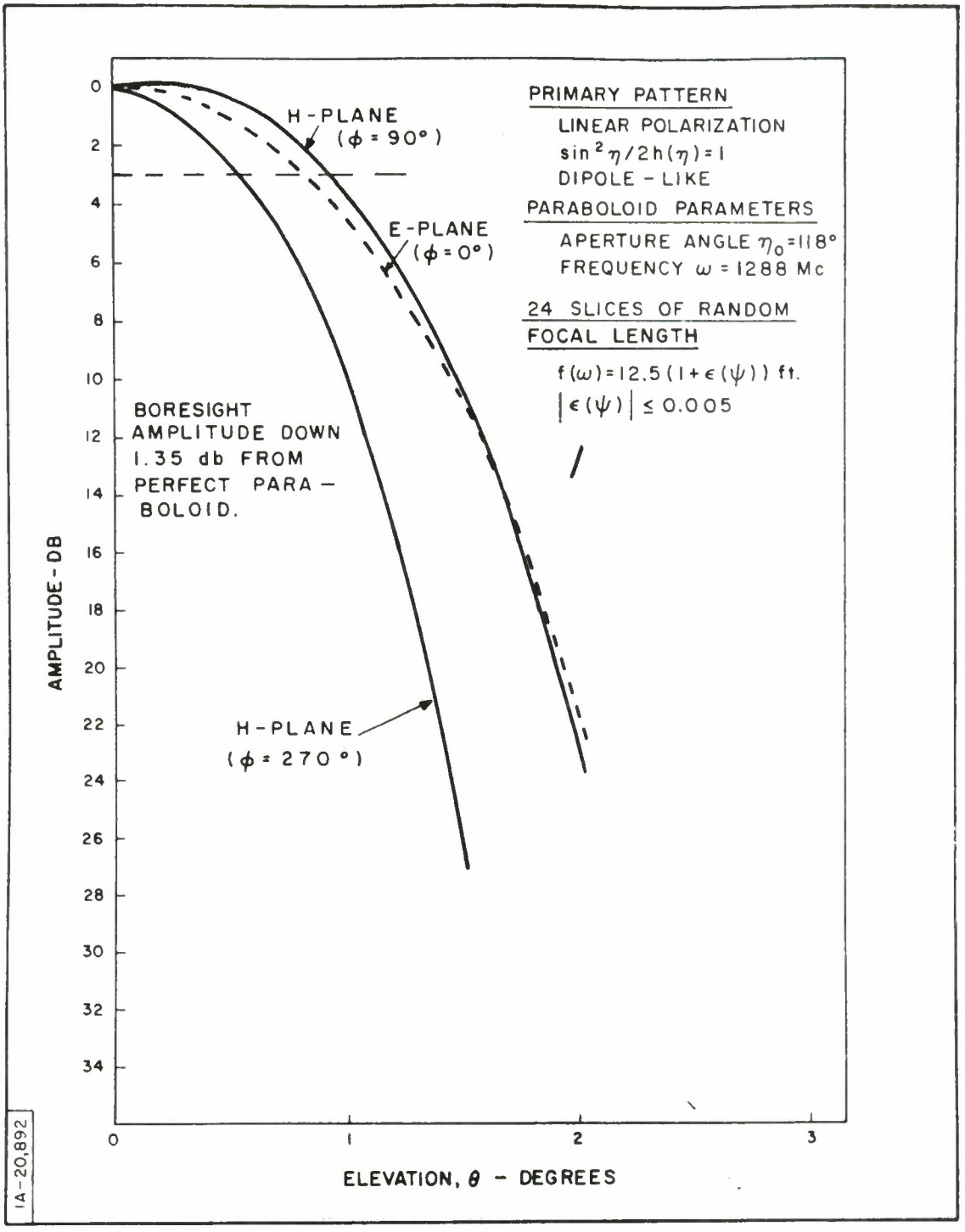

Figure 23. Focal Feed System: Amplitude Related to Paraboloid Imperfections (Far-Field)

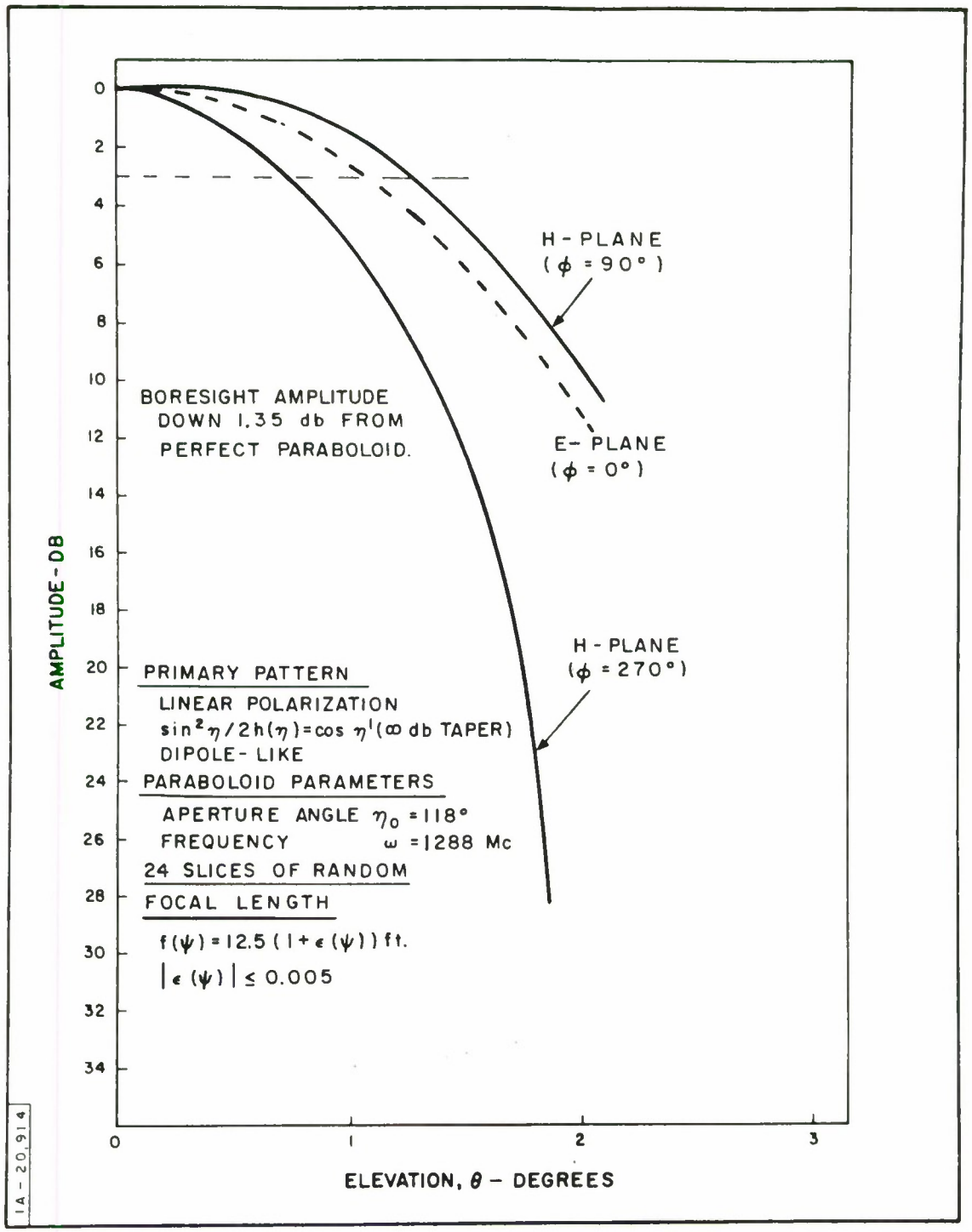

Figure 24. Focal Feed System: Amplitude Related to Paraboloid Imperfections (Far-Field)

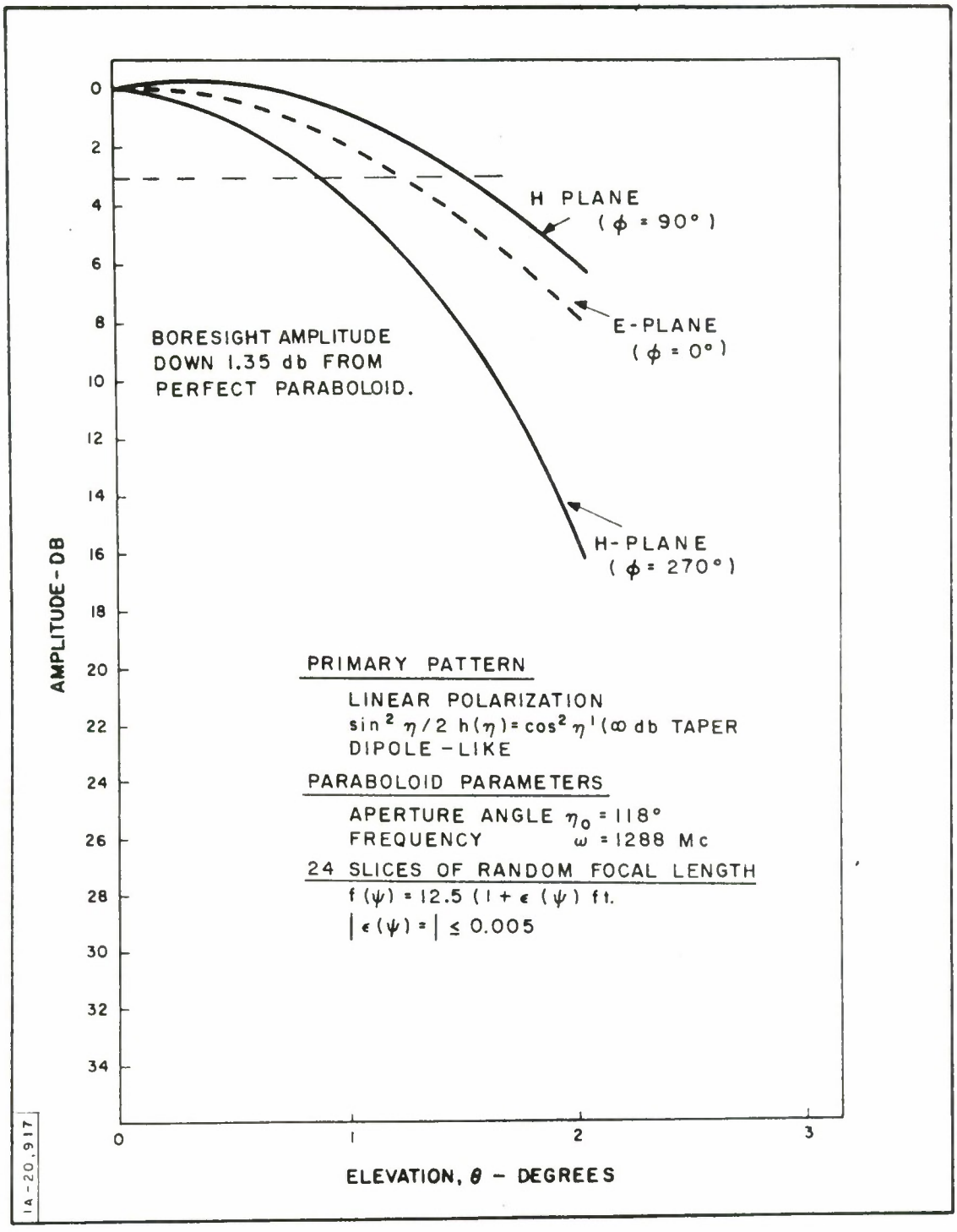

Figure 25. Focal Feed System: Amplitude Related to Paraboloid Imperfections (Far-Field)

ELLIPTICITIES

Figures 26 through 42 are plots of ellipticity at the observation point, P , as a function of the elevation angle, θ , when the feed system is circularly polarized. These plots are computed values of Equation (56). Quantities constant from graph to graph are the frequency (ω = 1288 Mc), and the paraboloid aperture (diameter = 30 ft).

Figures 26 through 31 show ellipticity variations, in the far-field, from graph to graph, as the primary illumination is varied. The various illumination conditions correspond, respectively, to Figures 9 through 14. Figure 32 pertains to a change in focal length and is the companion to Figure 15, which depicted amplitude changes. Figures 33 through 36 reflect ellipticity variations, from graph to graph, caused by changes in the range of the observation point, P. Finally, Figures 37 through 42 reflect changes in ellipticity as the surface of the paraboloid is perturbed.

Figure 26, where the taper function is $h(\eta) = \cos^{1.5}(\pi - \eta)$, can be considered as the case resulting from the "ideal" primary illumination: equibeam distribution, with a 10 db taper at the edge of the dish (exclusive of the effect of range variations from the phase center to the various points on the paraboloid). Ellipticity in the far-field is 0 db on boresight and remains less than 0.03 db at the 3-db half-beamwidth. Although there are no cross-polarized current components on the paraboloid, there are z-directed currents whose origins partake of both quadrature components. As a result, ellipticity increases as the elevation angle θ opens up. Although the extraordinary circular component is small and increases slowly with θ , ellipticity is enhanced near the null where the ordinary circular component dips to low values.

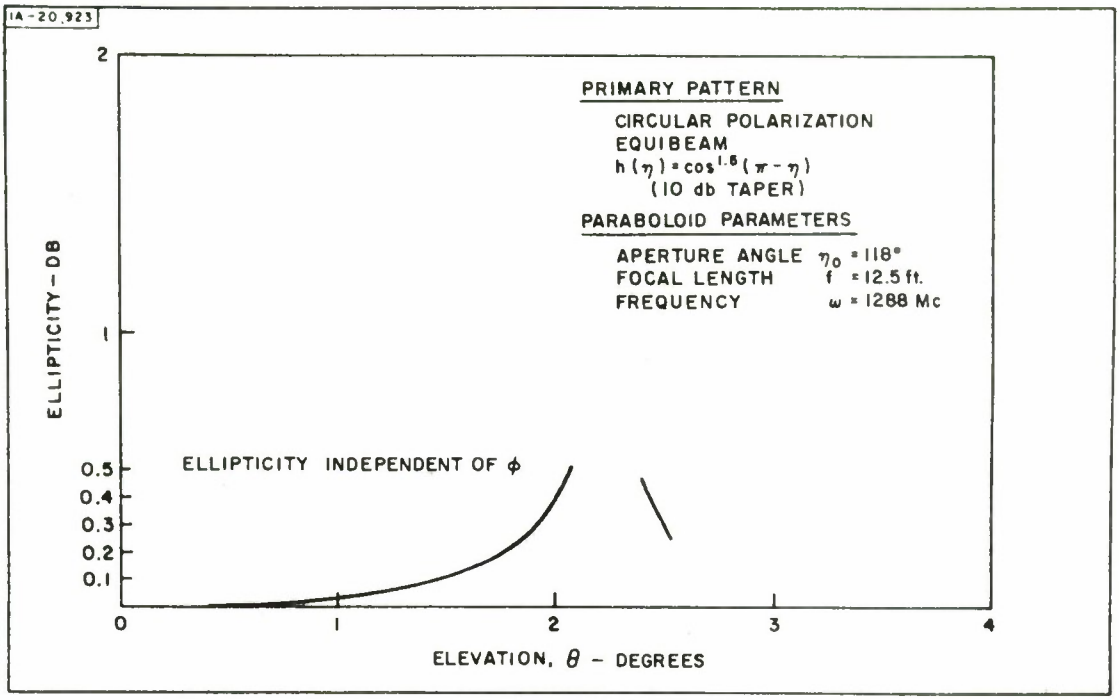

Figure 26. Focal Feed System: Ellipticity Related to Primary Distribution (Far-Field)

In Figure 27, the basic distribution is dipole-like, and $\sin^2 \eta/2\ h(\eta) = 1$, as in Figure 10. As shown in Section II, the ellipticity is 0 db on boresight, and, for a given elevation angle, is independent of the azimuth angle φ. The ellipticity increases first slowly, and then more rapidly, away from boresight. It is about 0.8 db for the average 3-db half-beamwidth. (Note the change of scale from Figure 26.) Ellipticity becomes very large and tends toward infinity (linear polarization) at the elevation region corresponding to the first null. Then, ellipticity decreases and tends again toward 0 db, as the observation point moves toward the peak of the first sidelobe.

In Figure 28, the distribution is dipole-like, and the taper function is implied in $\sin^2 \eta/2\ h(\eta) = \cos \eta'$, as in Figure 11. Again, ellipticity is 0 db on boresight, and again it is independent of φ for any given value of θ. The tapering of the illumination function proves beneficial to the

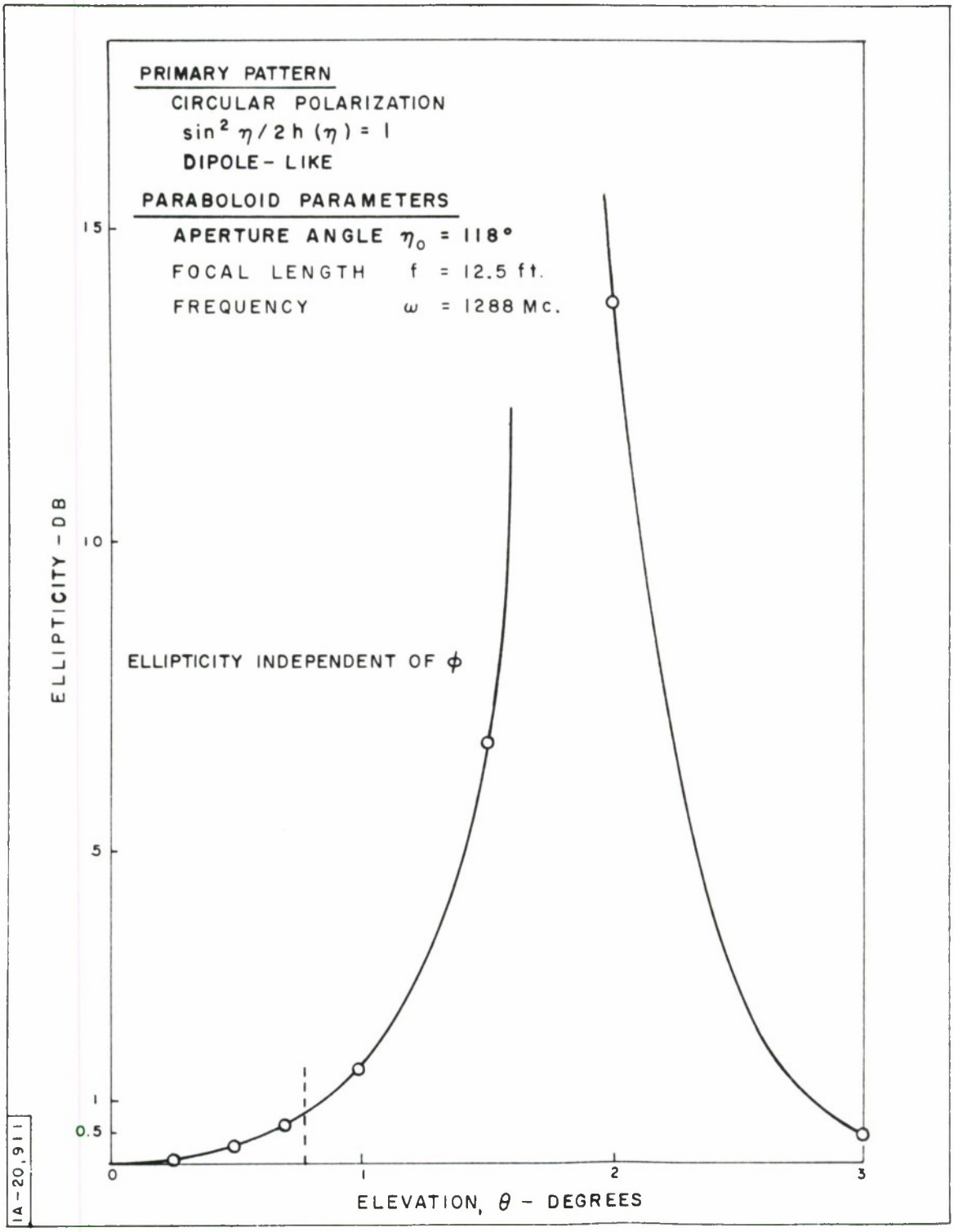

Figure 27. Focal Feed System: Ellipticity Related to Primary Illumination (Far-Field)

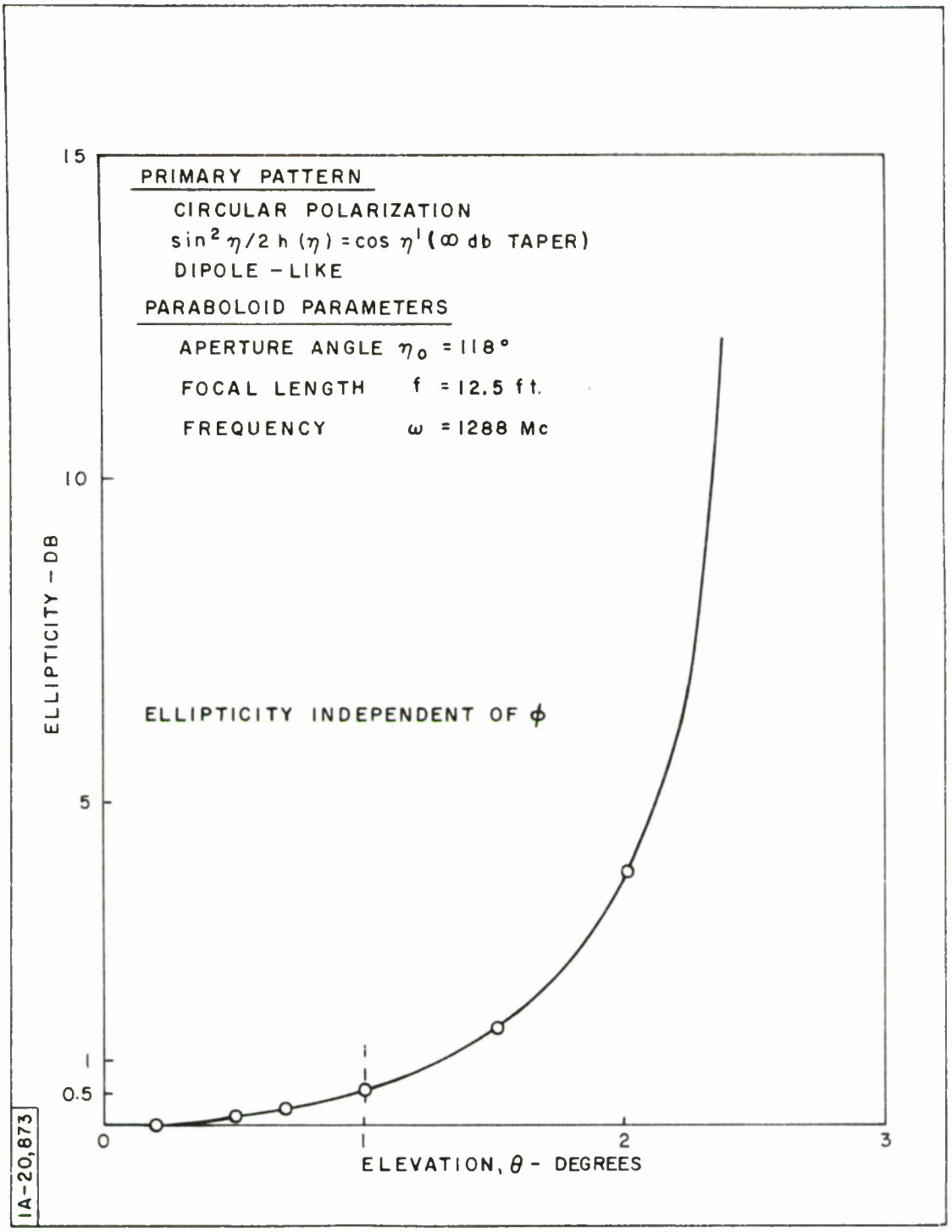

Figure 28. Focal Feed System: Ellipticity Related to Primary Illumination (Far-Field)

ellipticity since the region near the periphery of the dish which contributes most to the ellipticity (Equations (47) and (50)) is less fully utilized. Ellipticity corresponding to the average 3-db half-beamwidth is now 0.55 db.

In Figure 29, the distribution is dipole-like, and the taper function is $\sin^2 \eta / 2h(\eta) = \cos^2 \eta'$, as in Figure 12. Ellipticity is 0 db on boresight and is independent of φ for any value of θ. The tapering of the illumination function being even more pronounced than in the preceding graph, the ellipticity corresponding to the 3-db half-beamwidth is only 0.4 db.

In Figure 30, the distribution is dipole-like and the taper function is $h(\eta) = \cos^{1.5}(\pi - \eta)$ as in Figure 13. Ellipticity is 0 db on boresight and is independent of φ for any value of θ. The primary illumination being better utilized than in Figures 28 and 29, but not quite as well as in Figure 27, the ellipticity corresponding to the 3-db half-beamwidth is 0.7 db. It tends to increase near the null and decrease toward 0 db for an elevation angle corresponding to the peak of the first sidelobe.

In Figure 31, the distribution is now pseudo-equibeam, and the taper function is $h(\eta) = \cos^{1.5}(\pi - \eta)$ as in Figure 14. The character of the ellipticity versus elevation angle is changed drastically. It is now a function of φ and is essentially 0 db in the H- and E-planes for any value of θ. However, it reaches a maximum value in the 45-degree planes: there are now preferred planes corresponding to the planes on the spherical wavefront where the field is circularly polarized (quadrature components equal and orthogonal) and other planes where the ellipticity is maximum (quadrature components equal but of maximum space angle). It is noteworthy that the maximum ellipticity is essentially that of Figure 30 and that, in particular, the ellipticity corresponding to the 3-db half-beamwidth is also 0.7 db.

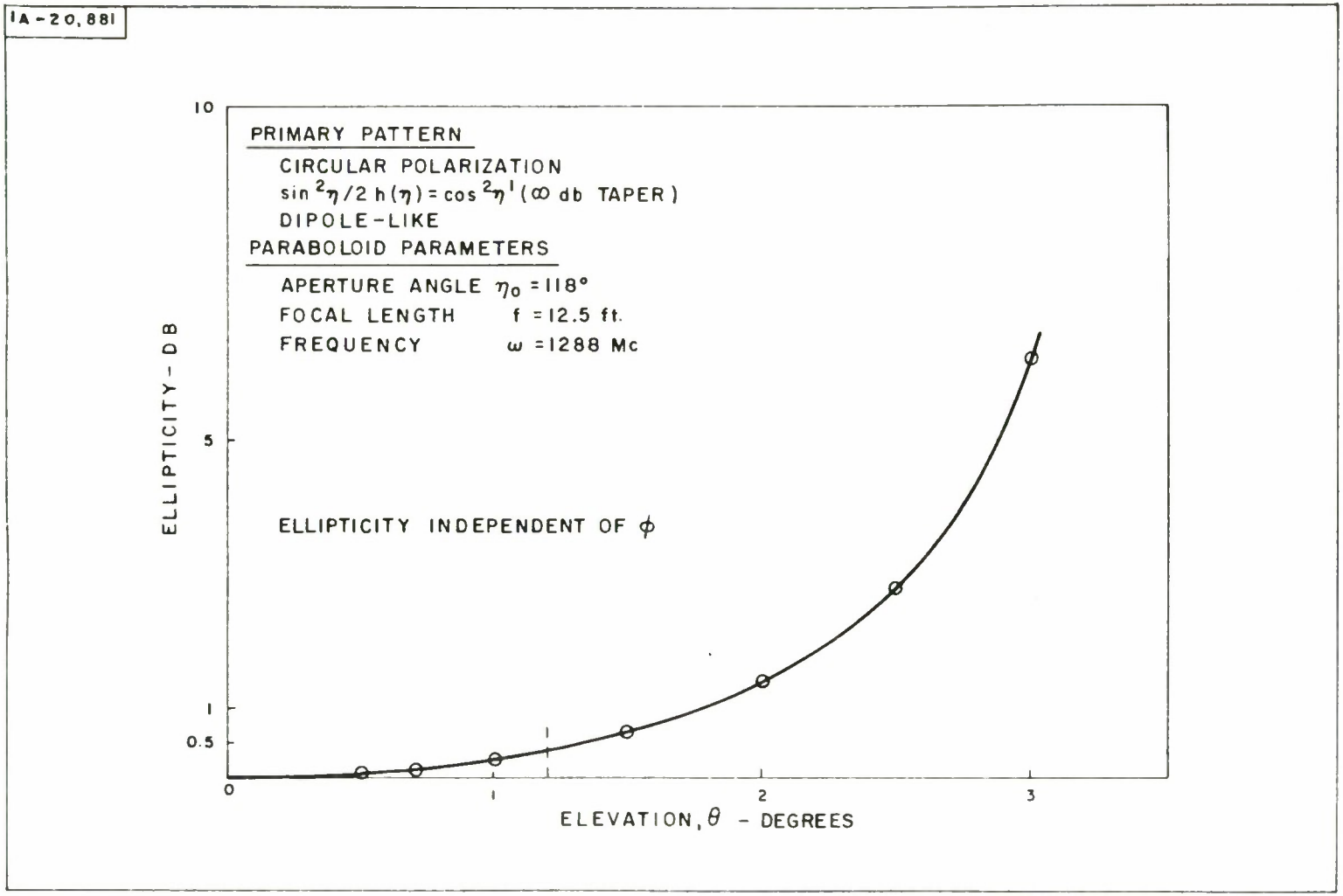

Figure 29. Focal Feed System: Ellipticity Related to Primary Illumination (Far-Field)

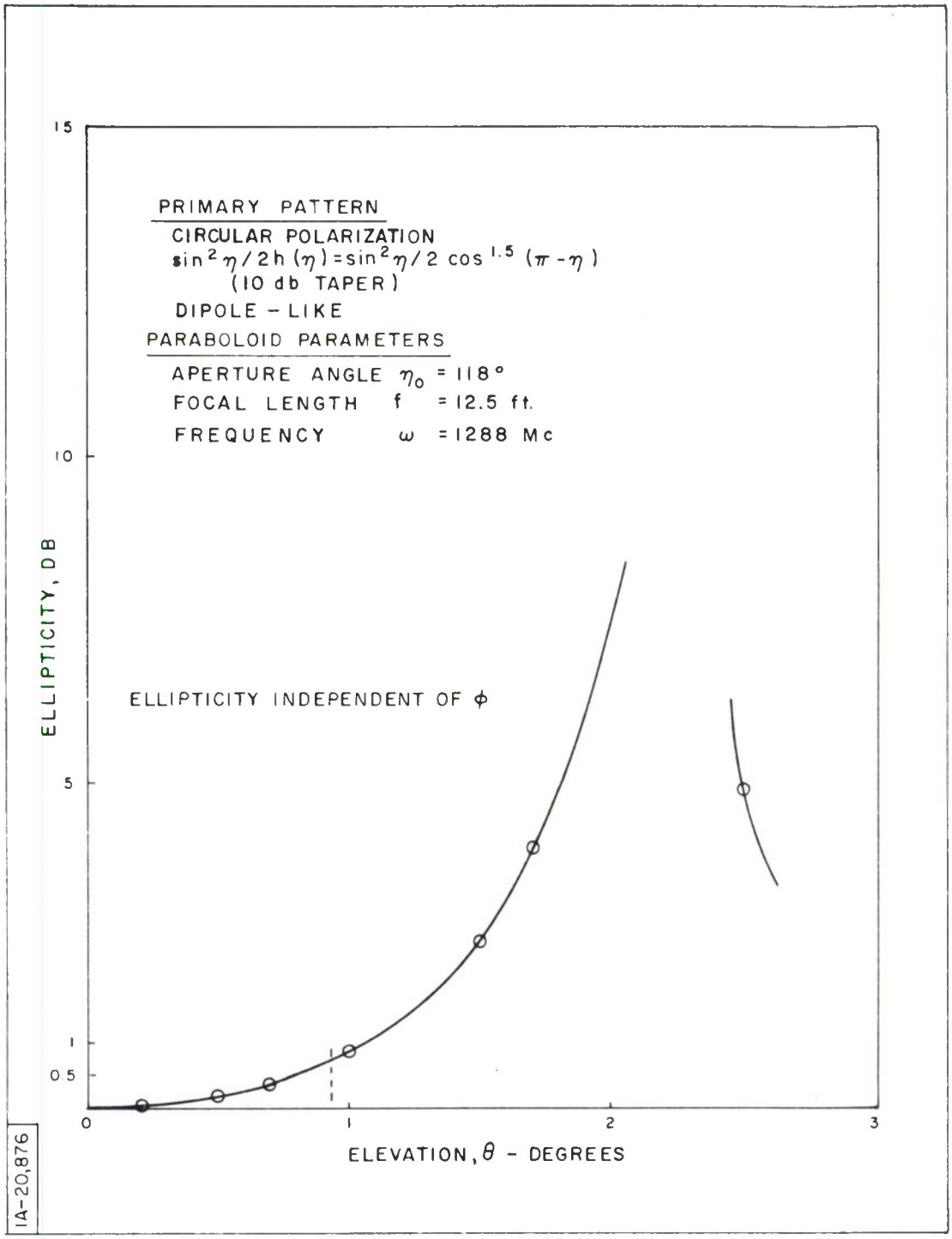

Figure 30. Focal Feed System: Ellipticity Related to Primary Illumination (Far-Field)

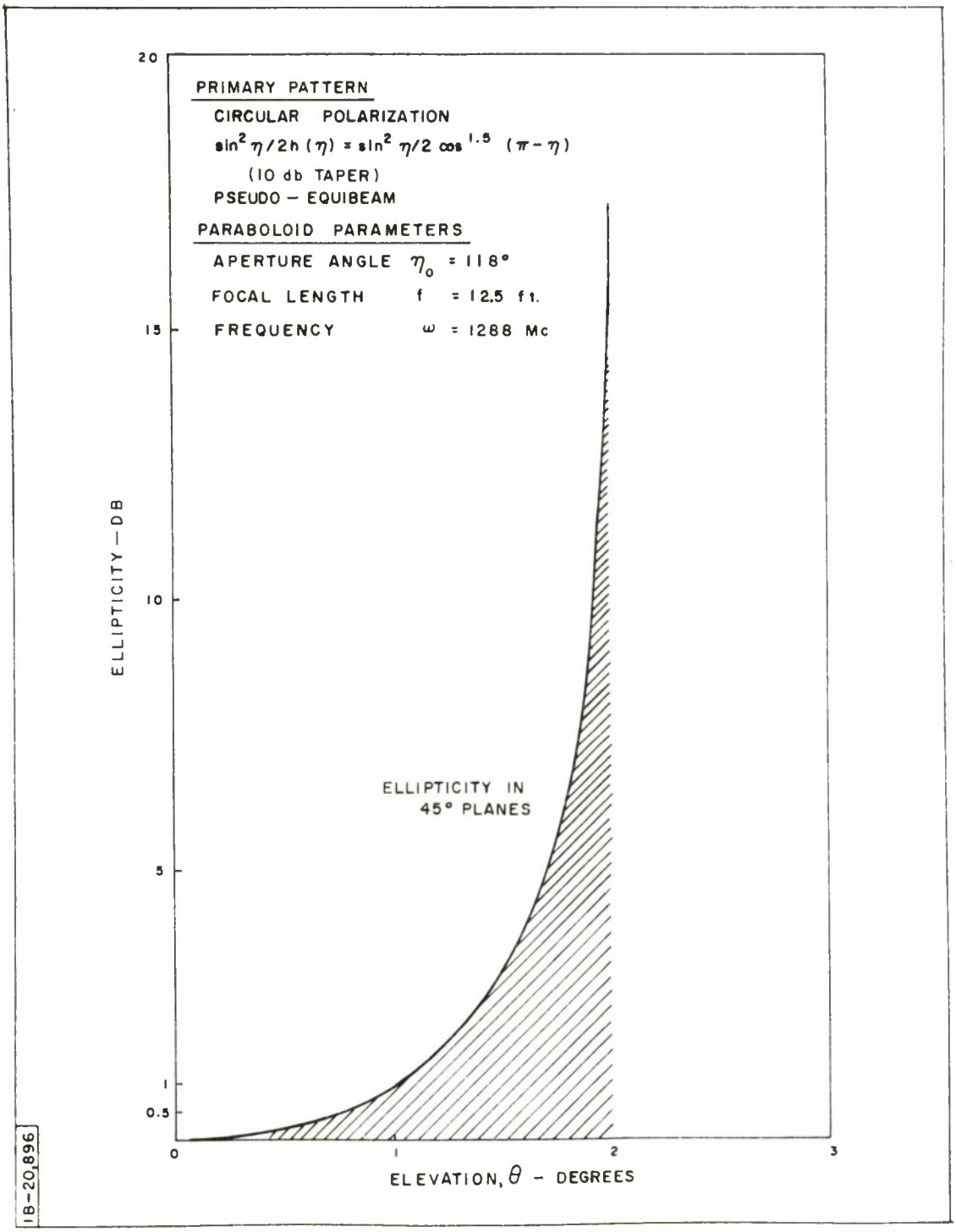

Figure 31. Focal Feed System: Ellipticity Related to Primary Illumination (Far-Field)

Figure 32 relates the ellipticities of three paraboloidal antennas of the same aperture, but of different focal lengths (12.5 ft, 29.7 ft, and 68 ft, respectively). The illumination is that of Figure 15. As the aperture angle becomes smaller, there is less difference between the dipole-like and the equibeam distributions, as noted in Appendix D. Corresponding to the 3-db half-beamwidth, ellipticity is only 0.03 db for the 68-ft focal length system, and 0.15 db for the 29.7-ft focal length system, as compared to 0.7 db for the 12.5-ft focal length system.

Figures 33 through 36 reflect the effect of the range of the observation point P on the ellipticity pattern.

Figures 32 through 36 reflect the effect of the range of the observation 10 db taper and compares ellipticities at a range of 400 ft to ellipticities in the far-field. Remarks applying to Figure 27 apply in the near-field, except that since the ordinary circular component of the field does not dip as much as in the far-field, the ellipticity peaks up to a small value near the null.

Figure 34 corresponds to the same illumination as Figure 27, but the range of point P is taken at 400 ft, 300 ft, and 200 ft. On boresight, the ellipticity is 0 db in all cases. Near boresight and within the 3-db half-beamwidth, the ellipticities are about the same as in the far-field case. Note, however, that the ellipticity for the 200-ft range is somewhat higher, near boresight, in anticipation of the near-by "dip" in amplitude (Figure 17). In the region of elevation angles corresponding to the far-field null, the near-field ellipticities are not as high as in the far-field case. Indeed, the closer the range and the shallower the amplitude "dip," the lower the maximum ellipticity.

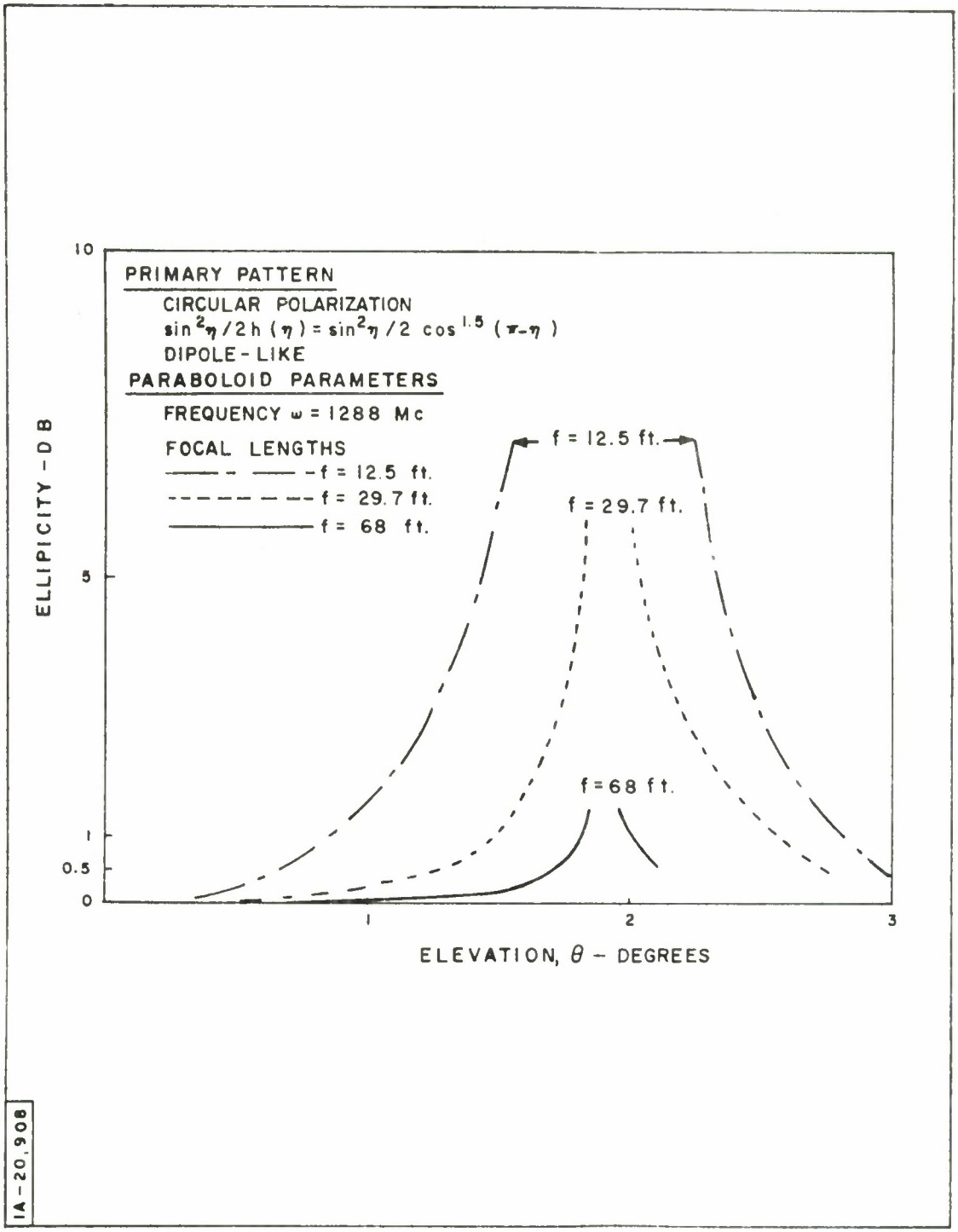

Figure 32. Focal Feed System: Ellipticity Related to Focal Length (Far-Field)

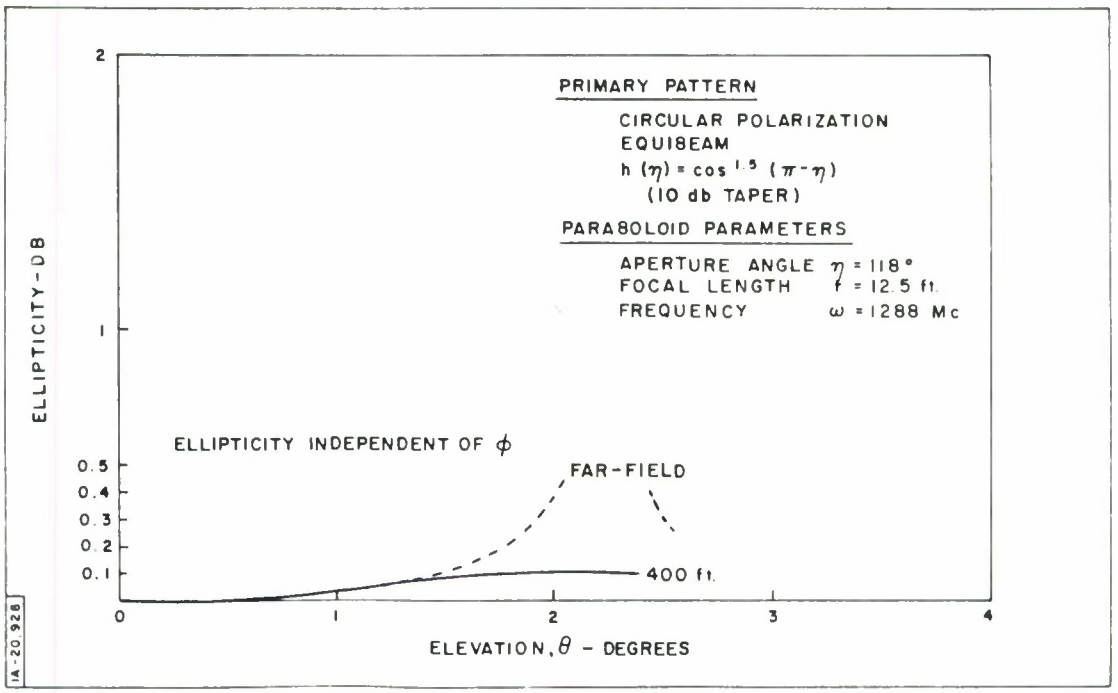

Figure 33. Focal Feed System: Ellipticity Related to Range

Figure 35 corresponds to the illumination of Figure 30, but the range of point P is taken at 400 ft. Ellipticity is essentially the same as in the far-field within the 3-db half-beamwidth, but, for elevation angles corresponding to the null of the far-field, the ellipticity at 400 ft is far smaller, in accordance with the shallow amplitude dip of Figure 18.

Figure 36 corresponds to the illumination of Figure 31 (pseudo-equibeam with 10-db taper illumination), but the range of point P is taken at 400 ft. As in Figure 31, ellipticity is now a function of φ and varies from essentially 0 db to a maximum in the 45-degree planes. Moreover, this maximum ellipticity at 400 ft exhibits the same characteristics as in the preceding graph (same values as in the far-field, within the beamwidth; much lower values than in the far-field, for elevation angles corresponding to the far-field nulls).

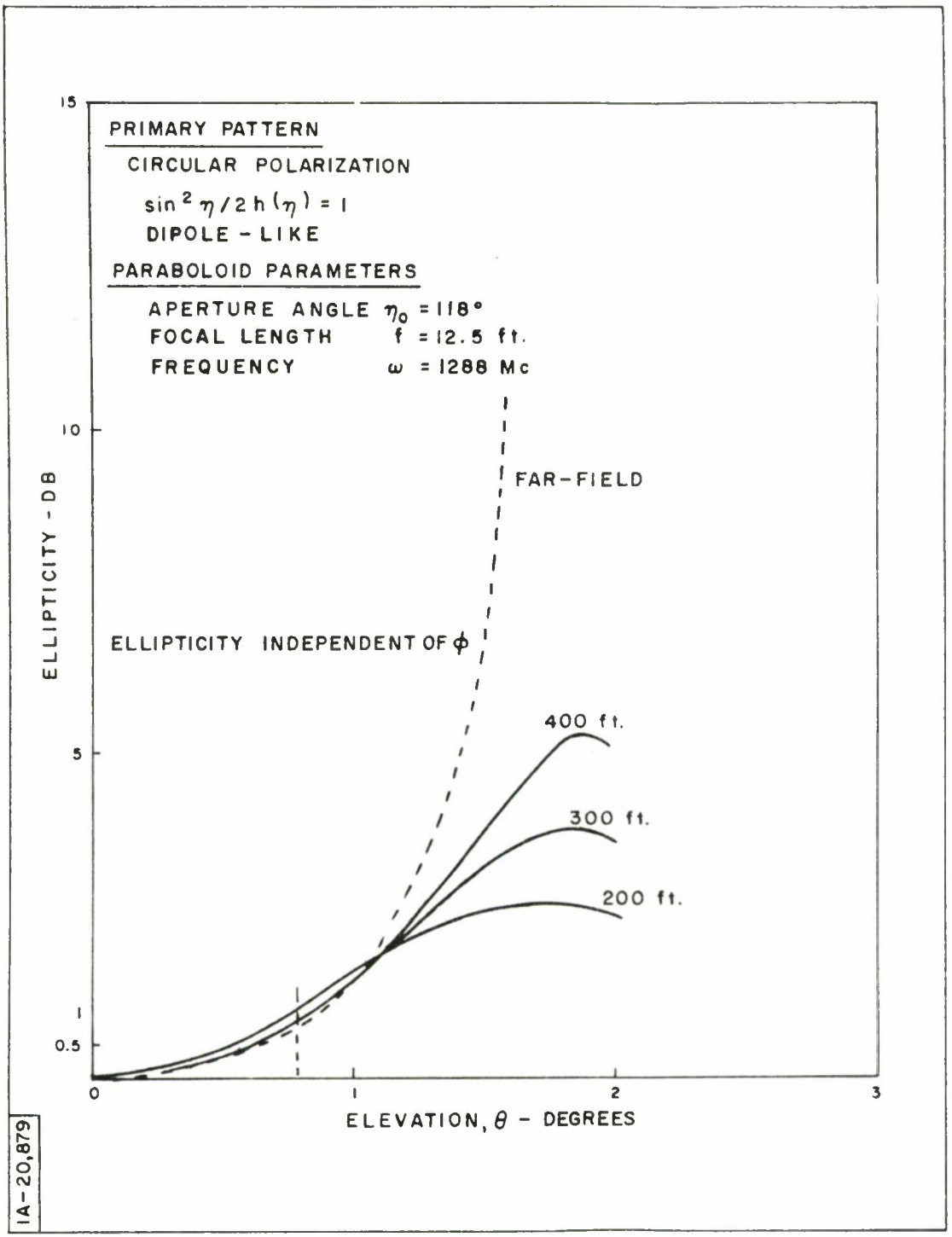

Figure 34. Focal Feed System: Ellipticity Related to Range

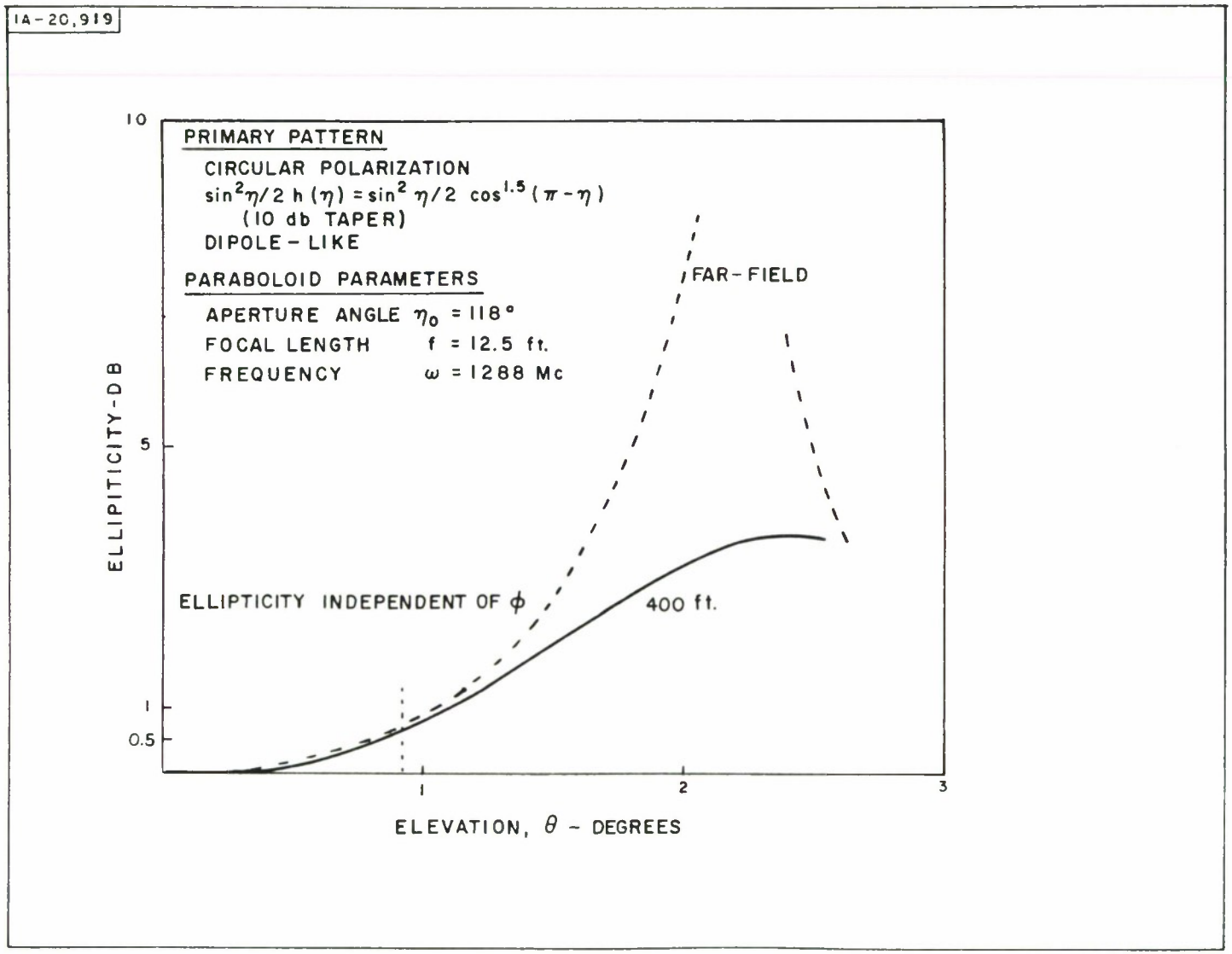

Figure 35. Focal Feed System: Ellipticity Related to Range

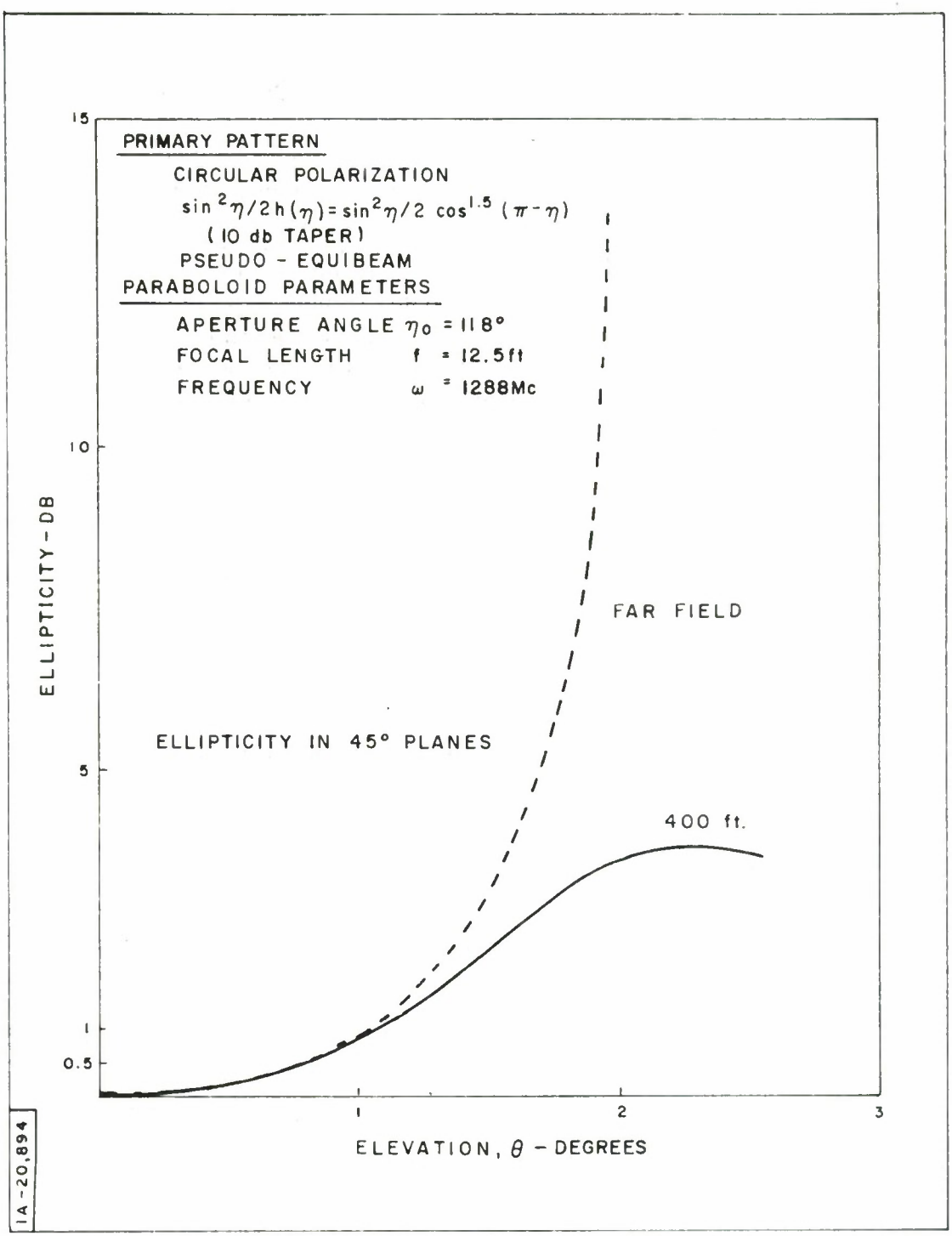

Figure 36. Focal Feed System: Ellipticity Related to Range

Figures 37 through 42 reflect changes (or lack thereof) in ellipticity when the paraboloidal surface is perturbed.

Figures 37, 38, and 39 correspond to Figures 20, 21 and 22, respectively, where randomly distributed imperfections on the paraboloidal surface are simulated by letting the focal length, f , vary randomly from point to point according to

$$f_{i,j} = (1 + \epsilon_{ij})\ 12.5 \text{ ft}$$

where

$$|\epsilon_{ij}| \leq 0.005$$

Ellipticities are no longer exactly 0 db on boresight, but are still extremely small (0.011 db, 0.0067 db, and 0.0043 db, respectively). The patterns themselves are essentially the same as for the unperturbed cases (Figures 27, 28, and 29), except that they present a small spread from the corresponding ideal cases. This spread, for a given value of the elevation angle, θ, varies randomly as a function of φ. Just as the random imperfections have no appreciable effect on the amplitude patterns (except for a substantial loss in gain), they have no appreciable effect on the ellipticity patterns.

Finally, in Figures 40, 41, and 42, the focal length was made to vary discontinuously as a function of ψ only, as in Figures 23, 24, and 25. The same table (Table III) applies to these cases. Ellipticities are not 0 db on boresight, but are still very small (0.066 db, 0.04 db, and 0.03 db, respectively). However, the ellipticity patterns spread considerably on either side of the curves pertaining to the perfect dish, as a random function of φ. This type of semi-correlated perturbation is far more disruptive than the random perturbations of Figures 37 through 39, even though their peak amplitudes are the same.

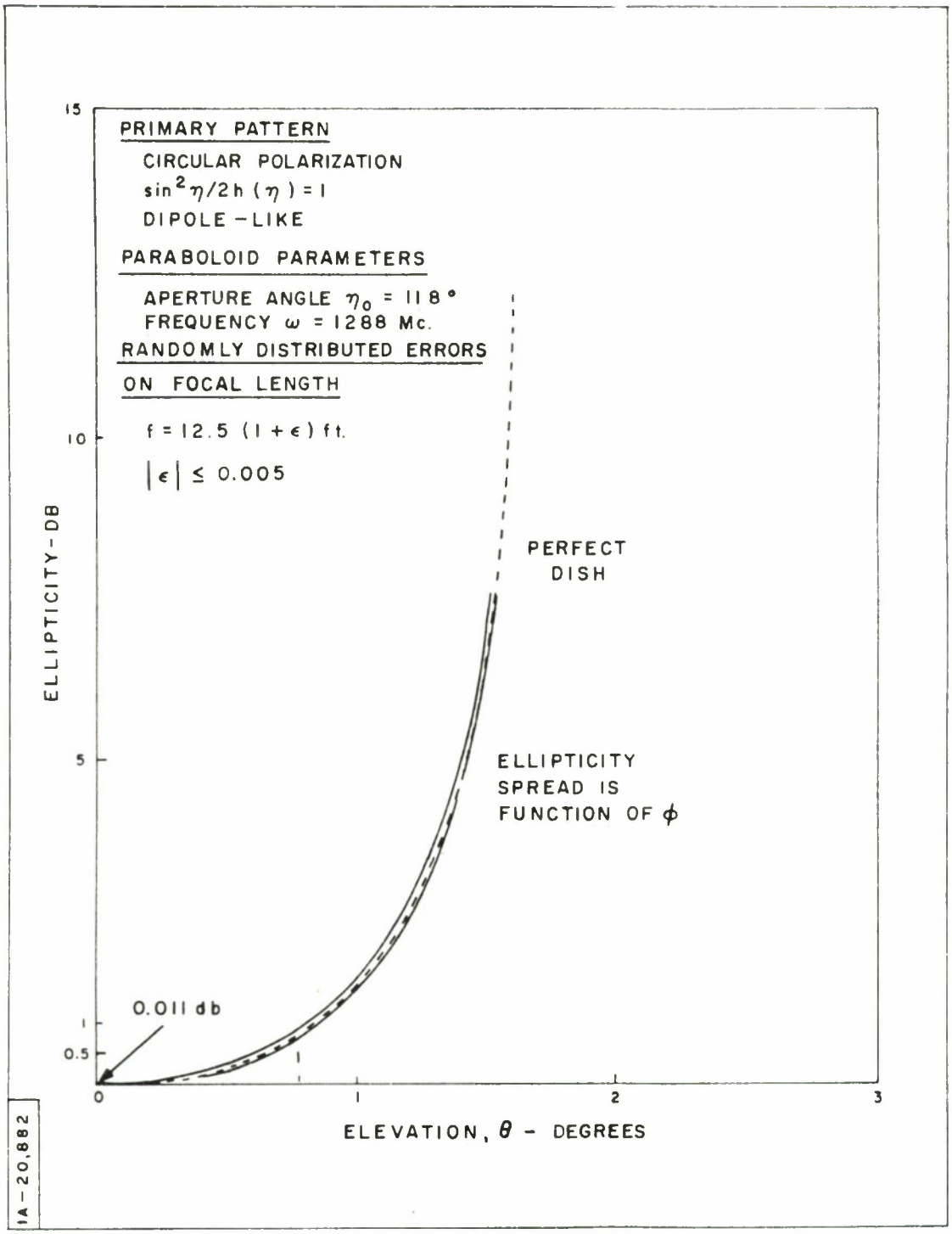

Figure 37. Focal Feed System: Ellipticity Related to Paraboloid Imperfections (Far-Field)

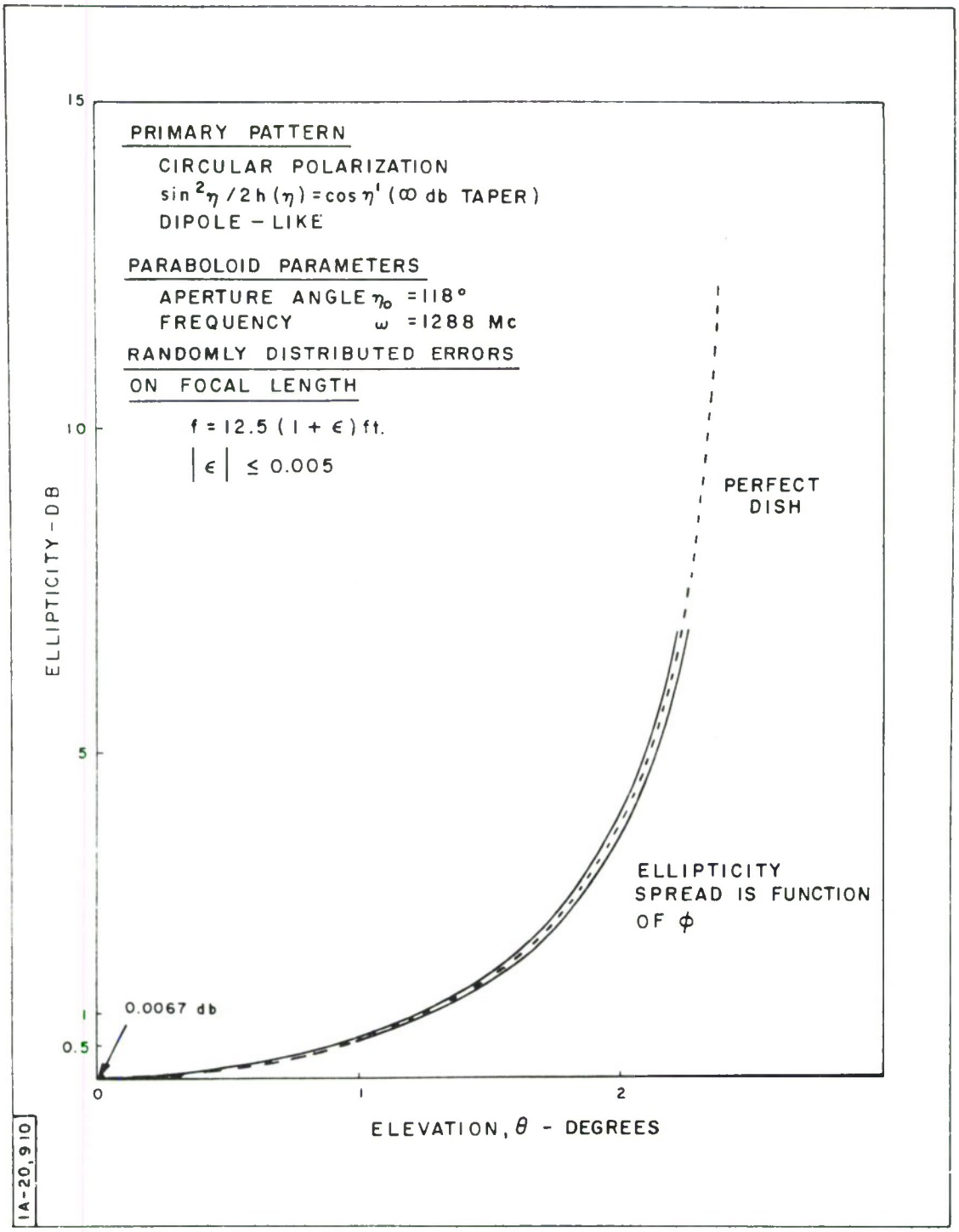

Figure 38. Focal Feed System: Ellipticity Related to Paraboloid Imperfections (Far-Field)

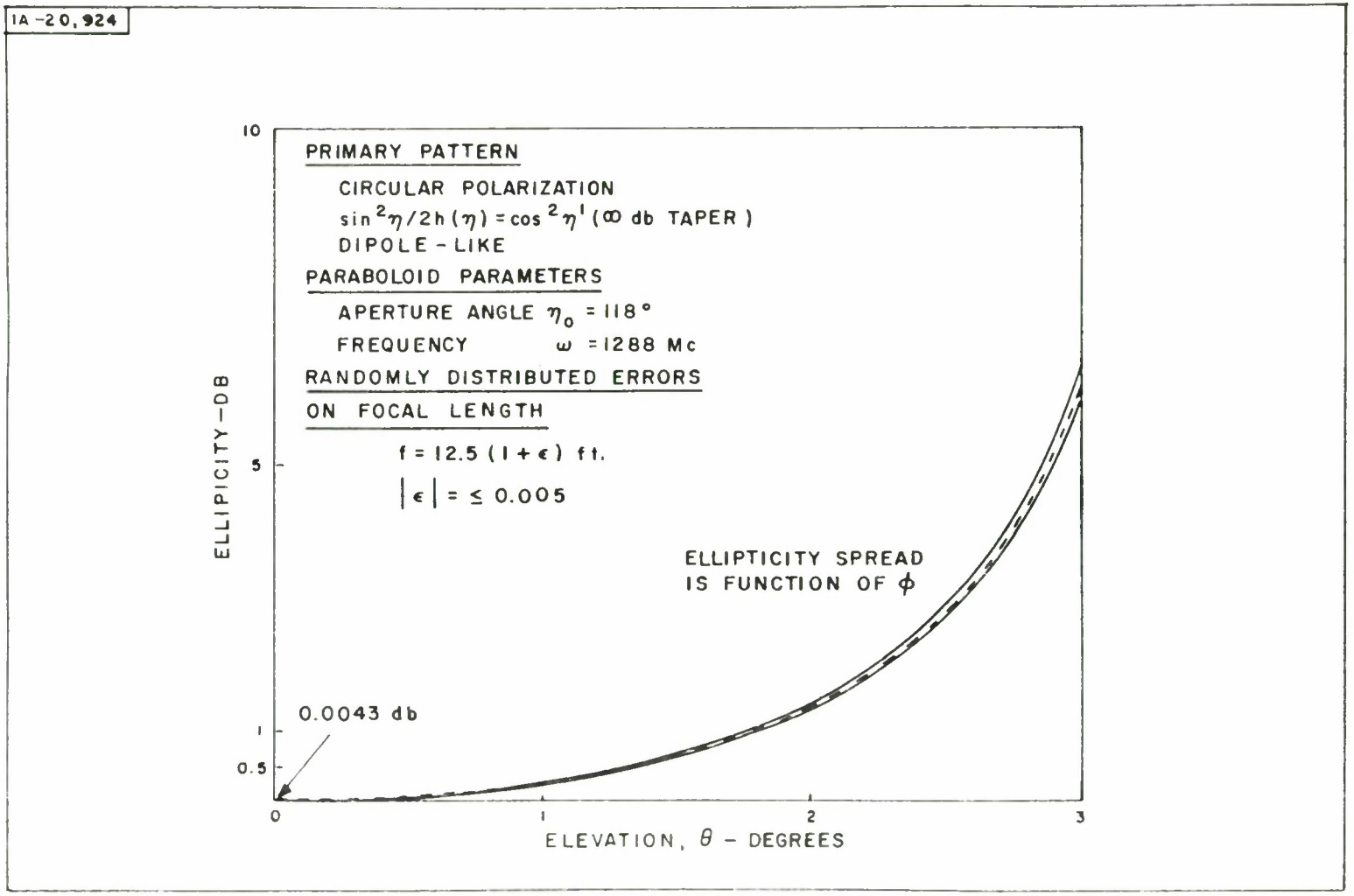

Figure 39. Focal Feed System: Ellipticity Related to Paraboloid Imperfections (Far-Field)

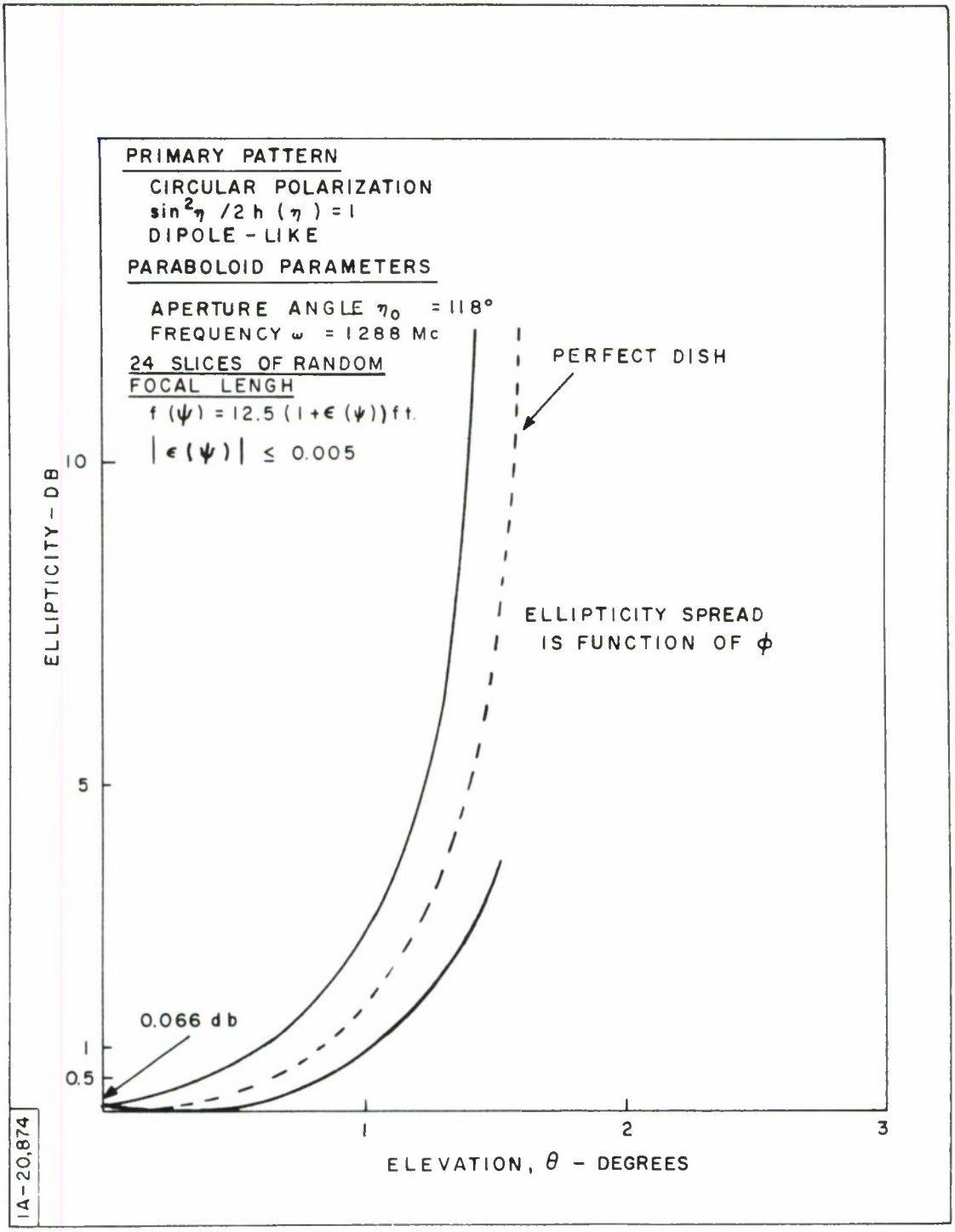

Figure 40. Focal Feed System: Ellipticity Related to Paraboloid Imperfections (Far-Field)

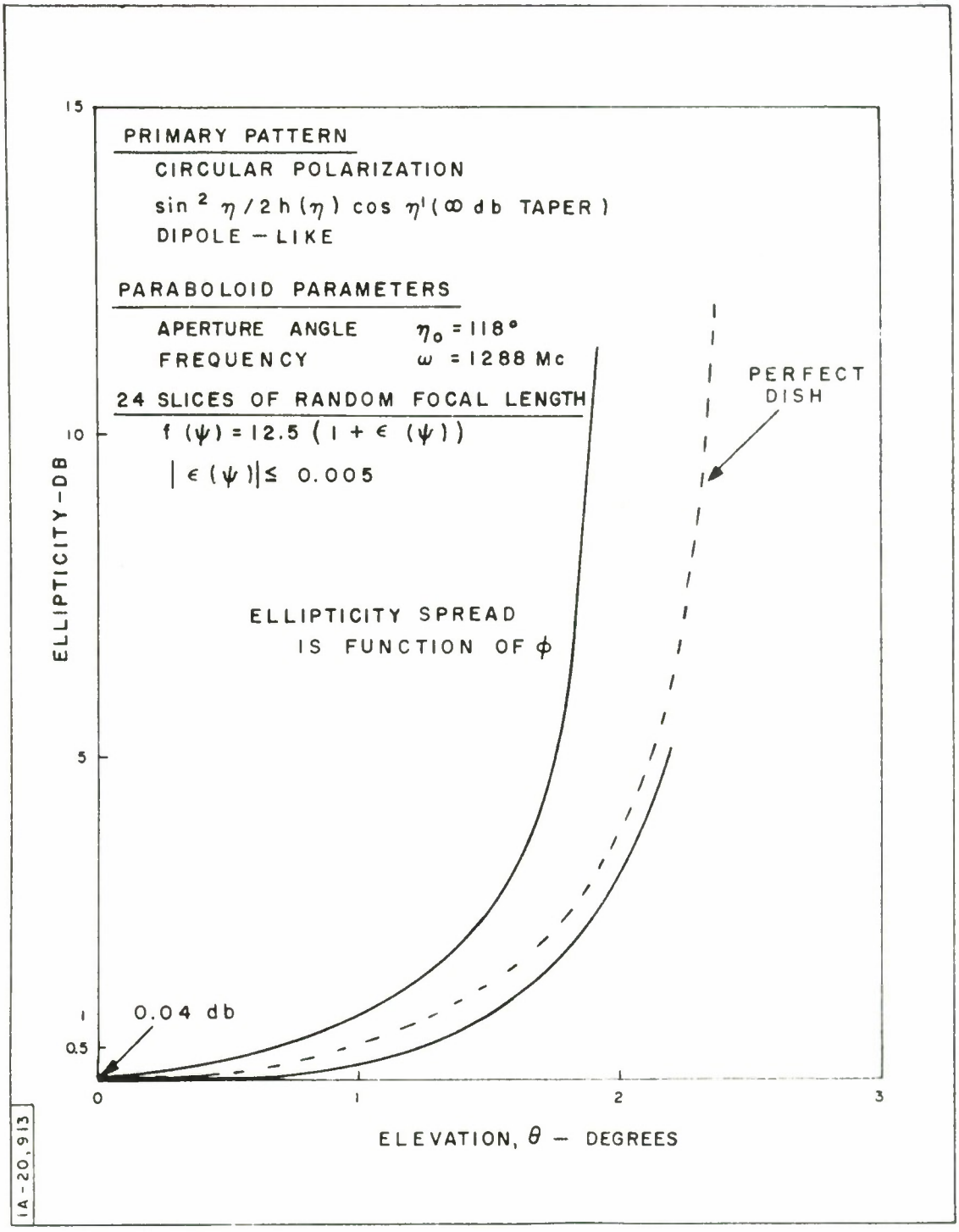

Figure 41. Ellipticity Related to Paraboloid Imperfections (Far-Field)

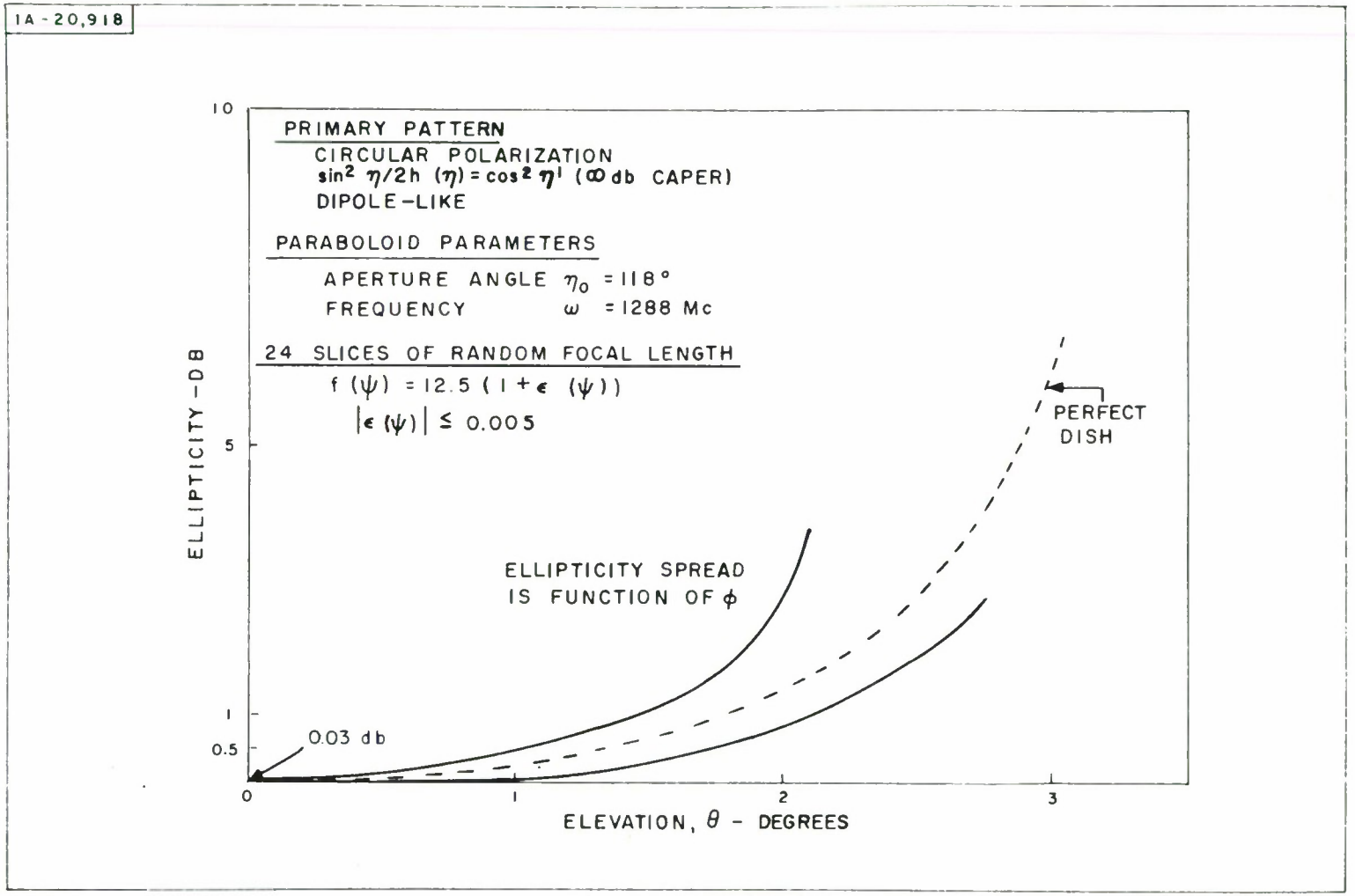

Figure 42. Ellipticity Related to Paraboloid Imperfections (Far-Field)

SHIFT IN LINEAR POLARIZATION

Figures 43 through 49 are plots of the deviation angle from the primary linear polarization to the polarization at the observation point, P , as a function of the azimuth angle, φ , for various values of the elevation angle, θ . They are plots of Equation (60), which relates the far-field cross-polarized terms to the "in-polarized" terms.

As discussed in Section II and proved in Appendix G, the cross-polarized terms are always zero in the H- and E-planes at the observation point, P. Consequently, regardless of whether the distribution is equibeam, dipole-like, or pseudo-equibeam, the deviation angle is zero for $\varphi = 0, \pi/2, \pi,$ and $3\pi/2$. Since the cross-polarized terms are maximum near the 45-degree planes, and since the ratio of cross-polarized to in-polarized terms increases from zero to a maximum value in the region of the amplitude null, the deviation angle is zero on boresight and increases with θ toward the amplitude null. For a given value of θ , it is maximum in or near the 45-degree planes. Thus, for the equibeam case (Figure 43), the deviation angles are maximum in the 45-degree planes as a result of the integration of Equation (33), but the amplitudes are rather small (one degree or so), even around the null. However, for the dipole-like distribution (Figures 44, 45, 46, and 47), the deviation angles are maximum near, but not in, the 45-degree planes, since amplitudes in the E-plane are larger than amplitude in the H-plane. Near the nulls, where the cross-polarized terms are much larger than the "in-polarized" terms, the deviation angles tend toward $\pm \pi/2$. Note that, past the nulls, the deviation angles decrease and change signs, for a given value of the azimuth angle, φ.

Figure 48 applies to the pseudo-equibeam distribution. The curves have essentially the same character as for the dipole-like distribution,

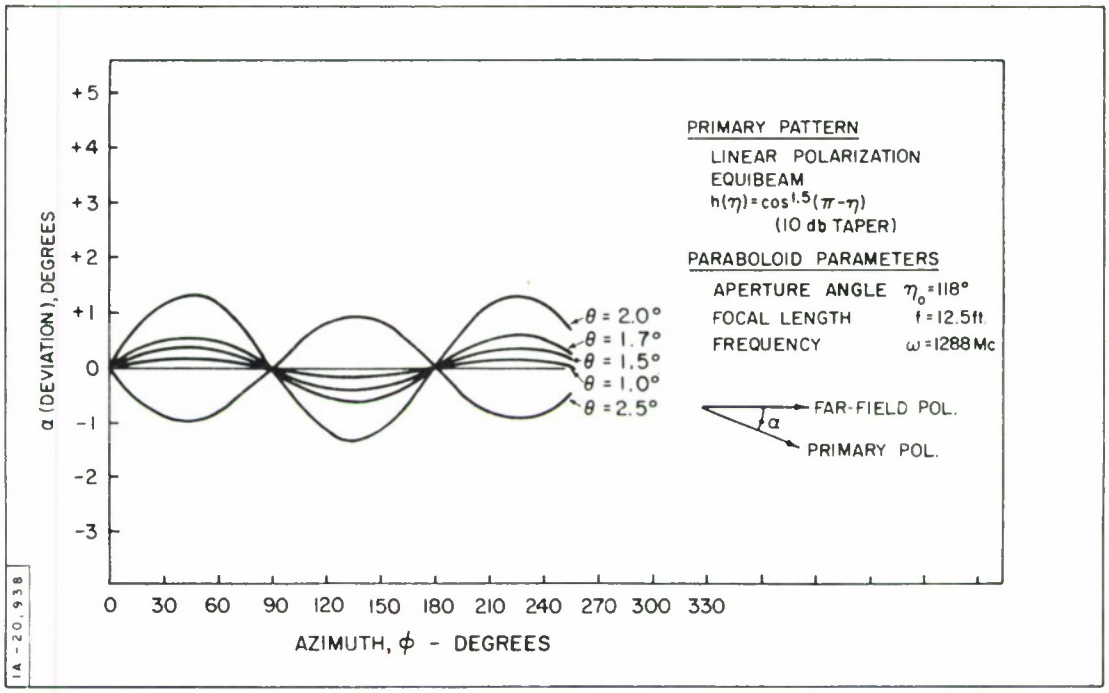

Figure 43. Focal Feed System: Polarization Deviation Related to Primary Illumination (Far-Field)

except that the deviation angles peak up in the 45-degree planes, since the amplitudes in the H- and E-planes are equal.

Figure 49 dramatizes the fact that for long focal lengths the cross-polarized terms are small, and consequently the deviation angles are small.

Those plots of polarization shifts can be directly related to the ellipticity plots: no deviation on boresight (0 db ellipticity); largest deviation near the nulls (largest ellipticity); low deviation and low ellipticity near the peak of the sidelobe.

Effects of range and surface perturbations have not been plotted, since, for the cases that were considered, those effects can be inferred readily from the amplitude and ellipticity graphs.

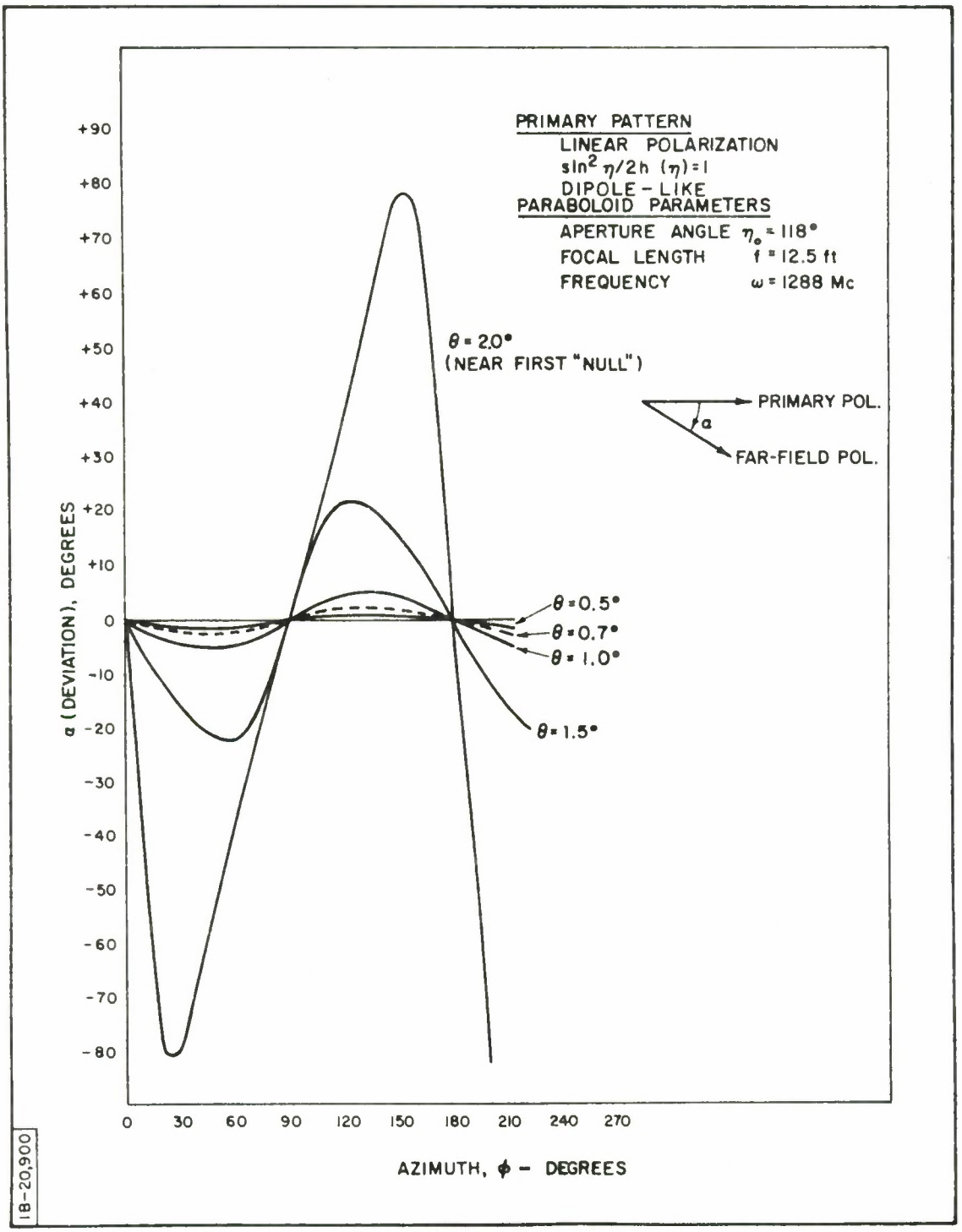

Figure 44. Focal Feed System: Polarization Deviation Related to Primary Illumination (Far-Field)

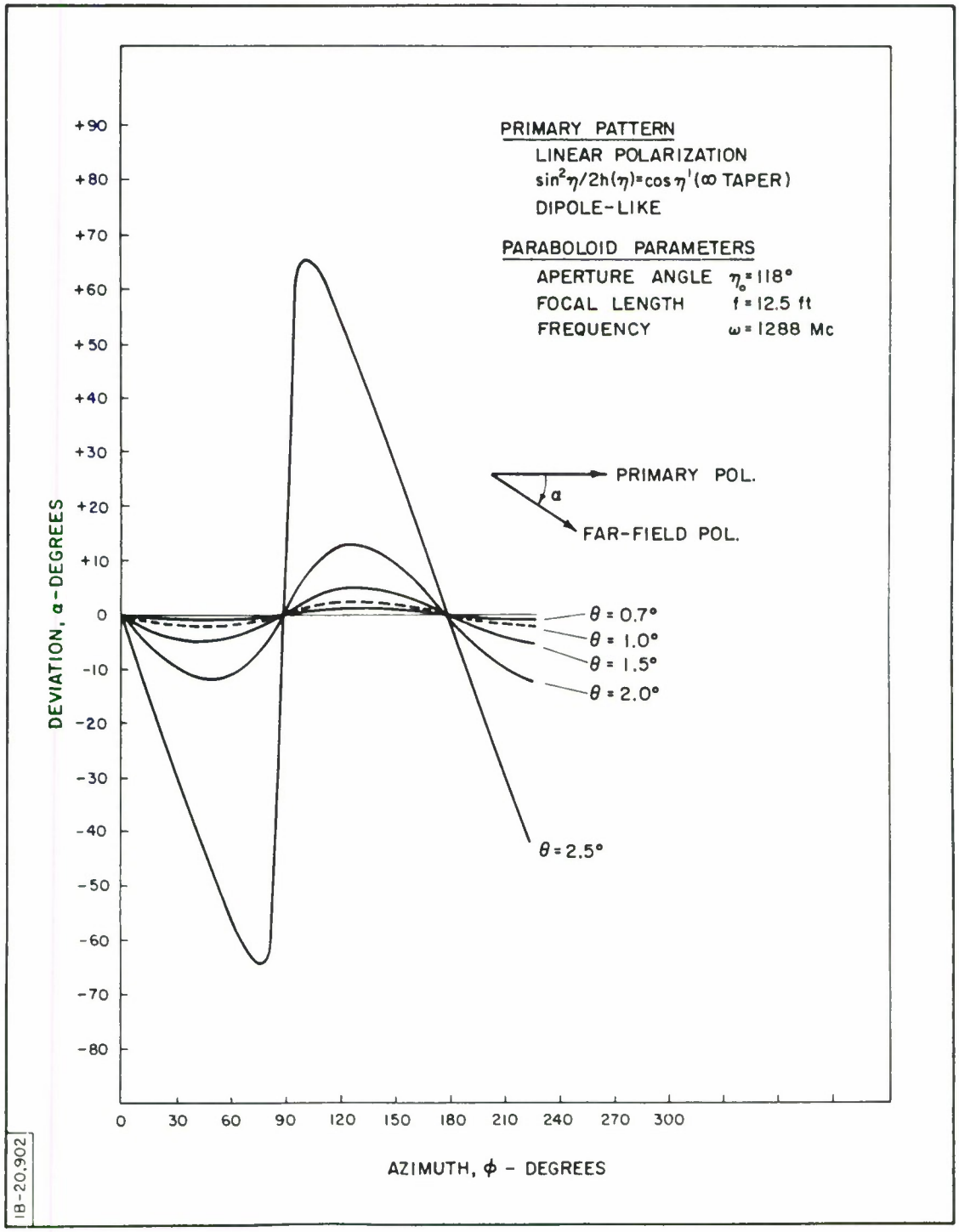

Figure 45. Focal Feed System: Polarization Deviation Related to Primary Illumination (Far-Field)

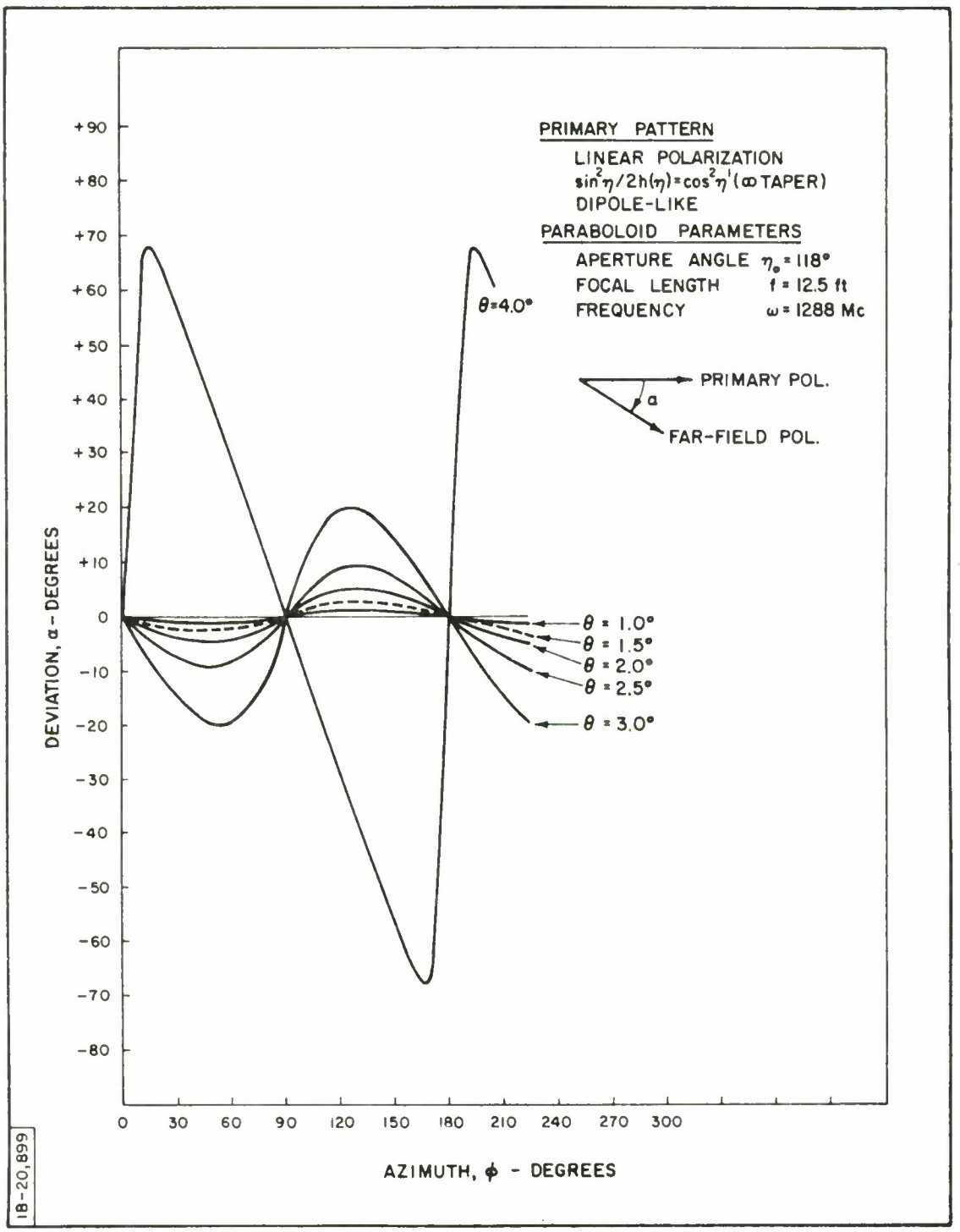

Figure 46. Focal Feed System: Polarization Deviation Related to Primary Illumination (Far-Field)

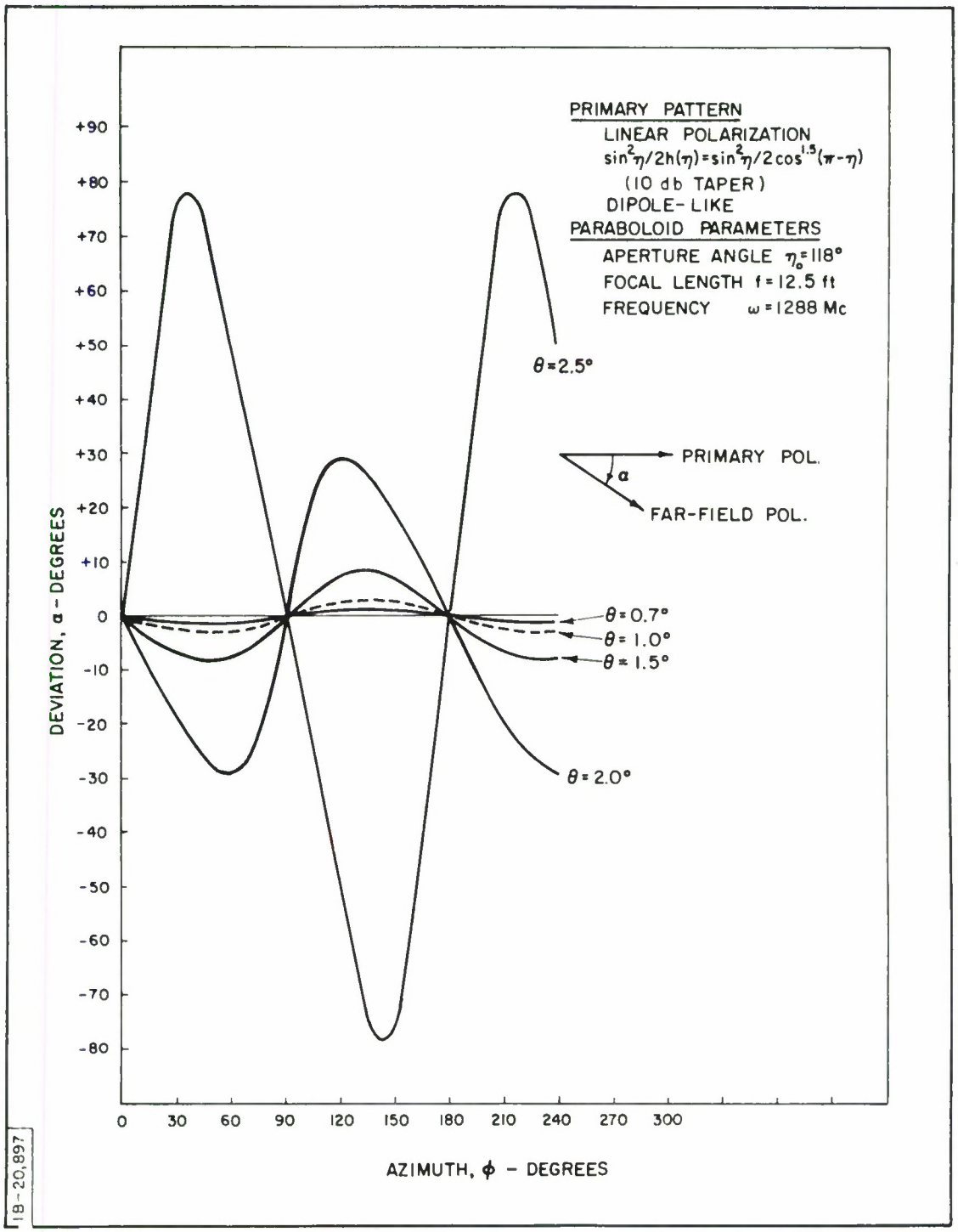

Figure 47. Focal Feed System: Polarization Deviation Related to Primary Illumination (Far-Field)

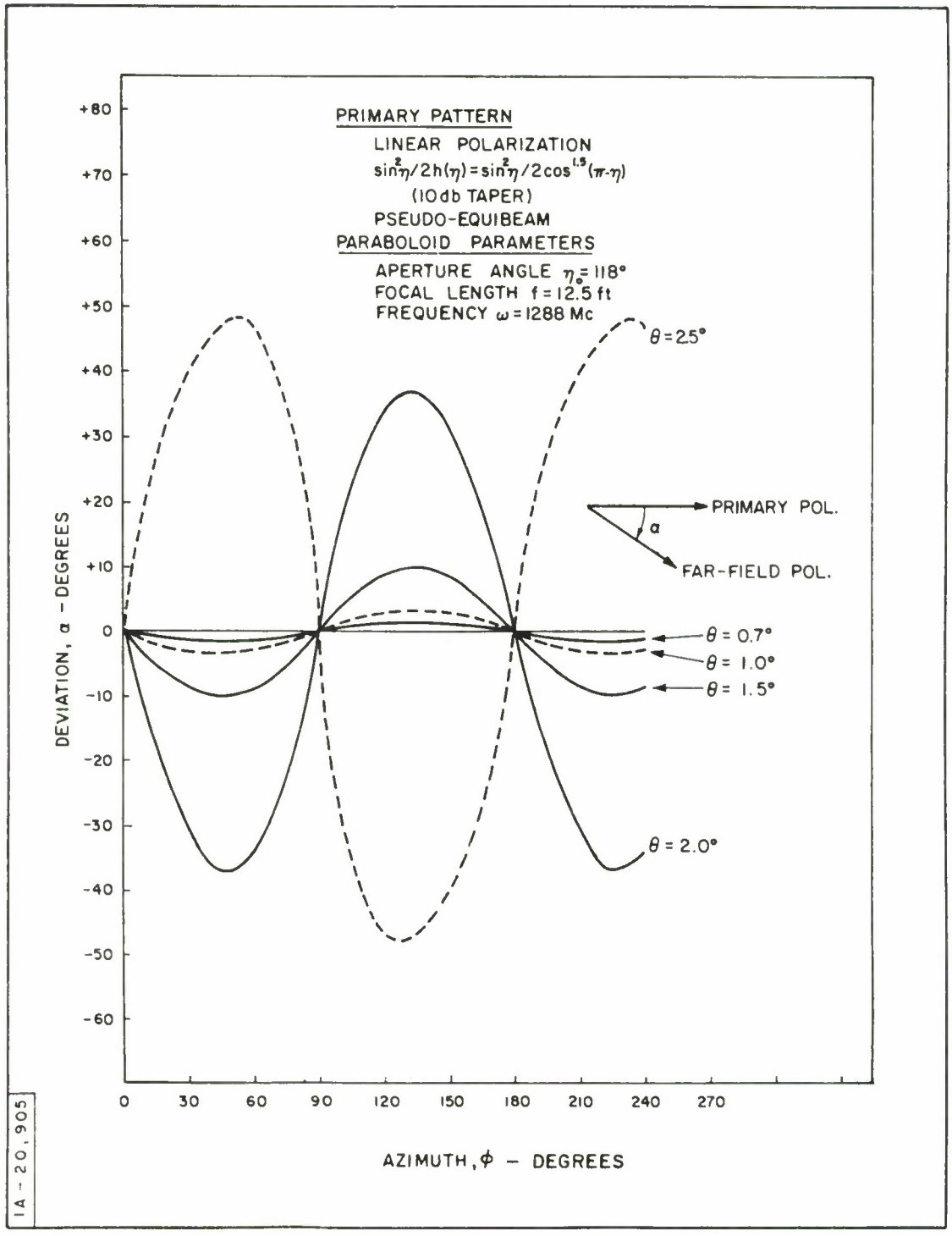

Figure 48. Focal Feed System: Polarization Deviation Related to Primary Illumination (Far-Field)

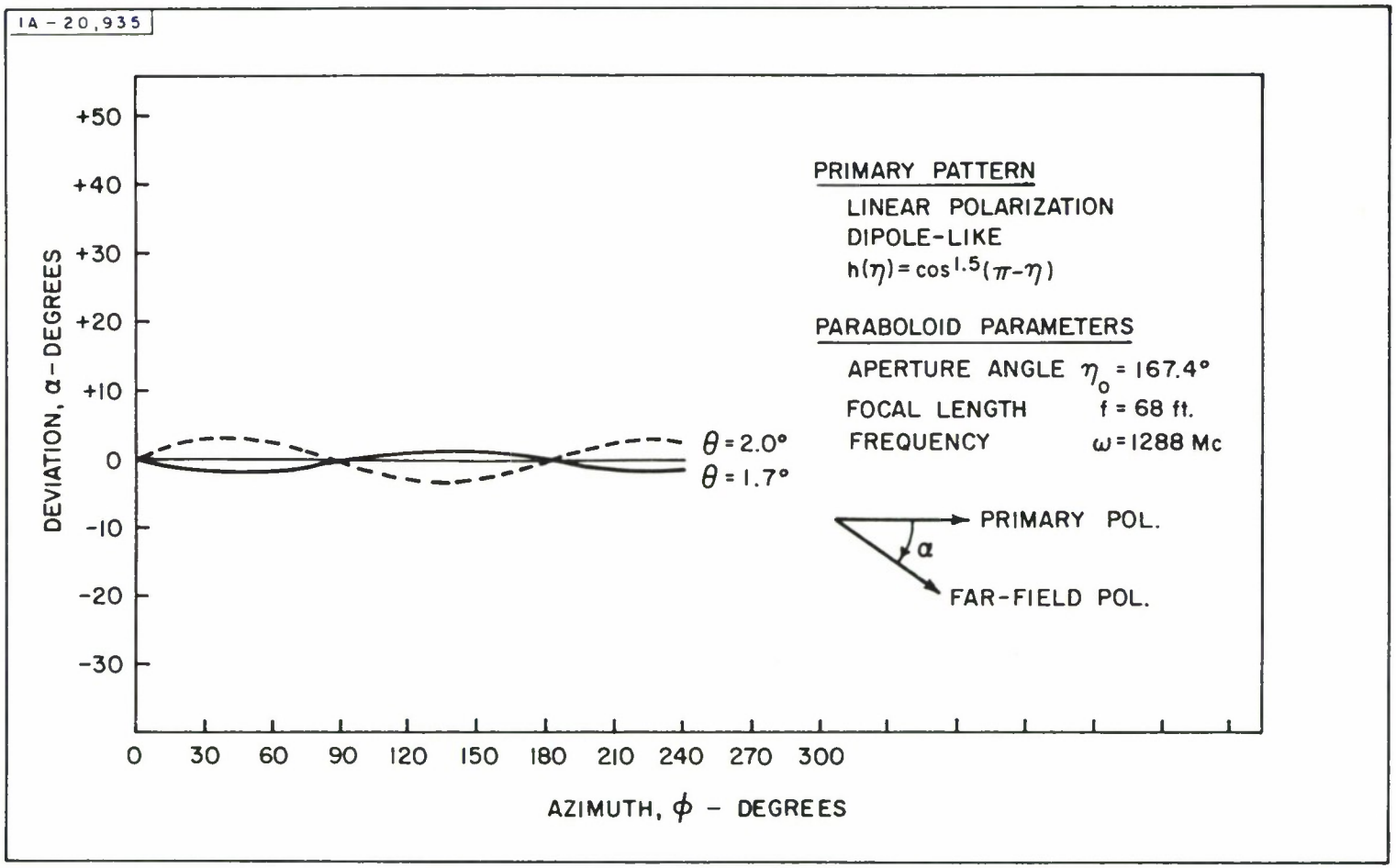

Figure 49. Focal Feed System: Polarization Deviation Related to Focal Length (Far-Field)

DEFOCUSING IN FOCAL PLANE: SUM OF TWO BEAMS

Figures 50 through 53 pertain to the situation of the paraboloidal dish being illuminated by two feeds, located at the intersection of the "vertical" plane and of the focal plane, each one a distance $d = 0.192$ ft from the boresight axis, on opposite sides of it (See Section II and Figure 5). Both feeds emit the same illumination. The plots describe the resultant far-field beam for the equibeam and dipole-like illumination functions.

Figure 50 is a plot of amplitude versus elevation angle, θ, in the far-field, for the equibeam distribution, with the taper function $\cos^{1.5}(\pi - \eta)$, under linear polarization. The beam does not exhibit cylindrical symmetry, but is broader in the "vertical" plane. Cuts through the vertical and horizontal planes are plotted in the graph. For the sake of convenience, the focal feed case (Figure 9) is redrawn (dotted line). The change of beam-width with azimuth is due to the particular orientation of the feeds. The distance d was "estimated" for a crossover angle $\theta_o = 0.8$ degrees (Section II). The situation around the "nulls" (not fully plotted) is very complex, but of little significance.

Figure 51 refers to the same situation as Figure 50, except that the feed illuminations are circularly polarized. Ellipticity is 0 db on boresight (perfect circularity) and increases with elevation, but very slowly. As expected, ellipticity is not independent of azimuth, since amplitude is not. Fundamentally, the reason that the ellipticity remains so low is that the only cross-coupling mechanism can still occur only through the z-directed currents whose contributions in the far-field are negligible (Equations (23) and (24)) for small elevation angles, except when the "dominant" terms sink to a null.

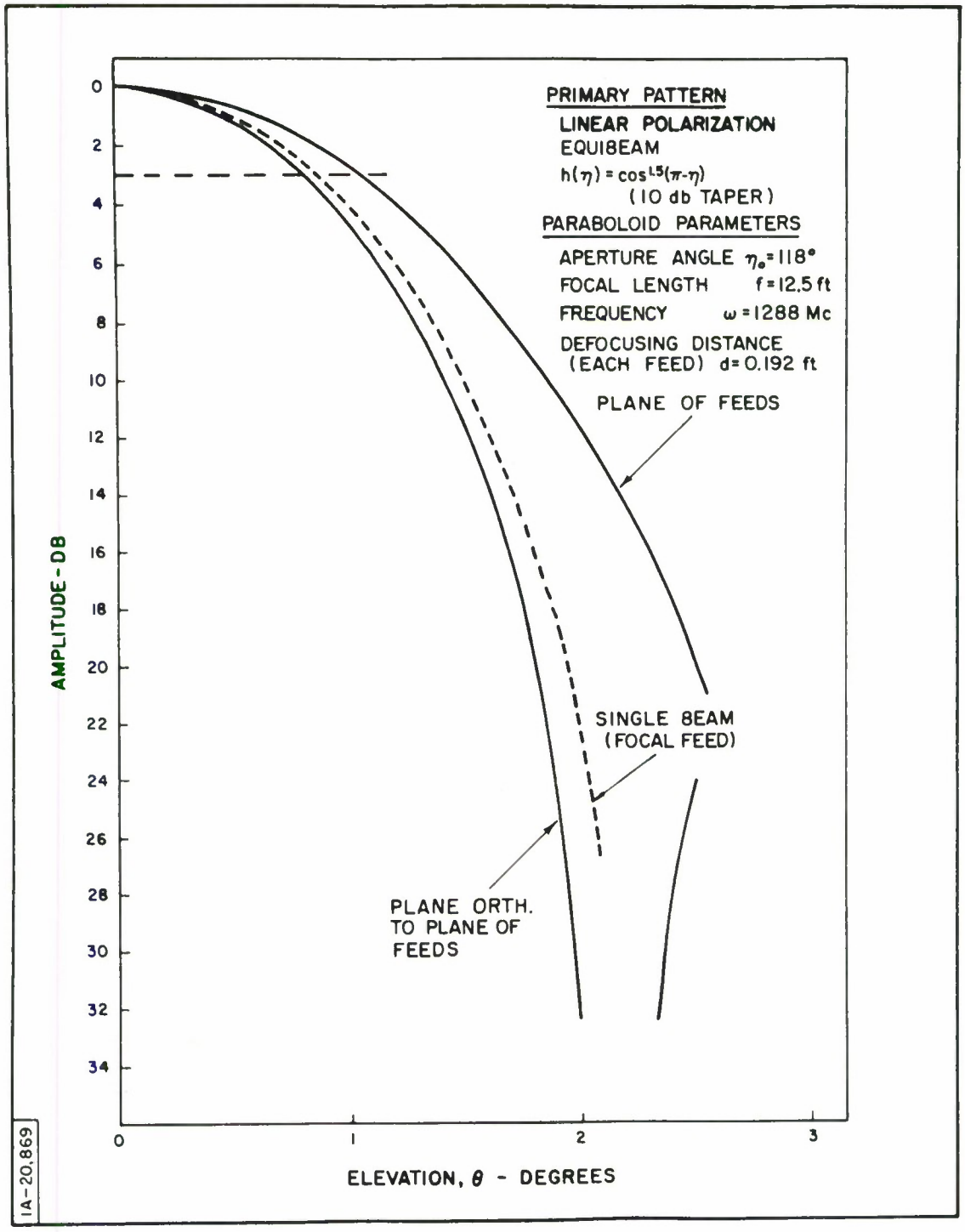

Figure 50. Defocusing in Focal Plane: Sum of Two Beams (Far-Field Amplitude)

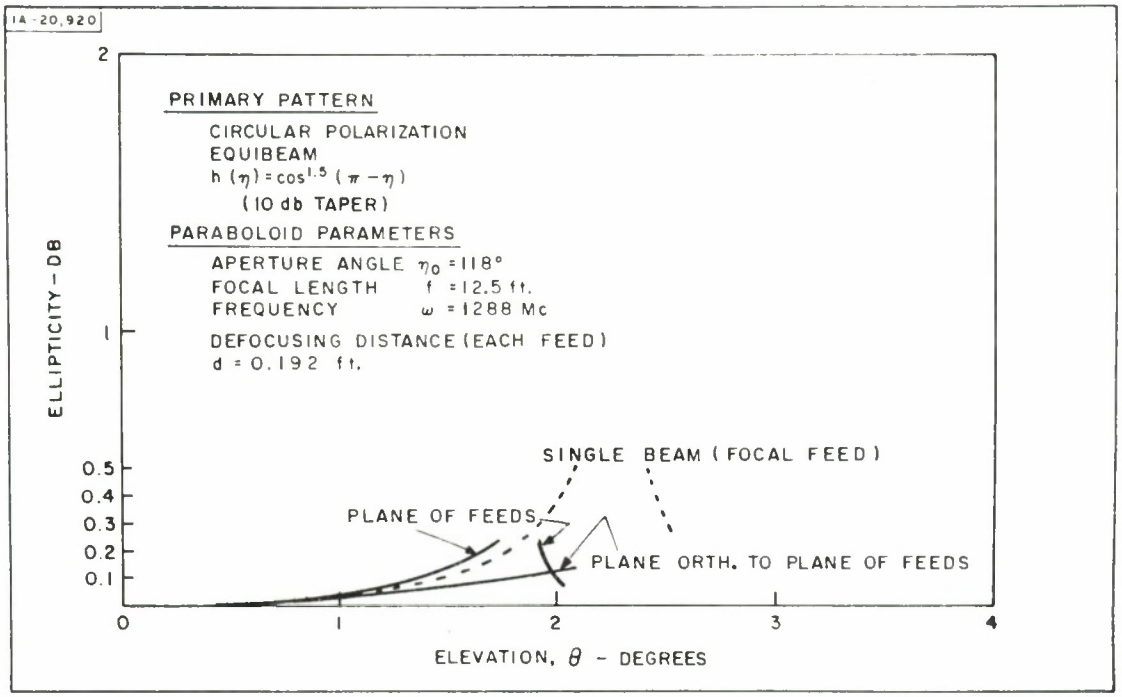

Figure 51. Defocusing in Focal Plane: Sum of Two Beams (Far-Field Ellipticity)

Figure 52 corresponds to Figure 50, except that the primary illumination function is dipole-like. Figure 13 has been redrawn for convenience of comparison with the single focal fed beam. The spread between vertical and horizontal patterns is not as large as in Figure 50, because the vertical plane has been made coincident with the H-plane. To some extent, the non-symmetry of each individual beam tends to cancel each other. Had the vertical plane been made to coincide with the E-plane, the spread between patterns would be larger than in Figure 50.

Figure 53 refers to the same situation as Figure 52, except that the feed illuminations are circularly polarized. The ellipticity on boresight is rather large (0.41 db). The reason is that, on boresight, the extraneous components X2 and Y2 are not equal to each other (Section II), since

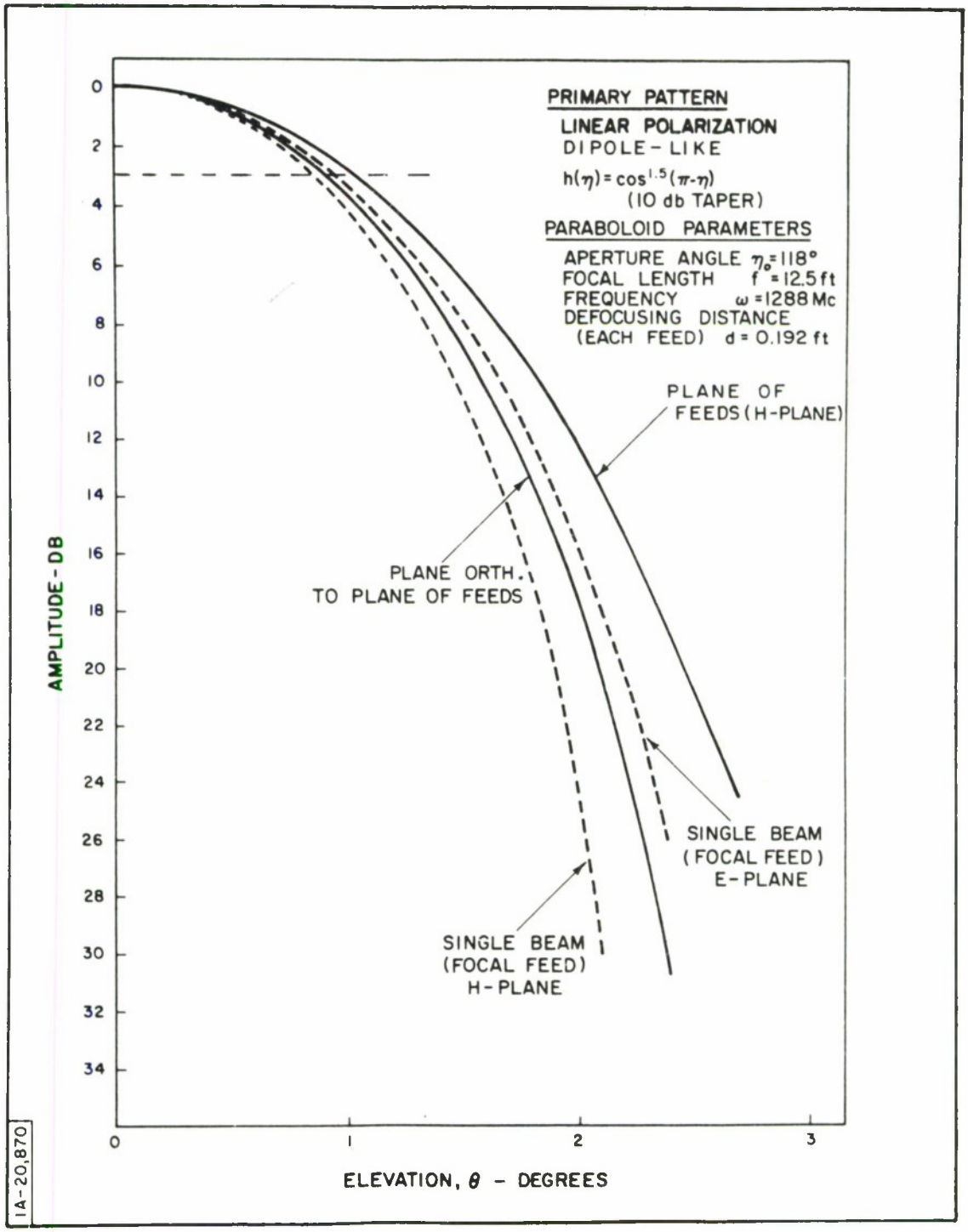

Figure 52. Defocusing in Focal Plane: Sum of Two Beams (Far-Field Amplitude)

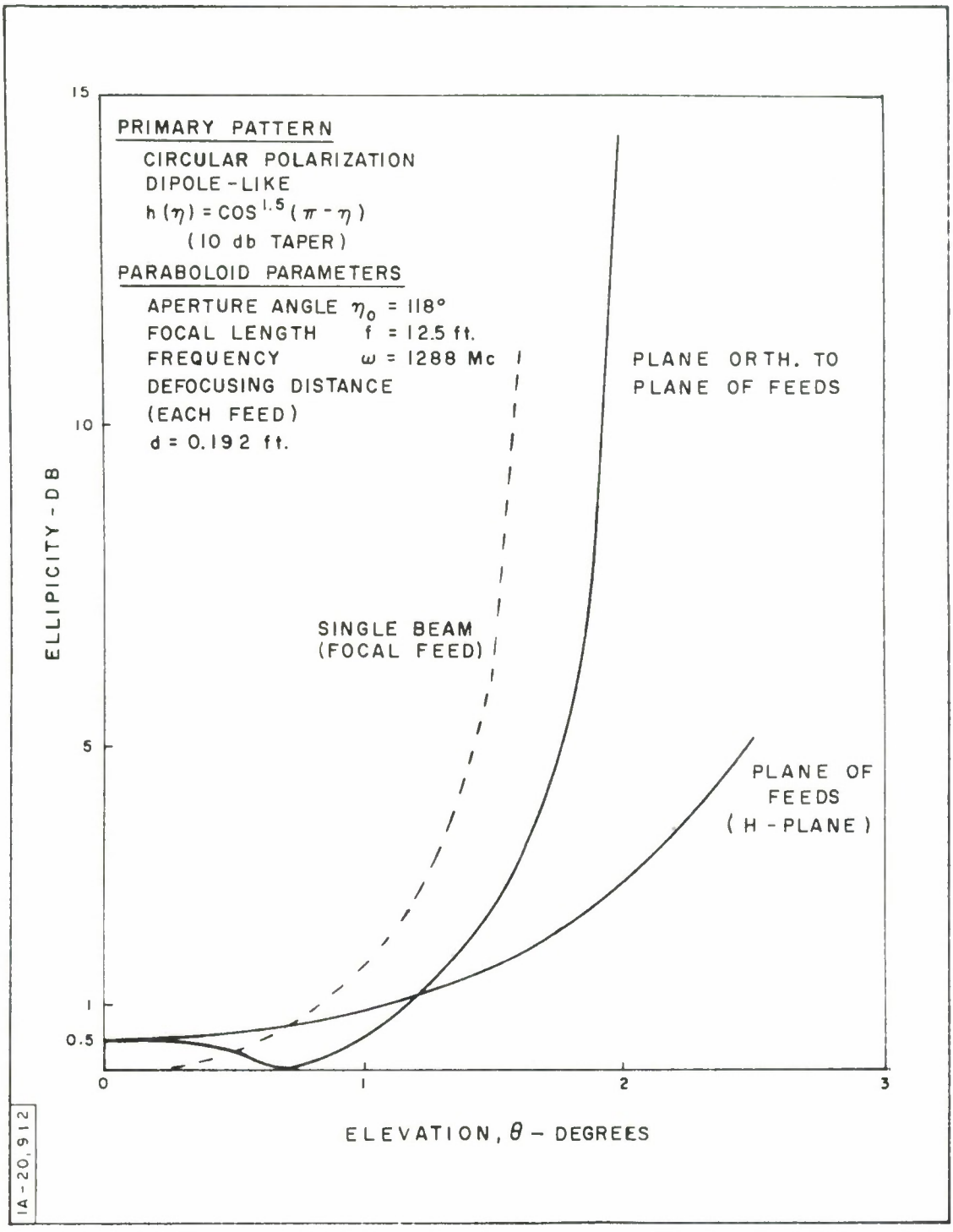

Figure 53. Defocusing in Focal Plane: Sum of Two Beams (Far-Field Ellipticity)

$$\int_0^{2\pi} \cos(k\,d\sin\eta\cos\psi)\cos^2\psi\,d\psi \neq \int_0^{2\pi} \cos(k\,d\sin\eta\cos\psi)\sin^2\psi\,d\psi$$

In the "vertical" plane (plane of feeds), the ellipticity keeps on rising slowly, whereas it first decreases in the horizontal plane before increasing rapidly (the minimum ellipticity is not far from θ_o).

In summary, the type of primary illumination plays a fundamental role in determining the character of the ellipticity. Whereas, in the circularly polarized focal feed case, ellipticity is always 0 db on boresight, regardless of the distribution over the dish, this is no longer the case under defocused conditions. For an imperfect illumination function, it would appear that the ellipticity on boresight is about one half of what it would be, for the focal feed single beam, at an elevation angle corresponding to "cross-over", that is, θ_o.

DEFOCUSING ALONG AXIS

Figures 54 through 57 pertain to the situation where the paraboloidal dish is illuminated from a feed that is displaced a distance $d = 0.417$ ft along the boresight axis, in an attempt to "focus" the field at a range $r_1 = 400$ ft. (See Section II and Figures 6 and 7). The displacement d was computed from Equation (96), where the constant 1.065 is "estimated."

Figure 54 contains plots of amplitude versus elevation for the equibeam distribution, with the taper function $\cos^{1.5}(\pi - \eta)$, under linear polarization. It is observed that the defocused amplitude curve (solid curve) for a range of 400 ft is very close to the far-field amplitude distribution, although it is still a little broader. It represents a dramatic improvement over the near-field pattern of the far-field focused beam. This slight broadening may be

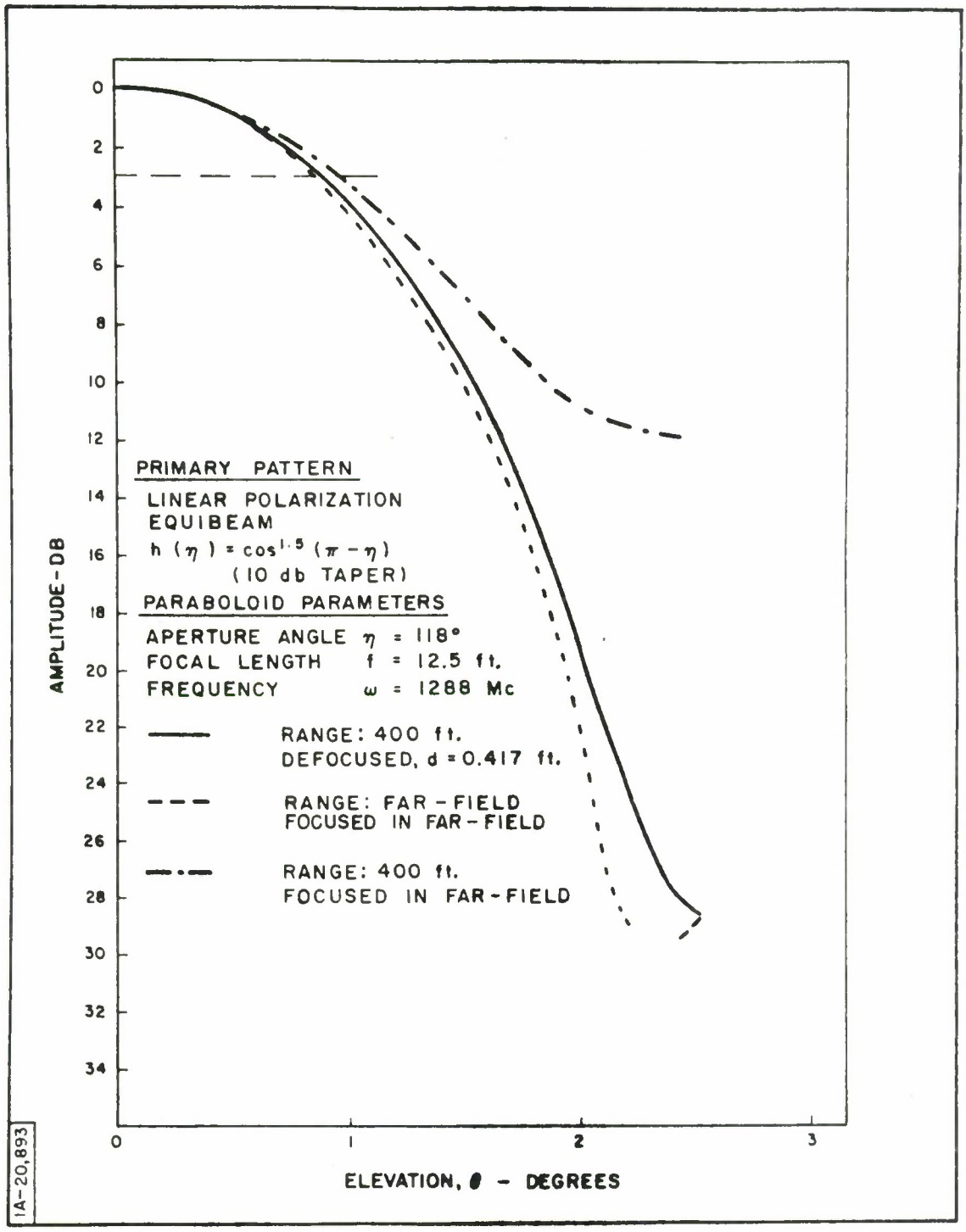

Figure 54. Focal Feed System: Amplitude Related to Defocusing Along Axis

accounted for by the facts that the displacement, d , is "estimated", and that even for the best estimate of d , some aberrations will always be present. The gain is essentially that in the far-field, whereas the gain of dot-dash curve is actually down 1.65 db.

Figure 55 refers to the same situation as Figure 54, except that the illumination is circularly polarized. The defocused ellipticity at 400 ft closely resembles the far-field ellipticity. Since the null is displaced to a larger elevation angle, so is the region of maximum ellipticity.

Figures 56 and 57 correspond, respectively, to Figures 54 and 55, except that the illumination is dipole-like. Since amplitude varies with azimuth, the amplitude plots refer to cuts in the φ = 45-degree planes. The same characteristics prevail so that the defocused patterns, at 400 ft, are almost exact replicas of the focused patterns at infinity.

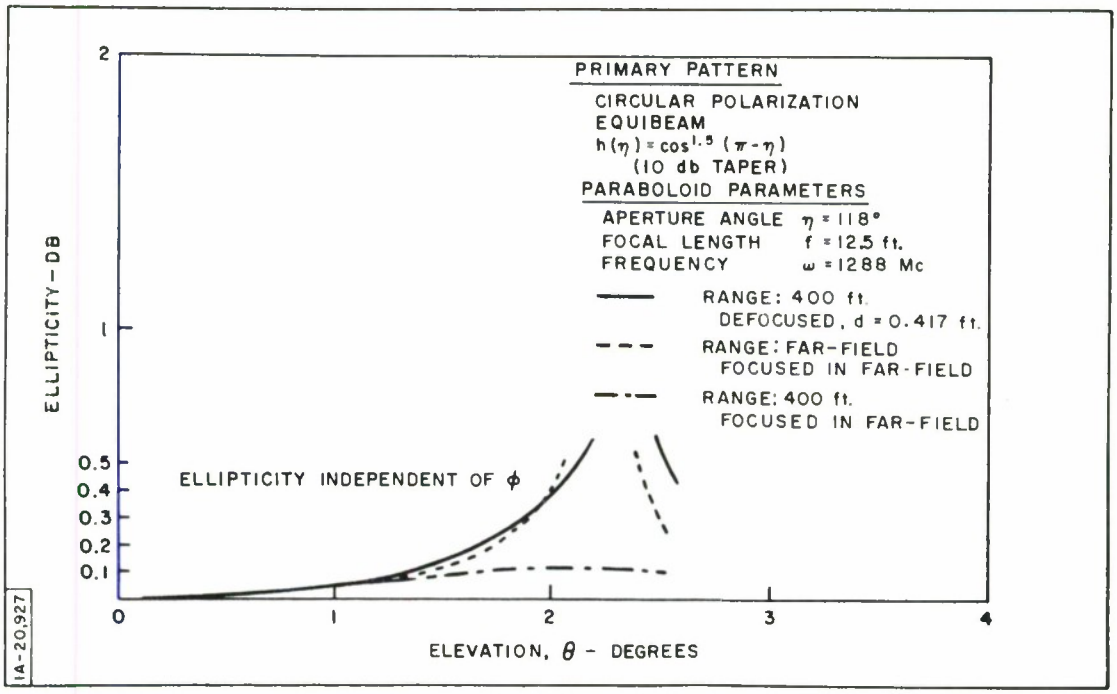

Figure 55. Focal Feed System: Ellipticity Related to Defocusing Along Axis

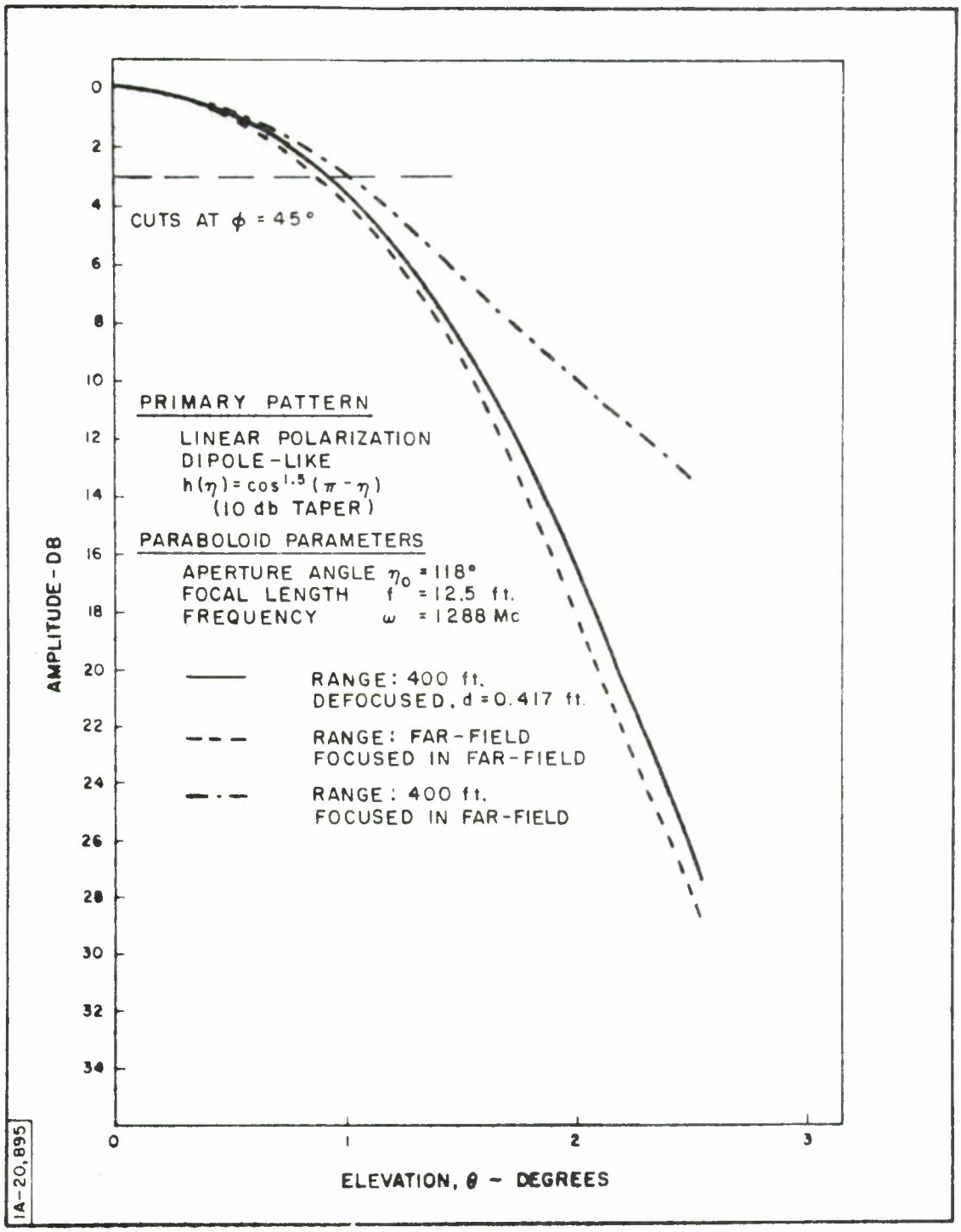

Figure 56. Focal Feed System: Amplitude Related to Defocusing Along Axis

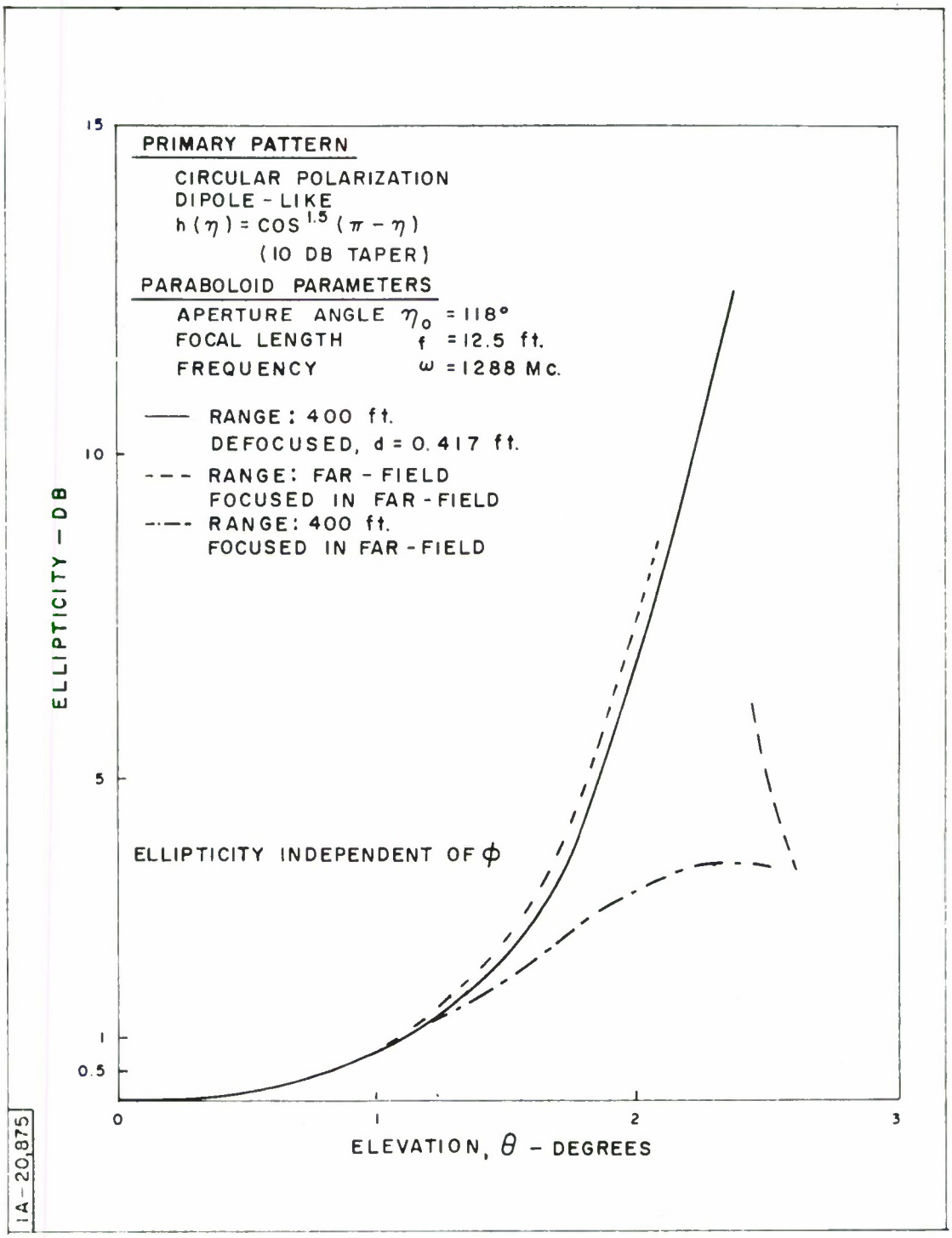

Figure 57. Focal Feed System: Ellipticity Related to Defocusing Along Axis

SECTION V

COMPUTED RESULTS – CASSEGRAIN SYSTEM

AMPLITUDES

Figures 58 and 59 are plots of the overall field amplitude at the observation point P as a function of elevation angle, θ , when the feed system is linearly polarized. Those plots are computed values of Equation (59) wherein Equations (158) and (161) have been substituted. The actual orientation of the total field at point P has not been considered separately, but can be deduced from the ellipticity curves (Figures 62 through 65).

Parameters applicable to those graphs are summarized in Table IV.

Table IV

Constants for the MITRE Antenna

FREQUENCY = 1288 Mc		
Taper function $h(\theta) = \cos^2(2\theta)$ (12 db taper)		
Sub-reflector		
Aperture half-angle	θ_o	$= 30^o$
Eccentricity	e	= 2.45
Parameter	a	= 1.063 ft
Main dish		
Aperture angle	η_o	$= 118^o$
Focal length	f	= 12.5 ft
Shadow aperture half-angle	η_1	$= 10.7^o$

Figure 58 compares the far-field amplitudes when the primary illumination is equibeam (solid line) and dipole-like (dashed line), with the same

taper function $h(\theta) = \cos^2(2\theta)$. It can be observed that both curves coalesce, except near the null. The reason is that the half-angle subtended by the subdish is relatively small (θ_o = 30 degrees) so that, as noted at the end of Appendix D, the two distributions are about the same. Thus, for the dipole-like distribution, the difference in field strength at the edge of the subdish between H-plane and E-plane is only 1.25 db.

The common 3-db half-beamwidth is 0.87 degrees.

The amplitude pattern is constant with azimuth for the equibeam distribution. For the dipole-like distribution, it is essentially constant, except near the null.

Figure 59 considers far-field amplitude changes induced by the shadowing effects of the subreflector and/or feed horn. Since, in the particular case under study, the two effects are approximately overlapping, the contributions from the main dish within an angle η_1 = 10.7 degrees have simply been omitted. This is equivalent to adding the negative field of a paraboloid of the same focal length, but of aperture angle = (180 - 10.7) degrees. The resultant field would be low in amplitude, but very broad. Thus, the overall field is slightly weaker on boresight (0.36 db loss), slightly sharper since the subtracting field is essentially constant near boresight (new 3-db half-beamwidth = 0.84 degrees), with a markedly deeper null and higher sidebands.

Figure 60 also considers the shadowing effect problem, but whereas the previous graph applies to the equibeam distribution, this one applies to the dipole-like distribution. The characters of the two graphs are essentially the same.

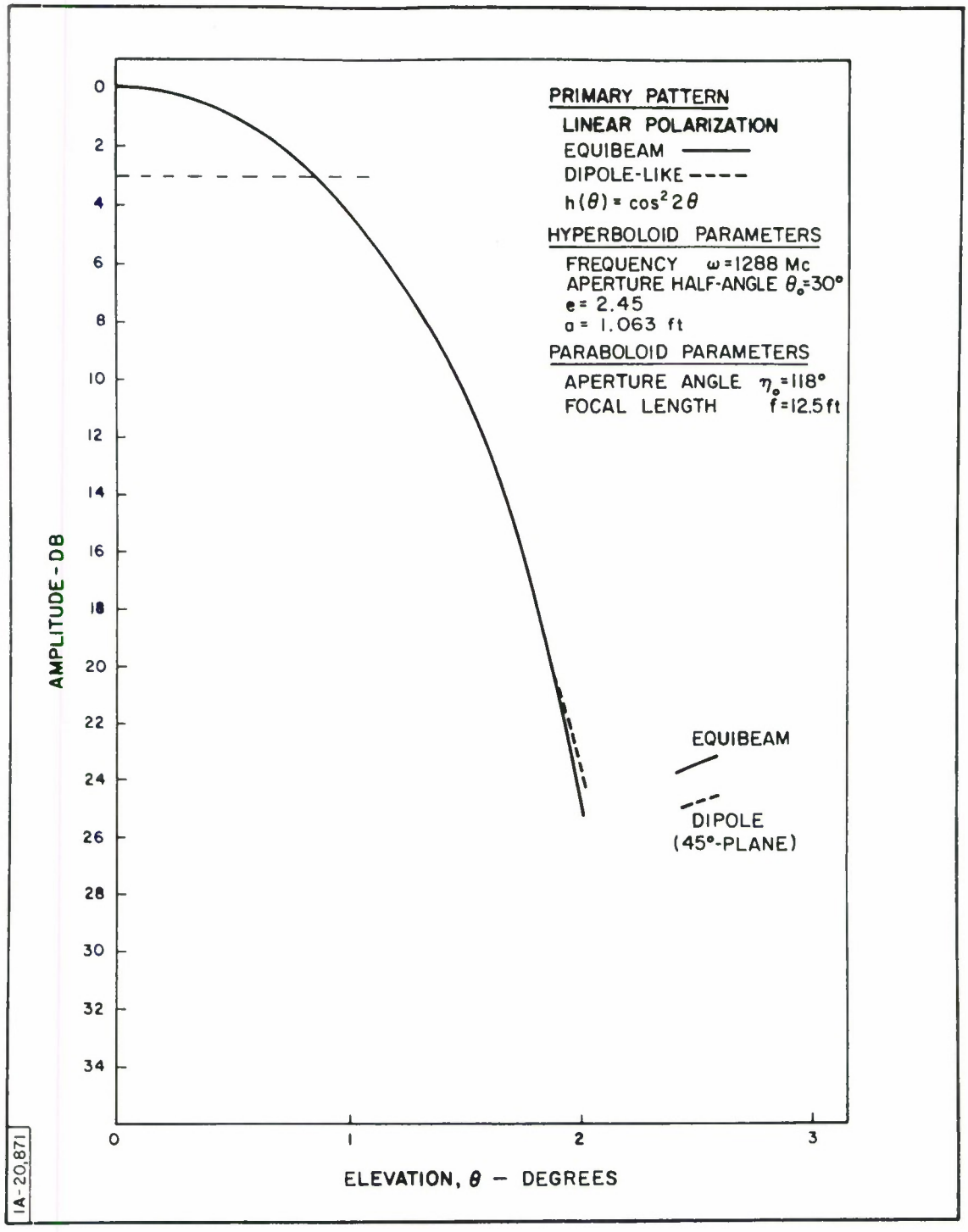

Figure 58. Cassegrain System: Amplitude Related to Primary Distribution (Far-Field)

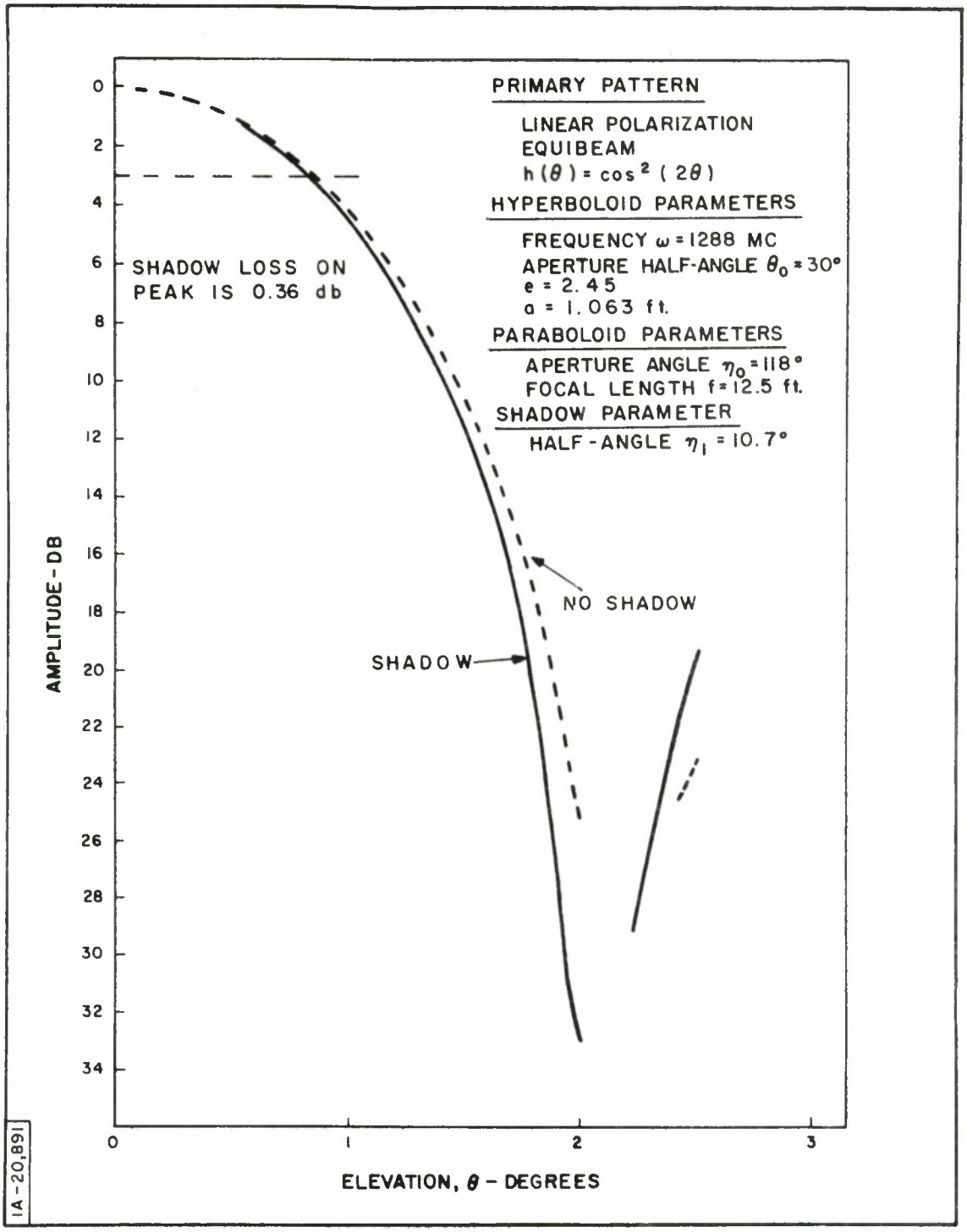

Figure 59. Cassegrain System: Amplitude Related to Shadowing Effects (Far-Field)

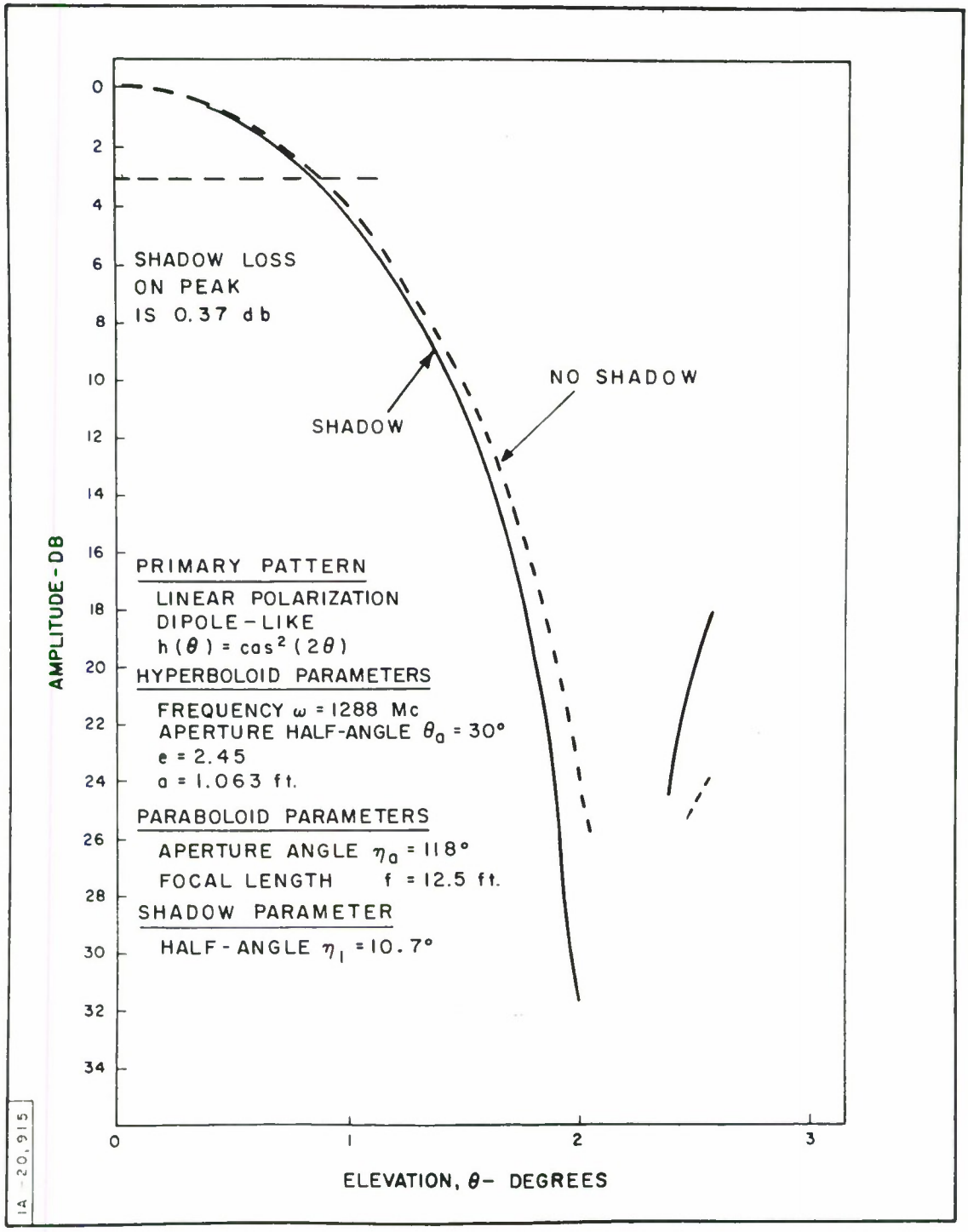

Figure 60. Cassegrain System: Amplitude Related to Shadowing Effects (Far-Field)

Figure 61 relates far-field amplitude to near-field amplitude (400 ft range) for the equibeam distribution, with shadow effects taken into account.

Remarks pertaining to the focal feed system apply here too. The amplitude distributions are practically the same near the peak of the beam, although the near-field 3-db half beamwidth is increased to 0.90 degrees at a range of 400 ft. The relative gain at 400 ft is down 1.67 db from the far-field gain, as referred to a standard horn. Major differences appear in the null region where, at 400 ft, the null is "filled-in" and the new null is pushed to a larger elevation angle.

ELLIPTICITIES

Figures 62 through 65 are plots of ellipticities at the observation point, P , as a function of the elevation angle, θ , when the feed system is circularly polarized. Those plots are computed values of Equation (56) wherein Equations (158) through (161) have been substituted. The conditions of Figures 62 through 65 parallel, respectively, conditions of 58 through 61.

Figure 62 shows the somewhat better performance of the equibeam distribution over the dipole-like distribution (far-field). However, the difference in ellipticity is very small, except in the null region. Ellipticities at the 3-db half-beamwidth: 0.14 db for the equibeam distribution; 0.17 for the dipole-like distribution. As discussed previously, at the edge of the subreflector, the dipole-like distribution shows a difference of only 1.25 db in amplitude between the H- and E-planes, that is, an ellipticity of 1.25 db. On the other hand, the equibeam distribution does not produce the perfect circularity exhibited in the focal feed system because of the existence of cross-polarized currents on the hyperboloidal subreflector.

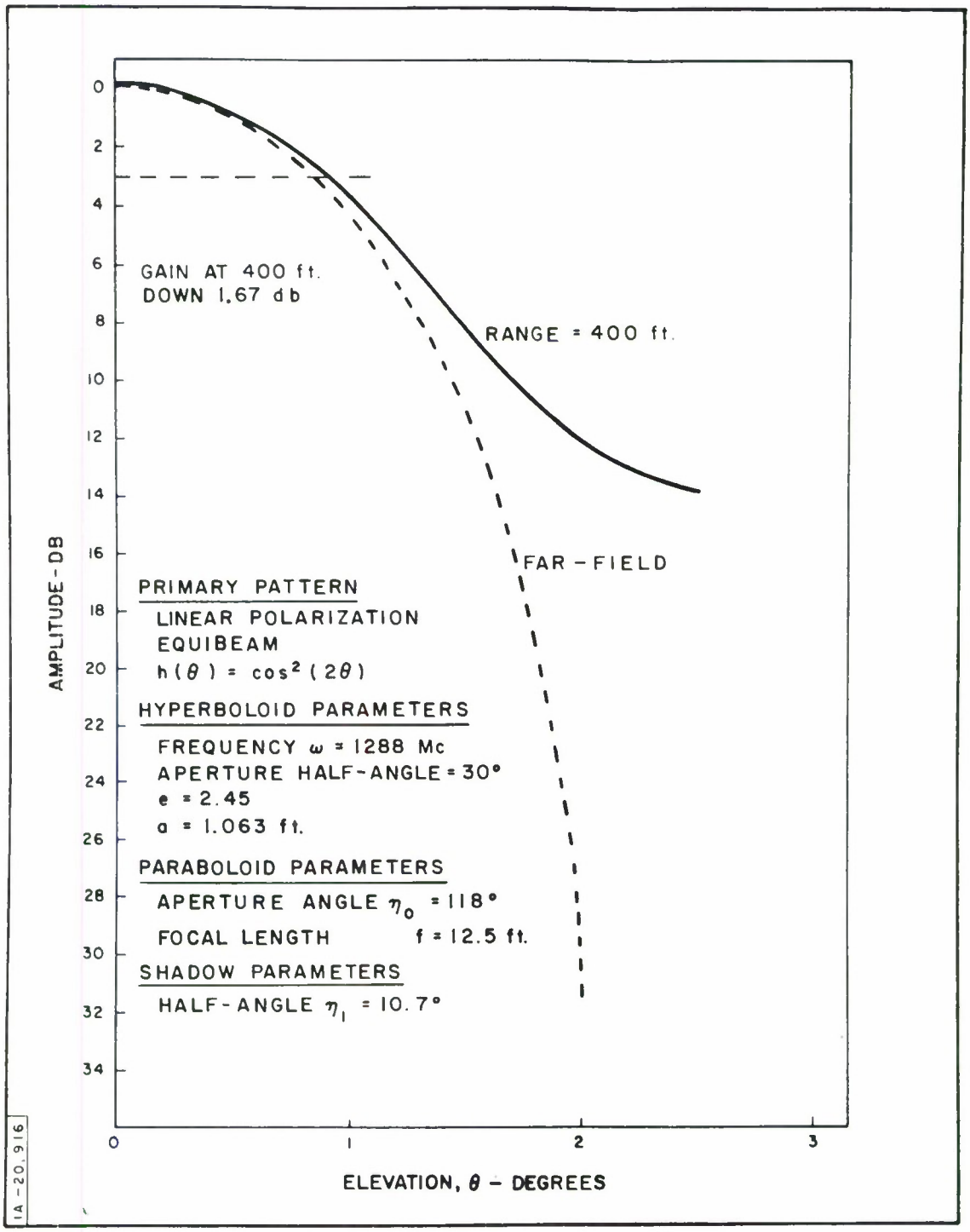

Figure 61. Cassegrain System: Amplitude Related to Range

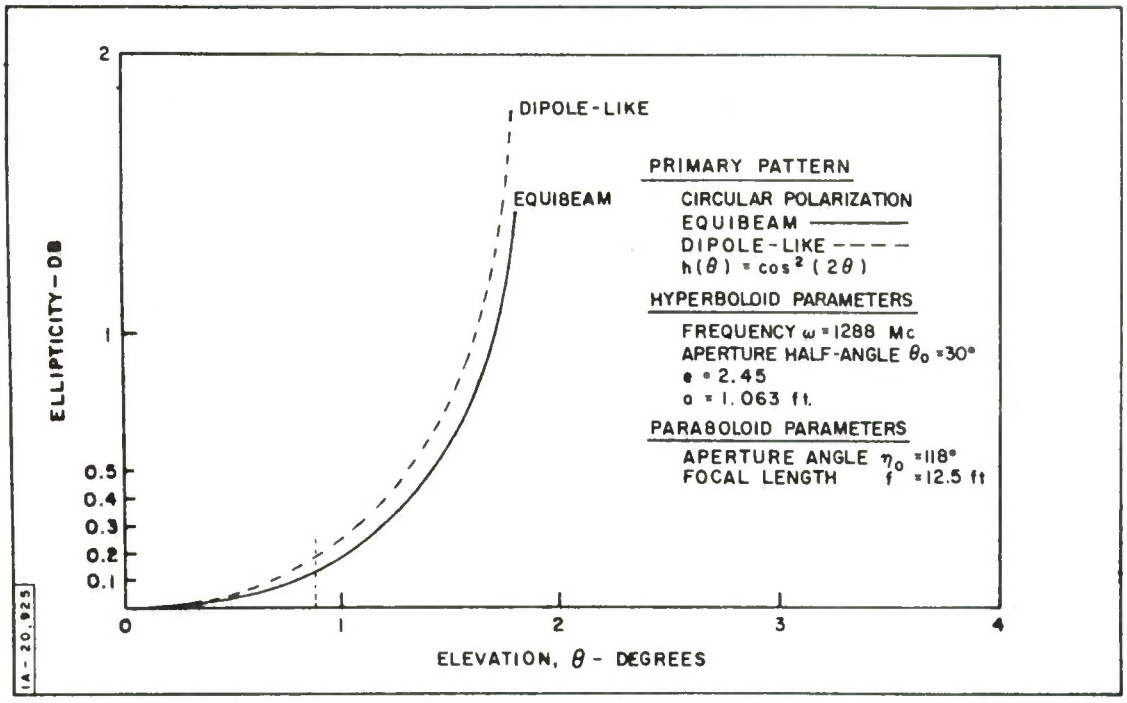

Figure 62. Cassegrain System: Ellipticity Related to Primary Distribution

Figure 63 considers far-field ellipticity changes induced by taking shadowing effects into account (equibeam distribution). The shadow tends to increase the ellipticity, but the effect is very small, except in the null region. Since the amplitude curve with shadow effects is slightly narrower, the ellipticities at the 3-db half-beamwidths are essentially the same for shadow and non-shadow conditions, that is, 0.14 db.

Figure 64 deals with the same situation as Figure 63 except that the primary distribution is dipole-like. The same remarks apply. The ellipticities at the 3-db half-beamwidths are essentially the same at 0.17 db.

Figure 65 relates far-field ellipticites to near-field ellipticities (400-ft range) for the equibeam distribution (shadow effects taken into account).

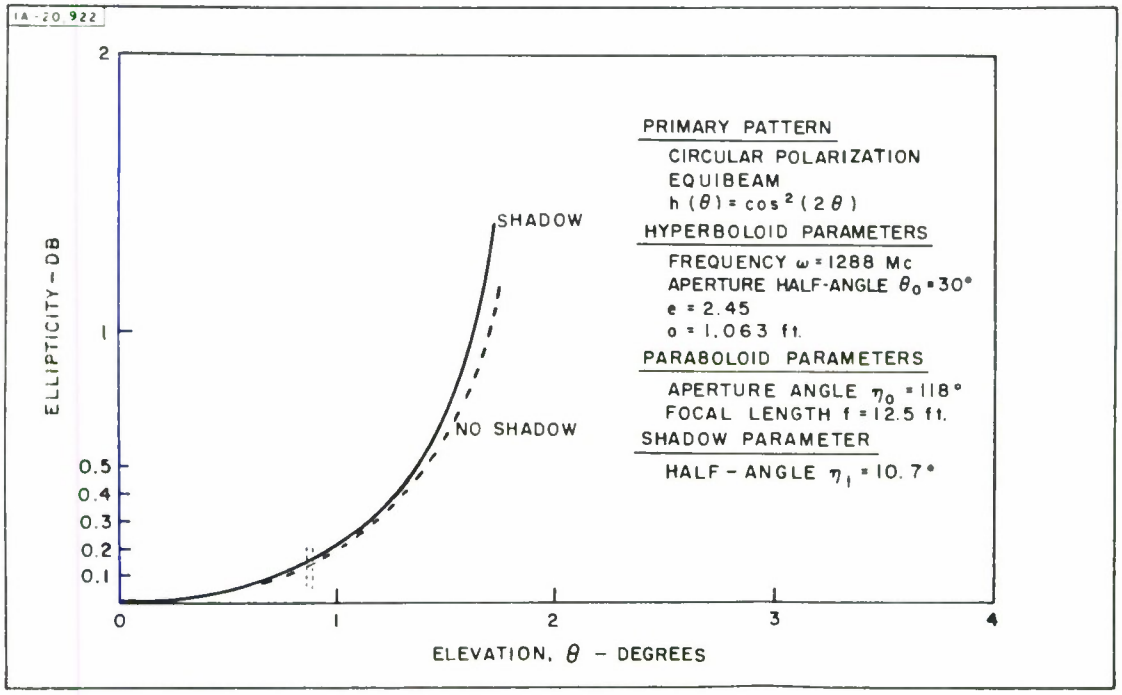

Figure 63. Cassegrain System: Ellipticity Related to Shadowing Effects (Far-Field)

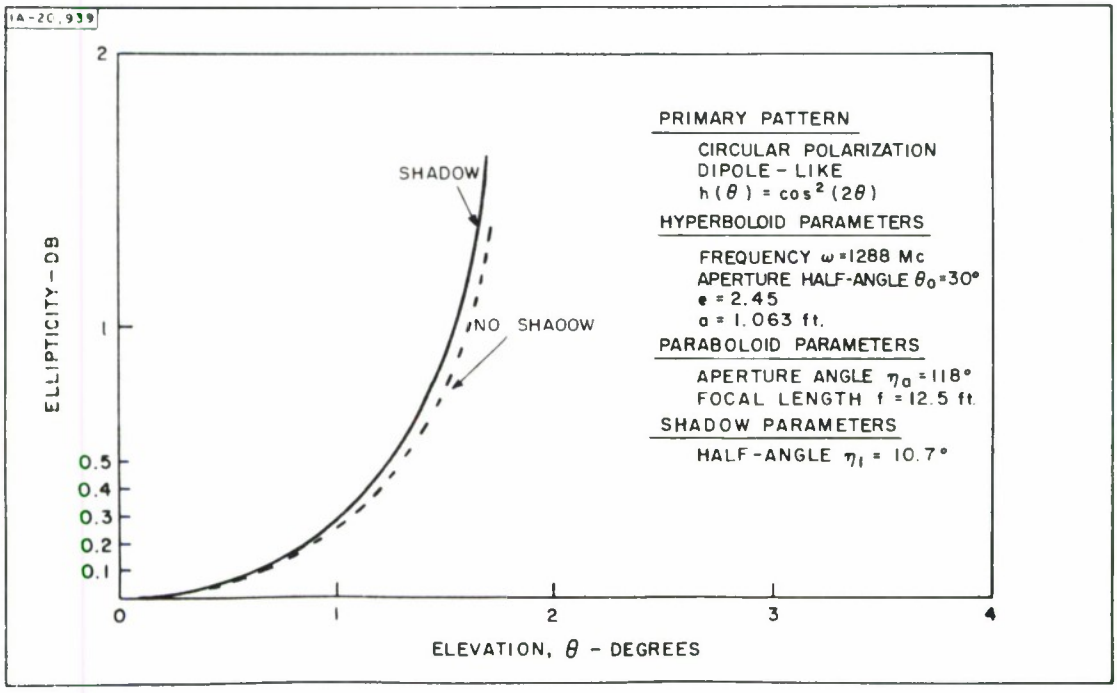

Figure 64. Cassegrain System: Ellipticity Related to Shadowing Effects (Far-Field)

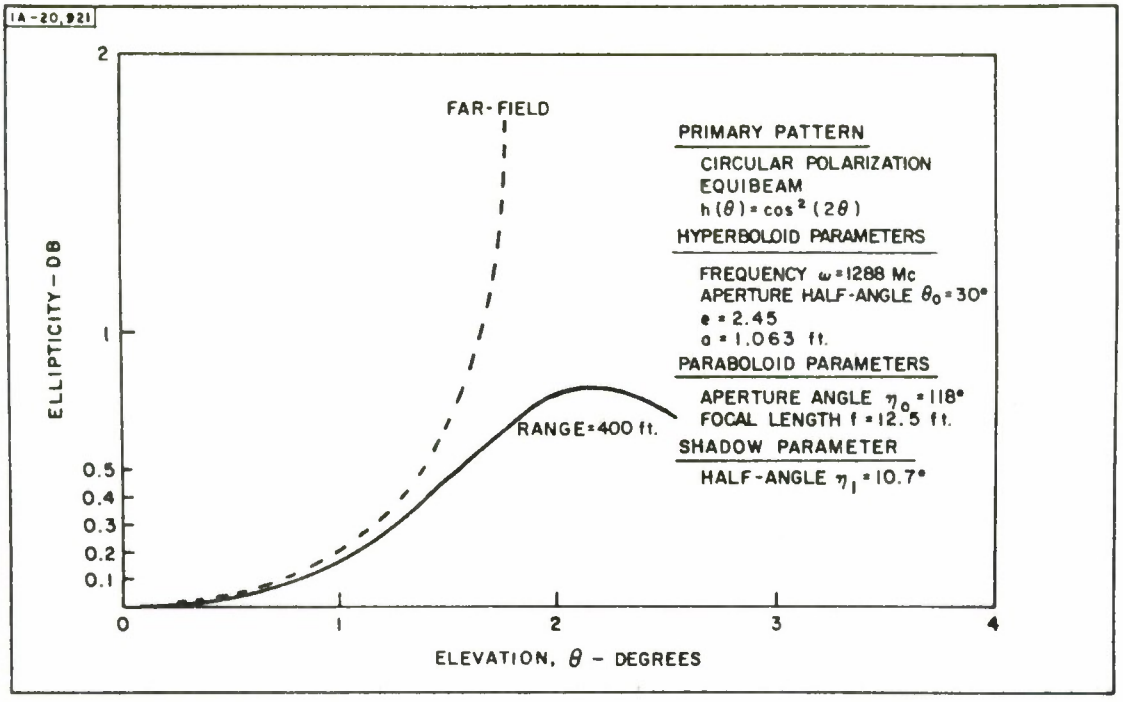

Figure 65. Cassegrain System: Ellipticity Related to Range

Near-field ellipticity peaks up to a low value in the corresponding near-field minimum amplitude region. Although this effect tends to lower the ellipticity curve, the ellipticities at the 3-db half-beamwidth remain essentially unchanged from far-field to near-field (400 ft) at 0.14 db.

PARABOLOID ILLUMINATION

Plots of the paraboloid illumination from the subreflector are contained in Figures 66 and 67.

Figures 66 considers H_{H1} Equation (153), the solid lines, and H_{E1} Equation (154), the dotted line, as functions of the elevation angle, η, for the equibeam primary distribution ($\cos^2 2\theta$ taper). Thus, H_{H1} is the field component in the H-plane ($\psi = 0, \pi$), at the paraboloidal dish, along the η-direction. The H_{H2} component is zero. The H_{H3} component (radial

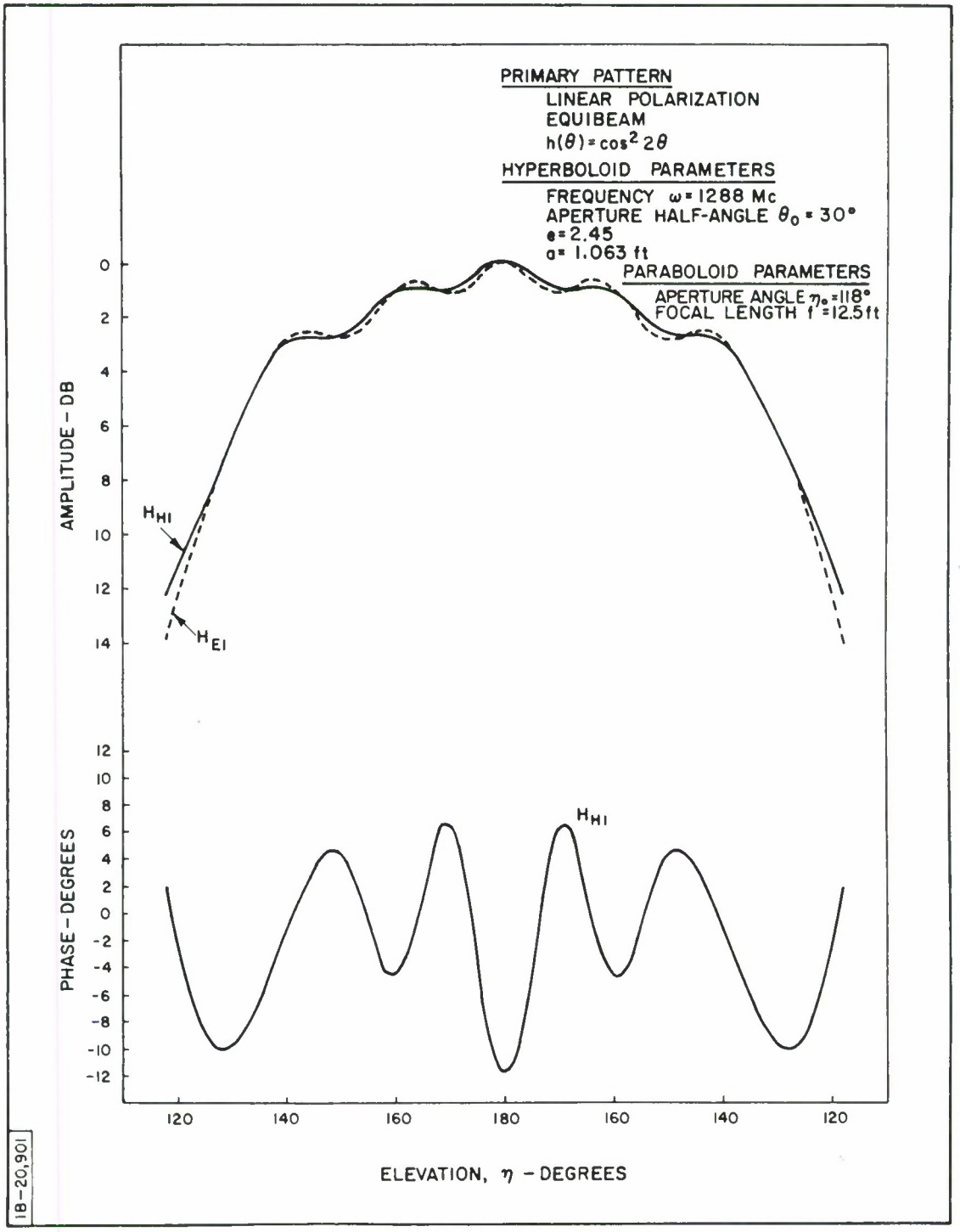

Figure 66. Cassegrain System: Paraboloid Illumination

component) is not zero, but, on the average, 40 db below the peak of H_{H1}. It does go up to 33 db below the peak of H_{H1} over small regions. H_{H3} is not plotted.

H_{E1}, the dotted line, is the field component in the E-plane ($\psi = \pm \pi/2$), directed along the x-direction. H_{E2} and H_{E3} are zero.

The H_{H1} and H_{E1} components are matched very closely to each other, but not exactly, although the primary illumination is equibeam. The difference is accentuated at the edge of the dish where it amounts to about 1.4 db. The curves, as a whole, exhibit shallow ripples which would become accentuated in the far-field (note that the curves refer to the fields at the paraboloid).

The phase of H_{H1} – relative to the focal feed phase – is also plotted. It oscillates about ±9 degrees about the value of -3 degrees. This average value depends on the a-parameter and has no special significance.

Figure 67 applies to the dipole-like distribution. The matching between H_{H1} and H_{E1}, although good, is not as close as in the preceding case. In particular, the mismatch at the edge amounts to about 2 db. Those results are consistent with computed ellipticities (Figure 62). Again, H_{H2} is zero; H_{H3} is very small (on the average, 40 db below the peak of H_{H1}); and H_{E2} and H_{E3} are zero.

This time, the phase H_{E1} relative to the focal feed phase, is plotted versus η. The phase oscillation amplitude is slightly larger than in the preceding case.

Figures 66 and 67 can be used to judge the amount of approximation resulting from treating the Cassegrain feed system by ray optics: in the latter case, H_{H1} and H_{E1} would be perfectly matched; H_{H3} would be

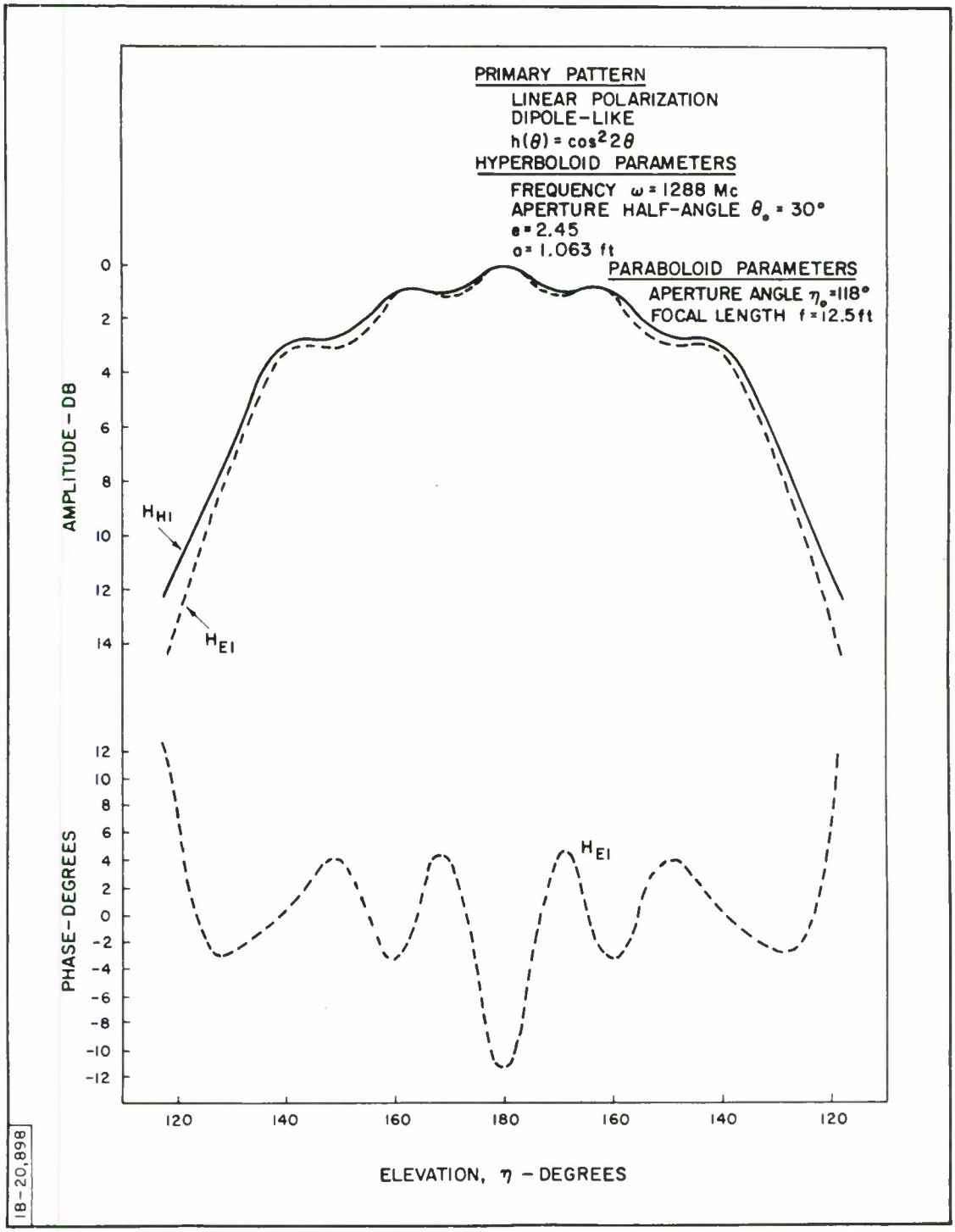

Figure 67. Cassegrain System: Paraboloid Illumination

zero; the phases (referred to the focal feed system) would be constant; there would be no amplitude ripple; the tapers would be those of the primary illumination function (except for range dependency); and in summary, the secondary illumination would be a replica of the primary illumination, except for angular magnification. On all counts, ray optics would give quantitatively inaccurate, but qualitatively valuable information.

APPENDIX A

EXPRESSION FOR $\hat{n}$ IN CARTESIAN COORDINATES (PARABOLOID)

The coordinate system used is shown in Figures 3 and 4. The origin is at point 0, the focus of the paraboloid, and the z-axis is oriented along the axis of symmetry. Let Q_o be a point on the paraboloid, located in the x-z plane, such that the angle of zOQ_o is η. Consider $\hat{n}_o$ at Q_o. The geometric properties of the parabola are such that a ray, transmitted from point 0 and incident at Q_o, will be reflected parallel to the z-axis. Consequently, the angle of $\hat{n}_o$ and the z-axis is $(\pi - \eta)/2$. The components of $\hat{n}_o$ at Q_o are

$$n_x = -\sin\left[\frac{1}{2}(\pi - \eta)\right] = -\cos \eta/2 \tag{166}$$

$$n_z = \cos\left[\frac{1}{2}(\pi - \eta)\right] = \sin \eta/2 \tag{167}$$

The components of $\hat{n}$ at any point Q are obtained by rotating Q_o about the z-axis through an angle ψ. Analytically, the results will be obtained by operating on Equations (166) and (167) by a rotation matrix

$$\begin{vmatrix} n_x \\ n_y \\ n_z \end{vmatrix} = \begin{vmatrix} \cos\psi & -\sin\psi & 0 \\ \sin\psi & \cos\psi & 0 \\ 0 & 0 & 1 \end{vmatrix} \begin{vmatrix} -\cos \eta/2 \\ 0 \\ \sin \eta/2 \end{vmatrix} = \begin{vmatrix} -\cos\psi \cos \eta/2 \\ -\sin\psi \cos \eta/2 \\ \sin \eta/2 \end{vmatrix} \tag{168}$$

APPENDIX B

EXPRESSION FOR $\vec{\rho}$ IN CARTESIAN COORDINATES (PARABOLOID)

Just as in Appendix A, the coordinate system used is shown in Figures 3 and 4. Let $\vec{\rho}_o$ correspond to point Q_o in the x-z plane. The components of $\vec{\rho}_o$ are

$$\rho_x = \rho \sin \eta \tag{170}$$

$$\rho_z = \rho \cos \eta \tag{171}$$

The expression for $\vec{\rho}$ at point Q is obtained by operating on Equations (170) and (171) with a rotation matrix (Appendix A),

$$\vec{\rho} = \begin{vmatrix} \cos\psi & -\sin\psi & 0 \\ \sin\psi & \cos\psi & 0 \\ 0 & 0 & 1 \end{vmatrix} \rho \begin{vmatrix} \sin\eta \\ 0 \\ \cos\eta \end{vmatrix} = \rho \begin{vmatrix} \sin\eta\cos\psi \\ \sin\eta\sin\psi \\ \cos\eta \end{vmatrix} \tag{172}$$

Since the equation of the parabola in polar form is

$$\rho = f/(\sin^2 \eta/2) \tag{173}$$

it follows that

$$\vec{\rho} = \frac{f}{\sin^2 \eta/2} \begin{vmatrix} \sin\eta\cos\psi \\ \sin\eta\sin\psi \\ \cos\eta \end{vmatrix} \tag{174}$$

It is noteworthy that ρ plus the distance from Q to the focal plane ($z = 0$) is a constant equal to 2f:

$$\rho + \rho \cos \eta = \rho (1 + \cos \eta) \tag{175}$$

$$= \frac{f}{\sin^2 \eta/2} (2 \sin^2 \eta/2) = 2f$$

so that any ray emanating from the focus loses the phase 2 kf to the focal plane.

If η_o is the value of η at the edge of the parabola, the aperture D can be expressed in terms of η_o and f according to

$$D = 2\rho \sin \eta_o = 4f \cot \eta_o/2 \tag{176}$$

APPENDIX C

DIFFERENTIAL AREA, dA, OF THE PARABOLOID

The differential element of area, dA , produced by a differential change $d\eta$ in η and $d\psi$ in ψ is (Figure 68)

$$dA = \rho \sin \eta \, d\psi \left[\rho^2 + \left(\frac{d\rho}{d\eta} \right)^2 \right]^{1/2} d\eta$$

But

$$\rho = \frac{f}{\sin^2 \eta/2}$$

which is the equation of the generating parabola in polar form. Hence,

$$\frac{d\rho}{d\eta} = -2f \sin^{-3} \eta/2 \cos \eta/2 \cdot \frac{1}{2} = -\frac{f \cos \eta/2}{\sin^3 \eta/2}$$

so that

$$\left[\rho^2 + \left(\frac{d\rho}{d\eta} \right)^2 \right]^{1/2} = \left(\frac{f^2}{\sin^4 \eta/2} + \frac{f^2 \cos^2 \eta/2}{\sin^6 \eta/2} \right)^{1/2} = \frac{f}{\sin^2 \eta/2} (1 + \cot^2 \eta/2)^{1/2} = \frac{f}{\sin^3 \eta/2}$$

It follows that

$$dA = \frac{f^2 \sin \eta}{\sin^6 \eta/2} \, d\eta \, d\psi \qquad (177)$$

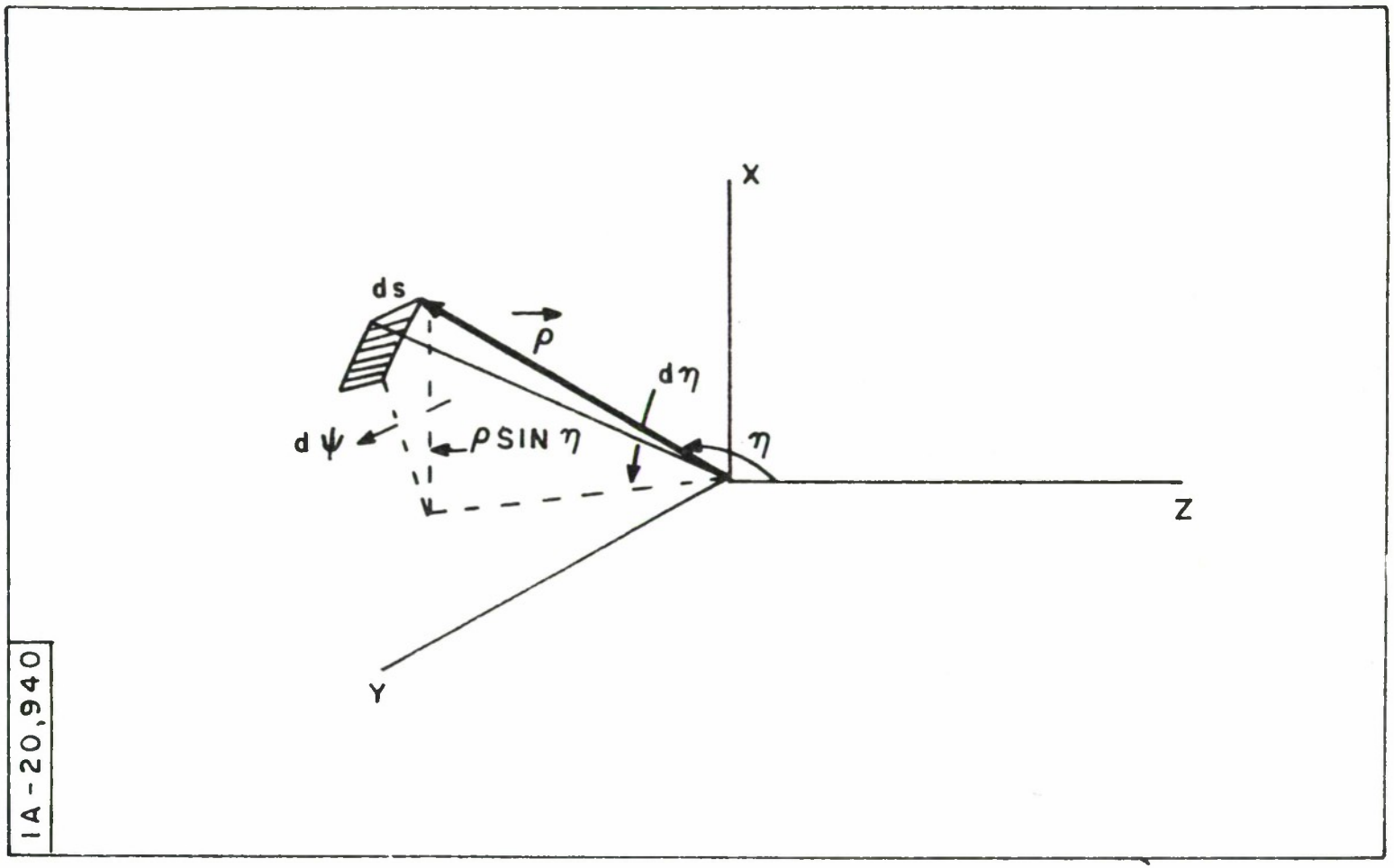

Figure 68. Differential Area

APPENDIX D

EXPRESSIONS FOR PRIMARY PATTERNS IN CARTESIAN COORDINATES

EQUIBEAM CONDITIONS

In deriving an analytic expression for the incident field $\vec{H}_i = \vec{H}_{io} e^{-jk}$ under equibeam conditions, the following properties pertaining to the feed horn and its primary pattern are postulated (those properties may also be used to define the equibeam conditions):

(1) The incident wave is spherical and issues from a well-defined "phase center."

(2) The H-field is perpendicular to the direction of propagation, that is, perpendicular to vector $\vec{\rho}$ (Figure 2).

(3) The "vertical" component of $\vec{H}_{io}$, $\vec{H}_V$, has no y-component (that is, no "horizontal" component) in the H- and E-planes ($\psi = 0, \pi$ and $\psi = \pm\frac{\pi}{2}$, respectively). The "horizontal" component of $\vec{H}_{io}$, $\vec{H}_H$, present under circular polarization, has no x-component (that is, no "vertical" component) in the H- and E-planes.

(4) Each linear component of $\vec{H}_{io}$ is equibeam in the sense that the strength of $\vec{H}$ in the H-plane is the same as the strength of $\vec{H}$ in the E-plane.

(5) Finally, it is not clear, at first, what directions must be assigned to the H-field in the other azimuthal planes. It turns out that the supplementary constraint is that orthogonal linear components in the feed give rise to orthogonal linear components

at any point on the spherical wavefront. Were it not so, the structure would exhibit "preferred" planes which would be inconsistent with the underlying goal of axial symmetry.

Thus, in summary, equibeam conditions are such that the field possesses axial symmetry in strength, but non-axial symmetry in direction. Rather, directions are constrained in such a manner that orthogonal families at the feed give rise to orthogonal families on the spherical wavefront.

Postulates (1) and (2) will be satisfied if, in the coordinate system $\eta - \psi - \rho$, $\vec{H}_V$ and $\vec{H}_H$ are expressed, respectively, as

$$\vec{H}_V = \begin{vmatrix} p \\ q \\ 0 \end{vmatrix} \quad ; \quad \vec{H}_H = \begin{vmatrix} p' \\ q' \\ 0 \end{vmatrix} \tag{178}$$

Postulate (4) requires that

$$p^2 + q^2 = 1$$

$$p'^2 + q'^2 = 1 \tag{179}$$

whereas Postulate (5) requires the equation

$$pp' + qq' = 0 \tag{180}$$

which is satisfied by

$$p' = \pm q$$

$$q' = \mp p \tag{181}$$

The simplest solution to Postulate (3), consistent with Equations (179) is

$$p = \mp \cos\psi$$

$$q = \mp \sin\psi \tag{182}$$

where the minus sign corresponds to a positive value of the x-component of $\vec{H}_{io}$, the positive sign to a negative value of the x-component.

To get an expression for $\vec{H}_V$ in the Cartesian coordinate system, one must first rotate the η - ψ - ρ system about the local ψ-axis through a - η angle, then – about the z-axis – through a -ψ angle (Appendix E). The transformation matrices are, respectively,

$$[T]_{-\eta} = \begin{vmatrix} \cos\eta & 0 & \sin\eta \\ 0 & 1 & 0 \\ -\sin\eta & 0 & \cos\eta \end{vmatrix} \tag{183}$$

and

$$[T]_{-\psi} = \begin{vmatrix} \cos\psi & -\sin\psi & 0 \\ \sin\psi & \cos\psi & 0 \\ 0 & 0 & 1 \end{vmatrix} \tag{184}$$

The expression for $\vec{H}_V$ in Cartesian coordinates becomes

$$\vec{H}_V = [T]_{-\psi}[T]_{-\eta} \begin{vmatrix} -\cos\psi \\ -\sin\psi \\ 0 \end{vmatrix} = \begin{vmatrix} -\cos^2\psi\cos\eta + \sin^2\psi \\ -\cos\psi\sin\psi(1+\cos\eta) \\ \sin\eta\cos\psi \end{vmatrix} \tag{185}$$

The projection of $\vec{H}_V$ onto the x-y plane is plotted semi-graphically in Figure (69).

From Equation (101), and by using the same procedure, one obtains for $\vec{H}_H$

$$H_H = [T]_{-\psi}\,[T]_{-\eta} \begin{vmatrix} -\sin\psi \\ \cos\psi \\ 0 \end{vmatrix} = \begin{vmatrix} -\cos\psi \sin\psi\,(1+\cos\eta) \\ -\sin^2\psi\cos\eta + \cos^2\psi \\ \sin\eta\sin\psi \end{vmatrix} \tag{186}$$

It may be readily verified that

$$\vec{H}_V \cdot \vec{H}_H = 0 \tag{187}$$

and that

$$|H_V|^2 = |H_H|^2 = 1 \tag{188}$$

regardless of ψ and η.

As a direct consequence, if $\vec{H}_V$ and $\vec{H}_H$ (as defined above) are applied simultaneously and in phase-quadrature, each point on the spherical wavefront will be circularly polarized.

Under conditions of equibeam circular polarization, the complete expression for $\vec{H}_{io}$ becomes

$$\vec{H}_{io} = h(\eta)\sin^2\eta/2 \begin{vmatrix} (-\cos^2\psi\cos\eta + \sin^2\psi)\cos\omega t \\ \quad + (-\cos\psi\sin\psi\,[1+\cos\eta])\sin\omega t \\ (-\cos\psi\sin\psi\,[1+\cos\eta])\cos\omega t \\ \quad + (-\sin^2\psi\cos\eta + \cos^2\psi)\sin\omega t \\ \sin\eta\cos\psi\cos\omega t + \sin\eta\sin\psi\sin\omega t \end{vmatrix} \tag{189}$$

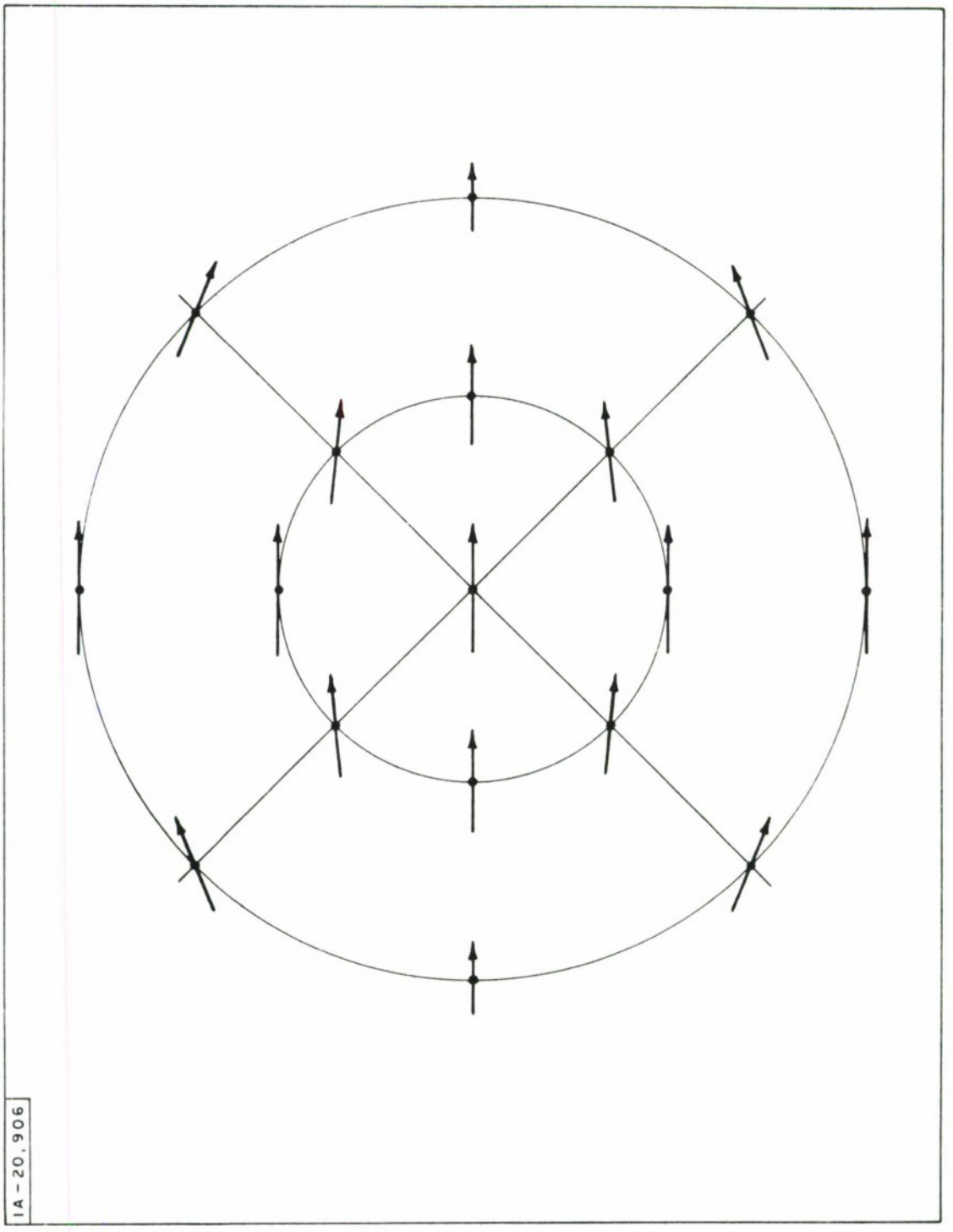

Figure 69. Equibeam Distribution: Projection of H-Field onto x-y Plane

where $\sin^2 \eta/2$ is a common factor reflecting the strength dependence on range ($1/\rho \propto \sin^2 \eta/2$), and $h(\eta)$ is a common tapering function dependent on η only.

It has been found that

$$h(\eta) = \cos^{1.5}(\pi - \eta) \tag{190}$$

fits the amplitude pattern very closely for an equibeam system with a 10 db taper at the edge of the dish (η_o = 118 degrees).

DIPOLE-LIKE DISTRIBUTION

The dipole-like distribution is considerably simpler than the equibeam distribution. Postulates (1) and (2) still apply, but Postulate (3) is modified to require that the "vertical" component of $\vec{H}_{io}$, $\vec{H}_V$, contain no y-component anywhere on the spherical wavefront, and that the "horizontal" component of $\vec{H}_{io}$, $\vec{H}_H$, contain no x-component anywhere on the spherical wavefront.

By Postulates (1) and (3), $\vec{H}_V$ and $\vec{H}_H$ are expressed, respectively, as

$$\vec{H}_V = \begin{vmatrix} m \\ 0 \\ n \end{vmatrix} ; \quad \vec{H}_H = \begin{vmatrix} 0 \\ m' \\ n' \end{vmatrix} \tag{191}$$

Postulate (2) expresses the conditions that

$$\begin{aligned} \vec{H}_V \cdot \vec{\rho} &= 0 \\ \vec{H}_H \cdot \vec{\rho} &= 0 \end{aligned} \tag{192}$$

But

$$\vec{\rho} = \rho \begin{vmatrix} \sin\eta\cos\psi \\ \sin\eta\sin\psi \\ \cos\eta \end{vmatrix}$$

by Equation (172). Hence, it follows that

$$\vec{H}_V = \begin{vmatrix} -\cos\eta \\ 0 \\ \sin\eta\cos\psi \end{vmatrix} \tag{193}$$

and

$$\vec{H}_H = \begin{vmatrix} 0 \\ -\cos\eta \\ \sin\eta\sin\psi \end{vmatrix} \tag{194}$$

Although the projections of $\vec{H}_V$ and $\vec{H}_H$ on the x-y plane are equal and orthogonal, it is apparent, from Equations (193) and (194), that

$$\vec{H}_V \cdot \vec{H}_H \neq 0 \tag{195}$$

that is, $\vec{H}_V$ and $\vec{H}_H$ are not orthogonal, except when $\psi = 0, \pi$ or $\pm\pi/2$ on the H- and E-planes. Also

$$|H_V| = \text{fc of } \psi; \qquad |H_H| = \text{fc of } \psi \tag{196}$$

In particular, when $\eta = 120$ degrees, $|H_V|$ is larger in the H-plane ($\psi = 0$) than in the E-plane ($\psi = \pm\pi/2$) by 6 db.

When $\vec{H}_V$ and $\vec{H}_H$ are applied simultaneously and in phase quadrature (circularly polarized feed), $\vec{H}_{io}$ becomes

$$\vec{H}_{io} = h(\eta) \sin^2 \eta/2 \begin{vmatrix} -\cos\eta\cos\omega t \\ -\cos\eta\sin\omega t \\ \sin\eta\cos(\omega t - \psi) \end{vmatrix} \tag{197}$$

where $\sin^2 \eta/2$ is the distance factor and $h(\eta)$ is a tapering function independent of azimuth.

In order to determine the ellipticity on the spherical wavefront, when the feed is circularly polarized, one can use the coordinate transformation method of Appendix E and the appropriate equations of Appendix F to compute the ellipticity of $\vec{H}_{io}$ on the dish. Replacing $\cos\omega t$ by 1 and $\sin\omega t$ by j, and neglecting the common η-dependency terms, one re-writes Equation (197) as

$$\vec{H}_{io} \propto \begin{vmatrix} -\cos\eta \\ -j\cos\eta \\ \sin\eta(\cos\psi + j\sin\psi) \end{vmatrix} \tag{198}$$

By the applications of Equation (210) (but with θ replaced by $(\eta - \pi)$, φ by ψ), one obtains

$$\dot{H}_{\text{io transf.}} = \begin{vmatrix} -\cos\eta\,(\cos\psi\,[-\cos\eta] + \sin\psi\,[-j\cos\eta] + \sin^2\eta\,(\cos\psi + j\sin\psi) \\ -\sin\psi\,(-\cos\eta) + \cos\psi\,(-j\cos\eta) \\ -\sin\eta\,[\cos\psi\,(-\cos\eta) + \sin\psi\,(-j\cos\eta)] - \cos\eta\,[\sin\eta\,(\cos\psi + j\sin\psi)] \end{vmatrix}$$

$$= \begin{vmatrix} \cos\psi + j\sin\psi \\ \cos\eta\,(\sin\psi - j\cos\psi) \\ 0 \end{vmatrix} \qquad (199)$$

Equation (199) represents the total field on the spherical wavefront in a right-hand coordinate system oriented along η, ψ, and $-\rho$. As expected, the ρ-component is zero. By Equations (217) and (218),

$$2\,|S^+|^2 = (\cos^2\psi + \cos^2\eta\sin^2\psi) + (\sin^2\psi + \cos^2\eta\cos^2\psi) - 2\cos\eta$$

$$2\,|S^-|^2 = (\cos^2\psi + \cos^2\eta\sin^2\psi) + (\sin^2\psi + \cos^2\eta\cos^2\psi) + 2\cos\eta$$

or

$$|S^+| = \frac{1}{\sqrt{2}}(1 - \cos\eta)$$

$$|S^-| = \frac{1}{\sqrt{2}}(1 + \cos\eta) \qquad (200)$$

so that

$$\text{Ellipticity} = \frac{1}{|\cos\eta|} \qquad (201)$$

It is remarkable that the ellipticity is independent of azimuth. The ellipticity goes to 1 when $\eta = \pi$ (on-axis) and to infinity (linear polarization) when $\eta = \pi/2$.

By application of Equation (221) to Equation (199), it is found that the orientation of the major axis is at zero degree in the local coordinate system. Consequently, in the fixed x-y-z coordinate system, the orientation of the ellipses is actually radial.

OTHER DISTRIBUTIONS

One may attempt to remedy the shortcomings of the dipole-like distribution by requiring that $\vec{H}_V$ and $\vec{H}_H$ be constant with azimuth. This will be the case for $\vec{H}_V$ if

$$|\gamma_c (-\hat{x} \cos\eta + \hat{z} \sin\eta \cos\psi)| = 1 \tag{202}$$

regardless of ψ . A solution for this equation is

$$\gamma_c = (\cos^2\eta + \sin^2\eta \cos^2\psi)^{-\frac{1}{2}} \tag{203}$$

In the same fashion, it will be found that $\vec{H}_H$ is constant with ψ if

$$|\gamma_s (-\hat{x} \cos\eta + \hat{z} \sin\eta \sin\psi)| = 1 \tag{204}$$

whose solution is

$$\gamma_s = (\cos^2\eta + \sin^2\eta \sin^2\psi)^{-\frac{1}{2}} \tag{205}$$

Thus, the expression for $\vec{H}_{io}$ in Cartesian coordinates for a circularly polarized feed system is

$$\vec{H}_{io} = h(\eta) \sin^2 \eta/2 \begin{vmatrix} -\cos\eta\,\gamma_c \cos\omega t \\ -\cos\eta\,\gamma_s \sin\omega t \\ (\sin\eta\cos\psi\,\gamma_c)\cos\omega t + (\sin\eta\sin\psi\,\gamma_s)\sin\omega t \end{vmatrix} \tag{206}$$

A few remarks are in order. Although $\vec{H}_V$ and $\vec{H}_H$ are equibeam in amplitude and can be applied in phase-quadrature, the resultant on the spherieal wavefront will not be circularly polarized everywhere, as in the case of the true equibeam distribution. Furthermore, in contradistinetion with the dipole-like distribution, the ellipticity is not constant with azimuth because the spaee angle of $\vec{H}_V$ and $\vec{H}$ varies with ψ (at eonstant η). Only in the vertical and horizontal planes are $\vec{H}_V$ and $\vec{H}_H$ orthogonal and $\vec{H}_{io}$ cireularly polarized.

This phenomenon ean be formally evideneed by applying the eoordinate transformation method of Appendix E and the appropriate equations of Appendix F. It is found that the magnitudes of the circular waves are

$$|S^+| = 1 - \gamma_c \gamma_s \cos\eta$$

$$|S^-| = 1 + \gamma_c \gamma_s \cos\eta \tag{207}$$

that is, they are functions of ψ, for a given value of η.

Because the ellipticity is not constant with azimuth, this pseudo-equibeam distribution eannot be produeed by a cylindrically symmetrical feed such as a cylindrieally symmetrical cireular horn. Another point of view is that the orthogonal and phase-quadratured sources of this pseudo-equibeam distribution eannot be considered infinitely small in extent and are not equivalent to a single, statieally charged, rotating souree.

Finally, note that when the elevation angle is small (near on-axis region with $\cos \eta \approx 1$, $\sin \eta \approx 0$), all three distributions are essentially the same on the spherical wavefront. Marked differences show up as the elevation angle opens up.

APPENDIX E

COORDINATE TRANSFORMATIONS AT OBSERVATION POINT P

For small values of $|\theta|$, the x and y coordinates, at the observation point P, are essentially perpendicular to the line of sight.

If the value of $|\theta|$ is not small, it is convenient to deal with a local coordinate system, x'', y'', z'', such that z'' is along the line of sight, for purposes of computing amplitudes and polarizations.

Let $\vec{H}_S\big|_P$ be (X, Y, Z), as given by Equations (52) and (53) (Z can be obtained from Equations (21) or (28), although this is not essential Equation (211).

First, rotate the coordinate system about the z-axis until the vector $\hat{a}_1$ lies in the z-x' plane (where x' is the rotated x-axis), that is, perform a ϕ-rotation (Figure 70). This is accomplished by the rotation matrix.

$$[T]_\phi = \begin{vmatrix} \cos\phi & \sin\phi & 0 \\ -\sin\phi & \cos\phi & 0 \\ 0 & 0 & 1 \end{vmatrix} \tag{208}$$

Next, perform a rotation about the y'-axis (the rotated y-axis), in the direction from z to x'. This is accomplished by the rotation matrix

$$[T]_\theta = \begin{vmatrix} \cos\theta & 0 & -\sin\theta \\ 0 & 1 & 0 \\ \sin\theta & 0 & \cos\theta \end{vmatrix} \tag{209}$$

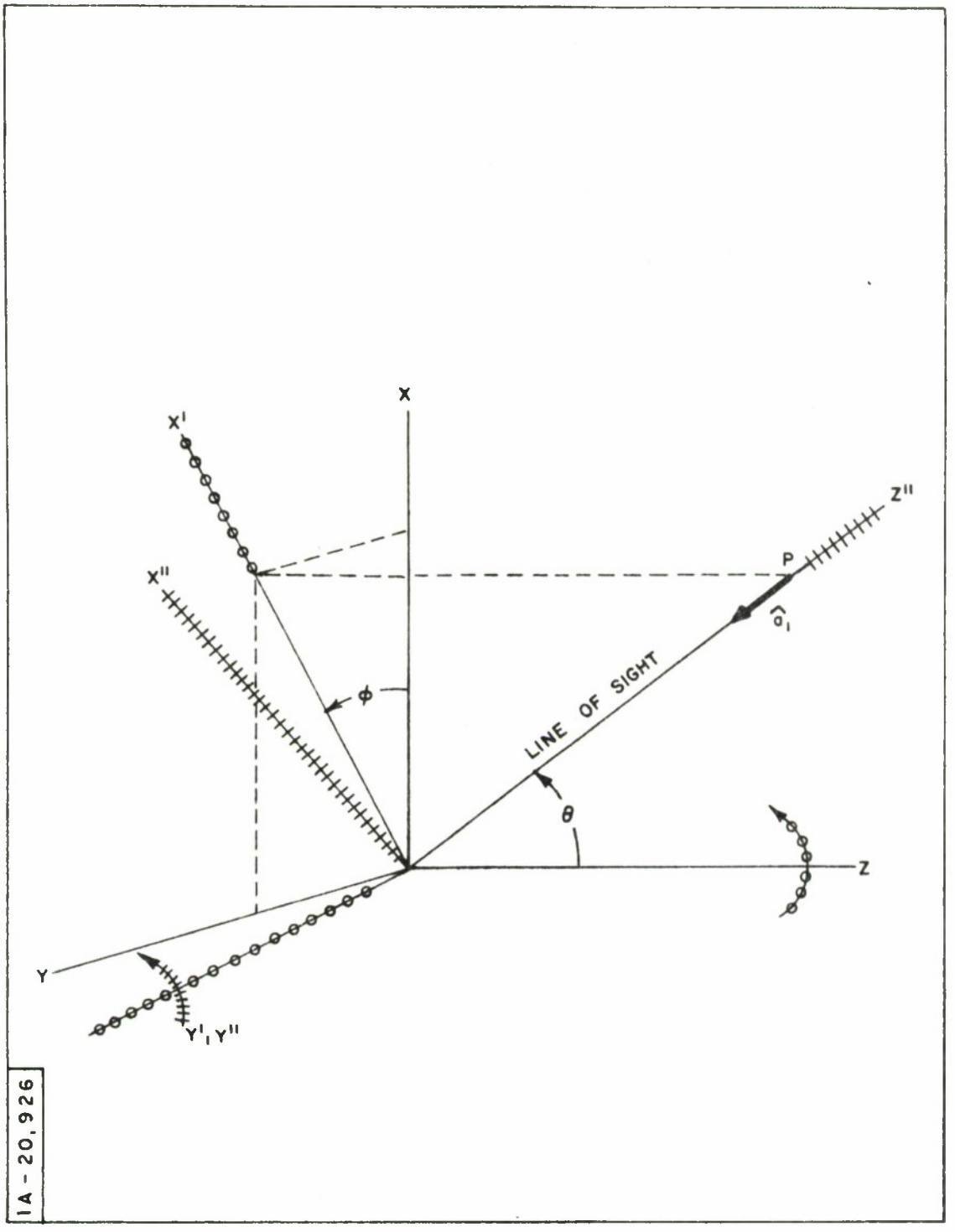

Figure 70. Rotations Related to Line-of-Sight Vector $\hat{a}_1$
(1) Rotation about z-axis
(2) Rotation about y'-axis

No more rotation appears to be necessary. The new z-axis, z'' , is now lined up with $\hat{a}_1$, the direction from the observation point, P, to the focus.

In the new coordinate system, the field components become

$$\begin{vmatrix} X'' \\ Y'' \\ Z'' \end{vmatrix} = [T]_\theta [T]_\phi \begin{vmatrix} X \\ Y \\ Z \end{vmatrix} = [T]_\theta \begin{vmatrix} \cos\phi\, X + \sin\phi\, Y \\ -\sin\phi\, X + \cos\phi\, Y \\ Z \end{vmatrix}$$

$$= \begin{vmatrix} \cos\theta\,(\cos\phi\, X + \sin\phi\, Y) - \sin\theta\, Z \\ -\sin\phi\, X + \cos\phi\, Y \\ \sin\theta\,(\cos\phi\, X + \sin\phi\, Y) + \cos\theta\, Z \end{vmatrix} \tag{210}$$

Since the z''-component must be 0, it follows that

$$Z = -\frac{\sin\theta}{\cos\theta}(\cos\phi\, X + \sin\phi\, Y) \tag{211}$$

and that

$$\begin{vmatrix} X'' \\ Y'' \\ Z'' \end{vmatrix} = \begin{vmatrix} \frac{1}{\cos\theta}(X\cos\phi + Y\sin\phi) \\ (-X\sin\phi + Y\cos\phi) \\ 0 \end{vmatrix} \tag{212}$$

APPENDIX F

COMPUTATION OF ELLIPTICITY

Given an x-component, $X = Ae^{j\alpha}$, and a y-component, $Y = B\,e^{j\beta}$, where the magnitudes A and B are real and arbitrary, and the phases α and β are real and arbitrary, what is the ellipticity (ratio of major to minor axis) ?

Write $A\,e^{j\alpha}$ in vector form as

$$\begin{vmatrix} A\,e^{j\alpha} \\ 0 \end{vmatrix} = \frac{1}{2} \left| \begin{pmatrix} A\,e^{j\alpha} \\ -j\,A\,e^{j\alpha} \end{pmatrix} + \begin{pmatrix} A\,e^{j\alpha} \\ j\,A\,e^{j\alpha} \end{pmatrix} \right| \tag{213}$$

that is, as the sum of two circularly polarized waves:

$$\frac{A}{2}\,e^{j\alpha} \begin{vmatrix} 1 \\ -j \end{vmatrix}$$, a right-hand wave advanced by α, $\frac{A^+}{2}\,e^{j\alpha}$

and

$$\frac{A}{2}\,e^{j\alpha} \begin{vmatrix} 1 \\ j \end{vmatrix}$$, a left-hand wave advanced (in its own direction) by α, $\frac{A^-}{2}\,e^{j\alpha}$.

In the same fashion, the y-component is

$$\begin{vmatrix} 0 \\ B\,e^{j\beta} \end{vmatrix} = \frac{1}{2} \left| \begin{pmatrix} j\,B\,e^{j\beta} \\ B\,e^{j\beta} \end{pmatrix} + \begin{pmatrix} -j\,B\,e^{j\beta} \\ B\,e^{j\beta} \end{pmatrix} \right| \tag{214}$$

that is, the sum of

$$B\, e^{j\left(\beta + \frac{\pi}{2}\right)} \begin{vmatrix} 1 \\ -j \end{vmatrix}$$, a right-hand wave, advanced by $\left(\beta + \frac{\pi}{2}\right)$, $\frac{B^+}{2}\, e^{j\left(\beta + \frac{\pi}{2}\right)}$

and

$$B\, e^{j\left(\beta - \frac{\pi}{2}\right)} \begin{vmatrix} 1 \\ j \end{vmatrix}$$, a left-hand wave, advanced by $\left(\beta - \frac{\pi}{2}\right)$, $\frac{B^-}{2}\, e^{j\left(\beta - \frac{\pi}{2}\right)}$

(Note how the right-hand wave is advanced by $\pi/2$, whereas the left-hand wave is retarded by $\pi/2$) .

The right-hand waves and the left-hand waves can be respectively added up together, that is

$$S^+ = \frac{1}{2}\left[A^+ e^{j\alpha} + B^+ e^{j\left(\beta + \frac{\pi}{2}\right)}\right]$$

$$= \frac{1}{2}\,[X + jY] \tag{215}$$

$$S^- = \frac{1}{2}\left[A^- e^{j\alpha} + B^- e^{j\left(\beta - \frac{\pi}{2}\right)}\right]$$

$$= \frac{1}{2}\,[X - jY] \tag{216}$$

The magnitudes of S^+ and S^- are, respectively,

$$|S^+| = \frac{1}{2}\left[(A\cos\alpha - B\sin\beta)^2 + (A\sin\alpha + B\cos\beta)^2\right]^{1/2}$$

$$= \frac{1}{2}\left[(\mathrm{Re}\,X - \mathrm{Im}\,Y)^2 + (\mathrm{Im}\,X + \mathrm{Re}\,Y)^2\right]^{1/2} \tag{217}$$

$$|S^-| = \frac{1}{2}\left[(A\cos\alpha + B\sin\beta)^2 + (A\sin\alpha - B\cos\beta)^2\right]^{1/2}$$

$$= \frac{1}{2}\left[(\mathrm{Re}\,X + \mathrm{Im}\,Y)^2 + (\mathrm{Im}\,X - \mathrm{Re}\,Y)^2\right]^{1/2} \tag{218}$$

The ellipticity is obtained by using those equations in

$$\text{Ellipticity} = \left| \frac{|S^+| + |S^-|}{|S^+| - |S^-|} \right| \tag{219}$$

The phase of S^+ with respect to the datum direction (x-axis) is

$$\arg S^+ = \tan^{-1} \left(\frac{\sin \alpha + \cos \beta}{\cos \alpha - \sin \beta} \right) = \tan^{-1} \left(\frac{B\ \mathrm{Im}\ X + A\ \mathrm{Re}\ Y}{B\ \mathrm{Re}\ X - A\ \mathrm{Im}\ Y} \right) \tag{220}$$

and, in the same fashion, the phase of S^- is

$$\arg S^- = \tan^{-1} \left(\frac{\sin \alpha - \cos \beta}{\cos \alpha + \sin \beta} \right) = \tan^{-1} \left(\frac{B\ \mathrm{Im}\ X - A\ \mathrm{Re}\ Y}{B\ \mathrm{Re}\ X + A\ \mathrm{Im}\ Y} \right) \tag{221}$$

Note that if $\arg S^+$ is positive, it denotes a right-hand angle; if $\arg S^-$ is positive, it denotes a left-hand angle.

The major axis corresponds to the situation when S^+ and S^- are in phase, that is, it lies half-way between $\arg S^+$ and $\arg S^-$ or

$$\text{Orientation of major axis} = \frac{1}{2} (\arg S^+ - \arg S^-) \tag{222}$$

APPENDIX G

THE FUNCTION $\int_0^{2\pi} \sin 2\psi \, e^{jm\cos(\psi-\phi)} \, d\psi$

This is the integration with respect to ψ for the phase-quadrature eomponents (Equations (47) and (50)).

First, let $\varphi = 0$ or π. Then

$$\int_0^{2\pi} \sin 2\psi \, e^{jm\cos\psi} \, d\psi =$$

$$\int_0^{\pi/2} \sin 2\psi \, e^{jm\cos\psi} \, d\psi + \int_{\pi/2}^{\pi} \sin 2\psi \, e^{jm\cos\psi} \, d\psi + \int_{\pi}^{3\pi/2} \sin 2\psi \, e^{jm\cos\psi} \, d\psi$$

$$+ \int_{3\pi/2}^{2\pi} \sin 2\psi \, e^{jm\cos\psi} \, d\psi$$

$$= \int_0^{\pi/2} \sin 2\psi \, e^{jm\cos\psi} \, d\psi + \int_{\pi/2}^{\pi} \sin 2\psi \, e^{jm\cos\psi} \, d\psi - \int_{\pi/2}^{\pi} \sin 2\psi \, e^{jm\cos\psi} \, d\psi$$

$$- \int_0^{\pi/2} \sin 2\psi \, e^{jm\cos\psi} \, d\psi = 0$$

since to eaeh value $\sin 2\psi \, e^{jm\cos\psi}$ in the first quadrant is assoeiated the value $-\sin 2\psi \, e^{jm\cos\psi}$ in the fourth quadrant, and to each value $-\sin 2\psi \, e^{jm\cos\psi}$ in the second quadrant, is associated the value $\sin 2\psi \, e^{jm\cos\psi}$ in the third quadrant.

Even faetors of ψ in the integrand will not ehange the result.

Now let $\varphi = \pm \pi/2$. Then the integral is again zero, exeept that now it is beeause values in the first quadrant cancel with corresponding values in the third quadrant, whereas values in the second quadrant caneel with corresponding values in the fourth quadrant.

Hence, the far-field quadrature terms become zero when the observation point is located in one of the two principal planes $\varphi = 0$ or $\varphi = \pi/2$.

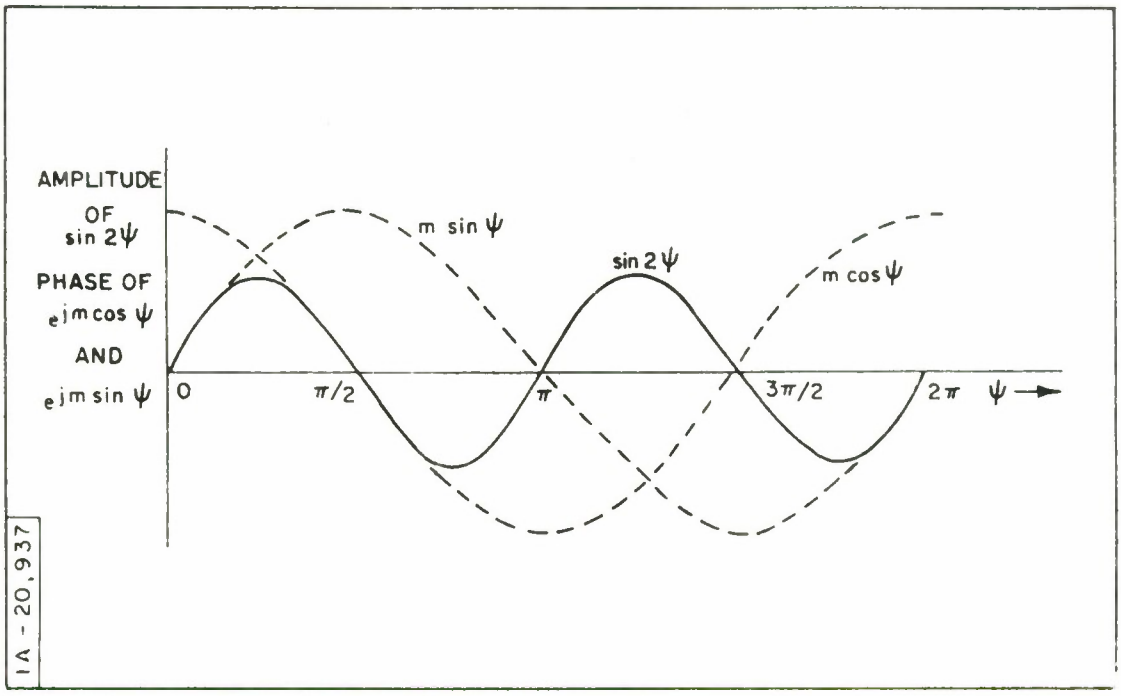

Figure 71. Amplitudes, Signs, and Phases

APPENDIX H

FLAT CIRCULAR PLATE ILLUMINATED BY PLANE, CIRCULARLY POLARIZED WAVE

This case may be considered as the limit of the paraboloid as the focal length is extended to infinity whereas the aperture remains constant. As a matter of fact, it is often substituted for the paraboloid in the literature,* but treated without regard to polarization.

The far-field equation is

$$\vec{H}_S\big|_p = \frac{jk}{2\pi r_1} e^{-jkr_1} \iint_S [(\hat{n} \times \vec{H}_i) \times \hat{a}_1] e^{-jk(\vec{\rho} \cdot \hat{a}_1)} dA \tag{223}$$

The vector $\hat{n}$ is simply (see Figure 72)

$$\hat{n} = \hat{z} \tag{224}$$

The vector $\hat{a}_1$ is still (see Equation (10))

$$\hat{a}_1 = -\begin{vmatrix} \sin\theta\cos\phi \\ \sin\theta\sin\phi \\ \cos\theta \end{vmatrix} \tag{225}$$

*See, for instance, L. Thourel, "The Antenna," pp. 260-262, John Wiley and Sons, Inc. New York, 1960.

The vector $\vec{\rho}$ ("center" of scattering is taken at center of the plate) is

$$\vec{\rho} = \rho \left[\hat{x} \cos \psi + \hat{y} \sin \psi \right] \tag{226}$$

so that

$$e^{-jk\vec{\rho} \cdot \hat{a}_1} = e^{jk\rho \sin\theta \cos(\psi - \phi)} \tag{227}$$

The differential area dA is simply

$$dA = \rho \, d\rho \, d\psi \tag{228}$$

The primary pattern, not necessarily uniform, is of the form

$$\vec{H}_i = h(\rho) \begin{vmatrix} \cos \omega t \\ \sin \omega t \\ 0 \end{vmatrix} \tag{229}$$

so that the eross-product $(\hat{n} \times \vec{H}_i)$ becomes

$$\text{Cofactors of } h(\rho) \begin{vmatrix} \hat{x} & \hat{y} & \hat{z} \\ 0 & 0 & 1 \\ \cos \omega t & \sin \omega t & 0 \end{vmatrix} = h(\rho) \begin{vmatrix} -\sin \omega t \\ \cos \omega t \\ 0 \end{vmatrix} \tag{230}$$

Finally, the cross-product of $(\hat{n} \times \vec{H}_i)$ and $\hat{a}_1$ becomes

$$\text{Cofactors of } h(\rho) \begin{vmatrix} \hat{x} & \hat{y} & \hat{z} \\ -\sin \omega t & \cos \omega t & 0 \\ -\sin\theta\cos\phi & -\sin\theta\sin\phi & \cos\theta \end{vmatrix} = h(\rho) \begin{vmatrix} \cos \omega t \cos\theta \\ \sin \omega t \cos\theta \\ (\sin\theta\sin\phi)\sin\omega t + (\sin\theta\cos\phi)\cos\omega t \end{vmatrix} \tag{231}$$

For small values of θ , the expression for the far-field becomes (Equation (77))

$$\vec{H}_S|_p \propto \hat{x} \cos \omega t \int_0^a J_o (k\rho \sin \theta)\, h(\rho)\, \rho\, d\rho$$

$$+ \hat{y} \sin \omega t \int_0^a J_o (k\rho \sin \theta)\, h(\rho)\, \rho\, d\rho \qquad (232)$$

Thus, it is seen that the x- and y-components are equal in magnitude, are in phase-quadrature, and are independent of φ .

For large values of θ , the coordinate transformation of Appendix E can be used. Thus, by Equation (211),

$$\vec{H}_S|_p \propto \hat{x}'' \cos (\omega t - \phi) \int_0^a J_0 (k\rho \sin \theta)\, h(\rho)\, \rho\, d\rho$$

$$+ y'' \sin (\omega t - \phi) [\cos \theta] \int_0^a J_o (k\rho \sin \theta)\, h(\rho)\, \rho\, d\rho \qquad (233)$$

Hence, except for the factor $\cos \theta$, the far-field is everywhere circularly polarized if the feed is circularly polarized. The φ-location of the observation point P only affects the phase of the circularly polarized wave.

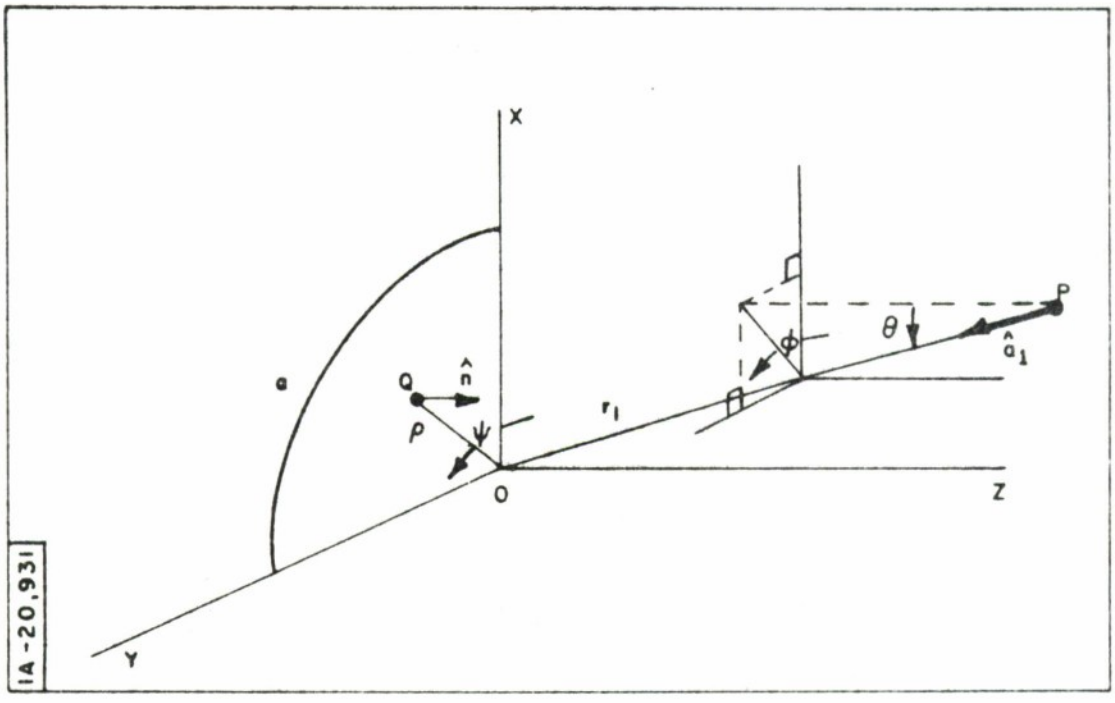

Figure 72. Geometry of the Flat Circular Plate

APPENDIX I

ANALYTICAL PROPERTIES OF THE HYPERBOLOID

Consider the locus of any point Q (Figure 73), such that

$$S = \rho + 2a \tag{234}$$

where a is a constant. If a perfectly conducting body of revolution is generated from such a curve, then the phase of a ray originating from a point source located at the origin will have the same phase, at point Q , as if it were originating from point C – within a constant phase corresponding to 2a.

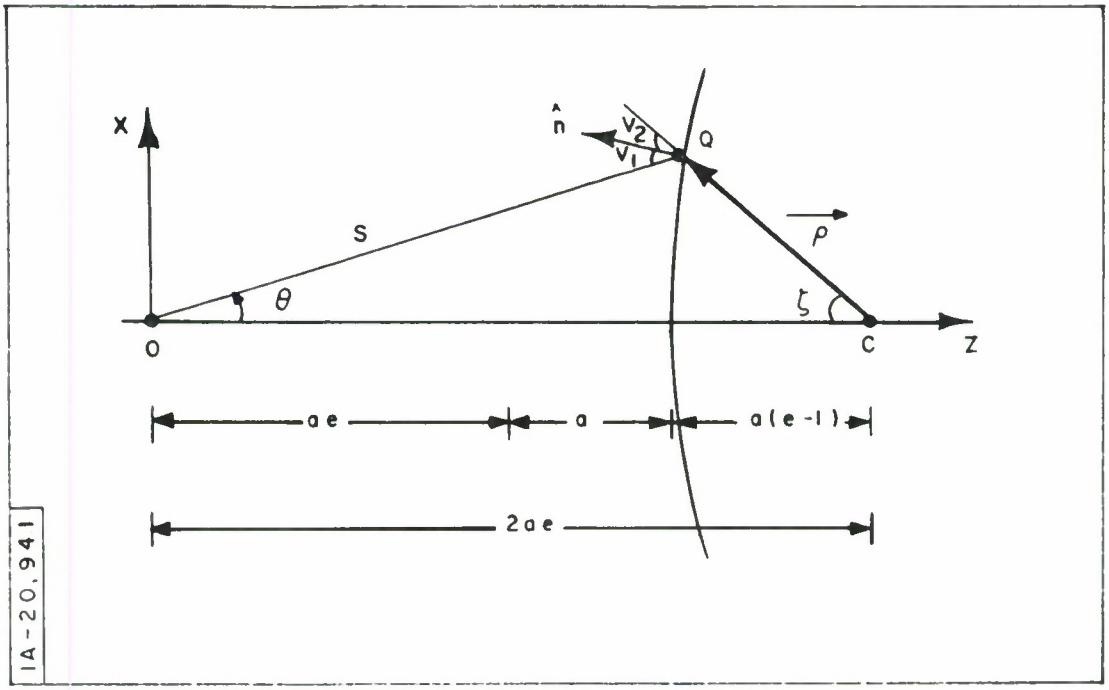

Figure 73. Geometry of Hyperboloid

Let the distance OC be 2ea. Then, by the law of cosines

$$\rho = (s^2 + 4e^2a^2 - 4s\,e\,a\cos\theta)^{1/2}$$

$$= s - 2a$$

by Equation (234). This equation can be solved for s, resulting in

$$s = \frac{a(1 - e^2)}{1 - e\cos\theta} \tag{235}$$

When

$$z = \frac{a(1 + e)(1 - e)}{(1 - e)} = a + ae$$

which is the location of the apex.

The quantity ρ can be evaluated from Equations (234) and (235) as

$$\alpha = s - 2a = \frac{a(1 - e^2) - 2a + 2ae\cos\theta}{1 - e\cos\theta}$$

or

$$\rho = \frac{a[2e\cos\theta - (1 + e^2)]}{1 - e\cos\theta} \tag{236}$$

In Cartesian coordinates, with Q in the x-z plane, the components of $\vec{\rho}$ are

$$\rho_x = s\sin\theta$$

$$\rho_z = -[2ae - s\cos\theta]$$

For any azimuthal angle φ, the expression for $\vec{\rho}$ is

$$\vec{\rho} = \begin{vmatrix} \cos\phi & -\sin\phi & 0 \\ \sin\phi & \cos\phi & 0 \\ 0 & 0 & 1 \end{vmatrix} \begin{vmatrix} s\sin\theta \\ 0 \\ s\cos\theta - 2ae \end{vmatrix} = \begin{vmatrix} s\sin\theta\cos\phi \\ s\sin\theta\sin\phi \\ s\cos\theta - 2ae \end{vmatrix}$$

But s depends on θ, and it is best to express $\vec{\rho}$ in terms of θ and φ (and constants) only, that is, by Equation (235)

$$\vec{\rho} = \frac{a}{1 - e\cos\theta} \begin{vmatrix} (1-e^2)\sin\theta\cos\phi \\ (1-e^2)\sin\theta\sin\phi \\ (1+e^2)\cos\theta - 2e \end{vmatrix} \tag{237}$$

The unit vector, normal to the surface at point Q, $\hat{n}$, can be obtained, in polar form, by taking the gradient of Equation (235), and dividing through by its magnitude, that is

$$\hat{n} = \frac{\nabla f}{|\nabla f|} = \left(\hat{a}_s \frac{\partial f}{\partial s} + \hat{a}_\theta \frac{1}{s} \frac{\partial f}{\partial \theta} \right) \Big/ |\nabla f|$$

where

$$f = s(1 - e\cos\theta) = a(1 - e^2)$$

It becomes

$$\hat{n} = \frac{[\hat{a}_s (1 - e\cos\theta) + \hat{a}_\theta e\sin\theta]}{[(1 - e\cos\theta)^2 + (e\sin\theta)^2]^{1/2}}$$

But, if Q is in the x-z plane,

$$\hat{a}_s = \begin{vmatrix} \sin\theta \\ 0 \\ \cos\theta \end{vmatrix}, \quad \hat{a}_\theta = \begin{vmatrix} \cos\theta \\ 0 \\ -\sin\theta \end{vmatrix}$$

so that, in that plane, the unit vector $\hat{n}$ is

$$\hat{n} = \frac{1}{(1 + e^2 - 2e\cos\theta)^{1/2}} \begin{vmatrix} \sin\theta \\ 0 \\ \cos\theta - e \end{vmatrix}$$

Hence, for any azimuthal angle φ, the expression for $\hat{n}$ becomes

$$\hat{n} = \begin{vmatrix} \cos\phi & -\sin\phi & 0 \\ \sin\phi & \cos\phi & 0 \\ 0 & 0 & 1 \end{vmatrix} \frac{1}{(1 + e^2 - 2e\cos\theta)^{1/2}} \begin{vmatrix} \sin\theta \\ 0 \\ (\cos\theta - e) \end{vmatrix}$$

$$= \frac{1}{(1 + e^2 - 2e\cos\theta)^{1/2}} \begin{vmatrix} \sin\theta\cos\phi \\ \sin\theta\sin\phi \\ (\cos\theta - e) \end{vmatrix} \tag{238}$$

It can be shown that the angle of incidence at point Q, namely $\cos^{-1}(-\hat{a}_s \cdot \hat{n})$, is equal to the angle of reflection, where the reflection seems to be originating from point C, namely angle $\cos^{-1}(\vec{\rho} \cdot \hat{n}/\rho)$: this property together with the property of Equation (234) constitute the

justification for the choice of the hyperboloid. Consider Equation (238) and a general expression for $\hat{a}_s$

$$\hat{a}_s = \begin{vmatrix} \cos\phi \sin\theta \\ \sin\phi \sin\theta \\ \cos\theta \end{vmatrix} \tag{239}$$

The dot product becomes

$$-\hat{a}_s \cdot \hat{n} = \frac{e\cos\theta - 1}{(1 + e^2 - 2e\cos\theta)^{1/2}}$$

By Equations (236), (237), and (238)

$$\frac{\hat{\rho}\cdot\hat{n}}{\rho} = \frac{(1 - e\cos\theta)}{a[2e\cos\theta - (1+e^2)]} \cdot \frac{1}{(1+e^2-2e\cos\theta)^{1/2}} \cdot \frac{a}{(1-e\cos\theta)} \cdot$$

$$\begin{vmatrix} (1-e^2)\sin\theta\cos\phi \\ (1-e^2)\sin\theta\sin\phi \\ (1+e^2)\cos\theta - 2e \end{vmatrix} \quad \begin{vmatrix} \sin\theta\cos\phi \\ \sin\theta\sin\phi \\ (\cos\theta - e) \end{vmatrix}$$

$$= \frac{1}{(1+e^2-2e\cos\theta)^{1/2}} \cdot \frac{(1-e^2)\sin^2\theta + [(1+e^2)\cos\theta - 2e](\cos\theta - e)}{[2e\cos\theta - (1+e^2)]}$$

The numerator can be transformed and factored as follows:

$$[(1-e^2)\sin^2\theta + (1+e^2)\cos^2\theta] - 2e\cos\theta - (1+e^2)e\cos\theta + 2e^2$$

$$= [1 + e^2 - 2e^2(1-\cos^2\theta)] - 2e\cos\theta - (1+e^2)e\cos\theta + 2e^2$$

$$= (1+e^2) + 2e^2\cos^2\theta - 2e\cos\theta - (1+e^2)e\cos\theta$$

$$= (e\cos\theta - 1)[2e\cos\theta - (1+e^2)]$$

Consequently, the expression for $(\vec{\rho} \cdot \hat{n})/\rho$ becomes

$$\frac{e \cos\theta - 1}{(1 + e^2 - 2e\cos\theta)^{1/2}}$$

that is, it is equal to $-\hat{a}_s \cdot \hat{n}$. Thus, in Figure 73, angles ν_1 and ν_2 are equal.

Finally, an expression for the differential area dA must be derived. In polar coordinates (Figure 73), the general expression for dA is

$$dA = [(s\,d\theta)^2 + (ds)^2]^{1/2} (s \sin\theta\, d\phi)$$

$$= \left[s^2 + \left(\frac{ds}{d\theta}\right)^2\right]^{1/2} s \sin\theta\, d\theta\, d\phi$$

By Equation (235), the derivative $ds/d\theta$ is evaluated as

$$\frac{ds}{d\theta} = \frac{-ae(1 - e^2)\sin\theta}{(1 - e\cos\theta)^2}$$

Upon substituting expressions for s and for $ds/d\theta$, we obtain

$$dA = \left[\left(\frac{a(1 - e^2)}{1 - e\cos\theta}\right)^2 + \left(\frac{-ae(1 - e^2)\sin\theta}{(1 - e\cos\theta)^2}\right)^2\right]^{1/2} \frac{a(1 - e^2)}{1 - e\cos\theta} \sin\theta\, d\theta\, d\phi$$

$$= \frac{a^2(1 - e^2)^2}{(1 - e\cos\theta)^3} (1 + e^2 - 2e\cos\theta) \sin\theta\, d\theta\, d\phi \qquad (240)$$

APPENDIX J

PRIMARY ILLUMINATION FUNCTION $h(\theta)$ FOR CASSEGRAIN SYSTEM

The amplitude pattern has been measured experimentally as a function of θ (Figure 74). If the maximum subtended angle θ, θ_o, is to be 30 degrees, an analytic expression can be obtained over the interval. By trial and error, it is found that the function $\cos^2(2\theta)$ provides an adequate fit, as shown in the following table:

θ	db (experimental)	db ($\cos^2 2\theta$)
0^o	0	0
10^o	1	1.07
20^o	5	4.63
30^o	12.5	12

The illumination function $h(\theta)$ will be multiplied by $1/s$, as given by Equation (107), so that the common amplitude factor is (within a constant)

$$(e \cos\theta - 1)\cos^2 2\theta$$

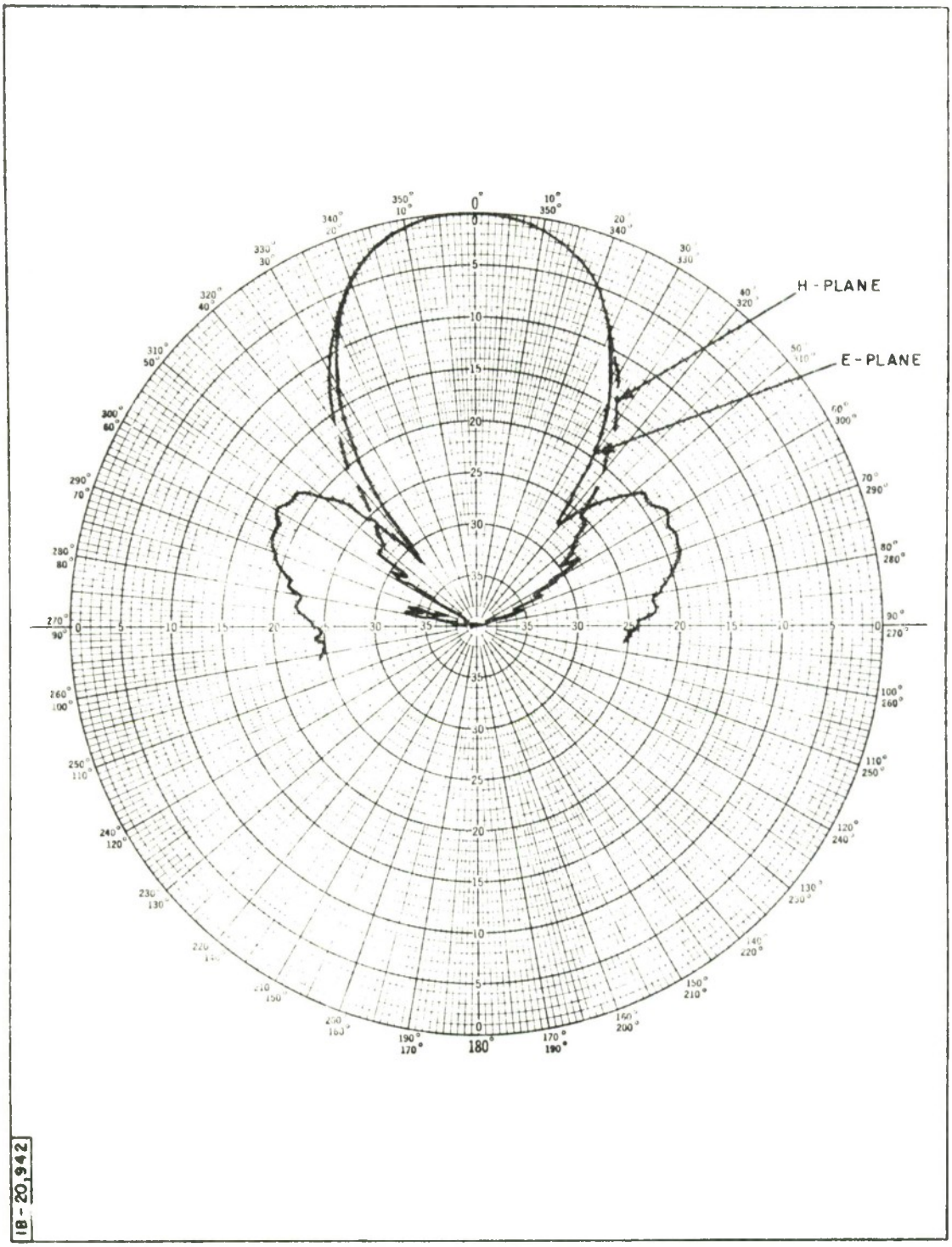

Figure 74. Primary Illumination Pattern

APPENDIX K*

COMPUTER PROGRAMS

EXAMPLE OF FOCAL FEED SYSTEM, FAR-FIELD, EQUIBEAM AND 10 db TAPER ILLUMINATION

Program "ANFPOLN" (Figure 75) is used to compute the plots of Figures 9, 26 and 43. It computes the field components at various locations in the far-field of a focal-plane antenna with equibeam distribution of the feed horn, and a $\cos^{1.5}(\pi - \eta)$ taper. The notation used in the program follows, as far as practicable, that used in the equations from which it was developed. Although this particular program represents a far-field case, very good near-field results may be calculated merely by changing the value of range, e.g., the field at a range of 600 ft. could be obtained by substituting the statement RANGE = 600. for the one shown.

The operation of the program is as follows. A value of elevation angle θ is read from a data card. Azimuth angle, ϕ, is initially set to zero. For this set of field-point coordinates, the individual contributions to the field vector components are computed for each incremental area of the reflector (in this case, 1 degree in Ψ and η) and a Simpson's rule numerical integration is performed over the surface of the reflector. After the computations are completed and the results printed, ϕ is incremented by 15 degrees and the computations are repeated for the new field point. Upon completion of the computations for ϕ = 180 degrees, the program is ready to read a new value of θ.

The Simpson's rule integration is performed by subroutine SRI, a listing of which is included.

*Written by J. L. Pearlman

```
$         JOB,ANFPOLN,PEARLMAN JL,8052.,D85,D15,E402,S
$         TYPE,COMPILGO,FORTRAN
$LIB1     ADDIO,PLBDL757
T         SUBTYPE,FORTRAN
C      NEAR FIELD POLARIZATION CALCULATIONS FOR J. ALTMAN  3/22/66
C      PER MEMO 3/11/66
C      ****************************************************************
C      ****** NOTE - EXPONENTIAL TERM MODIFIED  4/7/66 ******************
C      ****************************************************************
C      ****************************************************************
C      MODIFIED FOR EQUIBEAM DISTRIBUTION 9/13/66
C      ****************************************************************
       DIMENSION XY1RE (63), XY1IE (63), X2RE (63), X2IE (63), X3RE (63),
      1X3IE (63), XY4RE (63), XY4IE (63), X5RE (63), X5IE (63),
      2Y2RE (63), Y2IE (63), Y3RE (63), Y3IE (63), Y5RE (63), Y5IE (63),
      3XY1RP (361), XY1IP (361), X2RP (361), X2IP (361), X3RP (361),
      4X3IP (361), XY4RP (361), XY4IP (361), X5RP (361), X5IP (361),
      5Y2RP (361), Y2IP (361), Y3RP (361), Y3IP (361), Y5RP (361),
      6Y5IP (361), PHANG (25), Y2R (25), Y2I (25), Y3R (25), Y3I (25),
      7Y5R (25), Y5I (25), ELL (25), FMAG (25), DEV (25), HETA (63)
       PI=4.*ATAN(1.)
       F=12.5
C      ****************************************************************
C      ** NOTE - RANGE INCREASED INTO FAR FIELD 4/16/66 *****************
       RANGE=1.E7
C      ****************************************************************
       CONST1=-24./9.22*PI
       RSQ=RANGE**2
       FSQ=F**2
       TWOFR=2.*F*RANGE
       C2A=.5*F/RANGE
       C2B=4.*C2A
       DRC=PI/180.
       ETA0=118.07*DRC
       NTH=0
    20 READ 10,THANG
       NTH=1+NTH
       THETA=THANG*DRC
       STH=SIN(THETA)
       CTH=COS(THETA)
       PRINT 11,THANG
       DO 23 KC=1,13
       FKC=KC-1
       PHANG(KC)=15.*FKC
       PHI=PHANG(KC)*DRC
       SPHI=SIN(PHI)
       CPHI=COS(PHI)
       STSP=STH*SPHI
       STCP=STH*CPHI
       DO 22 KB=1,361
       FKB=KB-1
       PSI=DRC*FKB
       SP=SIN(PSI)
       CP=COS(PSI)
       SP2=SP**2
       CP2=CP**2
       S2PH=SP*CP
       CONST3=STH*COS(PSI-PHI)
       DO 21 KA=118,180
       KAA=KA-117
```

Figure 75. Program ANFPOLN

```
      FKA=KA
      ETA=DRC*FKA
      EO2=ETA/2.
      SE=SIN(ETA)
      CE=COS(ETA)
      SEO2=SIN(EO2)
      CEO2=COS(EO2)
      CTEO2=CEO2/SEO2
      C3AR=1./SEO2**2
      C3A=C3AR**2
C     ******************************************************************
C     H (ETA) AS FITTED TO MEASURED CURVE  4/26/66 **********************
      IF ((NTH.EQ.1).AND.(KC.EQ.1).AND.(KB.EQ.1))
     1HETA(KAA)=COS(PI-ETA)**(1.5)/C3AR
      HE=HETA(KAA)
C     ******************************************************************
      GE=HE*SE/SEO2**5
      C3B=.5*C2A*C3A
      CONST4=CONST1*(SQRT(RSQ+FSQ*C3A-TWOFR*C3AR*(SE*CONST3+CTH*CE))
     1+F*C3AR)
      AP=-SEO2*GE
      BP=0.
      EP=-CEO2*GE
      C2C=C2B*CTEO2
      CC4=COS(CONST4)
      SC4=SIN(CONST4)
      XY1RE(KAA)=AP*CC4
      XY1IE(KAA)=AP*SC4
      TA=(C2C*SP-STSP)*EP
      X3T=TA*SP
      X3RE(KAA)=X3T*CC4
      X3IE(KAA)=X3T*SC4
      X5T=-TA*CP
      X5RE(KAA)=X5T*CC4
      X5IE(KAA)=X5T*SC4
      TB=(C2C*CP-STCP)*EP
      Y3T=TB*CP
      Y3RE(KAA)=Y3T*CC4
      Y3IE(KAA)=Y3T*SC4
      Y5T=-TB*SP
      Y5RE(KAA)=Y5T*CC4
      Y5IE(KAA)=Y5T*SC4
   21 CONTINUE
      CALL SRI (XY1RE,DRC,KAA,XY1RP(KB))
      CALL SRI (XY1IE,DRC,KAA,XY1IP(KB))
      CALL SRI (X3RE,DRC,KAA,X3RP(KB))
      CALL SRI (X3IE,DRC,KAA,X3IP(KB))
      CALL SRI (X5RE,DRC,KAA,X5RP(KB))
      CALL SRI (X5IE,DRC,KAA,X5IP(KB))
      CALL SRI (Y3RE,DRC,KAA,Y3RP(KB))
      CALL SRI (Y3IE,DRC,KAA,Y3IP(KB))
      CALL SRI (Y5RE,DRC,KAA,Y5RP(KB))
      CALL SRI (Y5IE,DRC,KAA,Y5IP(KB))
   22 CONTINUE
      CALL SRI (XY1RP,DRC,361,XY1R)
      CALL SRI (XY1IP,DRC,361,XY1I)
      CALL SRI (X3RP,DRC,361,X3R)
      CALL SRI (X3IP,DRC,361,X3I)
      CALL SRI (X5RP,DRC,361,X5R)
      CALL SRI (X5IP,DRC,361,X5I)
```

Figure 75 (Continued). Program ANFPOLN

```
      CALL SRI (Y3RP,DRC,361,Y3R(KC))
      CALL SRI (Y3IP,DRC,361,Y3I(KC))
      CALL SRI (Y5RP,DRC,361,Y5R(KC))
      CALL SRI (Y5IP,DRC,361,Y5I(KC))
      XR=XY1R+X3R-X5I
      XI=XY1I+X3I+X5R
      YR=-XY1I-Y3I(KC)+Y5R(KC)
      YI=XY1R+Y3R(KC)+Y5I(KC)
      SPLU=.5*SQRT((XR-YI)**2+(XI+YR)**2)
      SMIN=.5*SQRT((XR+YI)**2+(XI-YR)**2)
      ELL(KC)=10.*ALOG10(((SPLU+SMIN)/(SPLU-SMIN))**2)
      XRN=-X5I
      XIN=X5R
      YRN=-XY1I-Y3I(KC)
      YIN=XY1R+Y3R(KC)
      XMAG=SQRT(XRN**2+XIN**2)
      YMAG=SQRT(YRN**2+YIN**2)
      FMAG(KC)=SQRT(XMAG**2+YMAG**2)
      DEV(KC)=ATAN(XMAG/YMAG)/DRC
      PRINT 10,PHANG(KC),XY1R,XY1I,X3R,X3I,X5R,X5I
   23 CONTINUE
      PRINT 12,THANG
      DO 24 L=1,13
      PRINT 10,PHANG(L),Y3R(L),Y3I(L),Y5R(L),Y5I(L)
   24 CONTINUE
      PRINT 14,THANG
      DO 25 L=1,13
      PRINT 13,PHANG(L),ELL(L),FMAG(L),DEV(L)
   25 CONTINUE
      GO TO 20
      RETURN
   10 FORMAT (F10.1,6E15.5)
   11 FORMAT (1$1$/110X$PAGE 1 OF 3$//
     110X$FAR FIELD CALCULATIONS FOR J. ALTMAN 4/16/66$/
     210X$EXACT NEAR FIELD EXPRESSION WITH VERY LARGE RANGE VALUE$/
     310X$ILLUMINATION FUNCTION FITTED TO MEASURED DATA 2/26/66$/
     C10X$MODIFIED FOR EQUIBEAM DISTRIBUTION  9/13/66$/
     410X$FOR THETA=$F6.1,$ DEGREES$/
     57X$PHI$5X$RE (X1,Y1)$5X$IM (X1,Y1)$5X$RE (X3)$8X$IM (X3)$
     68X$RE (X5)$8X$IM (X5)$)
   12 FORMAT ($1$/110X$PAGE 2 OF 3$//
     110X$FAR FIELD CALCULATIONS FOR J. ALTMAN 4/16/66$/
     210X$EXACT NEAR FIELD EXPRESSION WITH VERY LARGE RANGE VALUE$/
     310X$ILLUMINATION FUNCTION FITTED TO MEASURED DATA 2/26/66$/
     C10X$MODIFIED FOR EQUIBEAM DISTRIBUTION  9/13/66$/
     410X$FOR THETA=$F6.1,$ DEGREES$/
     57X$PHI$5X$RE (Y3)$8X$IM (Y3)$8X$RE (Y5)$8X$IM (Y5)$)
   13 FORMAT (F10.1,3F20.4)
   14 FORMAT ($1$/110X$PAGE 3 OF 3$//
     110X$FAR FIELD CALCULATIONS FOR J. ALTMAN 4/16/66$/
     210X$EXACT NEAR FIELD EXPRESSION WITH VERY LARGE RANGE VALUE$/
     310X$ILLUMINATION FUNCTION FITTED TO MEASURED DATA 2/26/66$/
     C10X$MODIFIED FOR EQUIBEAM DISTRIBUTION  9/13/66$/
     410X$FOR THETA=$F6.1,$ DEGREES$/
     57X$PHI$3X$ELLIPTICITY (DB.)$11X$MAGNITUDE$4X$DEVIATION (DEG.)$)
      END
         SUBTYPE,DATA
      .?
```

Figure 75 (Continued). Program ANFPOLN

```
T           SUBTYPE,FORTRAN,LSTRAP,NRL,SEQ
      SUBROUTINE SRI (Y,DX,N,YI)
C     NUMERICALLY INTEGRATES Y DX BY SIMPSON'S RULE
C     Y=ARRAY TO BE INTEGRATED
C     DX=X INCREMENT
C     N=NO. OF POINTS IN Y. IF N NOT ODD, SUBROUTINE CAUSES ABEOJ
C     WITH PRINTOUT OF CURRENT VALUE OF N.
      DIMENSION Y(N)
      IF ((MOD(N,2)).NE.1) GO TO 21
      SUM=Y(1)+Y(N)+4.*Y(2)
      NA=N-1
      DO 20 K=3,NA,2
      SUM=SUM+2.*Y(K)+4.*Y(K+1)
   20 CONTINUE
      YI=SUM*DX/3.
      RETURN
   21 PRINT 10,N
      STOP
   10 FORMAT ($CN=$I15,$, WHICH IS AN ILLEGAL VALUE.$)
      END
```

Figure 75 (Concluded). Program ANFPOLN

EXAMPLE OF CASSEGRAIN SYSTEM: FIELD ON PARABOLOID, DIPOLE-LIKE ILLUMINATION

Program "ACFSHB" (Figure 76) computes the vector components of the field scattered onto a parabolic reflector from a hyperbolic subreflector and stores the results on tape for further processing.

The operation of this program is similar to that of the previous program except that the coordinates of the field points are determined by the geometry of the parabolic reflector. The points on the reflector for which the field is calculated are separated by 15 degrees in Ψ and 1.9375 degrees in η (this value being the closest to two degrees which is an exact odd divisor of the angle subtended by the parabola). The components of the total field at each point on the parabola are integrated, using Simpson's rule, over the surface of the hyperbolic subreflector using an incremental area of the one degree in θ and ϕ.

A dipole-like distribution at the feed horn is assumed.

Again, subroutine SRI is used to perform the numerical integration.

EXAMPLE OF CASSEGRAIN SYSTEM: FAR-FIELD

Program "APCFA" (Figure 77) computes the components of the field vector in the far-field of a Cassegranian-feed antenna.

The operation is similar to that of "ANFPOLN" except that the field components on the surface of the reflector are not computed in this program, but are read in from a binary tape generated by another program (such as "ASFSHB"). Also, the incremental area on the surface of the reflector was 1.9375 degrees in η and 15 degrees in Ψ.

A recently added facility for handling complex numbers was used in this program.

```
B         JOB,ACFSHB,PEARLMAN JL,8052..D85,015,E402,S
B         TYPE,COMPILGO,FORTRAN
BLIB      ADDIO,PLBD1674
T         SUBTYPE,FIOD
B3B       IOD,TAPE,,,,,,SAVE
          END
T         SUBTYPE,FORTRAN
C      CALCULATION OF COMPONENTS OF H(S/P) AS PER MEMO BY J. ALTMAN
C      4/29/66
C      ***************************************************************
C      ORIGINAL PROGRAM WRITTEN 5/6/66 (J. L. P.) ********************
C      ***************************************************************
C      ***************************************************************
C      VERSION TO WRITE BINARY TAPE FOR CASSEGRANIAN FEED PROGRAM 7/19/66
C      ***************************************************************
C      ***************************************************************
C      DIPOLE - LIKE DISTRIBUTION
C      ***************************************************************
       DIMENSION PSANG (25), PS( (25), SPS (25), CPS (25),
      1XYZ (12), PHI (361), SPH (361), CPH (361), X1PR (361), X1PI (361),
      2X2PR (361), X2PI (361), Y1PR (361), Y1PI (361), Y2PR (361),
      3Y2PI (361), Z1PR (361), Z1PI (361), Z2PR (361), Z2P( (361),
      4THETA (31), STH (31), CTH (31), TTH(31), CSQTT (31), X1TR (31),
      5X1TI (31), X2TR (31), X2T( (31), Y1TR (31), Y1T( (31), Y2TR (31),
      6Y2T( (31), Z1TR (31), Z1TI (31), Z2TR (31), Z2T( (31)
       PI=4.*ATAN(1.)
       TWOPI=2.*PI
       FCON=12.5
       CONST1=12.*TWOPI/9.22
       ACON=1.063
       EXC=2.45
       EXSQ=EXC**2
       OPEXS=1.+EXSQ
       OMEXS=1.-EXSQ
       AOMEX=OMEXS*ACON
       DRC=PI/180.
       DRC2=31.*DRC/15.
       TFA=2.*FCON*ACON
       TWE=2.*EXC
       ASQ=ACON**2
       AOMEXS=AOMEX**2
       DO 30 NE=1,33
       FNE=33-NE
       ETA=PI-FNE*DRC2
       E02=ETA/2.
       SE=SIN(ETA)
       CE=COS(ETA)
       SE02=SIN(E02)
       SSE02=SE02**2
       FOM=FCON/SSE02
       RTA=FOM**2
       RTC1=TFA/SSE02
       RTC2A=SE*OMEXS
       RTC3A=CE*OPEXS
       RTC4=TWE*CE
       A1X1TA=-FOM*SE
       A1Z1T=-FOM*CE
       WRITE (3) ETA
```

Figure 76. Program ACFSHB

```
      DO 29 KC=1,25
      IF (NE.EQ.1) GO TO 21
      GO TO 22
   21 FKC=KC-1
      PSANG(KC)=15.*FKC
      PSI(KC)=PSANG(KC)*DRC
      SPS(KC)=SIN(PSI(KC))
      CPS(KC)=COS(PSI(KC))
   22 SECP=SE*CPS(KC)
      SESP=SE*SPS(KC)
      A1X1T=A1X1TA*CPS(KC)
      A1Y1T=A1X1TA*SPS(KC)
      DO 28 KB=1,361
      IF ((NE.EQ.1).AND.(KC.EQ.1)) GO TO 23
      GO TO 24
   23 FKB=KB-1
      PHI(KB)=FKB*DRC
      SPH(KB)=SIN(PHI(KB))
      CPH(KB)=COS(PHI(KB))
   24 SPHSQ=SPH(KB)**2
      CPHSQ=CPH(KB)**2
      SCPH=SPH(KB)*CPH(KB)
      CAD=COS(PSI(KC)-PHI(KB))
      RTC2B=RTC2A*CAD
      OMECP=OMEXS*CPH(KB)
      AOMESP=AOMEX*SPH(KB)
      AOMECP=ACON*OMECP
      DO 27 KA=1,31
      IF ((NE.EQ.1).AND.(KC.EQ.1).AND.(KB.EQ.1)) GO TO 25
      GO TO 26
   25 FKA=KA-1
      THETA(KA)=FKA*DRC
      STH(KA)=SIN(THETA(KA))
      CTH(KA)=COS(THETA(KA))
      TTH(KA)=2.*THETA(KA)
      CSQTT(KA)=COS(TTH(KA))**2
   26 ECTH=EXC*CTH(KA)
      OMECT=1.-ECTH
      R=SQRT(RTA+ASQ*((2.*ECTH-OPEXS)/OMECT)**2-RTC1/OMECT
     1*(RTC2B*STH(KA)+RTC3A*CTH(KA)-RTC4))
      RR=1./R
      A1XP=RR*(A1X1T+AOMECP*STH(KA)/OMECT)
      A1YP=RR*(A1Y1T+AOMESP*STH(KA)/OMECT)
      A1ZP=RR*(A1Z1T+ACON/OMECT*(OPEXS*CTH(KA)-TWE))
      TECTH=TWE*CTH(KA)
      HTH=-OMECT*CSQTT(KA)
      HTHP=HTH/SQRT(OPEXS-TECTH)
      STHSQ=STH(KA)**2
      SCTH=STH(KA)*CTH(KA)
      BCDT=HTHP*STHSQ
      EFT=HTHP*SCTH
      A=HTHP*CTH(KA)*(EXC-CTH(KA))
      B=-BCDT*SPHSQ
      C=-BCDT*SCPH
      D=BCDT*CPHSQ
      E=EFT*CPH(KB)
      F=EFT*SPH(KB)
```

Figure 76 (Continued). Program ACFSHB

```
      EXP=-CONST1*(AOMEX/OMECT-FOM+R)
      DAT=AOMEXS/OMECT**3*(OPEXS-TECTH)*STH(KA)
      EXPR=COS(EXP)
      EXPI=-SIN(EXP)
      APB=A+B
      DMA=D-A
      DAOR=RR*DAT
      X1T=DAOR*(A1ZP*DMA+A1YP*F)
      X2T=-DAOR*(A1ZP*C+A1YP*E)
      Y1T=DAOR*(A1XP*E-A1ZP*APB)
      Y2T=-DAOR*(A1ZP*C+A1XP*F)
      Z1T=DAOR*(A1YP*C-A1XP*DMA)
      Z2T=DAOR*(A1YP*APB+A1XP*C)
      X1TR(KA)=X1T*EXPR
      X1TI(KA)=X1T*EXPI
      X2TR(KA)=X2T*EXPR
      X2TI(KA)=X2T*EXPI
      Y1TR(KA)=Y1T*EXPR
      Y1TI(KA)=Y1T*EXPI
      Y2TR(KA)=Y2T*EXPR
      Y2TI(KA)=Y2T*EXPI
      Z1TR(KA)=Z1T*EXPR
      Z1TI(KA)=Z1T*EXPI
      Z2TR(KA)=Z2T*EXPR
      Z2TI(KA)=Z2T*EXPI
   27 CONTINUE
      CALL SRI (X1TR,DRC,31,X1PR(KB))
      CALL SRI (X1TI,DRC,31,X1PI(KB))
      CALL SRI (X2TR,DRC,31,X2PR(KB))
      CALL SRI (X2TI,DRC,31,X2PI(KB))
      CALL SRI (Y1TR,DRC,31,Y1PR(KB))
      CALL SRI (Y1TI,DRC,31,Y1PI(KB))
      CALL SRI (Y2TR,DRC,31,Y2PR(KB))
      CALL SRI (Y2TI,DRC,31,Y2PI(KB))
      CALL SRI (Z1TR,DRC,31,Z1PR(KB))
      CALL SRI (Z1TI,DRC,31,Z1PI(KB))
      CALL SRI (Z2TR,DRC,31,Z2PR(KB))
      CALL SRI (Z2TI,DRC,31,Z2PI(KB))
   28 CONTINUE
      CALL SRI (X1PR,DRC,361,XYZ(1))
      CALL SRI (X1PI,DRC,361,XYZ(2))
      CALL SRI (X2PR,DRC,361,XYZ(3))
      CALL SRI (X2PI,DRC,361,XYZ(4))
      CALL SRI (Y1PR,DRC,361,XYZ(5))
      CALL SRI (Y1PI,DRC,361,XYZ(6))
      CALL SRI (Y2PR,DRC,361,XYZ(7))
      CALL SRI (Y2PI,DRC,361,XYZ(8))
      CALL SRI (Z1PR,DRC,361,XYZ(9))
      CALL SRI (Z1PI,DRC,361,XYZ(10))
      CALL SRI (Z2PR,DRC,361,XYZ(11))
      CALL SRI (Z2PI,DRC,361,XYZ(12))
      WRITE (3) PSI(KC),XYZ
   29 CONTINUE
   30 CONTINUE
      END FILE 3
      REWIND 3
      RETURN
      END
```

Figure 76 (Concluded). Program ACFSHB

```
B         JOB,APCFA,PEARLMAN JL,8052..085,015,E402,S
B         TYPE,COMPILGO,FORTRAN
BLIB1     ADDIO,PLBD1954
T         SUBTYPE,FIOD
B3B       IOD,TAPE
B         REEL,PLBD1792
          END
T         SUBTYPE,FORTRAN
C      FAR FIELD POLARIZATION CALCULATIONS FOR J. ALTMAN
C      ************************************************************************
C      CASSEGRANIAN FEED   8/3/66
C      ************************************************************************
C      ************************************************************************
C      COMPONENTS OF FIELD SCATTERED ONTO PARABOLIC REFLECTOR FROM
C      HYPEBOLIC SUBREFLECTOR READ INTO ARRAY XYZ FROM BINARY TAPE (3)
C      GENERATED BY PROGRAM ACFSHB
C      ************************************************************************
C      ************************************************************************
C      ***** NOTE - DELTA ETA = 2 DEG. AND DELTA PSI = 15 DEG. **********
C      ************************************************************************
C      ************************************************************************
C      EXACT EXPONENTIAL TERM USED
C      ************************************************************************
       DIMENSION XPRE(33), XPIE (33), XQRE (33), XQIE (33), YPRE (33),
      1YPIE (33), YQRE (33), YQIE (33), SE (33), CE (33), SE02 (33),
      2CE02 (33), SE02F (33), ECHK (33), XPRP (25), XPIP (25), XQRP (25),
      3XQIP (25), YPRP (25), YPIP (25), YQRP (25), YQIP (25), SP (25),
      4CP (25), PSI (25), PSCHK (25), PHANG (13), YPR (13), YPI (13),
      5YQR (13), YQI (13), SPHI (13), CPHI (13), PHI (13), ELL (13),
      6DEV (13), FMAG (13), XYZ (12,25,33)
       COMPLEX EXPT, X1, X2, Y1, Y2, Z1, Z2, ZA1, ZA2, ZB1, ZB2, ZC1,
      1ZC2, XPCT, XQCT, YPCT, YQCT
       REWIND 3
       PI=4.*ATAN(1.)
       F=12.5
C      ************************************************************************
C      ***** RANGE EXTENDED TO FAR FIELD ************************************
       RANGE=1.E7
C      ************************************************************************
       CONST1=-24./9.22*PI
       RSQ=RANGE**2
       FSQ=F**2
       TWOFR=2.*F*RANGE
       C2A=.5*F/RANGE
       C2B=4.*C2A
       DRC=PI/180.
       DRC2=DRC*31./16.
       DRC15=15.*DRC
       NTH=0
   20  READ 10,THANG
       NTH=1+NTH
       THETA=THANG*DRC
       STH=SIN(THETA)
       CTH=COS(THETA)
       PRINT 11,THANG
       DO 30 KC=1,13
       IF (NTH.EQ.1)GO TO 21
       GO TO 22
```

Figure 77. Program APCFA

```
21 FKC=KC-1
   PHANG(KC)=15.*FKC
   PHI(KC)=PHANG(KC)*DRC
   SPHI(KC)=SIN(PHI(KC))
   CPHI(KC)=COS(PHI(KC))
22 STSP=STH*SPHI(KC)
   STCP=STH*CPHI(KC)
   DO 29 KB=1,25
   IF((NTH.EQ.1).AND.(KC.EQ.1)) GO TO 23
   GO TO 24
23 FKB=KB-1
   PSI(KB)=FKB*DRC15
   SP(KB)=SIN(PSI(KB))
   CP(KB)=COS(PSI(KB))
24 SP2=SP(KB)**2
   CP2=CP(KB)**2
   SP2PH=SP(KB)*CP(KB)
   CONST3=STH*COS(PSI(KB)-PHI(KC))
   DO 28 KAA=1,33
   IF ((NTH.EQ.1).AND.(KC.EQ.1).AND.(KB.EQ.1)) GO TO 25
   GO TO 27
25 FKA=33-KAA
   READ (3) ECHK(KAA)
   DO 26 KPH=1,25
   READ (3) PSCHK(KPH),(XYZ(L,KPH,KAA),L=1,12)
26 CONTINUE
   ETA=PI-FKA*DRC2
   EO2=ETA/2.
   SE(KAA)=SIN(ETA)
   CE(KAA)=COS(ETA)
   SEO2(KAA)=SIN(EO2)
   SEO2F(KAA)=SEO2(KAA)**5
   CEO2(KAA)=COS(EO2)
27 C3AR=1./SEO2(KAA)**2
   C3A=C3AR**2
   CONST4=CONST1*(SQRT(RSQ+FSQ*C3A-TWOFR*C3AR*(SF(KAA)*CONST3
  1+CTH*CE(KAA)))+F*C3AR)
   CTEO2=CEO2(KAA)/SEO2(KAA)
   C2C=C2B*CTEO2
   CC4=COS(CONST4)
   SC4=SIN(CONST4)
   GF=SE(KAA)/SEO2F(KAA)
   SPCEH=SP(KB)*CEO2(KAA)
   CPCEH=CP(KB)*CEO2(KAA)
   TA=C2C*SP(KB)-STSP
   TB=C2C*CP(KB)-STCP
   EXPT=CMPLX(CC4,SC4)*GF
   X1=CMPLX(XYZ(1,KB,KAA),XYZ(2,KB,KAA))
   X2=CMPLX(XYZ(3,KB,KAA),XYZ(4,KB,KAA))
   Y1=CMPLX(XYZ(5,KB,KAA),XYZ(6,KB,KAA))
   Y2=CMPLX(XYZ(7,KB,KAA),XYZ(8,KB,KAA))
   Z1=CMPLX(XYZ(9,KB,KAA),XYZ(10,KB,KAA))
   Z2=CMPLX(XYZ(11,KB,KAA),XYZ(12,KB,KAA))
   ZA1=-Y1*SEO2(KAA)-Z2*SPCEH
   ZA2=-Y2*SEO2(KAA)-Z1*SPCEH
   ZB1=X1*SEO2(KAA)+Z1*CPCEH
   ZB2=X2*SEO2(KAA)+Z2*CPCEH
   ZC1=X1*SPCEH-Y2*CPCEH
   ZC2=X2*SPCEH-Y1*CPCEH
   XPCT=-EXPT*(ZB1+ZC1*TA)
```

Figure 77 (Continued). Program APCFA

```
      XQCT=-EXPT*(ZB2+ZC2*TA)
      YPCT=EXPT*(ZA1+ZC2*TB)
      YQCT=EXPT*(ZA2+ZC1*TB)
      XPRE(KAA)=REAL(XPCT)
      XPIE(KAA)=AIMAG(XPCT)
      XQRE(KAA)=REAL(XQCT)
      XQIE(KAA)=AIMAG(XQCT)
      YPRE(KAA)=REAL(YPCT)
      YPIE(KAA)=AIMAG(YPCT)
      YQRE(KAA)=REAL(YQCT)
      YQIE(KAA)=AIMAG(YQCT)
   28 CONTINUE
      CALL SRI (XPRE,DRC2,33,XPRP(KB))
      CALL SRI (XPIE,DRC2,33,XPIP(KB))
      CALL SRI (XQRE,DRC2,33,XQRP(KB))
      CALL SRI (XQIE,DRC2,33,XQIP(KB))
      CALL SRI (YPRE,DRC2,33,YPRP(KB))
      CALL SRI (YPIE,DRC2,33,YPIP(KB))
      CALL SRI (YQRE,DRC2,33,YQRP(KB))
      CALL SRI (YQIE,DRC2,33,YQIP(KB))
   29 CONTINUE
      CALL SRI (XPRP,DRC15,25,XPR)
      CALL SRI (XPIP,DRC15,25,XPI)
      CALL SRI (XQRP,DRC15,25,XQR)
      CALL SRI (XQIP,DRC15,25,XQI)
      CALL SRI (YPRP,DRC15,25,YPR(KC))
      CALL SRI (YPIP,DRC15,25,YPI(KC))
      CALL SRI (YQRP,DRC15,25,YQR(KC))
      CALL SRI (YQIP,DRC15,25,YQI(KC))
      XR=XPR-XQI
      XI=XPI+XQR
      YR=YQR(KC)-YPI(KC)
      YI=YQI(KC)+YPR(KC)
      SPLU=.5*SQRT((XR-YI)**2+(XI+YR)**2)
      SMIN=.5*SQRT((XR+YI)**2+(XI-YR)**2)
      ELL(KC)=10.*ALOG10(((SPLU+SMIN)/(SPLU-SMIN))**2)
      XRN=XPR
      XIN=XPI
      YRN=YQR(KC)
      YIN=YQI(KC)
      XMAG=SQRT(XRN**2+XIN**2)
      YMAG=SQRT(YRN**2+YIN**2)
      FMAG(KC)=SQRT(XMAG**2+YMAG**2)
      DEV(KC)=ATAN(XMAG/YMAG)/DRC
      PRINT 10,PHANG(KC),XPR,XPI,XQR,XQI
   30 CONTINUE
      IF (NTH.EQ.1) CALL FFREE (3)
      PRINT 12,THANG
      DO 31 L=1,13
      PRINT 10,PHANG(L),YPR(L),YPI(L),YQR(L),YQI(L)
   31 CONTINUE
      PRINT 13,THANG
      DO 32 L=1,13
      PRINT 14,PHANG(L),ELL(L),FMAG(L)
   32 CONTINUE
      GO TO 20
      RETURN
   10 FORMAT (F10.1,7E15.5)
```

Figure 77 (Continued). Program APCFA

```
 11 FORMAT ($1$//11CX$PAGE 1 OF 3$//
   11OX$FAR FIELD POLARIZATION CALCULTIONS$/
   21OX$CASSEGRANIAN FEED ANTENNA$/
   31OX$FOR THETA=$F6.1,$ DEGREES$/
   47X$PHI$5X$RE (XP)$8X$IM (XP)$8X$RE (XQ)$8X$IM (XQ)$)
 12 FORMAT ($1$//11CX$PAGE 2 OF 3$//
   11CX$FAR FIELD POLARIZATION CALCULTIONS$/
   21CX$CASSEGRANIAN FEED ANTENNA$/
   31OX$FOR THETA=$Fo.1,$ DEGREES$/
   47X$PHI$5X$RE (YP)$8X$IM (YP)$8X$RE (YQ)$8X$IM (YQ)$)
 13 FORMAT ($1$//11CX$PAGE 3 OF 3$//
   11OX$FAR FIELD POLARIZATION CALCULTIONS$/
   21OX$CASSEGRANIAN FEED ANTENNA$/
   31CX$FOR THETA=$F6.1,$ DEGREES$/
   47X$PHI$3X$ELLIPTICITY (DB.)$11X$MAGNITUDE$)
 14 FORMAT (F1C.1,3F20.4)
    END
T      SUBTYPE,DATA
    .2

     0.5
     0.7
     1.C
     1.5
     1.7
     2.C
     2.5
```

Figure 77 (Concluded). Program APCFA

Security Classification

DOCUMENT CONTROL DATA - R & D

(Security classification of title, body of abstract and indexing annotation must be entered when the overall report is classified)

1. ORIGINATING ACTIVITY (Corporate author)
The MITRE Corporation
Bedford, Massachusetts

2a. REPORT SECURITY CLASSIFICATION
UNCLASSIFIED

2b. GROUP
N/A

3. REPORT TITLE
POLARIZATION PROPERTIES OF THE PARABOLOIDAL ANTENNA: AN ANALYTICAL STUDY

4. DESCRIPTIVE NOTES (Type of report and inclusive dates)
N/A

5. AUTHOR(S) (First name, middle initial, last name)
Jerome L. Altman

6. REPORT DATE
December 1967

7a. TOTAL NO. OF PAGES
210

7b. NO. OF REFS
6

8a. CONTRACT OR GRANT NO.
AF 19(628)-5165

b. PROJECT NO.
8052

c.

d.

9a. ORIGINATOR'S REPORT NUMBER(S)
ESD-TR-67-425

9b. OTHER REPORT NO(S) (Any other numbers that may be assigned this report)
MTP-52

10. DISTRIBUTION STATEMENT
This document has been approved for public release and sale; its distribution is unlimited.

11. SUPPLEMENTARY NOTES
N/A

12. SPONSORING MILITARY ACTIVITY
Development Engineering Division, Directorate of Planning and Technology, Electronic Systems Division, L. G. Hanscom Field, Bedford, Massachusetts.

13. ABSTRACT

This study is a theoretical investigation of the polarization properties of the paraboloidal antenna for both the focal feed system and the Cassegrain feed system when the feed horn is either circularly or linearly polarized. The properties are analyzed in terms of general analytic equations and also in terms of quantitative graphs pertaining to the specific case of the 30-foot diameter paraboloidal antenna which is part of The MITRE Corporation's Bedford Radar Installation.

DD FORM 1 NOV 65 1473

Security Classification

14 KEY WORDS	LINK A		LINK B		LINK C	
	ROLE	WT	ROLE	WT	ROLE	WT
RADAR						
ANTENNAS						
Polarization Properties of Antennas						
Paraboloidal Antennas						